

Novel therapies for diseases of the ocular surface



Yazad Irani

Department of Ophthalmology

Flinders University

Bedford Park, South Australia

March 2015

TABLE OF CONTENTS

DECLARATION	X
ABSTRACT	XI
ACKNOWLEDGEMENTS	XIII
PUBLICATIONS ARISING FROM THIS THESIS	XIV
CONFERENCE ABSTRACTS	XV
ABBREVIATIONS AND SYMBOLS USED IN THIS THESIS	XVII
CHAPTER 1 INTRODUCTION	1
1.1 OVERVIEW	1
1.2 THE STRUCTURE OF THE CORNEA AND THE OCULAR SURFACE.....	1
1.2.1 <i>The cornea and sclera</i>	1
1.2.2 <i>The conjunctiva</i>	5
1.2.3 <i>The limbus</i>	5
1.3 CORNEAL EPITHELIAL REGENERATION	8
1.3.1 <i>Renewal of the corneal epithelium</i>	8
1.3.2 <i>Corneal epithelial stem cells</i>	10
1.3.2.a ABCG2	11
1.3.2.b p63	11
1.3.2.c Cytokeratins	12
1.3.3 <i>The limbal stem cell niche</i>	12
1.4 LIMBAL STEM CELL DYSFUNCTION	14
1.4.1 <i>Treatments for ocular surface disease</i>	14
1.4.1.a Limbal grafts	14
1.4.1.b Ex vivo cultured limbal epithelial stem cells.....	16
1.4.1.c Oral mucosa as a source of stem cells	18
1.4.1.d Other sources of stem cells for ocular surface reconstruction	19
1.4.1.e Scaffolds for the transfer of stem cell to the ocular surface	21
1.4.1.e.1 Amniotic membrane	21

1.4.1.e.2	Alternative scaffolds for transfer of cells to the eye	22
1.5	CORNEAL NEOVASCULARIZATION	27
1.5.1	<i>Corneal avascularity</i>	27
1.5.2	<i>Physiological angiogenesis</i>	27
1.5.3	<i>Vascular endothelial growth factors and angiogenesis</i>	29
1.5.3.a	VEGF-A.....	29
1.5.3.b	VEGF-B.....	31
1.5.3.b.1	The role of VEGF-B in angiogenesis	32
1.5.3.b.2	The role of VEGF-B in the heart	33
1.5.3.b.3	The role of VEGF-B in neuroprotection.....	33
1.5.3.b.4	The role of VEGF-B in fatty acid transport.....	34
1.5.4	<i>Pathological neovascularization in the cornea</i>	34
1.5.5	<i>Treatments for corneal neovascularization</i>	36
1.5.5.a	Surgical therapy	36
1.5.5.a.1	Laser photocoagulation	36
1.5.5.a.2	Photodynamic therapy.....	37
1.5.5.a.3	Needle diathermy	38
1.5.5.b	Non-surgical therapy	38
1.5.5.b.1	Steroids and non-steroidal anti-inflammatory agents (NSAIDs).....	38
1.5.5.b.2	Cyclosporin A	39
1.5.5.b.3	Anti-VEGF agents.....	39
1.6	POROUS SILICON MATERIALS AS IMPLANTABLE SCAFFOLDS CARRYING STEM CELLS.....	42
1.6.1	<i>Nanostructured pSi implants</i>	42
1.6.1.a	Drug loading and delivery from pSi.....	44
1.6.1.b	Porous silicon as a scaffold for the culture of cells	45
1.7	POLY(E-CAPROLACTONE).....	46
1.7.1	<i>Porous silicon poly(ϵ-caprolactone) composite materials</i>	46
1.8	ANTIBODIES AND ANTIBODY FRAGMENTS	47
1.8.1	<i>Monoclonal antibodies</i>	49
1.8.1.a	Bevacizumab.....	49
1.8.2	<i>Engineered antibody fragments</i>	49
1.9	HYPOTHESIS AND AIMS	50

CHAPTER 2 MATERIALS AND METHODS.....	53
2.1 MATERIALS.....	53
2.1.1 Water.....	53
2.1.2 General chemicals.....	53
2.1.3 PCR primers.....	53
2.1.4 Enzymes.....	55
2.1.5 Recombinant proteins.....	56
2.1.6 Antibodies.....	57
2.1.7 Ophthalmic materials, reagents and eye drops.....	58
2.1.8 Porous silicon materials.....	58
2.1.8.a Porous silicon membranes and microparticles.....	58
2.1.8.b Porous silicon poly-(ϵ -caprolactone) composite materials.....	59
2.1.9 Animals.....	60
2.1.9.a Ethics approval.....	60
2.1.9.b Rats.....	60
2.2 MOLECULAR TECHNIQUES.....	61
2.2.1 DNA quantification.....	61
2.2.2 Agarose gel electrophoresis.....	61
2.2.3 Amplification of the V_H and V_L from the 2H10 hybridoma cDNA.....	61
2.2.4 Generation of the anti-VEGF-B scFv by SOE PCR.....	62
2.2.5 Amplification of the male specific sry gene.....	64
2.2.5.a Original sry PCR.....	64
2.2.5.b Novel sry PCR.....	65
2.2.6 Restriction endonuclease digestion with <i>Sfi</i> I.....	67
2.2.7 Ligation.....	67
2.2.8 Purification of anti-VEGF-B scFv by immobilised metal ion chromatography.....	69
2.2.9 Dialysis of purified scFv solution.....	69
2.2.10 Estimation of protein concentration.....	70
2.2.11 Visualization of purified protein by gel electrophoresis.....	70
2.2.12 Binding of anti-VEGF-B scFv to human VEGF-B and VEGF-A.....	70
2.2.13 Small and medium scale purification of plasmid DNA.....	71

2.2.14	<i>Sequencing of the anti-VEGF-B scFv in plasmid vectors</i>	71
2.3	BACTERIAL TECHNIQUES	72
2.3.1	<i>Preparation of electrocompetent cells</i>	72
2.3.2	<i>Electroporation of plasmid DNA</i>	73
2.3.3	<i>Colony blot for the detection of His tag</i>	73
2.3.4	<i>Bacterial culture</i>	74
2.3.5	<i>Small scale expression of recombinant scFv protein</i>	75
2.3.6	<i>Large scale production of anti-VEGF-B scFv</i>	76
2.4	CELLULAR TECHNIQUES	76
2.4.1	<i>Cell attachment and culture on pSi-PCL composite material</i>	76
2.4.2	<i>Enhanced attachment and growth of cells on composite material</i>	77
2.4.3	<i>Loading and release of biologics into pSi-PCL composite materials</i>	77
2.5	ANIMAL AND TISSUE TECHNIQUES	79
2.5.1	<i>Induction and assessment of corneal neovascularization in rats</i>	79
2.5.1.a	Induction of corneal neovascularization in rats by silver nitrate cautery	79
2.5.1.b	Topical scFv therapy	79
2.5.1.c	Subconjunctival injection of scFv	81
2.5.1.d	Haematoxylin perfusion to stain corneal blood vessels	81
2.5.1.e	Corneal flatmounting	84
2.5.1.f	Image analysis	84
2.5.2	<i>Harvest of rat oral mucosal epithelial cells and transfer to the rat eye</i>	86
2.5.2.a	Harvest and culture of oral mucosal epithelial cells from the rat	86
2.5.2.b	Antibody labelling of oral mucosal epithelial cells	88
2.5.2.c	Labelling rat OMEC with the cell tracker dye PKH26	89
2.5.2.d	Surgical implantation of porous silicon materials into the rat eye	90
2.5.2.e	Impression cytology using FTA paper	90
2.5.2.f	Induction of mild ocular surface disease by n-heptanol	91
2.5.2.g	Impression cytology of the rat eye to confirm OSD	91
2.5.2.h	Fixation, processing and embedding	92
2.5.2.i	Haematoxylin and eosin staining	92
2.6	STATISTICAL ANALYSES	93

CHAPTER 3 POROUS SILICON MATERIALS AS CARRIERS OF CELLS AND DRUGS

TO THE EYE	94
3.1 POROUS SILICON AS AN OCULAR IMPLANT.....	94
3.2 EXPLORATION OF POROUS SILICON MEMBRANES AS A STEM CELL NICHE	96
3.2.1 <i>Harvest and culture of oral mucosal epithelial cells from the rat</i>	96
3.2.2 <i>Oral mucosal epithelial cells grown on collagen IV coated pSi express corneal epithelial cell markers</i>	98
3.2.3 <i>Characterization of OMECs grown on pSi scaffolds coated with collagen IV and vitronectin</i>	100
3.2.4 <i>Stability and biocompatibility of pSi membranes in vivo</i>	105
3.2.5 <i>Detection of transplanted cells on the ocular surface</i>	108
3.2.6 <i>Novel sry PCR protocol for increased specificity and sensitivity</i>	109
3.2.6.a <i>Detection of transplanted male cells using the novel sry PCR</i>	113
3.2.7 <i>Induction of ocular surface disease prior to cell transplantation</i>	116
3.2.7.a <i>Implantation of pSi scaffolds carrying OMECs in h-heptanol debrided rat eyes</i>	118
3.2.8 <i>Fate of the transplanted oral mucosal epithelial cells</i>	118
3.3 POROUS SILICON POLYMER COMPOSITE MATERIALS	124
3.3.1 <i>Transfer of small molecule drugs to cells grown on pSi-PCL composite materials</i> ...	125
3.3.1.a <i>Effect of pSi particle size on transfer of drugs</i>	127
3.3.1.b <i>Effect of position of the cells on composite materials</i>	128
3.3.2 <i>Transfer of biologics to cells grown on pSi-PCL composite material</i>	132
3.3.2.a <i>Effect of FBS coating on cell growth on pSi-PCL composite materials</i>	132
3.3.2.b <i>Loading and release of biologic growth factors from composite materials post-fabrication</i>	135
3.3.3 <i>Biocompatibility of pSi-PCL composite material in the rat eye</i>	137
3.4 DISCUSSION.....	140
3.4.1 <i>Scaffolds to transfer stem cells to the eye for ocular surface regeneration</i>	141
3.4.2 <i>Source of stem cells</i>	144
3.4.3 <i>Characterization of OMECs on pSi scaffolds</i>	146
3.4.4 <i>Fate of OMECs after transplantation to the rat eye</i>	148
3.4.5 <i>Degradation of the pSi scaffold</i>	150

3.4.6	<i>Porous silicon polycaprolactone composite materials as ophthalmic implants</i>	151
3.4.6.a	Drug loading in the pSi-PCL composite materials	152
3.4.6.b	Biocompatibility of pSi-PCL composite material in the rat eye	154
3.5	CONCLUSIONS	155
CHAPTER 4 VEGF-B ANTAGONISM IN CORNEAL NEOVASCULARIZATION.....		156
4.1	GENERATION AND CHARACTERIZATION OF AN ANTI-VEGF-B scFv	157
4.1.1	<i>The 2H10 hybridoma</i>	157
4.1.2	<i>Amplification of the V_L and V_H and production of a scFv gene</i>	158
4.1.3	<i>Cloning of the anti-VEGF-B scFv in E.coli</i>	158
4.1.3.a	Restriction endonuclease digestion with SfiI	158
4.1.3.b	Ligation of scFv into the bacterial expression plasmid pHB400	161
4.1.3.c	Transfection of E.coli HB2151 with plasmid containing the anti-VEGF-B scFv	161
4.1.4	<i>Screening 2H10 scFv transfected clones</i>	164
4.1.4.a	Colony blot to detect recombinant protein in transfected HB2151 colonies	164
4.1.4.b	Detection of binding of scFv containing bacterial lysates to VEGF-B	166
4.1.4.c	Comparison of binding of anti-VEGF-B scFv clones to VEGF-B	166
4.1.4.d	Sequencing of anti-VEGF-B scFv clones	169
4.1.5	<i>Purification of anti-VEGF-B scFv</i>	171
4.1.6	<i>Binding of purified anti-VEGF-B scFv to VEGF-B</i>	171
4.2	CHARACTERIZATION OF ANTI-VEGF-B scFv PRODUCED IN MAMMALIAN CALLS	175
4.2.1	<i>Binding of anti-VEGF-B scFv to human VEGF-B and VEGF-A</i>	176
4.2.2	<i>Stability of the anti-VEGF-B scFv</i>	176
4.2.3	<i>Binding of the anti-VEGF-B scFv to human VEGF-B after formulation as an eye drop</i>	179
4.3	ANTI NEOVASCULAR ACTIVITY OF VEGF-B scFv IN A RAT MODEL OF CORNEAL NEOVASCULARIZATION	181
4.3.1	<i>Effect of topical anti-VEGF-B therapy on developing vessels</i>	181
4.3.2	<i>Effect of topical anti-VEGF-B scFv treatment on established vessels</i>	187
4.3.3	<i>Differences in the degree of neovascularization between males and females</i>	190
4.3.4	<i>Effect of anti-VEGF-B scFv delivered by subconjunctival injection on established vessels</i>	199

4.4	DISCUSSION.....	205
4.4.1	<i>VEGF-B as a therapeutic target for corneal neovascularization</i>	205
4.4.2	<i>Production of an anti-VEGF-B scFv</i>	206
4.4.3	<i>Characterization of the anti-VEGF-B scFv</i>	208
4.4.4	<i>Rat model of corneal neovascularization</i>	210
4.4.5	<i>Topical delivery of scFv for corneal neovascularization</i>	211
4.4.6	<i>Supplementation of topical therapy with subconjunctival anti-VEGF-B scFv</i>	213
4.4.7	<i>Difference in neovascular response in male and female rats</i>	214
4.5	CONCLUSION	216
CHAPTER 5 DISCUSSION		217
5.1	OVERVIEW OF STUDY FINDINGS	217
5.1.1	<i>Porous silicon materials as an artificial stem cell niche for the transfer of cells to the rat eye</i>	217
5.1.2	<i>Anti-VEGF-B therapy for corneal neovascularization</i>	218
5.2	GENERAL DISCUSSION	218
5.2.1	<i>The need for a specific limbal epithelial stem cell marker</i>	218
5.2.1.a	Cell surface markers for enrichment of stem cells	222
5.2.2	<i>Is a scaffold necessary for the transfer of cells to the ocular surface?</i>	223
5.2.3	<i>Recreating the limbal epithelial stem cell niche</i>	226
5.2.4	<i>Angiogenesis induced by treatments for ocular surface disease</i>	229
5.2.5	<i>VEGF-B, angiogenesis and the eye</i>	232
5.2.6	<i>Targeting VEGF-A and VEGF-B in corneal neovascularization</i>	234
5.2.7	<i>Is topical therapy for corneal neovascularization appropriate?</i>	236
5.2.8	<i>Gender differences in ocular pathology</i>	241
5.3	FINAL COMMENTS	243
APPENDIX A LIST OF GENERAL CHEMICALS.....		247
A.1	GENERAL CHEMICALS	247
APPENDIX B BUFFERS AND SOLUTIONS.....		251
B.1	2YT MEDIUM.....	251

B.2	2YT AGAR MEDIUM.....	251
B.3	6X GEL LOADING DYE	251
B.4	BUFFERED FORMALIN.....	252
B.5	BUFFERED GLYCEROL	252
B.6	CHROME ALUM SUBBING SOLUTION FOR SLIDES.....	252
B.7	CHLORAMPHENICOL FOR ANTIBIOTIC SELECTION.....	253
B.8	COMPLETE MEDIUM FOR OMEC CULTURE	253
B.9	ELISA BLOCKING BUFFER.....	253
B.10	ELISA DILUENT	254
B.11	ELISA WASH BUFFER.....	254
B.12	EOSIN STOCK SOLUTION	254
B.13	EYE DROP BASE SOLUTION	254
B.14	HAEMATOXYLIN STAIN	255
B.15	HAEMATOXYLIN PERFUSION BUFFER.....	255
B.16	IMAC ELUTION BUFFER	255
B.17	IMAC LOADING BUFFER	256
B.18	IMAC WASH BUFFER.....	256
B.19	LURIA BERTANI (LB) MEDIUM.....	256
B.20	PHOSPATE BUFFERED SALINE (PBS) 10X SOLUTION	257
B.21	PBS-AZIDE.....	257
B.22	PBS-TWEEN 20.....	257
B.23	SOC MEDIUM	257
B.24	TERRIFIC BROTH (TB)	258
B.25	TBE (5X STOCK).....	258
B.26	TBS pH 7.4	258
B.27	TNT BUFFER	258
B.28	TRYPsin-EDTA	259
APPENDIX C CHARACTERIZATION OF THE ANTI-VEGF-B SCFV AT CSL LTD.		260
C.1	BINDING OF THE PARENT 2H10 ANTIBODY TO HUMAN, MOUSE, AND RAT VEGF-B	260

C.2	ANALYSIS OF BINDING OF THE ANTI-VEGF-B scFv TO HUMAN VEGF-B BY SURFACE PLASMON RESONANCE.....	260
C.3	FUNCTIONAL CHARACTERIZATION OF THE ANTI-VEGF-B scFv	263
APPENDIX D ANIMAL MONITORING SHEETS		265
D.1	CORNEAL CAUTERY SCORING SHEET	265
D.2	CORNEAL NEOVASCULARIZATION MONITORING SHEET	268
D.3	RAT CONJUNCTIVAL SPACE IMPLANT SCORING SHEET	269
D.4	POST-pSi IMPLANTATION CLINICAL MONITORING SHEET	270
D.5	N-HEPTANOL CORNEAL DEBRIDEMENT PROCEDURE SHEET	271
D.6	POST-pSi IMPLANTATION CLINICAL MONITORING SHEET	272
BIBLIOGRAPHY.....		247

Declaration

I certify that this thesis does not incorporate without acknowledgement any material previously submitted for a degree or diploma in any university; and that to the best of my knowledge and belief it does not contain any material previously published or written by another person except where due reference is made in the text.

Yazad Irani

Abstract

Ocular surface disease and corneal neovascularization can lead to visual impairment. The principal aims of the work described in this thesis were to develop novel treatments for such conditions, and to assess their efficacy in rat models of disease.

Ocular surface disease results from loss of or damage to, corneal epithelial stem cells or their niche. Oral mucosal epithelial cells were harvested from male inbred Sprague-Dawley rats and cultured on porous silicon membrane scaffolds, coated with factors to replicate the stem cell niche. The cells were characterised, and found to express epithelial cell markers CK3 and CK19, as well as the putative stem cell markers p63 and ABCG2. Ocular surface disease was induced in female inbred Sprague-Dawley rats by n-heptanol debridement. Porous silicon scaffolds loaded with oral mucosal cells were implanted subconjunctivally. Cell samples were taken from the ocular surface and the presence of transplanted cells was detected by PCR for the male sry gene. Despite successful transfer of cells to the ocular surface, transplanted cells were not detected on the central cornea after 8 weeks, indicating daughter cells had not migrated over the ocular surface.

A novel composite of porous silicon and polycaprolactone was then developed as an improved dual purpose ophthalmic implant, to deliver drugs and cells to the eye. The composite biomaterial exhibited some characteristics, including flexibility and increased stability, which made it more suitable than porous silicon membrane for ocular implantation. The loading and subsequent release of a small molecule (fluorescein diacetate) and biologic growth factors (epithelial growth factor, insulin

and transferrin) in active form were demonstrated. Further, the composite supported attachment and growth of mammalian cells, and displayed acceptable biocompatibility when implanted in the eye of live rats. The material may be of use as an artificial stem cell niche for the transfer of epithelial stem cells to the cornea.

The normal cornea is avascular. Corneal neovascularization results from an imbalance in pro- and anti-angiogenic factors. Anti-vascular endothelial growth factor A (VEGF-A) therapy has shown promise in reducing progression of neovascularization in humans but has little effect on established vessels. The related molecule VEGF-B is a survival factor for endothelial cells. A recombinant antibody fragment reactive with human, rat and mouse VEGF-B was engineered from an established hybridoma. Corneal neovascularization was induced in Sprague-Dawley rats by silver nitrate cautery and the anti-VEGF-B antibody fragment or a control fragment was administered as eye drops or by subconjunctival injection. Treatment extended for 14 days either immediately, to determine the effect on growing vessels, or for 14 days after cautery to treat established vessels, at which time rats were killed, perfused with haematoxylin, and the corneal flatmounts imaged to quantify vascularization. Topical treatment neither prevented growth of vessels nor caused regression of established vessels. However, subconjunctival administration of the anti-VEGF-B antibody fragment significantly reduced the neovascular area of established vessels. Anti-VEGF-B biologics may thus hold promise for the regression of established corneal vessels.

Acknowledgements

First and foremost, I would like to thank my family for their love and support over the last four years. This work would not have been possible without the unconditional support of my dear wife Swati. To my parents I am thankful for instilling in me the desire to achieve and the courage to chase my dreams.

I am extremely fortunate to have such a supportive supervisor. Thank you Keryn, for your guidance and patience over the last four years. I would also like to take this opportunity to thank Sonja Klebe and Helen Brereton for their help with my experiments and in preparing this thesis.

I would also like to thank Dr. Steven McInnes and Prof. Nicolas Voelcker for providing the porous silicon membranes and Prof. Jeffery Coffey for fabricating the porous silicon polycaprolactone composite materials.

Finally I would like to thank all the members of the Department of Ophthalmology at Flinders University. Your friendship and camaraderie has made this journey an enjoyable one. In particular I would like to thank Madison Helm for all the help with animal husbandry.

Publications arising from this thesis

Steven J. P. McInnes, Chris T. Turner, Sameer A. Al-Bataineh, Marta J. I. Airaghi Leccardi, **Yazad Irani**, Keryn A. Williams, Allison J. Cowin and Nicolas H. Voelcker. 2015. Surface Q1 Q2 engineering of porous silicon to optimise therapeutic antibody loading and release. *Journal of Materials Chemistry B*. 2015;3(20):4123-33.

Williams, K. A., **Y. D. Irani**, and S. Klebe.. Novel therapeutic approaches for corneal disease. *Discovery Medicine*. 2013;15(84):291-9.

Appleby SL*, **Irani Y***, Mortimer LA, Brereton HM, Klebe S, Keane MC, *et al*. Co-expression of a scFv antibody fragment and a reporter protein using lentiviral shuttle plasmid containing a self-processing furin-2A sequence. *J Immunol Methods*. 2013;397(1-2):61-5.

McInnes SJ, **Irani Y**, Williams KA, Voelcker NH. Controlled drug delivery from composites of nanostructured porous silicon and poly (L-lactide). *Nanomedicine (Lond)*. 2012;7(7):995-1016.

* contributed equally to the publication

Conference abstracts

Yazad Irani[§], Pierre Scotney, Andrew Nash, Sonja Klebe, and Keryn A. Williams. 2015. Anti-VEGF-B therapy in a rat model of corneal neovascularization. ARVO Annual Meeting, Denver, Colorado, 3rd-7th May.

Yazad Irani[§], Pierre Scotney, Andrew Nash, Sonja Klebe, and Keryn A. Williams. 2015. Anti-VEGF-B therapy in a rat model of corneal neovascularization. 32nd Australia and New Zealand Cornea Society Meeting, Perth, 4th-7th March.

Yazad Irani, Yuan Tian, Mengjia Wang, Sonja Klebe, Nicolas H. Voelcker, Jeffery L. Coffey and Keryn A. Williams. 2014. A novel pressed porous silicon-polycaprolactone composite as a dual purpose ophthalmic implant. International Society for Eye Research XXI Biennial meeting, San Francisco, 20th-24th July.

Yazad Irani[§], Pierre Scotney, Andrew Nash, Sonja Klebe, and Keryn A. Williams. 2014. Topically-delivered anti-VEGF-B antibody fragment in a rat model of corneal neovascularization. 31st Australia and New Zealand Cornea Society Meeting, Brisbane, 6th-7th March.

Yazad Irani[§], Steven JP McInnes, Nicolas H Voelcker, Helen M Brereton, Keryn A Williams. 2013. Porous silicon scaffolds and new biologics for the treatment of corneal diseases. 30th Australia and New Zealand Cornea Society Meeting, Adelaide, 7th-8th March.

[§] Oral presentation

Yazad Irani, Steven JP McInnes, Nicolas H Voelcker, Helen M Brereton, Keryn A Williams. 2012. Culture and characterization of rat oral mucosal epithelial cells on nanostructured porous silicon. Australian Health and Medical Research Congress, Adelaide, 25th-28th November.

Yazad Irani*, Steven JP McInnes, Nicolas H Voelcker, Helen M Brereton, Keryn A Williams. 2012. Culture and characterization of rat oral mucosal epithelial cells on nanostructured porous silicon. 3rd International Nanomedicine Conference, Sydney, 2nd-4th July.

**Presented with the Australian Centre for NanoMedicine PhD Student Researcher Award for excellence in Nanomedicine research.*

Yazad Irani, Sarah Brice, Lauren Mortimer, Helen Brereton, Sonja Klebe, Miriam Keane, Peter Cowan, Doug Coster and Keryn Williams. 2011. Quantification of transgene expression targeted to different cell compartments from lentiviral plasmids containing a furin-2A sequence. Australasian Gene Therapy Society 7th Meeting, Melbourne, 4th-6th May.

Abbreviations and symbols used in this thesis

-	Minus
%	Percent
~	Approximately
+	Plus
<	Less than
>	Greater than
±	Plus minus
°C	Degrees centigrade
µg	Microgram
µl	Microliter
µm	Micrometre
3D	Three dimensional
ATCB5	ATP-binding cassette sub-family B member 5
ATCG2	ATP-binding cassette sub-family G member 2
AR	Analytical reagent
arp	Attachment region binding protein
ARMD	Age related macular degeneration
ARVO	Association for Research in Vision and Ophthalmology
BCA	Bicinchoninic acid
bFGF	Basic fibroblast growth factor
bp	Base pairs
BrdU	Thymidine analogue 5-bromo-2'-deoxy uridine
BSA	Bovine serum albumin

BSS	Balanced salt solution
CD	Cluster of differentiation
cDNA	Complementary DNA
CDR	Complementarity determining regions
CK	Cytokeratin
cm ³	Cubic centimetres
CNV	Choroidal neovascularization
CO ₂	Carbon dioxide
ddH ₂ O	Double distilled water
DEPC	Diethyl pyrocarbonate
Dept.	Department
DMSO	Dimethyl sulfoxide
DNA	Deoxyribonucleic acid
dNTP	Dinucleotide triphosphate
DR	Diabetic retinopathy
DTT	Dithiothreitol
<i>E. coli</i>	Escherichia coli
ECL	Enhanced chemiluminescence (Amersham Biosciences)
EDTA	Ethylene diamine tetra acetic acid
EGF	Epidermal growth factor
ELISA	Enzyme linked immunosorbent assay
Fab	Fragment antigen binding
FATP	Fatty acid transporter protein
FBS	Foetal bovine serum
Fc	Fragment crystallisable

FDA	Fluorescein diacetate
FGF-2	Fibroblast growth factor-2
FTA	Flinders technology associates – paper for cell sampling
Fv	Fragment variable
G	Gauge
g	Gram
g	Unit of gravity
gDNA	Genomic DNA
Gly	Glycine
h	Hour
H ₂ SO ₄	Sulphuric acid
HIF-1	Hypoxia inducible factor 1
His	Histidine
HRP	Horseradish peroxidase
Ig	Immunoglobulin
IgA	Immunoglobulin A
IgD	Immunoglobulin D
IgE	Immunoglobulin E
IgG	Immunoglobulin G
IgM	Immunoglobulin M
IMAC	Immobilised metal affinity chromatography
IP	Intraperitoneal
IPTG	Isopropyl β-D-thiogalactopyranoside
ITS	Insulin transferrin selenium supplement
K _d	Dissociation constant

kDa	Kilo Daltons
kV	Kilovolt
l	Litre
LCSD	Limbal stem cell dysfunction
LESC	Limbal epithelial stem cell
M	Molar
mAb	Monoclonal antibody
mAb	Monoclonal antibody
MCCF	Mean corrected cell fluorescence
mg	Milligram
MgCl ₂	Magnesium chloride
min	Minute
ml	Millilitre
mm	Millimetre
mM	Millimolar
ms	Millisecond
MSC	Mesenchymal stem cell
NaCl	Sodium chloride
ng	Nanogram
nm	Nanometre
NP	Neuropilin
NSAID	Non-steroidal anti-inflammatory agents
OM	Oral mucosa
OMEC	Oral mucosal epithelial cells
OSD	Ocular surface disease

p63	Transformation-related protein 63
PAS	Periodic acid Schiff
PBS	Phosphate buffered saline
PBS-tween	Phosphate buffered saline tween
PCL	Polycaprolactone
PCR	Polymerase chain reaction
PDT	Photodynamic therapy
PECAM-1	Platelet endothelial cell adhesion molecule
pH	Potential of hydrogen
PhD	Doctor of Philosophy
PI	Protease inhibitors (complete EDTA-free protease inhibitor cocktail)
PIGF	Placental growth factor
PSG	Penicillin streptomycin glutamine
pSi	Porous silicon
mRNA	Messenger ribonucleic acid
RPE	Retinal pigment epithelium
rpm	Revolutions per minute
s	Second
SA-HRP	Streptavidin horseradish peroxidase
scFv	Single chain antibody fragment
Ser	Serine
Sflt-1	Soluble fms-like tyrosine kinase-1
SOE-PCR	Splice by overlap extension polymerase chain reaction
SP	Side population
<i>sry</i>	Sex-determining region Y

TAC	Transient amplifying cell
TBE	Tris borate EDTA
TNT	Tris NaCl tween
TNTC	Too numerous to count
TSP-1	Thrombospondin-1
U	Units
UK	United Kingdom
USA	United States of America
V	Volts
v/v	Volume per volume
VEGF	Vascular endothelial growth factor
VEGF-A	Vascular endothelial growth factor-A
VEGF-B	Vascular endothelial growth factor-B
VEGFR	Vascular endothelial growth factor receptor
VEGFR	Vascular endothelial growth factor receptor
VH	Variable heavy chain
VL	Variable light chain
w/v	Weight per volume
WHO	World Health Organization
x	Times
YT	Yeast tryptone
α	Anti
β -NGF	Beta-nerve growth factor
λ	Lambda
Ω	Ohm

CHAPTER 1 INTRODUCTION

1.1 Overview

The focus of the work described in this thesis was to develop novel therapies for two common ocular conditions: corneal neovascularization, and ocular surface disease. In the introduction to the thesis, I will first discuss the normal anatomy of the ocular surface, followed by a summary of the mechanisms involved in regeneration of the corneal epithelium and the maintenance of corneal avascularity. The breakdown of normal conditions and the pathophysiology of disease will then be described, followed by current treatment strategies and the need for novel therapies. The potential use of porous silicon materials for the treatment of ocular surface disease, and anti-vascular endothelial growth factor B (VEGF-B) therapy for the treatment of corneal neovascularization, respectively, will then be discussed. The chapter will conclude with the aims of the project.

1.2 The structure of the cornea and the ocular surface

The ocular surface is a specialised structure that extends from the eyelid margins superiorly and inferiorly, and includes the conjunctival, limbal and corneal epithelia (Figure 1-1). It is exposed to the external environment and is subject to trauma, infection and drying. The ocular surface protects the eye from mechanical, toxic and infectious insults, and is kept hydrated by the tear film¹.

1.2.1 The cornea and sclera

The outermost fibrous layers of the eye consist of the cornea and sclera (Figure 1-1). Each is composed mainly of collagen, however the placement of collagen fibres is

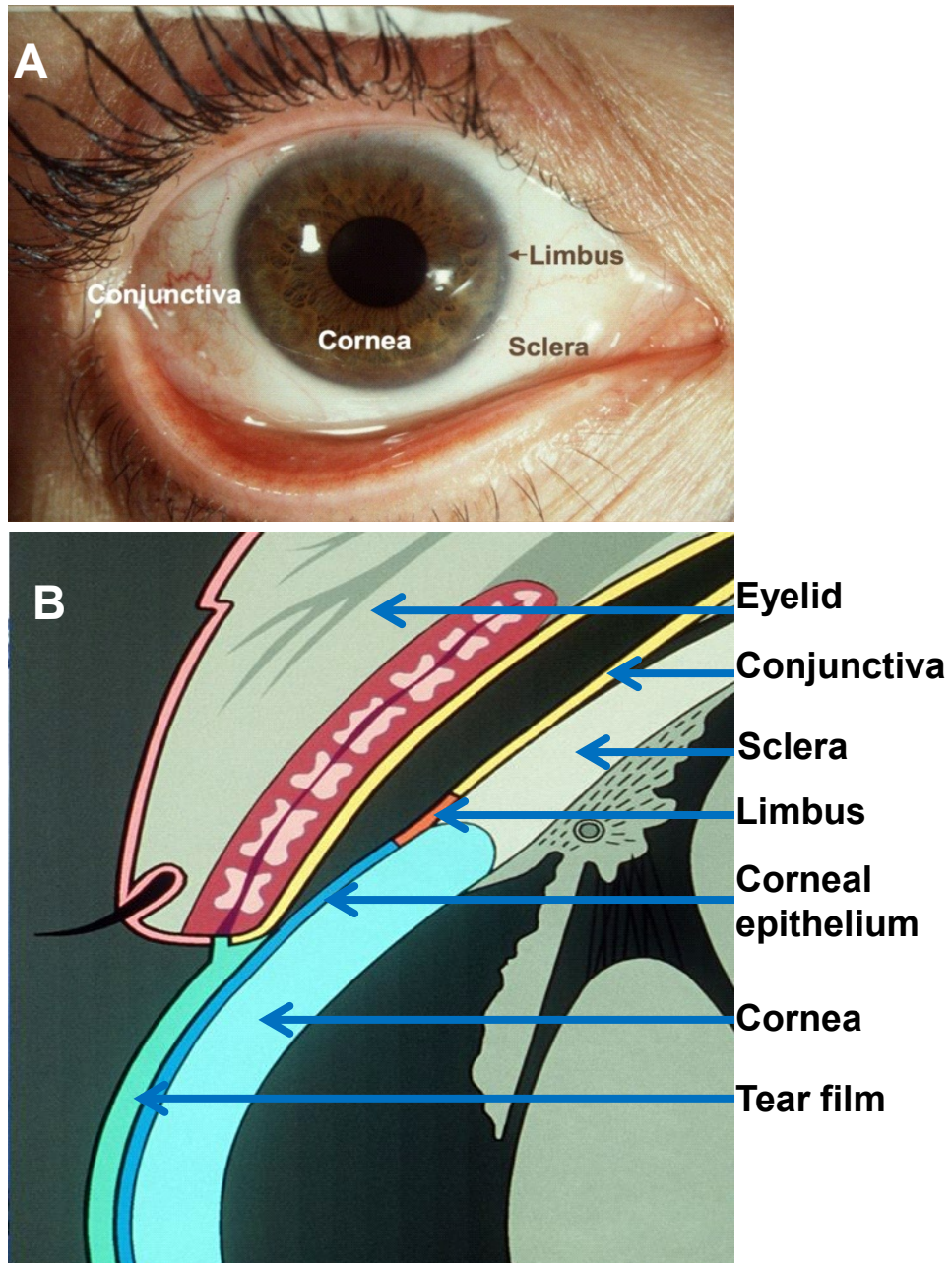


Figure 1-1 Structure of the anterior segment of the eye

(A) Image of the front of the human eye showing the positions of the conjunctiva, cornea, limbus and sclera. (B) Diagrammatic representation of a transverse section through the anterior segment of the eye. Diagram courtesy A/Prof. RAD Mills, Flinders University.

highly ordered in the cornea, making it transparent². The cornea and sclera provide mechanical strength to the eye, maintaining it in a regular near-spherical shape². The cornea is present at the anterior surface of the eye and is contiguous with the sclera, which is covered by the conjunctival epithelium anteriorly. The cornea is responsible for approximately 70% of the refractive power of the eye² and must remain transparent and avascular to maintain optimal light transmission³.

The human cornea comprises five distinct layers (Figure 1-2 A):

The corneal epithelium consists of five to six layers of stratified squamous cells, with a uniform thickness of around $50\ \mu\text{m}^4$ (Figure 1-2 B). The cells at the anterior surface of the epithelium are flattened, with a large surface area⁵. The middle layer consists of polyhedral cells that cap the basal epithelial cells. The basal epithelial cells are columnar, with flat bases and rounded heads. They are arranged in a highly ordered manner on the basal lamina, and are continuous with the limbal epithelium.

Bowman's layer is a modified region of the anterior stroma immediately posterior to the basement membrane of the corneal epithelium. It is approximately 8-14 μm thick and is devoid of cells. The corneal epithelial cells are thought to play a role in laying down Bowman's layer⁶.

The stroma makes up the bulk of the thickness of the cornea⁷. It consists of regularly arranged bundles of collagen fibres. Stromal keratocytes are responsible for the secretion of collagen and extracellular matrix components³.

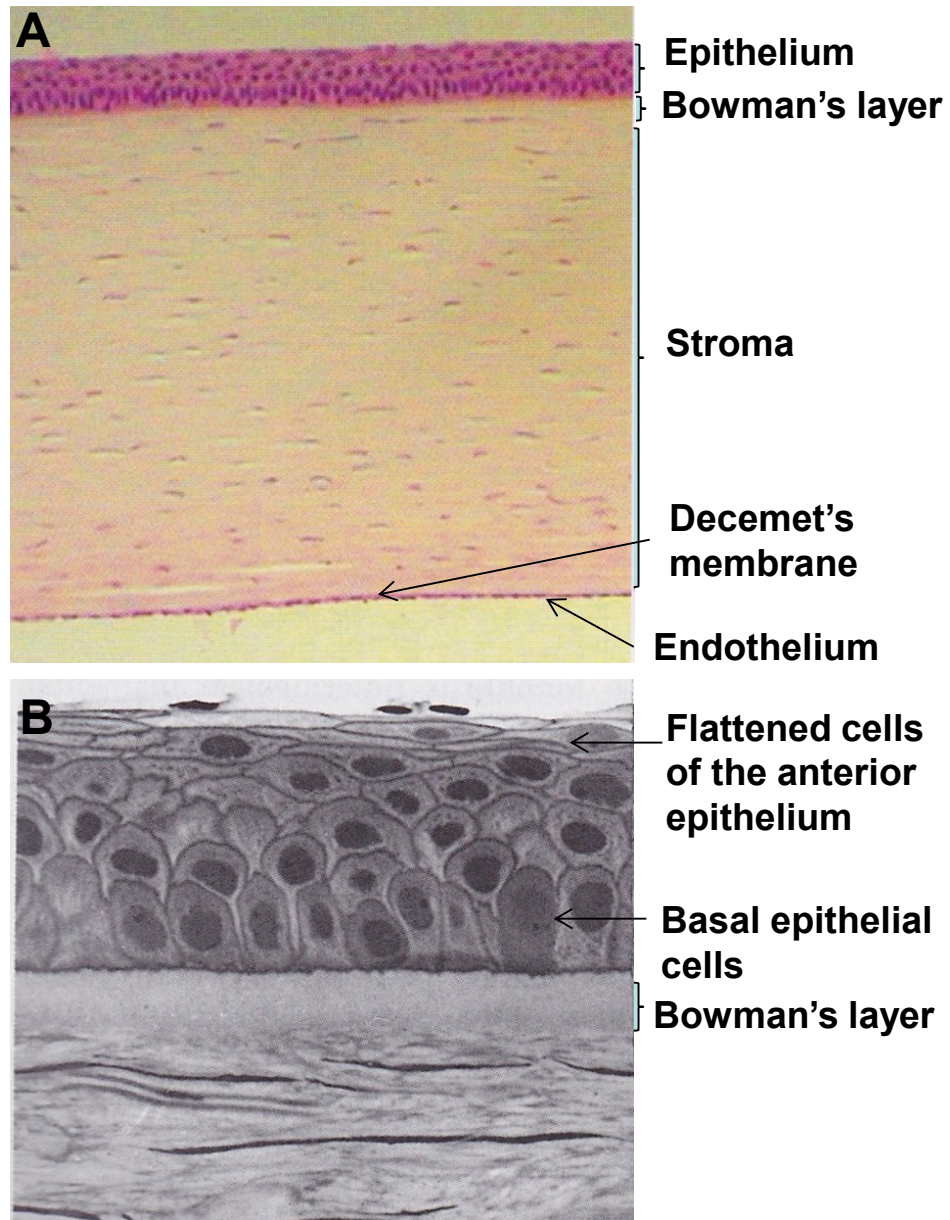


Figure 1-2 Layers of the cornea

(A) Haematoxylin and eosin stained section of the human cornea, showing the five anatomical layers (B) Typical architecture of corneal epithelial cells. The basal cells are columnar while the cells on the anterior surface are flattened and have pyknotic nuclei. Figure A adapted from Remington and Remington, 2012³ and Figure B from Bron *et al* 1997².

Decemet's membrane is the basement membrane of the endothelium. It is thin in childhood and thickens with age⁸.

The corneal endothelium consists of a single layer of amitotic cells, which pump water from the stroma into the anterior chamber, thus maintaining the stroma in a relatively dehydrated state⁹. This is essential for corneal transparency.

1.2.2 The conjunctiva

The conjunctiva is the mucous membrane that covers the posterior surface of the eyelids and the anterior surface of the sclera. It is translucent and consists of stratified squamous epithelium, is vascularised and is continuous with the limbal epithelium. The conjunctival epithelium is characterised by the presence of mucin-producing goblet cells¹⁰ (Figure 1-3). The conjunctiva plays an important role in defence against pathogens¹¹. Langerhans cells, which are antigen presenting cells, are present in the conjunctiva¹², the limbus and at a lower density in the cornea¹³.

1.2.3 The limbus

The limbus is the transitional zone between the cornea and the sclera². It functions as a barrier preventing the conjunctival epithelium from growing across the corneal surface and harbours a population of stem cells (at least in humans) responsible for the maintenance of the corneal epithelium¹⁴⁻¹⁹. The limbus contains radially-arranged ridge-like structures known as the palisades of Vogt²⁰ (Figure 1-4). The corneal epithelial stem cells are thought to reside in structures called limbal crypts, which extend from the interpalisade rete ridge²¹. The palisades offer a degree

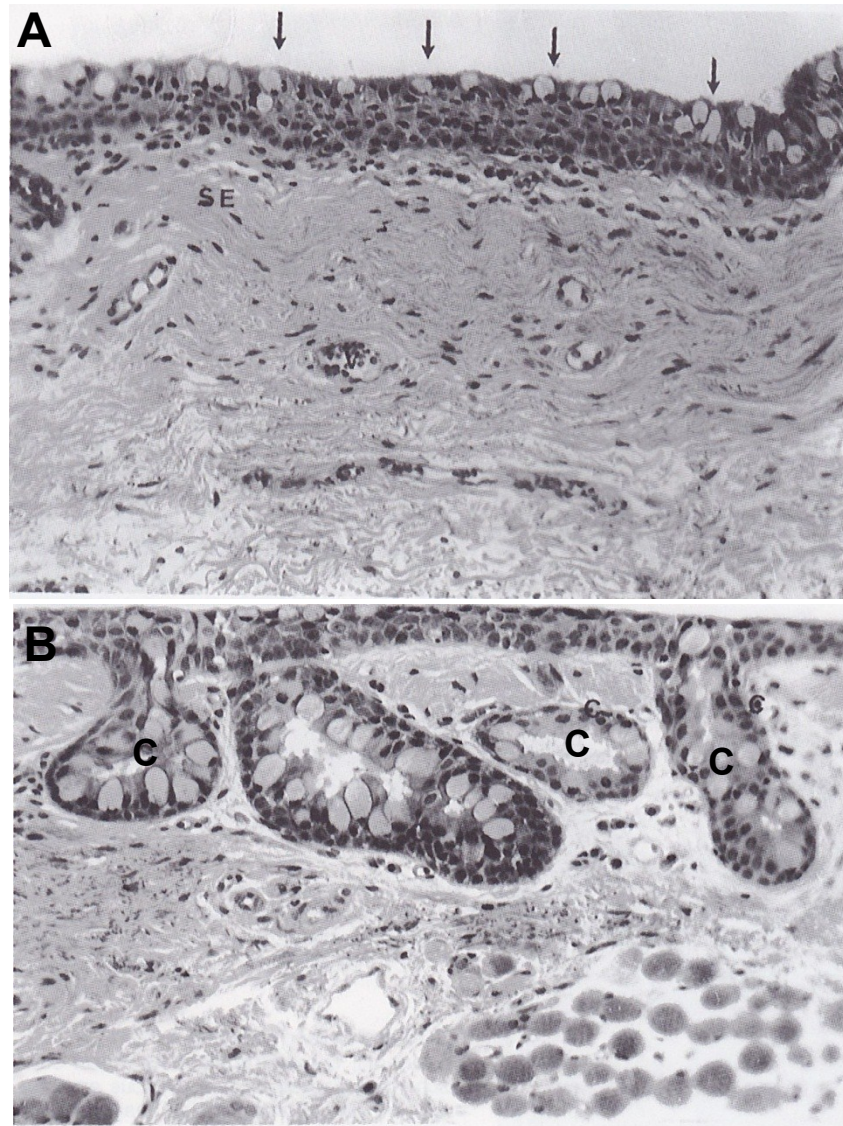


Figure 1-3 Histology of the conjunctiva

The conjunctiva is the mucous membrane that covers the anterior surface of the sclera and the posterior surface of the eyelids. **(A)** The conjunctiva is characterised by the presence of mucin-secreting goblet cells (arrows). **(B)** Higher magnification showing goblet cells (c) in the conjunctiva. Images from Bron *et al* 1997².

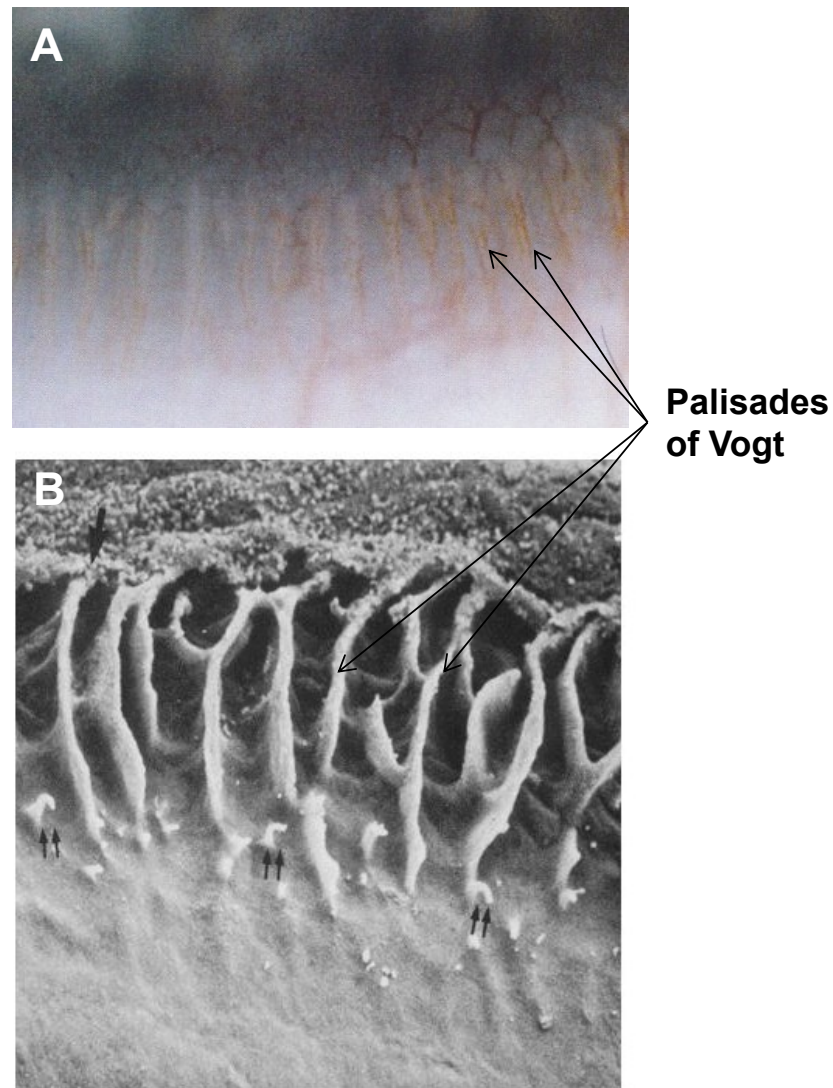


Figure 1-4 The limbus

The limbus is the transitional zone between the corneal and conjunctival epithelium. It contains a population of stem cells which are responsible for maintenance of the corneal epithelium. Anatomically the limbus is characterised by the palisades of Vogt. **(A)** Photograph of the limbus in a pigmented individual showing the rete ridges of the palisades of Vogt. **(B)** Electron micrograph of the palisades of Vogt. The stem cells are thought to reside in the interpalisade clefts (arrows) between the rete ridges. Image A from Bron *et al* 1997² and image B from Gipson *et al* 1989¹⁴.

of protection from ultraviolet light induced damage²², and a rich supply of blood vessels²³ to the corneal stem cells.

1.3 Corneal epithelial regeneration

The corneal epithelium is in a state of constant flux. The cells at the surface are sloughed off and replaced by cells from the basal layers. In order for renewal, progenitor cells need to divide, migrate and undergo differentiation³, so that the rate of cell renewal is equal to the rate of cell loss²⁴.

1.3.1 Renewal of the corneal epithelium

Human corneal epithelium was thought to be regenerated by the division of basal cells, with one daughter cell remaining in the basal layers, while the other migrates apically, differentiates, and is ultimately sloughed off²⁵. Experiments using tritiated thymidine estimated epithelial turnover over a period of seven days²⁵. The presence of stem cells at the limbus has been confirmed in rabbits²⁶ and in mice¹⁷. However, Majo *et al* have demonstrated that in the mouse, oligopotent stem cells with the ability to differentiate into corneal or conjunctival epithelial cells are present throughout the cornea²⁷. It is now widely accepted that in humans, the corneal epithelial stem cells reside at the limbus^{16, 21, 22, 28-36}. Thoft and Friend hypothesised that the proliferation of basal cells X, and the centripetal migration of cells Y, is equal to the epithelial cell loss Z, the so-called XYZ hypothesis³⁷ (Figure 1-5).

Stem cells proliferate at the limbus, dividing asymmetrically, to give rise to a daughter stem cell and a transient amplifying cell. A population of transient

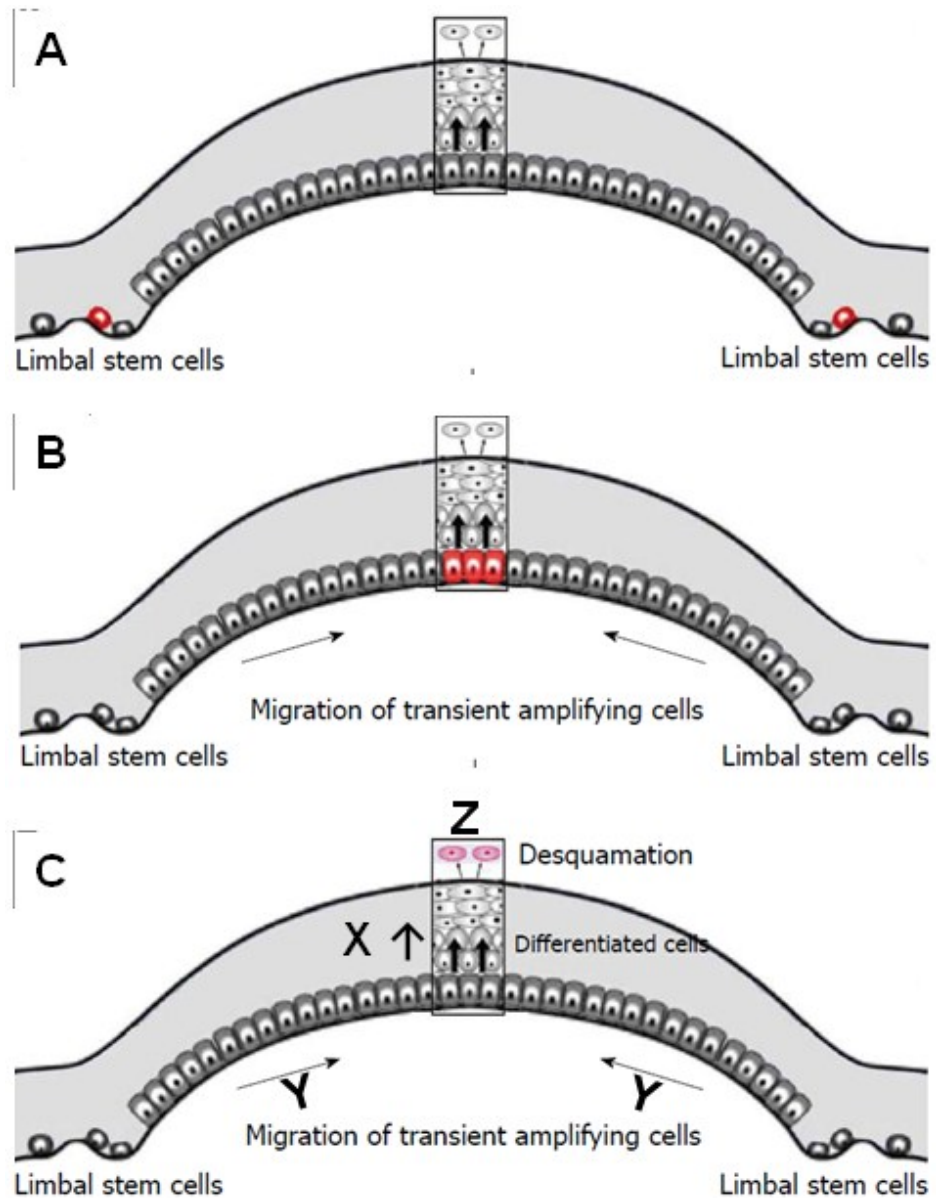


Figure 1-5 Corneal epithelial regeneration

The XYZ hypothesis of corneal epithelial cell regeneration states that the sum of proliferation and anterior migration, X, and centripetal migration, Y, is equal to the desquamation of superficial cells, Z. (A) Stem cells at the limbus undergo asymmetric division, giving rise to stem cells and transient amplifying cells (TACs). (B) TACs migrate centripetally, while undergoing a limited number of divisions. (C) The basal cells then migrate anteriorly, and are eventually sloughed off. Image modified from Yoon *et al* 2014³⁶.

amplifying cells has been identified at the basal junction of the limbus and the cornea^{38, 39}. The transient amplifying cells then proliferate and migrate centripetally (Y component). The centripetal migration of cells from the limbus to the central cornea has been demonstrated in mice by marking cells with Pelican India ink⁴⁰. The cells were measured to migrate at a rate of 17 microns per day and reached the central cornea in seven days⁴⁰. More recently, keratin14 positive progenitor cells have been shown to migrate centripetally in the mouse cornea at a rate of 10.8 microns per day⁴¹. Centripetal migration of cells has also been observed in the human cornea *in vivo* by confocal microscopy⁴². The migration of basal cells anteriorly (X component) has been demonstrated by labelling cells with tritiated thymidine in the mouse, rat, guinea pig and the dog⁴³. In humans, it is thought that the corneal epithelium is completely replaced over the course of 9 to 12 months⁴⁴.

1.3.2 Corneal epithelial stem cells

Corneal epithelial stem cells are characterised by a primitive phenotype, high nuclear to cytoplasmic ratio^{45, 46}, slow cell cycle^{46, 47}, high proliferative potential⁴⁸⁻⁵⁰ and the ability for self-renewal³⁰.

There are currently no unique and unambiguous phenotypic markers known for the identification of corneal epithelial stem cells. The presence of a group of putative stem cell markers in conjunction with the absence of differentiation markers is used to identify corneal epithelial stem cells. Some of these markers are described overleaf.

1.3.2.a *ABCG2*

The ATP binding cassette transporter protein (ABCG2) is a member of ATP binding cassette superfamily of drug transporters. Functionally, ABCG-2 is thought to protect stem cells from oxidative stress⁵¹. Several studies have reported expression of ABCG2 in stem cells of different tissues⁵²⁻⁵⁶. In the human limbus, 0.3-0.5% of cells display the “side population” (SP) phenotype, characterised by the efflux of Hoechst dye, and associated with expression of ABCG2, while no SP phenotype is observed in central corneal epithelium^{57, 58}. ABCG-2 expression has been detected in 2.5-3% of limbal cells by flow cytometry⁵⁹. Thus, ABCG-2 expressing cells outnumber “side population” cells, indicating that ABCG-2 not only marks the stem cells but likely a population of transient amplifying cells as well. Hence ABCG-2 alone cannot be used as a marker of corneal epithelial stem cells.

1.3.2.b *p63*

p63 is a transcription factor involved in morphogenesis. p63 knockout mice lack stratified epithelium^{60, 61}. Germline mutations in the p63 gene, in humans, cause the epithelial disorder ectrodactyly–ectodermal dysplasia–cleft syndrome⁶². These data indicate a possible role in maintenance of epithelial stem cell populations. p63 is thus a putative corneal epithelial stem cell marker. p63 has 6 isoforms⁶³ and in the uninjured eye, the $\Delta Np63\alpha$ is present in the limbus but not in the cornea⁶⁴. The $\Delta Np63\beta$ and the $\Delta Np63\gamma$ isoforms are seen in response to wounding, and are associated with limbal cell migration, corneal regeneration and differentiation⁶⁴. The $\Delta Np63\alpha$ isoform might potentially be a marker of corneal epithelial stem cells.

1.3.2.c *Cytokeratins*

Cytokeratins (CK) are cytoskeletal proteins that form intermediate filaments in epithelial cells. They show characteristic expression during development and differentiation, and are generally expressed in pairs. Because CK3/CK12 is expressed in corneal epithelium^{65, 66} but not in the basal layers of the limbus^{67, 68}, they are regarded as markers of corneal epithelial differentiation. CK14 has been used to identify epidermal stem cells in skin⁶⁹. CK5/CK14 has been identified in the basal cells of the limbus and the cornea^{70, 71}. Recently CK14 positive cells at the limbus have been shown to migrate centripetally *in vivo*⁴¹. CK19 is an epidermal stem cell marker in hair follicles⁷² and has been shown to localise to basal cells of human and murine limbal epithelium^{38, 66, 73}.

1.3.3 The limbal stem cell niche

A stem cell niche is a defined area that maintains stem cells in an undifferentiated state^{74, 75}. The limbus is highly vascularised, providing a rich supply of nutrients for stem cells^{17, 76} (Figure 1-6). It is also pigmented, which is thought to protect the stem cells from ultraviolet radiation^{14, 17}. The molecular composition of the limbal basement membrane is significantly different from that of the central basement membrane. Expression of ABCG2, collagen IV α 1 chain, lamina α 2, b1, b2, g1, g3 chains, again, BM40, tenascin-c, vitronectin, chondroitin sulphate and versican has been demonstrated at the limbus but not in the central cornea^{36, 67, 77-81}.

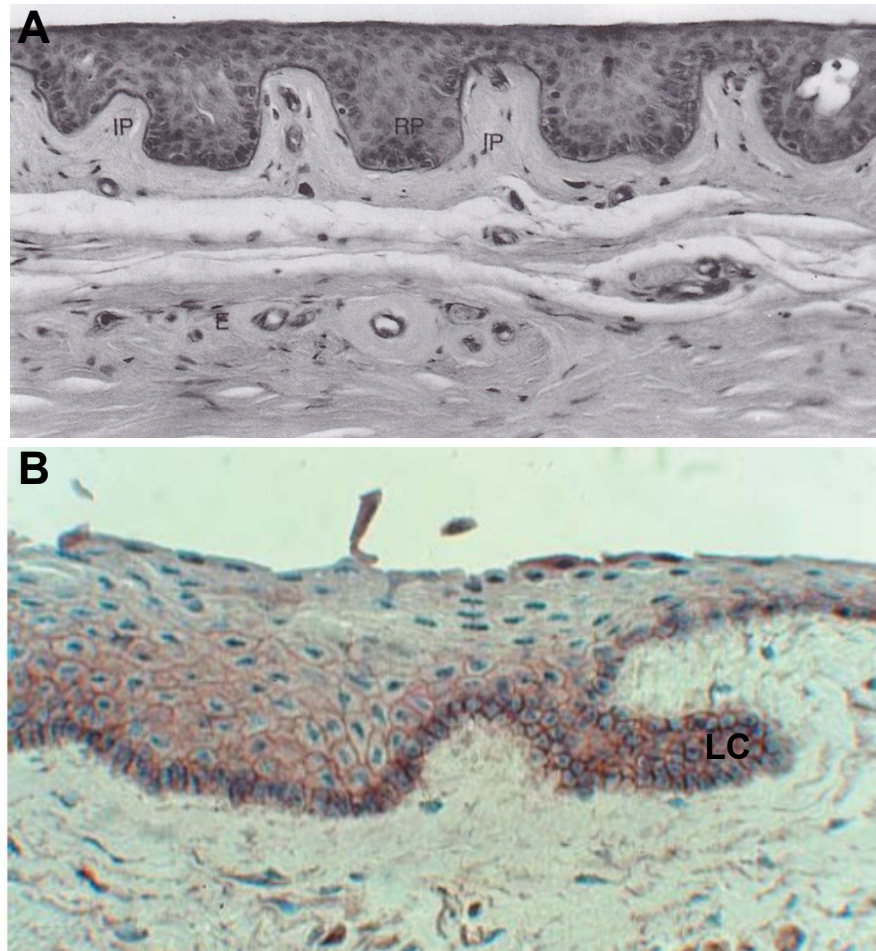


Figure 1-6 The limbal stem cell niche

The limbus is the niche for the corneal epithelial stem cells. **(A)** Transverse section of the anterior limbus. The rete pegs (RP) of the palisades of Vogt are separated by the interpalisade region (IP), and house a population of stem cells. A large number of blood vessels are located in close proximity to the limbus. **(B)** Immunohistochemistry for ABCG2, which is a cell membrane transport protein, with high expression in a number of stem cells. The cells in the limbal crypts (LC) show high expression of ABCG2. Image A from Bron *et al* 1997² and image B from Dua *et al* 2005²¹.

1.4 Limbal stem cell dysfunction

The loss or dysfunction of the corneal epithelial stem cells, or disruption of the limbal niche, can lead to limbal stem cell deficiency (LCS D). The causes of LCS D are manifold, and include aniridia⁸², autoimmune polyendocrinopathy candidiasis ectodermal dystrophy⁸³, and some epithelial or stromal corneal dystrophies⁸⁴. LCS D can also be acquired as a result of chemical and thermal burns⁴⁴, multiple surgeries involving the limbus⁸⁵, contact lens wear⁸⁶, drug toxicity⁸⁷, cicatricial pemphigoid⁸⁵, Stevens-Johnson syndrome⁸⁵, ocular surface squamous neoplasia⁸⁸, chronic inflammation⁸⁹, and pterygium⁹⁰. Some cases are idiopathic⁸⁵. LCS D can lead to ocular surface disease (OSD), which is characterised by conjunctivization of the ocular surface, corneal vascularization, pain, and oedema (**Error! Reference source not found.**). If left unchecked, LCS D can lead to blindness^{85, 91}. OSD can refer to a number of conditions with disparate causes, however for the purpose of this thesis, OSD refers to the disease caused by the loss of, or damage to, LESC s.

1.4.1 Treatments for ocular surface disease

1.4.1.a *Limbal grafts*

Limbal autotransplantation can be carried out for the treatment of unilateral disease⁹². Kenyon *et al* performed limbal autografts in 26 cases of chemical burns, with follow-up ranging from 2-45 months⁹². Of the 21 cases with 6 or more months follow-up, 17 cases had improved visual acuity, and 20 cases demonstrated a stable corneal surface without persistent epithelial defect⁹². The procedure involves transplantation of limbal tissue from the unaffected eye, however there is a risk of inducing disease in the donor eye⁸⁶. Bilateral disease necessitates the use of tissue

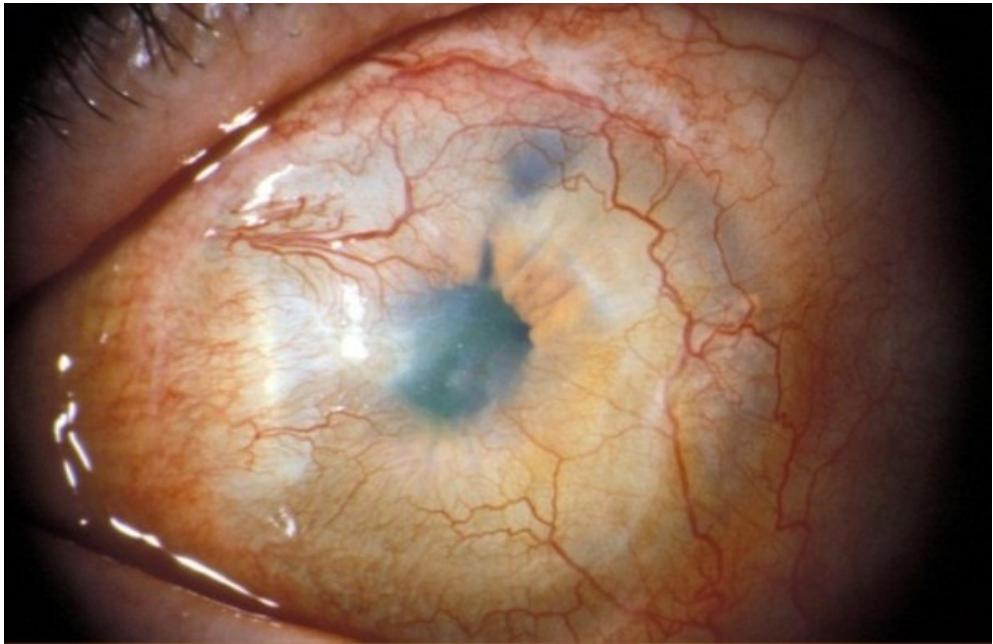


Figure 1-7 Ocular surface disease

Photograph of a human eye with ocular surface disease. Conjunctivization of the ocular surface and neovascularization is apparent. Provided by the ophthalmic photographer, FMC Eye Clinic.

from cadaveric donors^{93, 94}. Limbal transplantation has shown promise in terms of improved vision. However, limbal allografts tend to undergo immunological rejection^{95, 96}, require immunosuppression^{97, 98} and have a poorer survival rate when compared to corneal grafts⁹⁹ (Figure 1-8).

1.4.1.b *Ex vivo cultured limbal epithelial stem cells*

A biopsy of limbal tissue from an unaffected eye can be cultured to form an epithelial cell sheet which is then transferred on to the corneal surface of the affected eye on a scaffold. This method reduces the risk of LESC deficit in the healthy eye by reducing the amount of limbal tissue needing to be removed, and provides an autologous therapy. In case of bilateral disease, tissue from a related donor or cadaveric tissue has been used. Schwab *et al* used tissue from living-related donors in five patients with total LSCD. An improvement in visual acuity was observed in all patients, with a minimum follow-up time of six months^{100, 101}. The Kinoshita group evaluated the use of tissue from cadaveric donors for the treatment of OSD in two related studies^{109, 110}. Corneal epithelial cells cultured on denuded amniotic membrane were transplanted in 16 eyes in 13 patients with total LCSD. An improvement in visual acuity was observed in 13 of 16 treated eyes, with a mean follow-up of 11 months^{102, 103}. A separate study by the same group evaluated the use of autologous serum for the culture of donor epithelium, with all 7 eyes receiving transplanted cells demonstrating improved visual acuity¹⁰⁴. However, it must be noted that immunosuppression was required for the maintenance of allogeneic tissue, with episodes of rejection reported^{102, 105}. In light of these findings, alternative autologous sources of stem cells for ocular surface reconstruction have been explored, and are discussed in the following section.

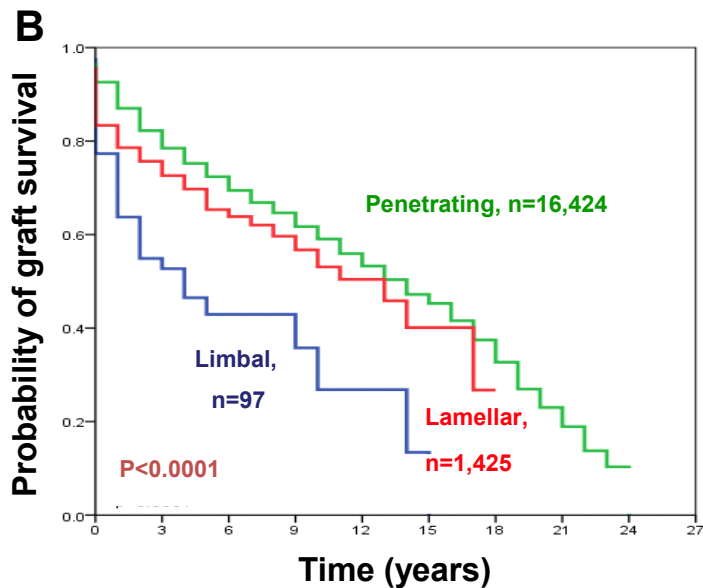
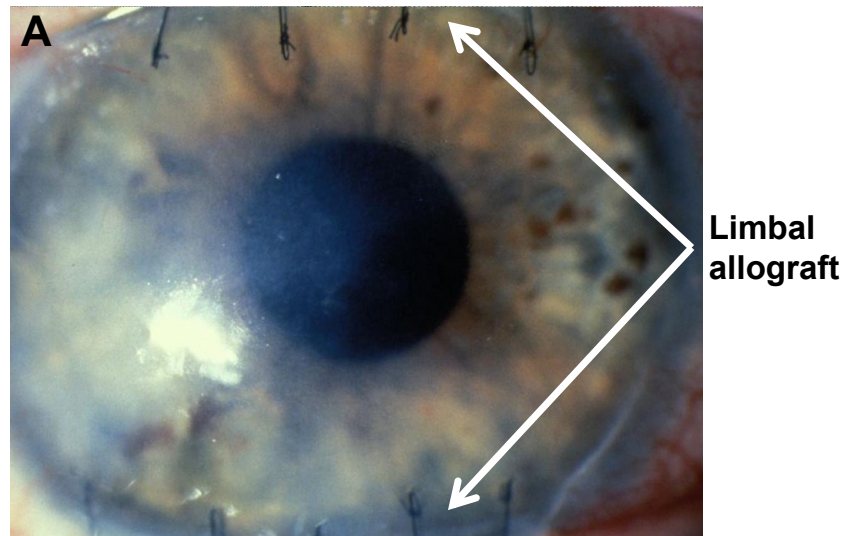


Figure 1-8 Limbal grafts

(A) Image of a failing human limbal allograft. Arrows point to the grafts, opacity indicates that the graft is failing. (B) A Kaplan-Meier plot comparing the probability of survival of limbal, lamellar and penetrating corneal grafts. Limbal grafts fail significantly faster than either partial or full thickness corneal grafts, data from the Australian Corneal Graft Registry report 2011⁹⁹. Image A provided by Prof. Keryn Williams, Flinders University.

1.4.1.c *Oral mucosa as a source of stem cells*

The use of autologous cells for transplantation avoids use of immunosuppressive agents. Oral mucosa (OM) is an attractive source of epithelial cells for corneal surface regeneration as like corneal epithelium, it is non-keratinised¹⁰⁶, is a source of stem cells^{107, 108}, and can be relatively easily harvested¹⁰⁹. Initial experiments in the rabbit demonstrated that autologous oral mucosal epithelium could restore the ocular surface in experimentally induced LCSD¹¹⁰⁻¹¹². Oral mucosal epithelial cells (OMECS) obtained from biopsies and cultured on denuded amniotic membrane in the presence of inactivated 3T3 fibroblasts have been transplanted to treat human ocular surface disease¹¹³. Six eyes of four patients with LCSD associated with Stevens-Johnson syndrome or chemical burns were treated with autologous oral mucosal epithelial cells. The corneal surface was free of epithelial defect 48 hours after transplantation in all six eyes, and remained stable during follow-up (mean 13.8 months). Improved visual acuity was reported, however peripheral vascularization was observed¹¹³.

Two long-term studies of autologous oral mucosal epithelial cell transplantation have been carried out. Nakamura *et al* reported successful re-epithelisation following oral mucosal epithelial cell transplants in 19 eyes in 17 patients with total LCSD¹¹⁴. The mean follow-up was 55 months, with the best corrected visual acuity improved in 10 eyes (53%) at the 36 month follow-up¹¹⁴. Satake *et al* demonstrated similar results in 40 eyes of 36 patients, with 53% of eyes having a stable ocular surface 3 years post treatment¹¹⁵. A number of other studies have demonstrated similar results with the use of *ex vivo* cultured autologous oral mucosal epithelial cells¹¹⁶⁻¹²¹.

The culture of oral mucosal epithelial cells (OMECs) employs the use of xenogeneic materials, which pose a risk to the recipient. There is a risk of transfer of pathogens with the use of amniotic membrane, bovine serum and 3T3 fibroblasts. Transplantation of OMECs without the use of amniotic membrane has been demonstrated¹⁰⁷. Nishida *et al* transplanted oral mucosal epithelial cell sheets to one eye each of four patients with bilateral total LCSD. Complete re-epithelialization was observed one week post-transplant, and the corneas remained transparent for up to 14 months, with improved visual acuity¹⁰⁷. In an attempt to further reduce the use of xenogeneic material, Oie *et al* explored the use of human dermal fibroblasts to replace the murine 3T3 feeder cells¹²². The colony-forming efficiency was comparable between oral mucosal cells grown on dermal fibroblasts and 3T3 cells, and stratified epithelium formed on both substrates¹²². Furthermore, the percentage of p63-positive cells was greater when grown on human dermal fibroblasts (46%) than on 3T3 cells (30%)¹²². A serum-free and feeder-cell free culture system was developed in 2008 for the expansion of human corneal epithelial equivalents¹²³. Epithelial cells grown in the absence of serum or feeder cells on human amniotic membrane formed stratified sheets and expressed CK3/12. The cells also showed a higher proliferative capacity and colony-forming efficiency than cells grown in standard conditions¹²³. However, human amniotic membrane was still used as a scaffold.

1.4.1.d ***Other sources of stem cells for ocular surface reconstruction***

Ex vivo expanded human¹²⁴ or rabbit¹²⁵ conjunctival epithelium on amniotic membrane has been used to treat experimentally-induced LCSD in rabbits. Conjunctival explants grew into stratified epithelium 3-6 layers thick on amniotic

membrane, and formed a stable transparent ocular surface when transplanted on the eyes of rabbits with experimentally induced LCSD^{124, 125}. Epidermis and corneal epithelium are derived from the ectoderm during embryogenesis. Autologous transplantation of epidermal stem cells led to restoration of corneal transparency and improved visual acuity in a goat model of ocular surface disease (OSD)¹²⁶. Human immature dental pulp stem cells (hDIPSC) share similar characteristics with limbal stem cells¹²⁷. Improved corneal transparency was reported after application of epithelial sheets derived from hDIPSC in a rabbit model of LCSD¹²⁸. Autologous nasal mucosa transplantation for ocular surface reconstruction has also been explored¹²⁹. Six eyes in six patients underwent ocular surface reconstruction with cultivated autologous nasal mucosal epithelial cells. The cells expressed CK3/12 and p63. A stable ocular surface was established at a mean follow-up of 14 months¹²⁹.

Stem cells derived from the hair follicle bulge have been successfully transdifferentiated into corneal epithelial-like cells¹³⁰. The cells expressed the corneal epithelial markers CK3/12 and pax6, as well as the putative stem cell markers CK15 and alpha6 integrin¹³⁰. Hair follicle bulge-derived cells grown on fibrin carriers were able to reconstruct the ocular surface in 80% of mice with experimentally-induced LCSD¹³¹. Furthermore, the cells transdifferentiated on the ocular surface expressed CK3/12, and prevented neovascularization and conjunctival ingrowth¹³¹. Mouse embryonic stem cells grown on collagen IV differentiated into keratin 12-expressing corneal epithelial progenitor cells, which were able to re-epithelialise the corneal surface after n-heptanol debridement¹³². Mesenchymal stem cells (MSCs) grown on amniotic membrane successfully re-epithelialised the ocular surface in a rat alkali burn model¹³³. MSCs delivered systemically were able

to home to the cornea and promote re-epithelialization after an alkali burn in a rabbit model¹³⁴.

Whatever the source of epithelial cells, they are generally transferred to the ocular surface on a scaffold. Clinically, amniotic membrane is widely used; however a number of alternatives are under investigation. Scaffolds for the transfer of epithelial cells to the eye are discussed below.

1.4.1.e *Scaffolds for the transfer of stem cell to the ocular surface*

1.4.1.e.1 **Amniotic membrane**

Epithelial cell sheets generally require a scaffold for successful transplantation. The current gold standard scaffold is human amniotic membrane, which is denuded of cells before seeding corneal epithelial cells¹³⁵. Epithelial cell sheets have been successfully grown on amniotic membrane *in vitro*¹³⁵⁻¹⁴⁰. A number of animal studies have demonstrated re-epithelialization of the corneal surface after transfer of epithelial cells on amniotic membrane^{110, 141-143}.

In humans, many groups have reported successful transfer of epithelial cells to the ocular surface using amniotic membrane. Tsai *et al* transplanted autologous limbal epithelial cells expanded on denuded amniotic membranes in 6 patients with unilateral LCSD¹⁴⁴. Complete reepithelialisation of the corneal surface was observed within 3-4 days, and visual acuity was improved in 5/6 patients with mean visual acuity improving from 20/112 to 20/45¹⁴⁴. The Kinoshita group has reported the transfer of autologous limbal epithelial cells on amniotic membrane, with

regeneration of a stable corneal surface up to 19 months post-transplant, in patients with unilateral LCSD¹⁴⁵. The same group transplanted autologous oral mucosal epithelial cells on amniotic membrane in 6 eyes in 4 patients with LCSD. The corneal surface was found to be intact in all eyes 48 hours after transplantation, and remained stable at a mean follow-up time of 13.8 months¹¹³. A further study from this group, in three patients, reported that regrafting with amniotic membrane carrying epithelial cells can be performed if the cornea opacifies after an initial graft¹⁴⁶. Similar results with the use of amniotic membrane as a carrier of epithelial cells for the treatment of OSD have been reported by others^{113, 147-151}.

1.4.1.e.2 **Alternative scaffolds for transfer of cells to the eye**

Amniotic membrane is at best translucent, does not degrade completely on the ocular surface and being biologically sourced, and poses a risk for transmission of pathogens. A number of alternative scaffolds have been trialled for the transfer of epithelial cells to the ocular surface, including contact lenses, human lens capsule, collagen, fibrin, silk fibroin, and polymers (Figure 1-9). The results obtained with these scaffolds will be discussed below.

Some contact lenses support the growth of human limbal epithelial cells. The Di Girolamo group reported that cells proliferated on the surface of the lens,

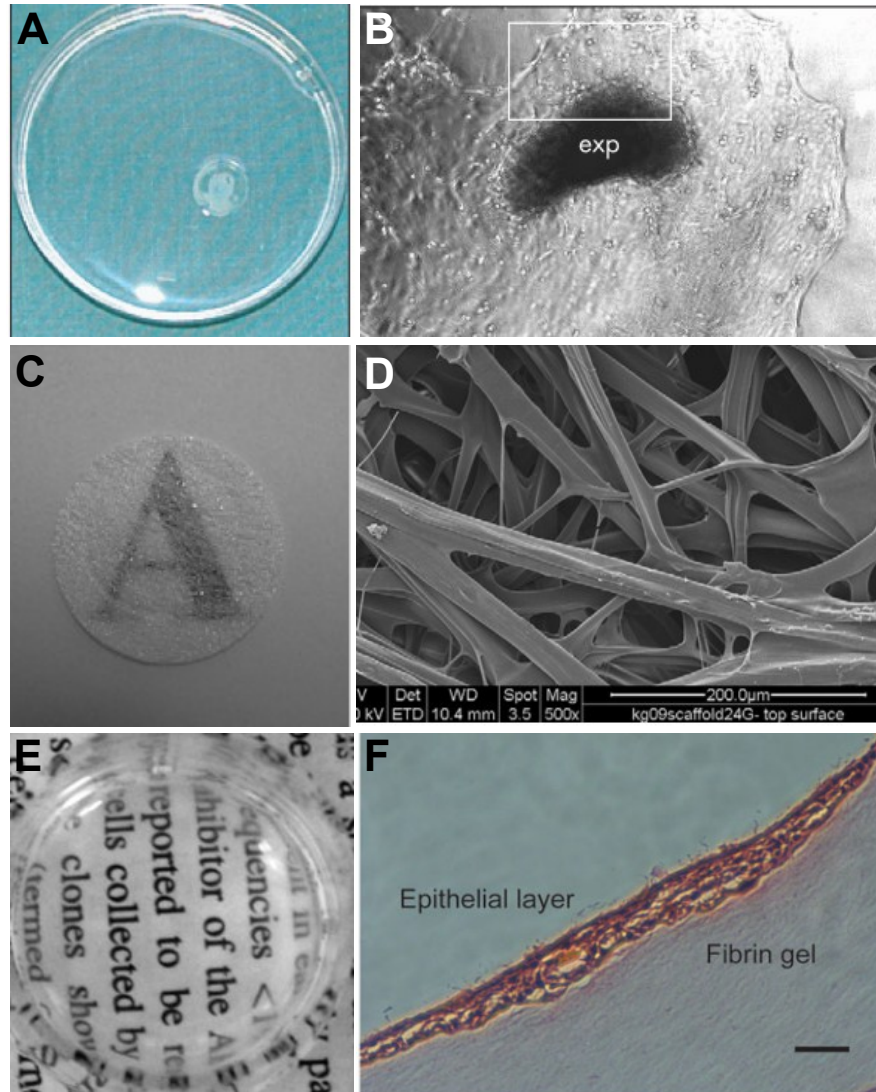


Figure 1-9 Scaffold for the transfer of cells to the ocular surface

(A) Image of a soft contact lens with limbal epithelial cells in a 90 mm petri dish. (B) Outgrowth of cells from a limbal explant seeded on a soft contact lens. (C) Silk fibroin membrane placed on written text, demonstrating transparency. (D) Electron micrograph of the fibrous silk fibroin mat used to culture mesenchymal stem cells. (E) The transparency of fibrin gels demonstrated by placing over text. (F) H&E stained oral mucosal epithelial cells on fibrin gel showing a multilayered epithelium. Images A and B from Di Girolamo *et al* 2007¹⁵², C and D from Bray *et al* 2012¹⁸⁶, and E and F from Sheth *et al* 2014¹⁷⁶.

were p63 positive, and formed a sheet 2-3 cells thick with expression of corneal epithelial cell markers CK3/12¹⁵². A recent study reported that acrylic acid modification of contact lenses led to increased proliferation of limbal epithelial cells, and maintained progenitor cells during *ex vivo* expansion¹⁵³. Acid modified contact lenses applied to rabbit eyes with induced LCSD were able to transfer epithelial cells to the ocular surface and partially reconstruct the corneal epithelium¹⁵⁴. Autologous limbal epithelial cells transferred to the eye on a soft contact lens were able to stabilise the ocular surface in one patient with severe alkali burns¹⁵⁵. A clinical trial exploring the use of contact lenses to deliver epithelial progenitor cells for the treatment of LCSD was carried out by Di Girolamo *et al*¹⁵⁶. Three patients with long-standing LCSD due to aniridia (n=1) or recurrent ocular surface melanoma (n=2) were included in the study. Autologous epithelial cells from limbal (n=2) or conjunctival (n=1) biopsies were expanded on siloxane-hydrogel contact lenses *ex vivo*, in the presence of autologous serum. Transplantation of the progenitor cells on the contact lens to the surface of the eye resulted in stabilization of the ocular surface in all patients, with an improvement in visual acuity. Follow-up ranged from eight to thirteen months¹⁵⁶.

Human anterior lens capsule is composed of collagen IV, laminins and heparin sulphate proteoglycans. It is easily sourced, as it is discarded following cataract surgery¹⁵⁷. Lens capsule was used successfully to treat mechanically-induced corneal ulcers in rabbits¹⁵⁸. Corneal ulceration was induced in 8 male rabbits by trephination. Allogeneic anterior lens capsule was implanted in four rabbits, and in the other four the wound was allowed to heal without intervention. Treated rabbits showed faster re-epithelialization of the corneal epithelium with reduced opacity when compared to

untreated animals¹⁵⁸. Human LESC's have also been expanded on lens capsule *ex vivo*¹⁵⁹, however more work is required to evaluate epithelial cell growth *in vitro* and *in vivo*.

Collagen is a major constituent of the cornea, is biocompatible, has low immunogenicity, and is easily produced^{160, 161}. Various formats of collagen carriers support the growth of epithelial cells *in vitro*¹⁶²⁻¹⁶⁷, and have been tested in rabbit¹⁶⁸, minipig^{169, 170} and porcine¹⁷¹ models of OSD¹⁶⁸. A cross-linked collagen material, without epithelial cells, designed as a biosynthetic mimic of extracellular matrix has shown promise as a corneal substitute in a phase I clinical trial¹⁷². The material was implanted in 10 patients with vision loss due to corneal pathology, and was stable up to 24 months post-implant. No immunosuppression was required and the material remained avascular. Complete re-epithelialization was apparent in all patients, with nerve regeneration and sensitivity to touch. Six out of ten patients showed an improvement in visual acuity¹⁷².

Fibrin is a low cost, degradable substrate that has been used as a tissue substitute for human skin^{173, 174}. Human corneal epithelial cells positive for CK3 have been grown on fibrin gels¹⁷⁵. Oral mucosal epithelial cells grown on a fibrin gel developed into a stratified epithelium, with the basal cells expressing p63 α , and the superficial cells expressing CK3/12¹⁷⁶. Rabbit LESC's on fibrin gels were able to regenerate the epithelium after superficial keratectomy¹⁷⁷. Autologous LESC's grown on fibrin gels restored the epithelium in 14 of 18 patients in an initial study by the Pellegrini group¹⁷⁸. Re-epithelialization was apparent within one week, with inflammation and vascularization regressing within 4 weeks, and a stable corneal epithelium at follow-up at 12-27 months¹⁷⁸. A larger study (112 patients), from the same group, with up to

10 years follow-up, demonstrated restoration of a transparent, renewing cornea in 76% of patients with LCSD¹⁷⁹.

Silk fibroin is a protein obtained from the cocoons of the silkworm *Bombyx mori*¹⁸⁰. It is transparent, non-immunogenic, and can be fabricated into a thin film^{181, 182}. Cells isolated from rabbit limbal epithelium have been cultured on porous silk fibroin membranes, and expressed CK3/12 and p63¹⁸³. Chirila *et al* demonstrated serum free expansion of human limbal epithelial cells on silk fibroin membranes¹⁸⁴. Bray *et al* compared the growth of human limbal epithelial cells on silk fibroin and amniotic membrane. Attachment of cells to tissue culture plastic and silk fibroin membranes was comparable, but was six fold less than attachment to amniotic membrane¹⁸⁵. The cells attached to silk fibroin expressed CK3/12, and similar distribution of p63 positive cells were observed on silk fibroin and amniotic membrane¹⁸⁵. The same group explored dual-layer culture of epithelial and stromal cells on silk fibroin membranes, with a view to creating an artificial limbus¹⁸⁶. Epithelial cells co-cultured with stromal cells displayed similar expression of CK3/12 and p63 to cells grown without stromal cells¹⁸⁶.

Polymers are inexpensive and straightforward to prepare. They can be easily moulded to form a suitable scaffold for cell culture. Poly(ϵ -caprolactone)^{187, 188}, poly(lactide-co-glycolide)¹⁸⁹, polymethacrylate^{190, 191}, and hydroxyethyl-methacrylate¹⁹² have been shown to support the growth of epithelial cells *in vitro*. Rabbit conjunctival epithelial cells grown on poly(ϵ -caprolactone) underwent proliferation and stratification after implantation into the corneas of severe combined immunodeficiency (SCID) mice¹⁸⁷.

1.5 Corneal neovascularization

1.5.1 Corneal avascularity

In most species including humans, the cornea remains avascular even although a number of angiogenic factors are present. Vascular endothelial growth factor A (VEGF-A)¹⁹³, platelet-derived growth factor, insulin-like growth factor, fibroblast growth factor and matrix metalloproteinases have all been detected in the cornea¹⁹⁴. Under normal conditions, there is high expression of anti-angiogenic factors and low levels of pro-angiogenic factors. Soluble vascular endothelial growth factor receptor-1 (sflt-1) is the principal anti-angiogenic agent in the cornea¹⁹⁵. It is responsible for maintenance of corneal avascularity by sequestering VEGF-A, preventing it from binding to VEGF receptor-2 on endothelial cells and exerting its mitogenic effect¹⁹⁵. Expression of Fas ligand¹⁹⁶ and thrombospondin-1¹⁹⁷ have also been shown to induce apoptosis in Fas positive endothelial cells, and to reduce the angiogenic response to injury, respectively, and thus play a role in maintaining corneal avascularity.

1.5.2 Physiological angiogenesis

Angiogenesis can be defined as the formation of new blood vessels from existing vessels. Two forms of angiogenesis are recognised: sprouting angiogenesis, which involves chemotactic migration and proliferation of endothelial cells, and non-sprouting angiogenesis, which is the splitting of existing vessels by formation of transcapillary pillars¹⁹⁸. The growth of tissue beyond the diffusion limit of oxygen, approximately 100-200 μm from a blood vessel¹⁹⁹, leads to hypoxic induction of angiogenesis²⁰⁰ through hypoxia-inducible factor-1 (HIF-1)^{201, 202}. Physiological angiogenesis is important in the remodelling of the vasculature and vascularization of

hypoxic tissue, but pathological angiogenesis has been implicated in a number of ischaemic, malignant, inflammatory, infectious and immune disorders²⁰⁰.

The seed for the development of the vascular system is sown during embryogenesis by the differentiation of mesodermal cells known as angioblasts¹⁹⁸. The angioblasts form the primitive plexus of blood vessels by a process termed vasculogenesis²⁰³. After vasculogenesis, the remodelling and maturation of the vascular system takes place through angiogenesis. Structures such as the neural tube and retina are vascularised by angiogenic sprouting during normal development²⁰⁴. An important step in the maturation of vessels is the association of the endothelial cells with smooth muscle cells and pericytes²⁰⁴.

Vascular endothelial cells have a low turnover in adult vascular beds²⁰⁵, and angiogenesis is a rare event in the mature vasculature. Physiological angiogenesis does play an important role in adult vasculature in the female reproductive system²⁰⁶, especially during cyclic endometrial changes^{207, 208}. Angiogenesis also plays an important role in wound healing^{198, 204}. Physiological angiogenic events are highly regulated and persist for short periods before being completely suppressed²⁰⁹.

Angiogenesis is controlled by a fine balance of pro- and anti-angiogenic factors. A number of molecules have been identified as inducers of angiogenesis, such as members of the vascular endothelial growth factor (VEGF) family, angiopoietins, transforming growth factors, tumour necrosis factor- α , platelet-derived growth factor, interleukins and members of the fibroblast growth factor family²¹⁰. The major initiator of angiogenesis is believed to be VEGF-A, which is a secreted growth factor that stimulates the proliferation of endothelial cells^{211, 212}.

The vascularization of tissue is determined by its metabolic activity. The presence of hypoxic tissue is known to stimulate angiogenesis. Tissue hypoxia has been shown to upregulate VEGF-A expression^{213, 214} by the induction of HIF-1, which increases VEGF-A transcription, and also by an increase in the stability of VEGF-A mRNA²¹⁵. VEGF-A has been shown to be expressed during both vasculogenesis²¹⁶ and angiogenesis²¹⁷. VEGF-A acts specifically on endothelial cells, and shows little mitogenic activity on other cell type^{212, 218}.

VEGF-A acts in conjunction with other pro-angiogenic agents in a strictly regulated manner to mediate physiological angiogenesis. After sufficient vascularization of hypoxic tissue, the signals that mediate induction of pro-angiogenic factors soon disappear. The levels of VEGF-A return to normal, resulting in cessation of angiogenesis and return of the endothelial cells to their quiescent state²⁰⁰.

1.5.3 Vascular endothelial growth factors and angiogenesis

The VEGF family consists of 7 members: VEGF-A, VEGF-B, VEGF-C, VEGF-D, VEGF-E, VEGF-F and placental growth factor (PlGF)²¹⁹. The VEGFs bind to transmembrane tyrosine kinase receptors VEGFR-1, VEGFR-2, VEGFR-3, neuropilin-1 and neuropilin-2 (Figure 1-10). VEGF-A and VEGF-B, which have endothelial cell growth and survival properties respectively, will be discussed further.

1.5.3.a VEGF-A

VEGF-A was first discovered as a factor secreted by tumours²²⁰. It exists as a covalently linked²²¹ homodimer of ~45 kDa²¹¹. Differential splicing of the VEGF-A

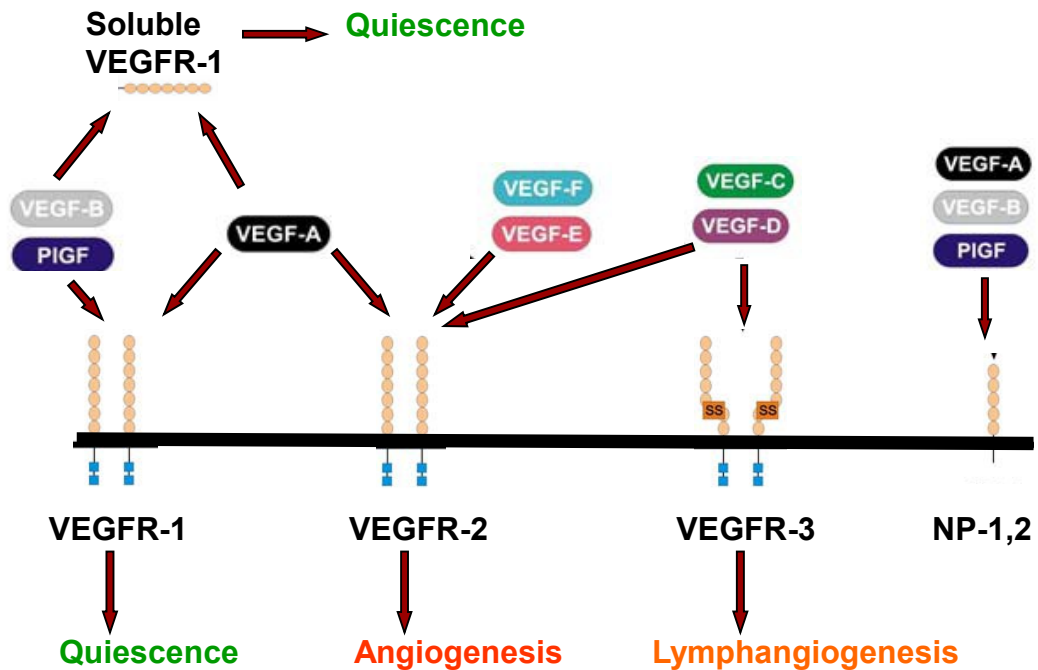


Figure 1-10 The vascular endothelial growth factor family

The VEGF family of growth factors consists of 7 members VEGF-A to F and PIGF, and their receptors VEGFR-1 to 3 and neuropilin-1 and 2. VEGF-A brings about angiogenesis through binding to VEGFR-2. VEGFR-1 acts as a dummy receptor to keep the levels of VEGF-A in check. The soluble portion of this receptor has been shown to be responsible for corneal avascularity. VEGF-B binds to VEGFR-1 and the neuropilin receptors. It does not induce angiogenesis or lymphangiogenesis. It is more of a survival factor than a growth factor. VEGFR-3 and its ligands VEGF-C and D regulate lymphangiogenesis. VEGF-E is an angiogenic stimulator encoded by the genome of the orf virus. VEGF-F is a VEGF-like molecule in viper venom. PIGF is expressed in the placenta, heart and lung and is important in vascular remodeling. Figure adapted from Otrrock *et al* 2007²¹⁰.

gene yields a number of isoforms, namely VEGF₁₂₁, VEGF₁₄₅, VEGF₁₆₅, VEGF₁₈₃, VEGF₁₈₉ and VEGF₂₀₆^{222, 223}, with VEGF₁₆₅ being the most highly expressed. VEGF-A binds to VEGFR-1, VEGFR-2 and both neuropilin receptors. VEGF-A promotes angiogenesis *in vitro*²²⁴ and *in vivo*^{225, 226} and is a survival factor for newly formed vessels²²⁷. Deletion of a single allele of the VEGF-A gene in mice leads to vascular defects and is embryonic lethal²²⁸, indicating its essential role in vasculogenesis. VEGF-A also plays a key role in pathological angiogenesis. Most solid tumours express VEGF-A²²⁹, and high levels of VEGF-A have been found in the vitreous and blood of patients with active proliferative retinopathy²³⁰⁻²³³, and in human and animal models of corneal neovascularization^{193, 234, 235}. Dysregulation of VEGF-A expression leads to uncontrolled angiogenesis and formation of immature blood vessels that are leaky and prone to haemorrhage. VEGF-A is thus an attractive target for the treatment of proliferative neovascular diseases.

1.5.3.b *VEGF-B*

The VEGF-B gene was initially cloned and characterised as VEGF-related-factor (VRF) in 1996²³⁶. It was shown to have structural similarities to VEGF-A and PlGF, and described as an endothelial cell mitogen²³⁷. Alternative splicing of the VEGF-B gene yields two isoforms which differ in their heparin binding properties²³⁸. VEGF-B is a secreted protein and associates to form a homodimer²³⁹. VEGF-B is expressed in a wide range of tissue but shows high levels of expression in the heart and skeletal muscles both during development²⁴⁰ and in adult tissue²³⁷. Isoform-specific expression has also been reported²⁴¹. VEGF-B binds to VEGFR-1²⁴² and neuropilin-1²⁴³ and was initially believed to have angiogenic properties²⁴⁴.

The function of VEGF-B is not completely understood, but recent studies have shown it to be more of a cell survival factor than a growth factor²⁴⁵. VEGF-B knockout mice are healthy and fertile, however they do have minor vascular abnormalities^{246, 247}. This is in contrast to VEGF-A or VEGF-C knock outs, which are embryonic lethal²²⁸. These data suggest that VEGF-B is not essential for formation of the vascular system. Transgenic overexpression of VEGF-B does not induce angiogenesis, or lymphangiogenesis^{248, 249}, which is in stark contrast to other members of the VEGF family. Furthermore, unlike VEGF-A, VEGF-B lacks the ability to induce vascular permeability^{247, 248, 250, 251}.

1.5.3.b.1 **The role of VEGF-B in angiogenesis**

Initial reports suggested VEGF-B could stimulate the growth of endothelial cells *in vitro*²³⁷. VEGF-B was also shown to increase vascular growth in an ischaemic limb model^{252, 253}, however, other studies showed no vascular growth²⁵⁴. The majority of published data suggest that VEGF-B does *not* induce neovascularization. VEGF-B over-expression in muscle²⁵⁵, periadvential tissue²⁵⁶ and heart²⁴⁹ did not cause blood vessel growth, though an increase in capillary diameter was observed²⁴⁹. VEGF-B over-expression potentiated rather than initiated angiogenesis in transgenic mouse cells²⁴⁸. VEGF-B was found to be dispensable for blood vessel growth, but required for blood vessel survival in a mouse model of corneal neovascularization²⁵⁷. Furthermore, VEGF-B addition was found to augment neovessel formation in models of choroidal and retinal neovascularization²⁵⁸, possibly by increasing endothelial cell survival.

1.5.3.b.2 The role of VEGF-B in the heart

VEGF-B deficient mice had essentially normal hearts, but minor abnormalities in the coronary vasculature were noted²⁴⁷. Similarly VEGF-B deficient rats did not exhibit any obvious vascular abnormalities²⁵⁹. In mice, VEGF-B deficiency was shown to confer some resistance to hypertension and vascular remodelling induced by hypoxia²⁶⁰. The levels of VEGF-B were observed to be downregulated in a model of left ventricular hypertrophy in the mouse²⁶¹. VEGF-B₁₈₆ delivered by an adeno-associated virus preserved cardiac function, possibly by inhibition of apoptosis²⁶¹. A similar downregulation of VEGF-B was observed in rats following myocardial infarction²⁶², and levels of myocardial VEGF-B have been shown to be reduced in heart failure in humans²⁵⁹. VEGF-B did not induce capillary angiogenesis but caused enlargement of myocardial capillaries in both mouse and rat^{249, 263-265}.

1.5.3.b.3 The role of VEGF-B in neuroprotection

VEGF-B is expressed in neurons in the central nervous system²⁴⁰ and elsewhere²⁶⁶. Expression has been shown in the brain of humans with Parkinson's disease²⁶⁷. VEGF-B also increased neuron survival in a model of Parkinson's disease *in vitro*²⁶⁸ and *in vivo*²⁶⁹. VEGF-B stimulated neurogenesis in mice²⁷⁰ and prevented motor neuron degeneration *in vitro*²⁷¹. VEGF-B appears to be a survival factor for different types of neurons including brain cortical neurons^{272, 273}, retinal neurons²⁷³ and motor neurons in the spinal cord²⁷¹. The neuroprotective effects appear to be mediated through VEGFR1^{266, 271}, by inhibition of apoptosis²⁷³. The neuroprotective role of VEGF-B might be important in the context of the cornea, as VEGF-B inhibition could potentially lead to apoptosis of corneal nerves. VEGF-B has been found to be

expressed in the normal mouse cornea, and increased expression was observed in response to epithelial debridement²⁷⁴. Furthermore, VEGF-B deficient mice had impaired nerve regeneration, which was rescued by exogenous VEGF-B, in a mouse model of peripheral nerve injury²⁷⁴.

1.5.3.b.4 The role of VEGF-B in fatty acid transport

VEGF-B has an effect on the expression of fatty acid transporter proteins (FATPs). Deletion of VEGF-B has been shown to reduce the levels of FATP3 and 4²⁷⁵. VEGF-B deficient mice fed a high fat diet had improved insulin sensitivity and blood lipid profiles²⁷⁶. Cold exposure reduced the levels of VEGF-B and FATP3 in brown adipose tissue²⁷⁷. VEGF-B also affected FATP1 and 4 levels in a neuroblastoma cell line *in vitro*²⁶⁷. Downregulation²⁷⁸ and overexpression^{279, 280} of VEGF-A have been shown to prevent obesity and insulin resistance in response to a high fat diet, and the levels of VEGF-B and FATP1-4 were increased in the white adipose tissue of these mice²⁷⁸. Both VEGF-B and VEGFR1 are highly expressed in white and brown adipose tissue²⁸¹, however their role in fatty acid metabolism is not completely understood.

1.5.4 Pathological neovascularization in the cornea

Angiogenesis, the sprouting of blood vessels from existing vessels, is highly regulated and occurs for very short periods of time²⁰⁹. Corneal neovascularization occurs when the balance of pro- and anti-angiogenic factors shifts towards angiogenesis (Figure 1-11 A). Pathological angiogenesis is the result of prolonged pro-angiogenic stimuli, and can be caused by infection, chemical or mechanical

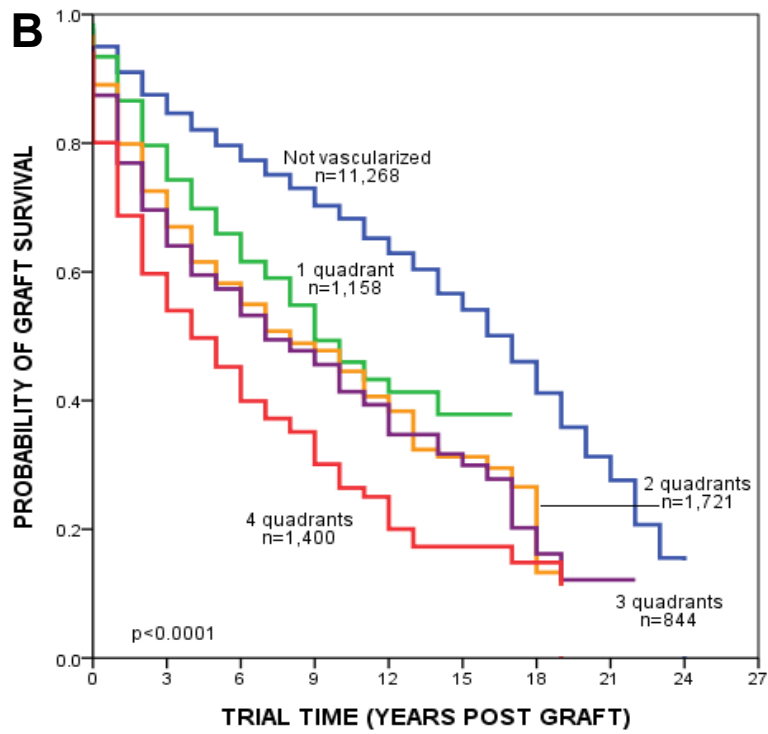
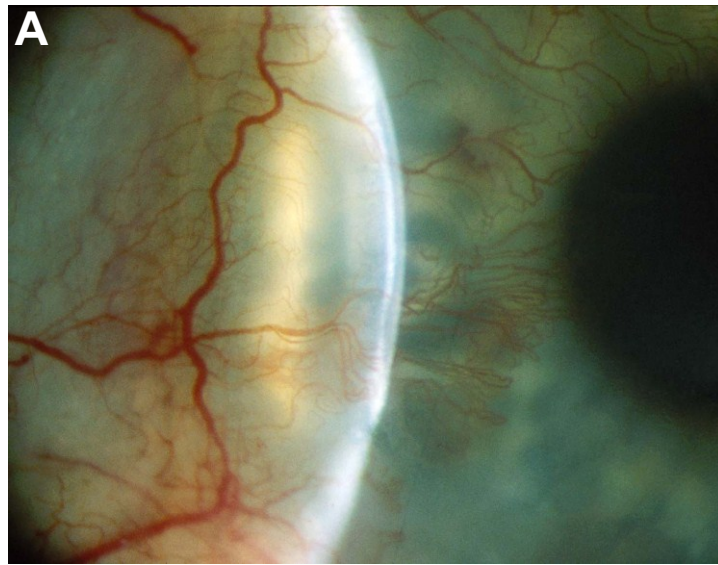


Figure 1-11 Corneal neovascularization

(A) Image of a vascularised human cornea. (B) Kaplan-Meier plot comparing the probability of human corneal allograft survival in vascularised and non-vascularised recipient beds. Grafts into non-vascularised recipient beds survive significantly longer than if there are vessels present at the time of graft. Data from the Australian Corneal Graft Registry report 2011⁹⁹.

insults, and inflammation^{282, 283}, leading to unregulated growth of blood vessels. Neovessels arise from the pericorneal limbal plexus and invade the cornea^{284, 285}. Pathological neovessels tend to be immature and hyperpermeable, which can lead to corneal oedema, scarring, lipid deposition and inflammation^{194, 286, 287}. The presence of corneal vessels is a risk factor for failure of a subsequent corneal graft (Figure 1-11 B). Corneal neovascularization is a potentially sight-threatening condition estimated to affect 1.4 million people per year in the USA²⁸².

1.5.5 Treatments for corneal neovascularization

A number of strategies are employed for the treatment of corneal neovascularization. In early stages of disease, anti-angiogenic therapies can be employed to prevent the formation of blood vessels, while angio-regressive methods are used to treat established vessels.

1.5.5.a *Surgical therapy*

Surgical techniques used to treat corneal neovascularization include laser photocoagulation, photodynamic therapy and needle diathermy.

1.5.5.a.1 Laser photocoagulation

This technique uses a laser to induce thermal damage to vessels. The laser energy is absorbed by haemoglobin leading to coagulation, followed by collapse of the vessel and cessation of blood flow. The shortcomings of this technique are that feeding arteries and arterioles can be difficult to identify at the slit-lamp, the occlusive effect can be impermanent²⁸⁸ and the vessels can regrow²⁸⁹. Laser therapy can also lead to

upregulation of inflammatory cytokines and VEGF-A²⁹⁰, resulting in further angiogenesis. A number of complications of laser photocoagulation such as peripheral corneal haemorrhage, iris atrophy and pupil ectasia, corneal thinning²⁹¹ and necrotising scleritis²⁹² have been described.

1.5.5.a.2 **Photodynamic therapy**

Photodynamic therapy (PDT) aims to target vessels selectively by using a photosensitising agent which is selectively absorbed and retained by neovascular tissue. Application of laser energy thereafter leads to production of free radicals and targeted tissue damage. Verteporfin²⁹³⁻²⁹⁵, fluorescein²⁹⁶ and dihematoporphyrin (DHE)²⁸⁸ have been used as photosensitising agents. A pilot study in 15 patients with corneal neovascularization showed fluorescein-potentiated argon laser therapy resulted in a slow regression of neovascularization and clinically significant reduction in corneal oedema, however multiple treatments were required²⁹⁶. DHE was found to be effective in reducing established vessels, but showed significant systemic and local side effects²⁸⁸. Verteporfin PDT caused complete occlusion of vessels in 50% of cases, however repeat treatments were required in 60% of patients, and it failed to cause occlusion in 11% of cases²⁹⁵. The dyes and lasers used for PDT are expensive^{293, 294}, and coupled with the potential for local and systemic side effects, PDT is not commonly used for the treatment of corneal neovascularization²⁹⁷.

1.5.5.a.3 **Needle diathermy**

This technique involves occlusion of vessels by passing an electric current, using a diathermy unit, through a stainless steel needle placed in or near the vessel²⁹⁸. A modification of this technique uses an electrolysis needle which is more flexible and applies thermal energy²⁹⁹. A recently published long-term evaluation of the technique in 56 eyes in 52 patients, demonstrated regression of vessels in 68% of eyes 6 weeks post therapy, however multiple treatments were required to maintain regression, and there was only a modest improvement in visual acuity³⁰⁰. These techniques have been used in a limited number of patients and require further evaluation.

1.5.5.b *Non-surgical therapy*

Non-surgical treatments for corneal neovascularization are based on anti-angiogenic and anti-inflammatory agents.

1.5.5.b.1 **Steroids and non-steroidal anti-inflammatory agents (NSAIDs)**

Topical steroids are used as a front-line treatment for corneal neovascularization³⁰¹. The anti-angiogenic activity of a number of corticosteroids such as cortisone³⁰², dexamethasone³⁰³, hydrocortisone³⁰⁴, prednisolone³⁰⁵ and triamcinolone³⁰⁶ has been assessed. The mechanism of anti-angiogenic action of these agents is poorly understood³⁰⁷. The anti-angiogenic effect is believed to result from anti-inflammatory properties such as inhibition of cell chemotaxis^{305, 308}, modulation of proteolytic activity of vascular endothelial cells^{301, 308} and inhibition of pro-inflammatory cytokines^{309, 310}. Steroids are unable to completely suppress corneal neovascularization²⁹¹, cannot induce regression of vessels, and may elicit a

number of side-effects such as glaucoma and cataract in steroid-sensitive individuals. Non-steroidal anti-inflammatory drugs (NSAIDs) provide similar efficacy as do steroids, without the ocular side effects. NSAIDs target prostaglandin production by inhibition of the cyclooxygenase enzymes²⁹⁷. The anti-angiogenic activity of topically delivered flurbiprofen³⁰⁸, indomethacin³⁰⁸, ketorolac³¹¹, diclofenac³¹² and nepafenac³¹³ has been reported in corneal neovascularization. However, NSAIDs do cause corneal ulceration and melting and have shown variable clinical efficacy²⁹¹.

1.5.5.b.2 Cyclosporin A

Cyclosporin A is an immunosuppressive agent that specifically acts on T-lymphocytes³¹⁴. It elicits an anti-angiogenic response through inhibition of interleukin-2. Cyclosporin A is sometimes used when steroids need to be tapered, but is used sparingly due to systemic toxicity³¹⁵ and corneal deposits³¹⁶. Furthermore, there have been reports of the inability of topical cyclosporine A to inhibit corneal neovascularization in the context of corneal graft rejection³¹⁷.

1.5.5.b.3 Anti-VEGF agents

VEGF-A is the primary pro-angiogenic factor in the eye and is largely responsible for pathological neovascularization³¹⁸. VEGF-A promotes growth of endothelial cells and is a survival factor for newly formed vessels²²⁷. Blockade of the VEGF-A signalling cascade has been attempted with the use of neutralizing antibodies³¹⁹, VEGF receptor antibodies^{320, 321}, recombinant soluble VEGF receptor protein³²², VEGF antisense nucleotides³²³, ribozymes³²³ and receptor tyrosine kinase inhibitors^{297, 324, 325}. Bevacizumab, a full length humanised murine monoclonal

antibody that neutralises VEGF-A activity³²⁶, has been trialled for the treatment of Corneal neovascularization. Several animal studies have shown that topical bevacizumab can reduce corneal neovascularization. Topical administration in rats^{327, 328} and rabbits³²⁹ limited the growth of neovessels. However, it must be noted that bevacizumab binds to murine VEGF-A with significantly lower affinity than to human VEGF-A. A recent study demonstrated that bevacizumab penetrates only superficially in healthy mouse corneas, and penetration in corneas with neovascularization was variable³³⁰.

Subconjunctival injection of bevacizumab is an alternative route of administration, and has been shown to be safe and efficacious in reducing corneal neovascularization in rat^{331, 332}, guineapig³³³ and rabbit³³⁴⁻³³⁶ models. Combination therapy of topical bevacizumab and doxycycline enhanced the anti-neovascular effect of bevacizumab and decreased side effects associated with the anti-VEGF-A agent, such as delayed wound healing, in the rat³³⁷. These results are surprising, considering the weak species cross-reactivity of bevacizumab.

Clinically, monoclonal antibody therapy is being trialled in a number of centres. Both topical and subconjunctival administration of bevacizumab result in partial regression of neovascularization, with limited side effects³³⁸⁻³⁴⁶. Regression of vessels without recurrence was observed with combination therapy of bevacizumab with argon laser photocoagulation²⁹⁰ or superficial keratectomy³⁴⁷. The most promising results are from a recent randomised control trial, which showed subconjunctival bevacizumab, administered in new Corneal neovascularization cases, reduced the corneal vessel area by 36% over a 12 week period³⁴⁸ (Figure 1-12). However, bevacizumab therapy does not cause complete regression of vessels, is

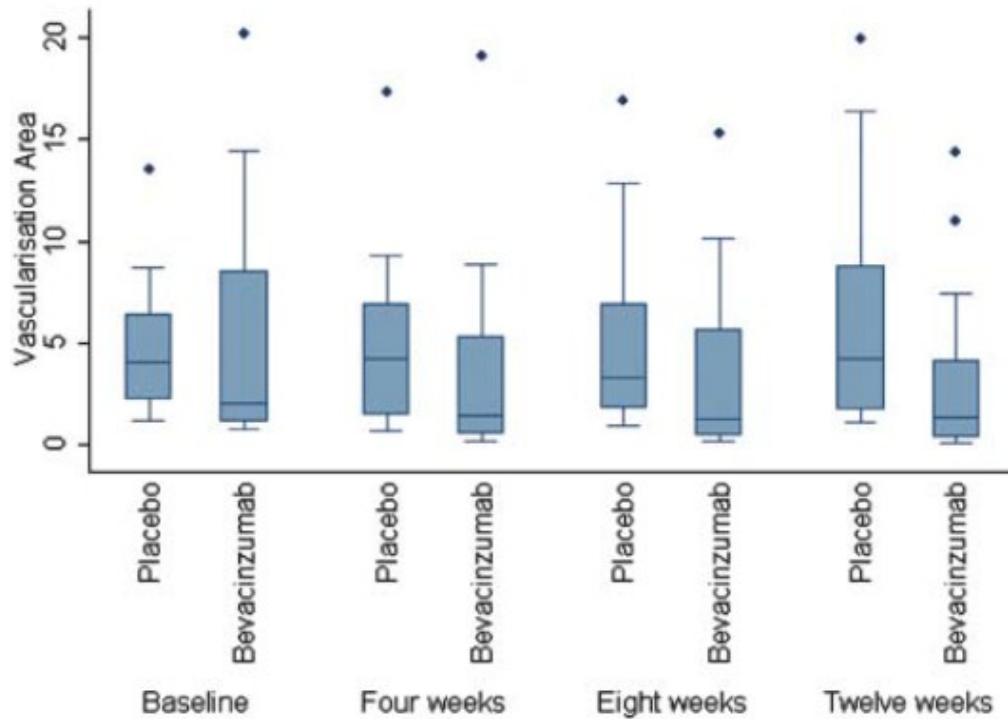


Figure 1-12 Bevacizumab prevents growth of blood vessels

Result of a double masked, randomised clinical trial comparing 3 monthly subconjunctival injections of 2.5mg bevacizumab to placebo (0.9% saline) in patients (n=15 per group) with newly growing corneal vessels. The box and whisker plot shows the area of the cornea that was vascularised. Outliers are marked by circles. There was a 90% increase in corneal neovascular area in the control group over 12 weeks, while bevacizumab treatment reduced corneal neovascular area by 36%, over the same time. From Petsoglou *et al* 2013³⁴⁸.

more effective in treatment of newly formed vessels, and has little effect on established vessels^{338, 345}.

1.6 Porous silicon materials as implantable scaffolds carrying stem cells

Silicon is the second most abundant element in the earth's crust. Elemental silicon was initially considered bioincompatible and was isolated from contact with human tissue in medical devices such as pacemakers. Porous silicon (pSi) was first discovered in the 1950's and found a use in transistors³⁴⁹, however its possible uses in medicine have been explored more recently³⁵⁰⁻³⁵⁸.

1.6.1 Nanostructured pSi implants

Flat silicon can be converted to pSi by etching pores into its surface (Figure 1-13 A). The pSi is said to be nanostructured when these pores are on the nano scale (one to several hundred nanometres). The engineering of nanopores into silicon gives it a huge surface area, in the range of 400-1000 m²/g³⁵⁹. This property allows for loading of large amounts of substances such as proteins, nutrients and drugs³⁶⁰. Moreover, the size and shape of the pores can be “tuned” for the appropriate application.

Porous silicon membranes demonstrate biocompatibility both *in vitro*^{352, 361-365}, and *in vivo*^{363, 366} (Figure 1-13 B), and accommodate the attachment and growth of cells³⁶⁷⁻³⁷¹. On implantation, pSi degrades completely into silicic acid^{361, 372} which is bioavailable³⁷³ and is the major form of silicon in the human body³⁷⁴. The degradation rate of pSi can be effectively controlled by surface modification. For

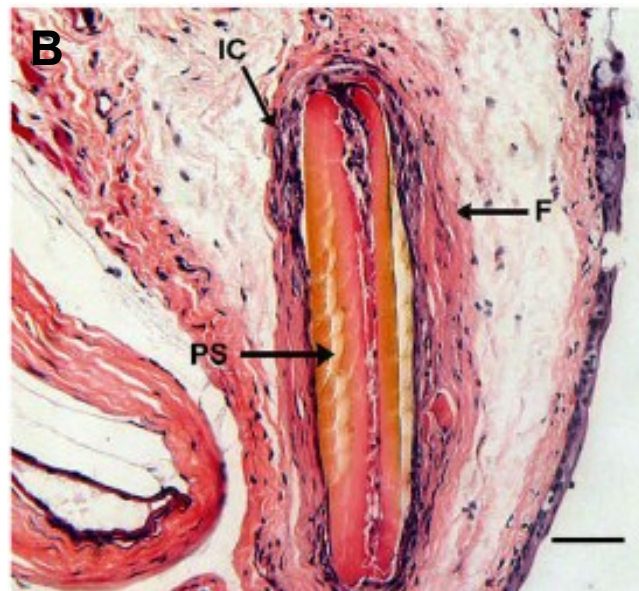
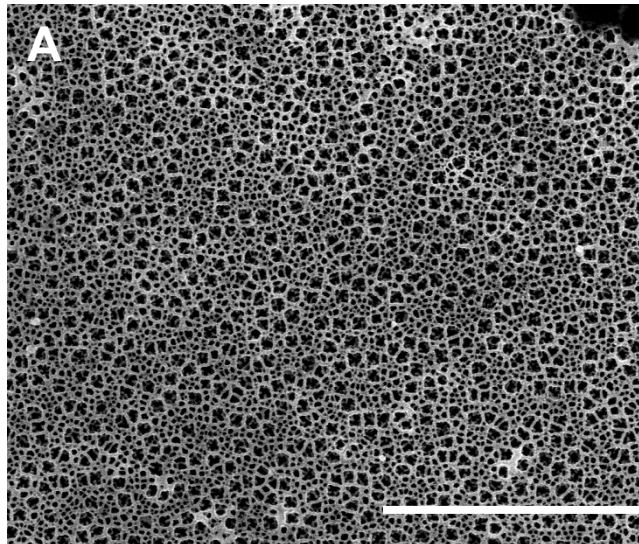


Figure 1-13 Porous silicon

(A) Scanning electron micrograph of porous silicon membrane showing its highly porous nature. Scale bar 4 μm . Image courtesy of Steven McInnes.

(B) Haematoxylin and eosin stained section of a pSi membrane (PS) implanted under the rat conjunctiva. A fibrous capsule (F) formed around the implant, and some inflammatory cells (IC) were observed. Image from Low *et al* 2009³⁹¹.

example, unmodified pSi degrades over a period of a few hours in aqueous solution, while highly oxidised pSi shows significantly greater stability^{358, 375, 376}.

pSi can be fabricated in a number of formats such as films, which remain attached to the bulk silicon, membranes, which consist of only porous material, and microparticles, which are generated by mechanical disruption of membranes³⁵⁴. The versatility of formats, surface chemistry, porosity and biocompatibility of pSi make it a promising biomaterial for use in implants for applications such as drug delivery and as a scaffold for cells.

1.6.1.a ***Drug loading and delivery from pSi***

Porous silicon may be of use in a number of drug delivery applications, particularly as a controlled drug delivery device. The large surface area and high porosity of the material allow loading of a large amount of drug³⁷⁷. Loading of drugs into pSi is relatively simple and can be achieved by immersing the pSi in a solution of the drug³⁷⁸⁻³⁸¹. Alternatively, a small amount of drug solution can be impregnated into the pores^{350, 381-383}.

A wide variety of molecules such as proteins, enzymes, drugs and DNA can be loaded³⁶⁰. The surface chemistry and degradation rate of the pSi can be modified to tailor the drug release profile. This allows for release of drugs over a period of a few hours or slow release over longer timeframes^{358, 384, 385}. A unique property of pSi is the ability to ‘self-report’ the amount of drug loaded or released. Loading of a molecule into thin film or multilayered pSi alters the index of refraction and the spectrum obtained, giving a visual indication of the amount of drug. This permits *in*

vivo monitoring of the amount of drug diffused out of the pSi³⁸⁶ or the degree of degradation³⁸⁷.

The potential use of pSi microparticles for drug delivery to the eye has already been explored³⁸⁸. No toxicity was observed up to 4 months after intravitreal injection of microparticles in rabbits³⁸⁸. Injection of daunorubicin loaded microparticles into the rabbit vitreous led to slow release of the drug without toxicity^{389, 390}.

1.6.1.b *Porous silicon as a scaffold for the culture of cells*

The bioactivity of pSi was described when hydroxyapatite crystals were successfully grown upon it³⁶¹. Bioactivity linked with biocompatibility make pSi an ideal scaffold for the transfer of cells to the body. We have previously shown that pSi membranes implanted under the conjunctiva in rats did not cause significant inflammation, neovascularization, nor erode the underlying or overlying tissue³⁹¹. An added advantage of pSi is that it is completely inorganic and easily sterilisable by autoclaving³⁹². The surface chemistry can be altered³⁹³⁻³⁹⁵ to promote the attachment and growth of cells³⁹⁶. Surface modification also affects the degradation kinetics of the pSi, which can be designed to dissociate at a specific rate. Furthermore, pSi can be coated with proteins and growth factors to maintain an optimal growth environment for cultured cells. A number of studies have reported culture of mammalian cells such as B50³⁷¹, hepatocytes³⁷⁰, PC12 and lens epithelial cells³⁶⁷ on pSi.

Nanostructured pSi has been used as a scaffold in orthopaedic implants³⁹⁷ and can potentially be used in ophthalmology. Work in our laboratory has shown that human

corneal epithelial cells can be grown on pSi membranes coated with rat tail collagen I³⁹¹. The cells proliferated and grew to colonise the surface of the pSi membrane, and migrated across the ocular surface after subconjunctival implantation in the rat eye³⁹¹.

1.7 Poly(ϵ -caprolactone)

Poly(ϵ -caprolactone) (PCL) was first generated in the 1930's through ring opening polymerization³⁹⁸. It is hydrophobic, semi-crystalline, soluble in a wide range of organic solvents, and has a low melting point (59-64°C)³⁹⁹. It is easily manufactured and can be engineered into a large range of scaffolds, including nanospheres, nanofibers, foams and knitted textiles⁴⁰⁰⁻⁴⁰⁴.

Mammals lack the enzymes required to degrade PCL⁴⁰⁵. It is however bioresorbable, as it undergoes hydrolysis, and degrades over a period of 2-4 years^{406, 407}. *In vivo* the initial hydrolysis^{408, 409} of the material is followed by phagocytosis by macrophages, giant cells and fibroblasts when the polymer molecular mass is below 3000 Daltons⁴¹⁰. PCL microspheres implanted into muscle and bone in rats caused a localised inflammatory response with recruitment of neutrophils⁴¹⁰. However, PCL microsphere implantation in the brain did not cause necrosis⁴¹¹. Implantation of a PCL scaffold in rats and rabbit calvaria was well tolerated and induced new bone formation when loaded with recombinant human bone morphogenic protein 2^{412, 413}.

1.7.1 Porous silicon poly(ϵ -caprolactone) composite materials

Although porous silicon has a number of properties that make it an attractive material for an ophthalmic implant, it does have some drawbacks. pSi membranes are ridged,

inflexible, brittle and prone to mechanical damage⁴¹⁴, and erode in aqueous environments^{415, 416}. Some of these disadvantages can be mitigated by incorporation of a soft flexible polymer such as poly(ϵ -caprolactone) into a composite material (Figure 1-14).

Composite materials of pSi and PCL can have superior properties compared to the individual components. For example, a two-stage drug delivery profile can be achieved or different drugs can be loaded into the pSi and polymer³⁶⁰. Polymers can compensate for the brittle nature of pSi and can increase the stability of the pSi in biological fluids⁴¹⁷.

Composite materials can be prepared in a number of formats, such as capping pSi with polymer⁴¹⁸, coating with polymer³⁵³, polymer infiltration into the pSi⁴¹⁹, pSi films supported by polymer⁴²⁰, and pSi micro- and nano-particles encapsulated by polymer^{421, 422}. The properties of composite materials can be tailored to suit the intended application, such as drug delivery, bio-sensing, or as resorbable implants.

1.8 Antibodies and antibody fragments

Antibodies are immunoglobulins, glycoproteins that circulate in the blood and are also found in milk, mucous, tears and other body fluids⁴²³. They are an important part of the humoral immune system and function to protect against infection and toxins⁴²⁴.

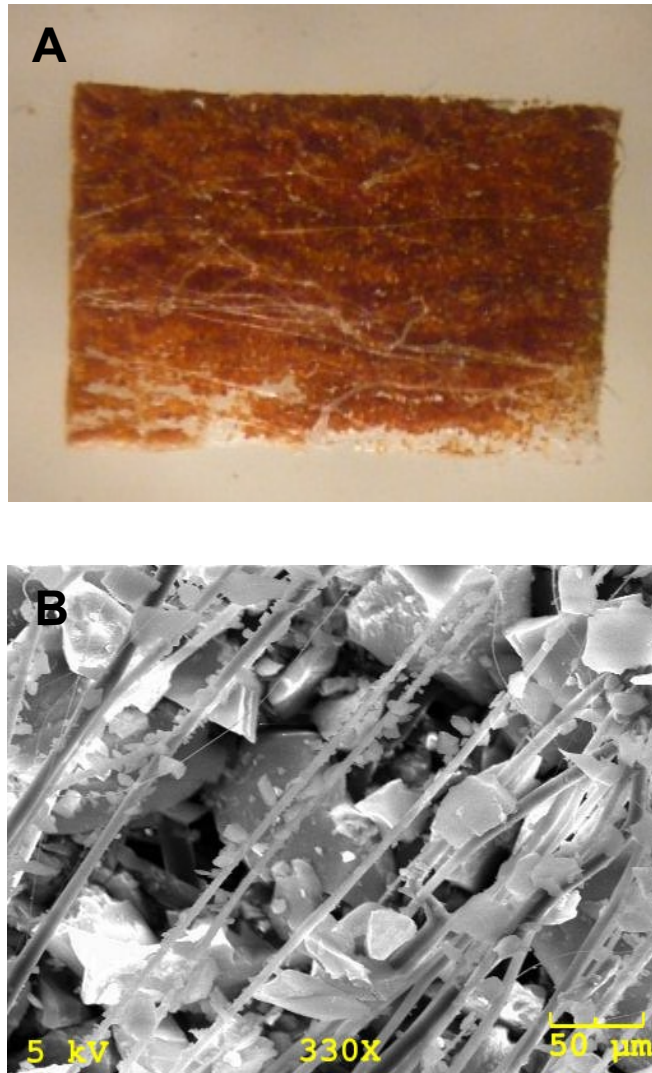


Figure 1-14 Porous silicon polycaprolactone composite materials

(A) Macroscopic image of a piece of pSi-PCL composite material prepared by embedding pSi microparticles in a polycaprolactone fabric. (B) Scanning electron micrograph of pSi-PCL composite material showing pSi microparticles intimately associated with the PCL fibers. Images provided by Prof. Jeff Coffey, Texas Christian University.

1.8.1 Monoclonal antibodies

Antibodies with a defined specificity produced using hybridoma technology are termed monoclonal antibodies. A hybridoma cell is produced by the fusion of an antibody secreting B lymphocyte with a myeloma cell⁴²⁵. Hybridoma cells can be cultured indefinitely and secrete specific antibodies. Many monoclonal antibodies are of murine origin and elicit an immune response mediated by generation of anti-mouse antibodies when used in humans^{426, 427}, limiting their use. Methods such as chimerization⁴²⁸ and humanization⁴²⁹ have overcome this problem and allowed widespread use of monoclonal antibodies as therapeutic agents.

1.8.1.a Bevacizumab

Bevacizumab (Avastin) is a humanised monoclonal antibody that binds to human VEGF-A³¹⁹. It was originally developed for cancer therapy and has shown safety and efficacy in the treatment of a number of cancers⁴³⁰. VEGF-A, a pro-angiogenic cytokine, is involved in the pathogenesis of a number of ocular neovascular diseases, and is an attractive therapeutic target. Clinically, in ophthalmology, bevacizumab is used for the treatment of diabetic retinopathy^{431, 432}, age related macular degeneration⁴³³, neovascular glaucoma⁴³⁴ and macular oedema⁴³⁵⁻⁴³⁷, in each case with some success. Bevacizumab has also been shown to be effective in reducing newly-formed corneal vessels in a human randomised control trial³⁴⁸, as described earlier in Figure 1-12.

1.8.2 Engineered antibody fragments

Antibody fragments maintain antigen binding specificity of the parent antibody but lack some of their undesirable properties such as poor tissue penetration, long half-

life in blood and activation of the effector arm of the immune system. Some of the formats of antibody fragments are depicted in Figure 1-15.

The most popular approach to generating antibody fragments is to genetically engineer a molecule for bacterial expression⁴³⁸. *E.coli* is the bacterium of choice as it is well characterised and inexpensive⁴³⁹. Single chain variable fragments (scFvs) are commonly used antibody fragments and consist of the variable light (V_L) and variable heavy (V_H) regions of an antibody joined by a polypeptide linker^{439, 440}. ScFvs, being small (~26 kDa), show good tissue penetration and as they lack the Fc region, they are cleared quickly from circulation, primarily by elimination in the kidneys^{441, 442}. Alternatively, a number of expression systems such as yeast, algae, plants, insect cells and mammalian cells can be used to express antibody fragments. The major drawback of using scFvs is that they have a single antigen binding site, which results in shorter retention times on antigen, that is, lower avidity. However, the use of antibody fragments is particularly attractive for the treatment of ocular diseases, as they can be applied topically, and penetrate the cornea⁴⁴³.

1.9 Hypothesis and aims

The overarching aim of the work described in this thesis was to develop novel therapies for two common ocular conditions, ocular surface disease and corneal neovascularization. Although ocular surface disease and corneal neovascularization are disparate conditions, ocular inflammation and neovascularization are part of the pathogenesis of both.

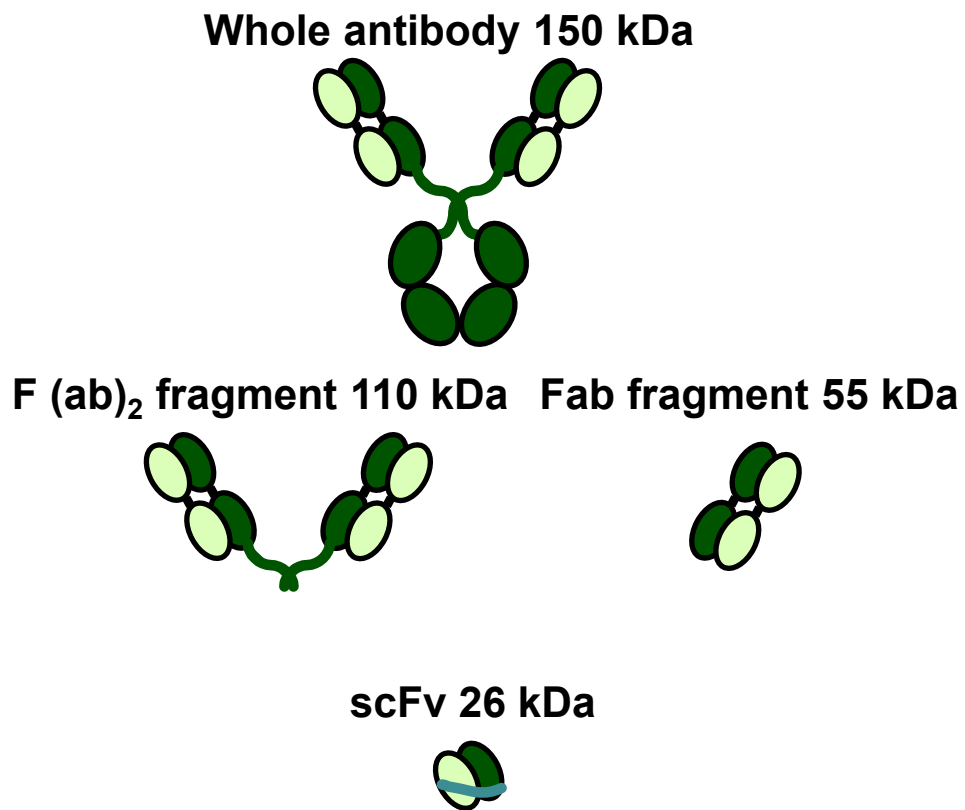


Figure 1-15 Formats of antibody fragments

Whole antibodies are large molecules, with a molecular weight of approximately 150 kDa (IgG). Antibody fragments such as F(ab)₂, Fab, and scFvs are much smaller with molecular weights of 110 kDa, 55 kDa and 26 kDa respectively. Antibody fragments retain the binding specificity of the parent antibody, but as they are smaller have better tissue penetration. scFvs have been shown to penetrate the cornea on topical application Thiel *et al* 2002⁴⁴³.

Ocular surface disease is a painful disease characterised by damage to or loss of the corneal stem cells and/or their niche at the limbus. Clinically, OSD is treated by transplanting epithelial cells to repair the damaged ocular surface. The cells are carried on a scaffold, currently human amniotic membrane. We hypothesised that porous silicon materials would be a suitable scaffold for the transfer of rat oral mucosal epithelial cells to the eye, with the aim of recreating an artificial stem cell niche. I aimed to assess two pSi materials, pSi membranes and pSi-PCL composite materials, for their ability to be loaded with drugs including biologics, support the growth of oral mucosal epithelial cells, and for their biocompatibility when implanted under the conjunctiva of the rat eye.

Corneal neovascularization is characterised by the growth of blood vessels in the normally avascular cornea. The current therapies for corneal neovascularization can prevent the progression of newly formed vessels, but are ineffective at treating established vessels. We hypothesised that blockade of VEGF-B, a survival factor for endothelial cells, might lead to regression of established corneal vessels in a rat model of corneal neovascularization. I aimed to assess the ability of an anti-VEGF-B scFv, delivered topically and by subconjunctival injection, to inhibit the growth of developing as well as established vessels.

CHAPTER 2 MATERIALS AND METHODS

2.1 Materials

2.1.1 Water

Double glass-distilled water (ddH₂O) was used for the preparation of all solutions and buffers unless otherwise mentioned. Autoclaved Milli-Q water was used for all polymerase chain reactions (PCR).

2.1.2 General chemicals

A list of general chemicals can be found in Appendix A. All chemicals used were analytical grade unless otherwise noted. A list of commonly used buffers and solutions can be found in Appendix B.

2.1.3 PCR primers

Primers used for all PCR reactions were purchased from GeneWorks Pty Ltd (Thebarton, SA, Australia) at sequencing-grade purity. Primers used for the generation and sequencing of the anti-VEGF-B scFv are described in Table 2-1. Primers used for the detection of transplanted cells on the rat ocular surface are described in Table 2-2.

Table 2-1 Primers used to generate and sequence the anti-VEGF-B scFv

Primer	Sequence (5' →3')	Description
2H10V_Lfor	GGAGCCGCCGCCGAGAACCA CCACCACCAGAACCACCACCAC CCCTCTTGATTCCCAGCTTTGT	Amplifies the V _L from the 2H10 hybridoma
2H10V_Lback	GCCATGGCGGACTACAAAGAGA TCCAGATGACCCAGACC	Amplifies the V _L from the 2H10 hybridoma
2H10V_Hfor	GGAATTCGGCCCCCGAGGCCCT GGACACGGTCACGC	Amplifies the V _H from the 2H10 hybridoma
2H10V_Hback	GGCGGCGGCGGCTCCGGTGGTG GTGGATCCCAGGTGCAGCTGCA GCAGCC	Amplifies the V _H from the 2H10 hybridoma
Scfor	GGAATTCGGCCCCCGAG	SOE* primer
Sback	TTACTCGCGGCCAGCCGGCCAT	SOE* primer
SeqV_Lfor	GGAGCCGCCGCCCA	Sequencing primer
SeqV_Hback	GGCTCCGGTTGGTGGTGA	Sequencing primer

* SOE: splice by overlap extension

Table 2-2 Primers used to detect the male specific gene *sry*

Primer	Sequence (5' →3')	Description
SRYfor	CCCGCGGAGAGAGGCACAAGT	Original <i>sry</i> PCR primer
SRYrev	TAGGGTCTTCAGTCTCTGCGC	Original <i>sry</i> PCR primer
SRY1for	TGCATTTATGGTGTGGTCCCG	<i>sry</i> multiplex primer
SRY1rev	CTGTGTAGGGTCTTCAGTCTCTGC	<i>sry</i> multiplex primer
SRY2for	TGTCTAGATAGCATGGAGGGC	Second round primer
SRY2rev	CCTCTGTGGCACTTTAACCCTT	Second round primer
ARBPfor	CCATCTGCATTTGCGGC	Housekeeping gene
ARBPprev	GCAGGCTGACTTGGTGTGA	Housekeeping gene

2.1.4 Enzymes

Table 2-3 List of enzymes

Enzyme	Description	Company
PlatinumTaq® DNA polymerase	Used for amplification of DNA in end-point PCR	Life Technologies, Carlsbad, CA, USA
Elongase® Enzyme Mix	Used for amplification of DNA in end-point PCR	Life Technologies, Carlsbad, CA, USA
Pfx50™ DNA polymerase	Proofreading enzyme used for generation of scFv	Life Technologies, Carlsbad, CA, USA
SfiI	Restriction endonuclease used for cloning of scFv	England Biolabs, Ipswich, MA, USA
T4 DNA ligase	Ligase used for cloning of scFv	Promega, Madison, WI, USA
Dispase I	Used to detach the oral mucosal epithelium	Life Technologies, Carlsbad, CA, USA
Trypsin	Used to disaggregate oral mucosal epithelial cells	Sigma-Aldrich, St. Louis, MO, USA

2.1.5 Recombinant proteins

Table 2-4 List of recombinant proteins

Protein	Description	Company
Collagen IV	Recombinant human	Sigma-Aldrich, St. Louis, MO, USA
EGF	Recombinant human epidermal growth factor	Prospec-Bio, Rehovot, Israel
Insulin transferrin selenium supplement	Catalogue number 41400-045	Life Technologies, Carlsbad, CA, USA
Vitronectin	Recombinant human	R&D Systems, Minneapolis, MN, USA
β-NGF	Recombinant rat beta-nerve growth factor	R&D Systems, Minneapolis, MN, USA

2.1.6 Antibodies

Table 2-5 List of antibodies

Antibody	Description	Company
CK3/12	Clone AE5	Millipore, Billerica, MA, USA
CK19	Clone E6	Abcam, Cambridge, United Kingdom
p63	Clone 4A4	Abcam, Cambridge, United Kingdom
ABCG2	Clone 5D3	Chemicon, Temecula, CA, USA
Goat anti-Mouse IgG Alexa Fluor[®] 488	2 ^o antibody used for immunofluorescence	Life Technologies, Carlsbad, CA, USA
Anti-polyhistidine	Clone HIS-1 used in scFv ELISA	Sigma-Aldrich, St. Louis, MO, USA
Anti-mouse IgG HRP conjugated	Goat anti mouse IgG horseradish peroxidase conjugated used in ELISA	Millipore, Billerica, MA

2.1.7 Ophthalmic materials, reagents and eye drops

Table 2-6 Ophthalmic reagents and eye drops

Reagent	Description	Company
Ophthalmic balanced Salt Solution (BSS)	Sterile irrigating solution (ophthalmic)	Alcon Laboratories, Inc. TX, USA
Chlorsig™ eye ointment	Chloramphenicol 10 mg/g	Sigma Pharmaceuticals, Rowville, VIC
Eye spears	BVI Weck-Cel®	Beaver Visitec International, Inc. Waltham, MA USA
Mydriacyl® eye drops	Topicamide 1%	Alcon Laboratories (Australia), Frenchs Forest, NSW
Surgical sutures, 10-0	Monofilament nylon	Alcon Laboratories, Inc. TX USA

2.1.8 Porous silicon materials

2.1.8.a Porous silicon membranes and microparticles

Samples of pSi were generously provided by Professor L Canham and Dr A Loni, pSiMedica Ltd, Malvern, United Kingdom. All pSi membranes and microparticles were prepared in the laboratories of Prof. Nicolas Voelcker, Mawson Institute, University of South Australia. Porous silicon membranes were produced by electrochemical anodization of p-type (0.01-0.02 Ohm cm) single-crystal silicon wafers in hydrofluoric acid, followed by separation from the bulk silicon membranes were subsequently milled to produce microparticles. Membranes were ammosilanised by immersion in 50mM 3-aminopropyltrimethoxysilane prior to use as scaffolds for the culture of oral mucosal epithelial cells. Microparticles were used to prepare composite materials as described below.

2.1.8.b *Porous silicon poly-(ϵ -caprolactone) composite materials*

All pSi-PCL composite materials were prepared in the laboratories of Prof. Jeffery Coffer, Texas Christian University, Fort Worth, TX, USA. Porous silicon microparticles were generated as described in section 2.1.8.a. The particles were sieved to two size ranges: 150-250 μm , and $<40 \mu\text{m}$. For fabrication of composite materials, two different methods were evaluated.

Method A. To embed pSi microparticles in the outer surface of microfibers of PCL, the particles were warmed to a temperature above the polymer melting point, followed by brief exposure to the PCL fabric, forcing a modest blending between the contacting interfaces. Specifically, pSi particles were heated in an oven at 110°C , then immediately transferred to a glass plate. A $1 \times 1 \text{ cm}^2$ piece of PCL fabric was physically pressed on to the hot particles. The hot particles caused localised melting of the PCL fibres and thus resulted in the pSi being partially embedded in the polymer. Loadings of the order of 5-6% pSi by mass were obtained, with retention of PCL fibre morphology.

Method B. Improved embedding of pSi microparticles in the PCL was achieved by the brief addition of chloroform to pSi microparticles after removal from the oven, resulting in a surface etch/dissolution of the PCL surface and better adhesion of the pSi particles to the PCL matrix. This processing step was followed by an additional electrospinning event, to physically entrap more pSi into the composite. Specifically, pSi particles were heated in an oven at 220°C for 10 minutes (min), and then transferred to a cold glass plate. One drop of chloroform was added to the pSi and quickly mixed. After $\sim 10 \text{ s}$, a $1 \times 1 \text{ cm}^2$ piece of PCL fabric was physically pressed on

to the moist pSi particles. An additional thin layer of PCL fibres was then generated on to the pSi-PCL, resulting in the formation of a “net”. Loadings of the order of 32-34% pSi by mass were obtained, with retention of PCL fibre morphology.

2.1.9 Animals

2.1.9.a *Ethics approval*

All animal experiments described in this thesis were approved by the Animal Welfare Committee of Flinders University of South Australia. All experiments were in accordance with the ARVO Statement for the Use of Animals in Ophthalmic and Vision Research, as well as the Australian Code of Practice for the Care and Use of Animals for Scientific Purposes.

2.1.9.b *Rats*

Male and female Sprague-Dawley rats (at least 6 weeks old) were sourced from the Flinders University Animal Facility or the Animal Resources Centre (Perth, Western Australia). Rats were housed at the Flinders University Animal Facility and exposed to a 12 hour light-dark cycle. The room temperature was maintained at 24°C with 50% ambient humidity. Access to food and water was *ad libitum*. Animals were monitored using the sheets in Appendix D.

2.2 Molecular techniques

2.2.1 DNA quantification

The concentration of DNA in purified plasmid preparations and purified PCR products was estimated using a NanoDrop 8000 UV-Vis spectrophotometer (Thermo Fisher Scientific, Waltham, MA, USA).

2.2.2 Agarose gel electrophoresis

Agarose was added to 0.5x TBE to make a gel of suitable concentration (e.g. 2g agarose in 100ml 0.5x TBE for 2% gel). A microwave oven was used to heat the solution to dissolve the agarose. The gel was allowed to cool and Gel Red (Biotium, Hayward, CA) was added to a final concentration 1/10,000 of stock. The solution was poured into a gel tray and allowed to set at room temperature. Once set, the gels were placed in an electrophoresis tank containing 0.5x TBE. 1µl of 6x loading dye was added for every 5 µl of sample prior to loading. A DNA marker was also run. A potential difference of 110V was applied across the gels for 90 mins using a BioRad Power Pac 200. DNA was visualised and photographed under ultraviolet light using a Syngene Gene Genius bio-imaging system.

2.2.3 Amplification of the V_H and V_L from the 2H10 hybridoma cDNA

cDNA from the 2H10 hybridoma, which secretes an antibody with affinity for human, mouse and rat VEGF-B, was provided by Pierre Scotney (CSL Ltd.). The PCR master mix was prepared as described overleaf.

Reagent	Volume (μ l)
Water	34.5
10x Pfx50 reaction buffer	5
dNTPs (10 μ M each)	1.5
Pfx50 DNA polymerase (5 U/ μ l)	1
Sense primer	1.5
Antisense primer	1.5
Template DNA	5

The primers used for amplification are described in Table 2-1. The thermal cycling conditions used were as follows:

	Temperature ($^{\circ}$ C)	Time (s)	Number of repetitions
Enzyme activation	94	300	1
Denaturation	94	60	30
Annealing	63	60	
Extension	72	60	
Final extension	72	240	1

2.2.4 Generation of the anti-VEGF-B scFv by SOE PCR

A single chain variable fragment (scFv) consists of the V_L and V_H regions of an antibody joined together by a polypeptide linker. DNA coding for the V_L and V_H of the 2H10 hybridoma was isolated and gel purified in order to be spliced together to generate scFv DNA. An approximately equimolar mixture of the V_L and V_H was made. An assembly PCR mix was made as follows:

Reagent	Volume (μl)
Water	19.25
10X Pfx50 reaction buffer	2.5
dNTPs (10 μ M each)	0.75
Pfx50 enzyme (U/ μ l)	0.5
Template V _L and V _H	2

The mixture was subjected to two rounds of primerless PCR as shown in panel A. The SOE primer mix containing 50 μ M each of the primers Scfor and Scback (Table 2-1) was then added and the mixture was amplified for 25 rounds as shown in panel B.

A

	Temperature ($^{\circ}$C)	Time (s)
Denaturation	92	60
Annealing	63	30
Touchdown	58	50
Extension	72	60

B

	Temperature ($^{\circ}$C)	Time (s)
	92	60
	63	30
	72	60

The results of the assembly PCR were analysed by separating the products on a 1% agarose gel.

2.2.5 Amplification of the male specific sry gene

Cell samples were collected from the ocular surface of female rats implanted with pSi loaded with male oral mucosal epithelial cells, using FTA paper (Millipore, Billerica, MA, USA) as described in section 2.5.2.e (below). The presence of transplanted cells was detected by PCR amplifying the male specific *sry* gene in the collected samples. The FTA discs were washed in FTA purification reagent (Millipore, Billerica, MA, USA) and TE buffer, twice for five minutes each. The discs were air dried and used as the template in a PCR reaction.

2.2.5.a *Original sry PCR*

The PCR master mix was prepared as follows:

Reagent	Volume (μ l)
Water	17.4
10x Buffer	2.5
MgCl ₂	0.75
dNTPs (10 μ M each)	0.25
SRYfor and SRYrev	2
Platinum Taq	0.1

The thermal cycling conditions were as follows:

	Temperature (°C)	Time (s)	Number of repetitions
Enzyme activation	95	300	1
Denaturation	95	30	65
Annealing	55	30	
Extension	72	30	
Final extension	72	300	1

The results of the PCR were visualised by running 5 µl of the PCR product on a 2% agarose gel. The expected size of the sry band was 167 bp.

2.2.5.b *Novel sry PCR*

The PCR master mix was prepared as follows:

Reagent	Volume (µl)
Water	17.4
10x Buffer	2.5
MgCl ₂	0.75
dNTPs (10µM each)	0.25
Primer mix with SRY1for, SRY1rev, ARBFor and ARBPrev	2
Platinum Taq	0.1

The primer mix contained a 20:1 ratio of the ARBP and SRY1 primers (Table 2-2). Two microliters of male rat genomic DNA (courtesy of Dr. Helen Brereton) was used as a positive control. Washed FTA discs were added to the PCR mix and subjected to thermal cycling as follows:

	Temperature (°C)	Time (s)	Number of repetitions
Enzyme activation	95	300	1
Denaturation	95	30	30
Annealing	62	30	
Extension	72	30	
Final extension	72	240	1

The results of the PCR were visualised by running 5 µl of the PCR product on a 2% agarose gel. Detection of *arbp* (a housekeeper gene) indicated the presence of DNA on the FTA disc, and detection of *sry* indicated the presence of transplanted cells on the corneal surface. If no *sry* was detected, a second PCR was performed using the PCR product from the first reaction. The master mix for the second round PCR was as follows:

Reagent	Volume (µl)
Water	17.4
10x Buffer	2.5
MgCl ₂	0.75
dNTPs (10µM each)	0.25
SRY1for	1
SRY1rev	1
Platinum Taq	0.1

The product from the first PCR reaction was diluted 1/100 and 2 μ l was used as a template in the second reaction. The thermal cycling conditions used was the same as for reaction one, with the exception that the annealing temperature was 60°C.

2.2.6 Restriction endonuclease digestion with SfiI

The restriction endonuclease digestion mix was prepared as follows:

	Vector	Insert
DNA	10 μ g	28 μ l (varying concentration)
10X Buffer	5 μ l	5 μ l
SfiI (20 U/ μ l)	2 μ l	1 μ l

The volume was made up to 50 μ l with ddH₂O. The solution was vortexed briefly and overlaid with mineral oil before being incubated overnight at 50°C.

2.2.7 Ligation

Ligation reactions were carried out using molar ratios of pHB400 vector to insert of 1:1 and 1:3. Since the vector is ~4800 bp and the insert ~800 bp (Figure 2-1), this is equal to a mass ratio of 6:1 and 2:1 respectively. Two hundred micrograms of vector and either 30 μ g or 90 μ g of insert were ligated in a 20 μ l reaction, which contained 2 μ l of 10 x ligase buffer and 1 μ l of 40,000 U/ μ l T4 DNA ligase (New England Biolabs, Ipswich, MA, USA.). Two control reactions were set up with each sample.

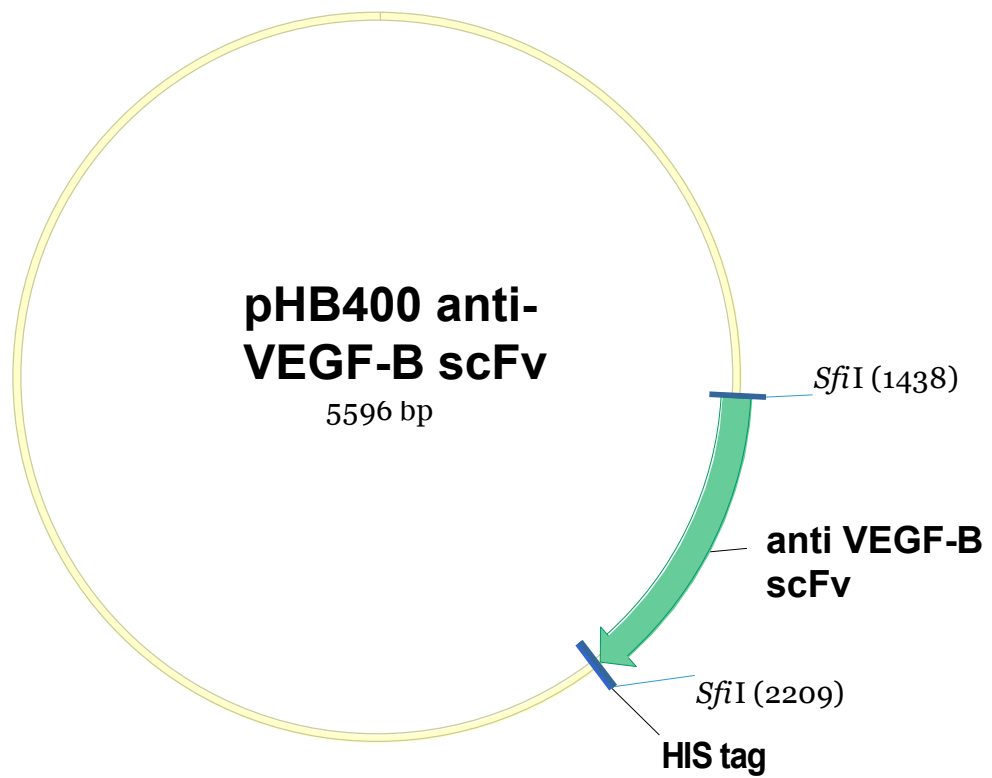


Figure 2-1 Plasmid map of the anti-VEGF-B scFv in pHB400

The anti-VEGF-B scFv was ligated into the plasmid pHB400 using a *sfi*I restriction endonuclease site. The plasmid adds a polyhistidine tag to the n-terminal end of the anti-VEGF-B scFv.

The first control contained digested plasmid and 10X ligase buffer only, the second contained digested plasmid, 10X ligase buffer and 40,000 U of T4 DNA ligase. Once all the components had been added to the respective tubes, they were mixed briefly and incubated overnight at 4°C.

2.2.8 Purification of anti-VEGF-B scFv by immobilised metal ion chromatography

Bacterial lysates containing anti-VEGF-B scFv were prepared as described in section 2.3.6 (*vide infra*). Lysates were transferred into a 60 ml conical bottom centrifuge tube and incubated with 8 ml of Profinity IMAC resin (BioRad, Hercules, CA, USA) overnight at 4°C on a rotating wheel. The scFv was bound to the nickel charged resin through interaction with the polyhistidine tag (Figure 2-1).

The following day, the solution was centrifuged at 1000 g for 5 minutes and the supernatant was removed. The resin was washed 3 x with 10 ml of binding buffer (section B.17) and loaded on to a chromatography column attached to a BioLogic LP chromatography system (BioRad, Hercules, CA, USA). The resin was washed with 10 ml of binding buffer, successively followed by 10 ml of wash buffers containing 20 mM or 30 mM imidazole (section B.18). The bound protein was eluted by addition of buffer containing 250 mM imidazole.

2.2.9 Dialysis of purified scFv solution

Purified scFv was placed in dialysis tubing (Thermo Fisher Scientific, Waltham, MA, USA) with a 10 kDa cut-off. The tubing was placed in 2 l of PBS for 2 hours at 4°C with constant mixing. The PBS was replaced with 2 l of fresh PBS for a further

2 hours. Finally the PBS was replaced with 4 litres of fresh PBS and dialysis carried out overnight at 4°C.

2.2.10 Estimation of protein concentration

The protein concentration of solutions containing scFv was determined using a microplate BCA protein assay kit (Thermo scientific, Waltham, MA, USA). Samples were assayed in triplicate according to the manufacturer's instructions. A standard curve was prepared using dilutions of bovine serum albumin. The protein concentration of each sample assayed was determined by comparison to the values of the standard curve.

2.2.11 Visualization of purified protein by gel electrophoresis

Visualization of the components of protein solutions containing scFv was achieved by separation by gel electrophoresis. Five micrograms of protein samples were mixed with 4x loading buffer (BioRad, Hercules, CA, USA) with dithiothreitol and incubated at 95°C for 2 minutes. The samples were then loaded into the wells of a 4-20% Biorad TGX stain free precast gel in a Criterion gel tank. A voltage of 300 V was applied for 20 minutes. The gel was then imaged using the BioRad gel-Doc EZ imager.

2.2.12 Binding of anti-VEGF-B scFv to human VEGF-B and VEGF-A

A direct ELISA was used to detect binding of scFv to VEGF-B. ELISA plates were coated with 1 µg/ml recombinant human VEGF-B (CSL, Melbourne, Australia) or human VEGF-A (ProspecTany, Rehovot, Israel) overnight at 4°C in a humidified box, then blocked with 5% skim milk powder in phosphate buffered saline (PBS) for

1.5 hours. Anti-VEGF-B scFv was then added for 1.5 hours at room temperature. Diluent (0.1% skim milk) was added as a negative control. Bound scFv was detected with 1:2000 diluted anti-HIS antibody (Sigma-Aldrich, St. Louis, MO, USA) and 1:1000 horseradish peroxidase conjugated anti-mouse antibody (Millipore, Billerica, MA) for 1.5 hours each. TMB (BD, Franklin Lakes, NJ) was used as the substrate and absorbance was measured at 450 nm.

2.2.13 Small and medium scale purification of plasmid DNA

For the small scale production of plasmid DNA, *E.coli* HB2151 cells containing the required plasmid were grown overnight in 3 ml cultures as described in section 2.3.4. For the medium scale production of plasmid DNA, a 3 ml bacterial culture was set up for 8 h as described earlier. One hundred microliters of this culture was used to inoculate 50 ml of 2YT medium containing 35 µg/ml chloramphenicol and 1% glucose in a 250 ml conical flask. The flask was incubated at 37°C with 250 rpm shaking overnight. The bacterial cells were harvested by centrifuging at 6000 g for 15 min at 4°C. The Qiagen mini or midi plasmid purification kits (Qiagen, Valencia, CA, USA) were used to purify plasmid DNA from the bacterial cells according to the manufacturer's instructions.

2.2.14 Sequencing of the anti-VEGF-B scFv in plasmid vectors

DNA to be sequenced was gel purified using the Qiagen gel purification kit (Qiagen, Venlo, Limburg, Netherlands). The concentration of the DNA was adjusted to ~100 ng/µl for plasmid DNA and ~10 ng/µl for every 100 bp of PCR product (e.g. 30 ng/ml for a 300 bp product). 5 µM sequencing primers were used. The samples were sequenced bi-directionally using BigDye Terminator v3.1 Cycle Sequencing kit and

resolved using an ABI 3100 Genetic Analyser (Applied Biosystems, Foster City, CA, USA), by Oliver van Wageningen at The Flinders Sequencing Facility. Sequence analysis was carried using Vector NTI Advance™ 10 software (Invitrogen, Carlsbad, CA, USA).

2.3 Bacterial techniques

2.3.1 Preparation of electrocompetent cells

E. coli HB2151 cells were streaked on a 2YT agar (section B.2) plate from glycerol stocks. The plate was incubated at 37°C overnight. Isolated colonies were picked from the plate and used to inoculate several 10 ml aliquots of 2YT medium (Appendix B.1) in a 50 ml container. The culture was incubated at 37°C overnight with shaking. Two 500 ml cultures in low salt Luria Bertani (LB) (Appendix B.19) medium were set up using 10 ml of the overnight culture as inoculum. The cultures were incubated at 37°C with shaking for ~3 h or until the absorbance at 660 nm (OD₆₆₀) was ≥ 0.6 . The cultures were transferred to centrifuge bottles and chilled on ice before centrifuging at 2,500 g for 15 min at 4°C. The supernatant was discarded without disturbing the pellet. The cells were washed twice with 500 ml of ice cold distilled water and centrifuged at 2,500 g for 15 min at 4°C, discarding the supernatant gently each time. Each pellet was then resuspended in 10 ml of 10% glycerol. The suspensions were then pooled and transferred to a 50 ml Oakridge tube (Thermo Fisher Scientific, Waltham, MA, USA). The mixture was centrifuged at 2,500 g for 15 min at 4°C and the pellet was suspended in 0.5 ml of 10% glycerol. Sixty microliter aliquots of the suspension were placed in chilled labelled eppendorf tubes. The aliquots were snap frozen in liquid nitrogen and stored at -80°C.

2.3.2 Electroporation of plasmid DNA

Aliquots of competent cells were thawed on ice. Two microliters of purified ligation mix was added to each aliquot of competent cells. The mixture was gently mixed by tapping the sides of the tube and allowed to stand for 5 min. The mixture was then transferred to an ice-cold electroporation cuvette with a gap size of 1 mm, making sure no bubbles were formed. If bubbles formed, they were removed by teasing with a 19 gauge (G) needle. The cells were electroporated at 1.8 kV, 25 μ F and 200 Ω using a BioRad Genepulser (BioRad, Hercules, CA, USA). The displayed time constant was noted, with a time constant of 3 ms or more considered acceptable. One millilitre of SOC medium (section B.23) was added to the cuvette and mixed gently by pipetting up and down. The mixture was transferred to an Eppendorf tube and incubated for 1 h at 37°C and then centrifuged at 3000 g for 1 min. Eight hundred microliters of supernatant was discarded and the cells suspended in the remaining fluid. The cell suspension was spread onto an agar plate containing 35 μ g/ml chloramphenicol and 1% glucose and incubated overnight at 37°C. The number of colonies was counted on the next day.

2.3.3 Colony blot for the detection of His tag

The colonies obtained after electroporation with the scFv-containing plasmid were picked and plated in a grid pattern on two 2YT agar plates containing 35 μ g/ml chloramphenicol and 1% glucose and grown overnight at 37°C. The colonies from one of the replica plates were lifted on to labelled nitrocellulose discs (Hybond-ECL, Amersham Biosciences, Amersham, United Kingdom). The discs were placed on 2YT agar plates containing 35 μ g/ml chloramphenicol and 1 mM isopropyl β -D-thiogalactopyranoside (IPTG), colony side up. The plates were incubated at room

temperature for 24 h for the production of recombinant protein. The discs were then placed on two layers of filter paper soaked with Tris NaCl tween (TNT) solution (section B.27) in a box. An open container of chloroform was placed in the box and the lid was closed. The colonies were incubated at room temperature in the box for 30 min to lyse cells and allow the released protein to bind to the nitrocellulose discs. The debris from lysed colonies was removed from the discs by squirting with TNT solution using a spray bottle. The discs were placed in a box containing blocking solution (section B.9) for 1 h on a shaker. The discs were washed with PBS-tween (PBS-t) (section B.22) and sealed in polythene bags, 5 ml of mouse anti-histidine antibody (Sigma-Aldrich, St. Louis, MO, USA) diluted 1/2000 in PBS-tween containing 2% w/v skim milk powder was added to the bag before sealing. The discs were placed on a rotating wheel for 1 h at room temperature. Unbound antibody was washed away by placing discs in a box with PBS-tween for 5 min on a shaker. The discs were resealed in a polythene bag with 5 ml of 1/1000 diluted anti-mouse antibody conjugated to horseradish peroxidase (Millipore, Billerica, MA) and incubated at room temperature on a rotating wheel for 1 h. The discs were washed thrice in PBS-t, 2.5 ml of a 1:1 mixture of enhanced chemiluminescence (ECL) reagents 1 and 2 (GE Healthcare, Buckinghamshire, UK) was applied to the discs and incubated for 5 min. The discs were placed between two sheets of clear plastic and imaged using a LAS4000 imager (Fujifilm, Tokyo, Japan).

2.3.4 Bacterial culture

E. coli HB2151 cells were transferred from glycerol stock to 3 ml of 2YT medium containing 1% glucose and 35 µg/ml chloramphenicol using a sterile loop and grown overnight on a shake tray at 37°C. A sterile loop was used to streak the cells on to

2YT agar containing 1% glucose and 35 µg/ml chloramphenicol. The plates were incubated overnight at 37°C. Single colonies were picked using a sterile toothpick and placed in 3 ml of 2YT medium containing 1% glucose and 35 µg/ml chloramphenicol. The cultures were grown in an incubator at 37°C with shaking at 250 rpm.

2.3.5 Small scale expression of recombinant scFv protein

Single colonies of *E. coli* HB2151 transfected with scFv-constructs were picked into 1 ml of 2YT medium containing 35 µg/ml chloramphenicol and 1% glucose in the wells of a 24 well plate and grown overnight at 37°C with shaking at 250 rpm shaking. 400 µl of overnight bacterial culture was used to inoculate 3 ml of 2YT medium containing 35 µg/ml chloramphenicol in a 30 ml tube. The cultures were incubated for 2 h at 37°C with constant shaking. Recombinant protein production was induced by the addition of IPTG at a concentration of 0.25 mM. The culture was incubated for 4 h at room temperature with shaking.

The culture was transferred to centrifuge tubes and centrifuged for 15 min at 6000 g at 4°C. The pellet was resuspended in 1 ml (2 ml) of ice cold PBS with protease inhibitors (one tablet complete EDTA free protease inhibitors, Roche, Basel, Switzerland, was added to 50 ml PBS). The cells were lysed by sonication (using a W375 cell disruptor, Heat Systems Ultrasonics, Newton, CT, USA.) and the suspension was centrifuged for 10 min at 13,000 g in a microfuge at 4°C. Sodium azide (20 mM) was added to the supernatant as a preservative. The resulting solution was stored at 4°C.

2.3.6 Large scale production of anti-VEGF-B scFv

Single colonies of E.coli HB2151 transfected with scFv construct were picked into 3 ml of 2YT medium containing 35 µg/ml chloramphenicol and 1% glucose (growth medium) in a 30 ml tube and grown for 8 hours at 37°C with shaking at 250 rpm. 1 ml of this culture was used to inoculate 50 ml growth medium in a 250 ml conical flask. The culture was incubated overnight at 37°C with shaking at 250 rpm overnight. Twenty millilitres of the overnight culture was used to inoculate 500 ml of pre-warmed TB broth with, 35 µg/ml chloramphenicol and 0.25% glucose, in a 2 litre conical flask. The culture was incubated for 2 hours at 37°C with 200 rpm shaking. Recombinant protein production was induced by the addition of IPTG to a concentration of 0.25 mM. The culture was incubated for 4 hours at room temperature with shaking at 200 rpm.

The culture was transferred to 500 ml centrifuge tubes and centrifuged for 15 min at 6000 g at 4°C. The pellet was resuspended in 50 ml ice cold PBS with protease inhibitors and homogenised with a dounce homogeniser. The cells were lysed using an Emulsiflex C5 cell disruptor. The lysates were centrifuged at 13,000 g at 4°C for 15 minutes and the resulting supernatant was labelled as crude bacterial scFv lysate.

2.4 Cellular techniques

2.4.1 Cell attachment and culture on pSi-PCL composite material

Pieces of composite material A were sterilised by immersion in 70% ethanol for 5 min, then washed three times with sterile Dulbecco's A phosphate buffered saline (PBS), pH 7.2. The pieces were then transferred into sterile 96-well plates (Becton

Dickinson Labware, Franklin Lakes, NJ, USA) and held in place by polytetrafluoroethylene O-rings. Prior to seeding cells, the material was immersed in DMEM containing 10% FBS, 100 IU/ml penicillin, 100 µg/ml streptomycin sulphate and 0.29 mg/ml glutamine (complete medium) for 5 min. Human lens epithelial cells designated SRA01/04, the kind gift of Professor V. Reddy, Kellogg Eye Centre, University of Michigan, Ann Arbor, MI, USA, were used as a model ocular epithelial cell line. SRA01/04 cells were seeded at 1×10^5 cells per well in 200 µl complete medium. Cells were maintained at 37°C with 5% CO₂ in air.

2.4.2 Enhanced attachment and growth of cells on composite material

The ability of growth factors loaded in the pSi to enhance attachment and growth of cells was examined. Initial experiments focussed on the use of FBS. Composite materials were sterilised and washed as above, then incubated with FBS for 2 h at room temperature. Material incubated in serum-free medium was used as a control. FBS was removed and SRA01/04 cells were seeded as above. After 6 or 24 h of culture, the medium was replaced with complete medium containing 10 nM Hoechst 33342 dye (Sigma-Aldrich, St. Louis, MO, USA) and incubated for 30 min. Unbound dye was removed by washing three times with complete medium. The cells were imaged on an Olympus IX71 inverted microscope or mounted on a slide in complete medium and imaged on an Olympus BX50 fluorescence microscope.

2.4.3 Loading and release of biologics into pSi-PCL composite materials

Pieces of composite material were transferred to a 48 well plate, air-dried and exposed to UV radiation in a laminar air-flow hood for 5 min. Test composites were incubated in 500 µl of 1 mg/ml insulin, 0.55 mg/ml transferrin, 0.67 µg/ml sodium

selenite and 10 µg/ml EGF for 16 h at 4°C in a humidified box, to maintain activity of the biologics. Insulin, transferrin, and selenite improve cell growth in serum-free or serum-low medium⁴⁴⁴. Composites incubated in PBS were used as controls. The materials were washed 5 times in sterile PBS and transferred to a 96 well plate. EGF is a potent mitogen for many mammalian cells, but not for SRA01/04 cells. Thus, BALB/c 3T3 cells (the kind gift of Dr. E. Lousberg, Adelaide University, Adelaide, Australia), which are EGF-responsive⁴⁴⁵, were seeded on the materials at 2×10^4 cells per well and incubated at 37°C and 5% CO₂ in air for 48 h. The number of cells in each well was enumerated using the CellTiter 96® AQueous One Solution (Promega, Madison, WI, USA), according to the manufacturer's instructions.

The release of biologics from the pSi-PCL composite materials was first measured functionally, by their ability to induce proliferation in BALB/c 3T3 cells. Composite materials were loaded as described above. Conditioned medium was prepared by incubating the pSi-PCL composite material in 400 µl DMEM at 37°C for 24 h, transferring to fresh medium for 24 h and finally into fresh medium for 96 h. Unloaded pSi-PCL composite material was used as a control. A proliferation assay with BALB/c 3T3 cells was performed using the CellTiter 96® AQueous One Solution assay as described above, with 50 µl conditioned medium used in place of the pSi-PCL composite materials. Next, the release of insulin from the composite materials was measured. Materials were loaded with insulin, transferrin, and selenite as above and incubated in 200 µl serum free DMEM in a 96 well plate at 37°C. Samples were taken at the end of day 1, day 2 and day 6. The medium was replaced with fresh serum-free DMEM at each time point. The amount of insulin in the conditioned medium was assayed using the Insulin Human ELISA kit (Abcam,

Cambridge, MA, USA), according to the manufacturer's instructions.

2.5 Animal and tissue techniques

2.5.1 Induction and assessment of corneal neovascularization in rats

2.5.1.a *Induction of corneal neovascularization in rats by silver nitrate cautery*

Male or female Sprague-Dawley rats, which were at least 12 weeks old, were anaesthetised using inhaled isoflurane in a glass chamber. Anaesthesia was maintained by administration of 2 l per minute isoflurane (Bomac, NSW, Australia) in oxygen delivered via a nose cone. Topical anaesthetic (0.5% proxymethacaine eye drop, Alcon, Fort Worth, TX, USA) was applied to the right eye for two minutes. A silver nitrate potassium nitrate applicator (Grafc0, QLD, Australia) was dipped in sterile water and the excess liquid removed using a surgical spear. The applicator was gently placed on the central cornea for five seconds (Figure 2-2). The eye was washed with sterile BSS, and Chloromycetin ointment was applied and the eyelid was sutured shut with a 10-0 nylon monofilament sutures. The eyelid suture was removed the following day and inflammation, blister response and neovascularization were monitored daily until euthanasia, using the assessment sheets in appendix A3.2.

2.5.1.b *Topical scFv therapy*

Anti-VEGF-B and control scFv was formulated as eye drops as described in appendix B.13. Rats with induced corneal cautery were treated either immediately

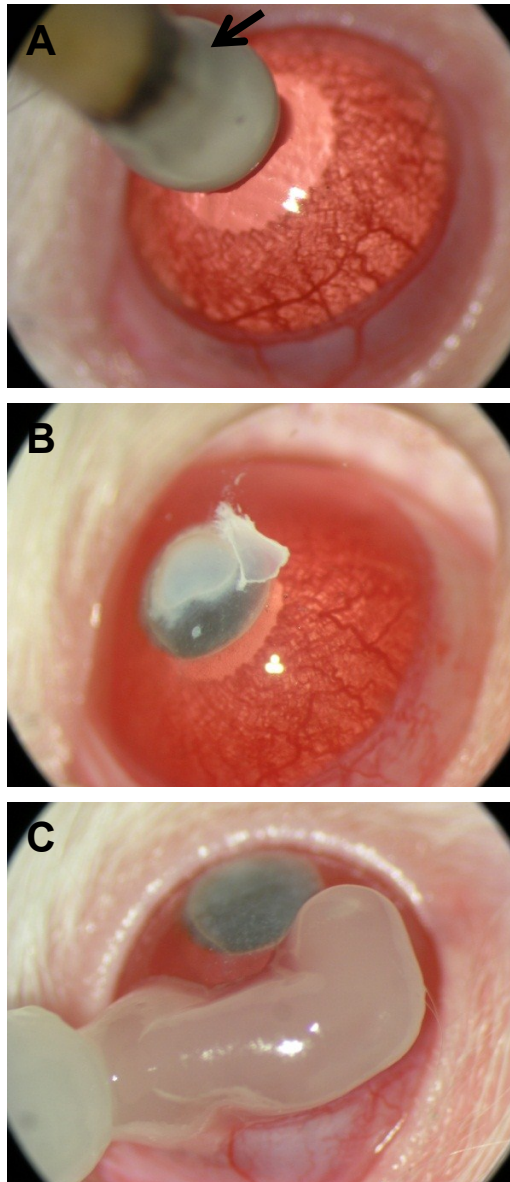


Figure 2-2 Corneal cautery

Sprague-Dawley rats were anaesthetised using inhaled isoflurane. A drop of topical proxymethacaine solution was applied to the right eye. (A) A silver nitrate applicator (Arrow) was wetted in ddH₂O and applied to the central cornea for 5 seconds. (B) A drop of ophthalmic BSS solution was then applied to wash the eye. A white precipitate is seen in the image above the cauterised portion of the cornea. (C) Chloromycetin ointment was applied and the eyelids were closed with a 10-0 monofilament suture for 1 day.

after cautery to assess the effect on developing vessels or the vessels were allowed to develop before commencing of therapy. Rats were restrained using a cloth drape with only their heads remaining uncovered. Five microliters of scFv eye drops were applied to the corneal surface using a micropipette (Figure 2-3). The treatments were repeated for a total of five eye drops per day at 2 hour intervals.

2.5.1.c *Subconjunctival injection of scFv*

Anti-VEGF-B and control scFv were formulated into a temperature responsive gel. A sterile solution of 5 mg/ml scFv and 20% Pluronic F127 (Sigma-Aldrich, St. Louis, MO, USA) was prepared in PBS. The resulting solution is a liquid at 4°C but rapidly gels at body temperature. Ten microliters of the solution was loaded into pre-chilled 31G sterile insulin syringes. Rats were anaesthetised as described in section 2.5.1.a, and the depth of anaesthesia was confirmed by absence of pedal and blink reflexes. The conjunctiva was pulled up with forceps to form a “tent” into which the needle was introduced. The scFv solution was gently injected and the needle was kept in place for approximately 30 seconds to allow the solution to gel (Figure 2-4). 1% Chloromycetin ointment was applied to the eye.

2.5.1.d *Haematoxylin perfusion to stain corneal blood vessels*

Sprague-Dawley rats with induced corneal neovascularization were injected with 35 units of heparin IP per 100g body weight intraperitoneally. The rats were killed by an overdose of inhaled isoflurane 30 mins after injection of heparin. The chest and abdominal cavities were opened and the descending aorta exposed. The inferior vena cava and the descending aorta were clamped close to the heart. A large incision was made in the right auricle and a 22G butterfly needle was inserted into the cavity of



Figure 2-3 Application of eye drops

Rats were carefully restrained using a cloth swaddle, making sure the head remained exposed. Five microliters of eye drop was loaded into a micropipette. The liquid was ejected from the pipette to form a drop at the end of the pipette tip. The drop was carefully applied to the eye of the rat.

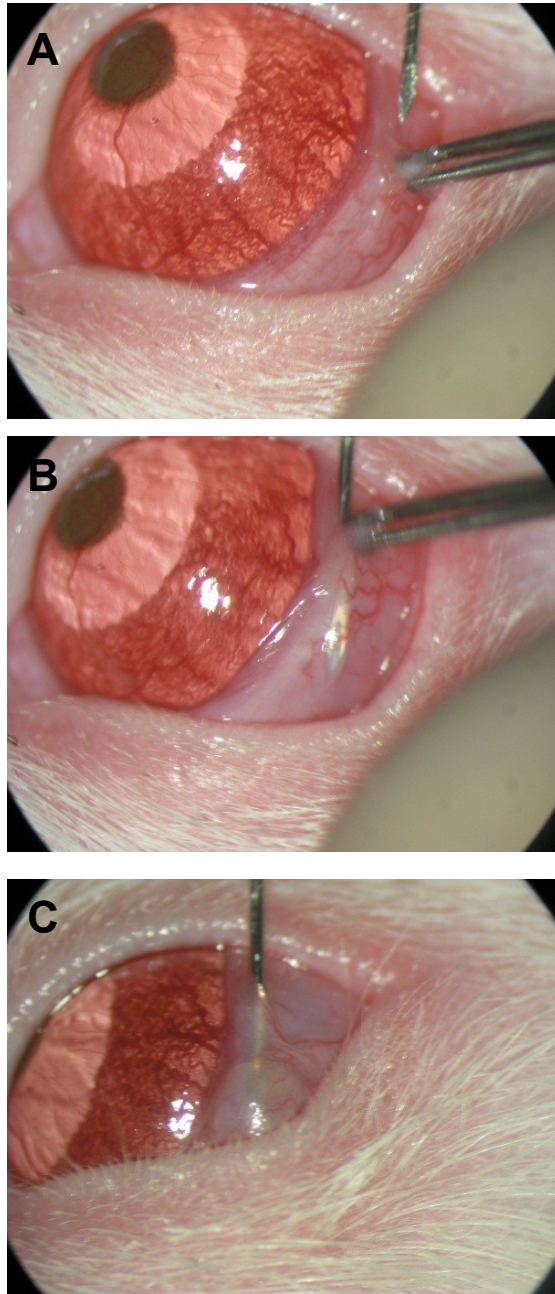


Figure 2-4 Subconjunctival injection of scFv

Sprague-Dawley rats were anaesthetised using inhaled isoflurane.

(A) Subconjunctival injection of scFv was performed using a 31 G needle. The conjunctiva was lifted using forceps (B) and the needle was inserted at the base of the lifted area.(C) scFv was injected and the needle was withdrawn after 20-30 seconds after the solution had gelled.

the left ventricle. The rat was perfused with 50 ml warm saline containing 4 U/ml heparin and 0.32 ml/l papaverine HCl, followed by 50 ml of 1:3 haematoxylin: PBS pH6.0 containing 0.32 ml/l papaverine HCl, at 120 mmHg through the butterfly needle using the setup depicted in Figure 2-5. The eyes were enucleated and placed in buffered formalin for 1 h at room temperature and then placed in PBS. The cornea was then dissected out and flatmounted as described in section 2.5.1.e.

2.5.1.e *Corneal flatmounting*

Haematoxylin perfused formalin fixed rat eyes were removed from PBS and blotted on tissue paper. An incision was made in the sclera approximately 2 mm from the limbus. The cornea with a scleral rim was excised using scissors. The iris was removed using forceps. The cornea was placed on a slide with 2-3 drops of buffered glycerol. A scalpel blade was used to make four radial cuts at 90° to each other and extending $\frac{3}{4}$ of the way to the centre of the cornea. The cornea was then flattened using a forceps and a coverslip applied. A weight was placed on the coverslip to further flatten the cornea and the coverslip sealed with nail polish. Flatmounts were imaged using an Olympus BX51 microscope.

2.5.1.f *Image analysis*

Images of corneal flatmounts were processed in Photoshop CS2 (Adobe, San Jose, USA) using the auto level command. Montages were prepared using the photomerge function. Montaged images were then coded so that the quantification of corneal vessel area was performed in a masked fashion. Images were processed in ImageJ (National Institutes of Health, USA) and the area of the central corneal burn was selected using the freehand selection tool. The selected area was then removed. The

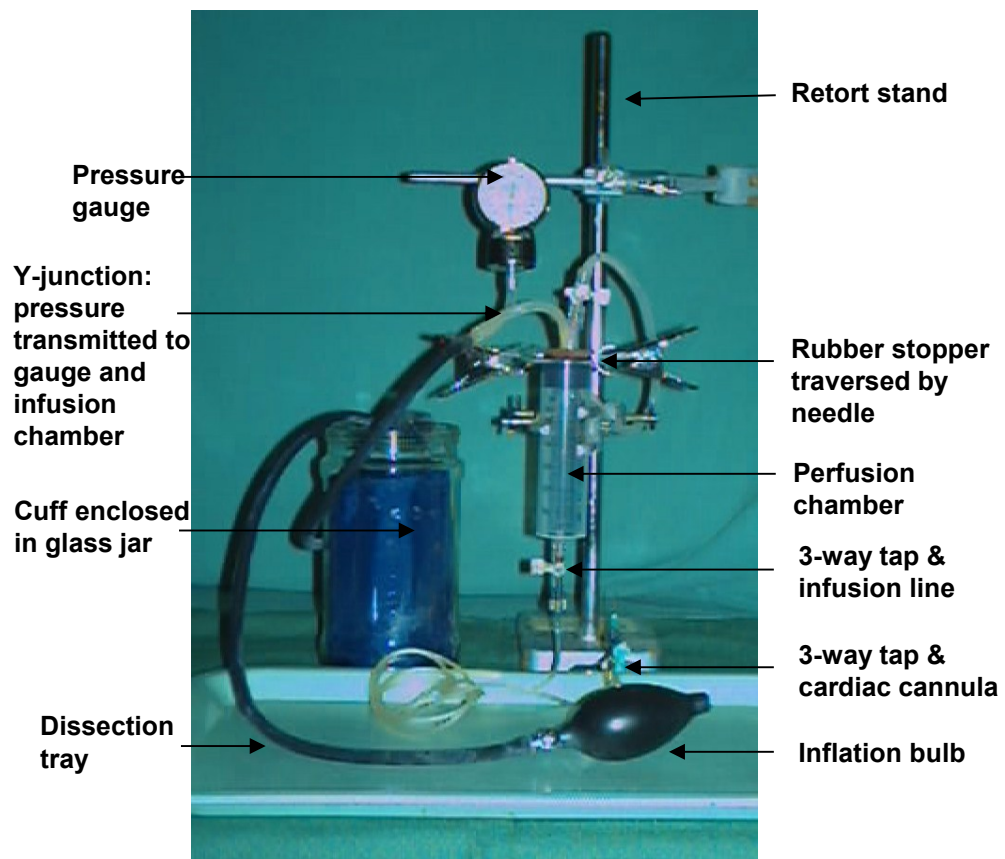


Figure 2-5 Haematoxylin perfusion setup

The apparatus used to perfuse the vasculature of rats with haematoxylin, in order to stain corneal vessels, is pictured above. A sphygmomanometer was modified to provide regulated pressure. The perfusion chamber (60 ml syringe) contained the perfusion solution, which was delivered through a 23 G cannula at 120 mmHg, attached to the perfusion chamber with rubber tubing. Image provided by Dr. Peter van Wijngaarden, Flinders University.

freehand selection tool was used to select the corneal area including some sclera. The selection was copied to a new image file. The paintbrush tool was used to remove all areas beyond the limbal arcades. The image was converted to a RGB stack and the green channel, which had the maximum contrast, was copied to a new file. The brightness and contrast of the file was optimised to show vessels. The colour threshold function was applied and the level was adjusted to select the vessels with minimal background (Figure 2-6). The “analyse particles” function was used to measure the area covered by vessels. The freehand selection and measure tools were used to measure the total corneal area. The following formula was used to calculate the percentage of corneal area covered by vessels.

$$\text{Percent area of vessels} = \left(\frac{\text{Measured vessel area}}{\text{Total corneal area} - \text{cauterised area}} \right) * 100$$

2.5.2 Harvest of rat oral mucosal epithelial cells and transfer to the rat eye

2.5.2.a Harvest and culture of oral mucosal epithelial cells from the rat

Male Sprague-Dawley rats aged between 4 to 6 weeks were euthanised by an overdose of inhaled isoflurane. The rat was immersed in povidone iodine solution for 2 minutes ensuring that the buccal cavity was bathed in liquid. The buccal cavity was washed with ophthalmic BSS-antibiotic solution (BSS supplemented with 200U/ml penicillin, 200 µg/ml streptomycin and 10 ng/ml amphotericin). The rat was placed on a sterile field in a laminar flow hood and oral mucosal tissue was dissected out using a scalpel blade and dissecting scissors, making sure the underlying tissue was not taken. The tissue was washed with BSS-antibiotic solution and placed in one

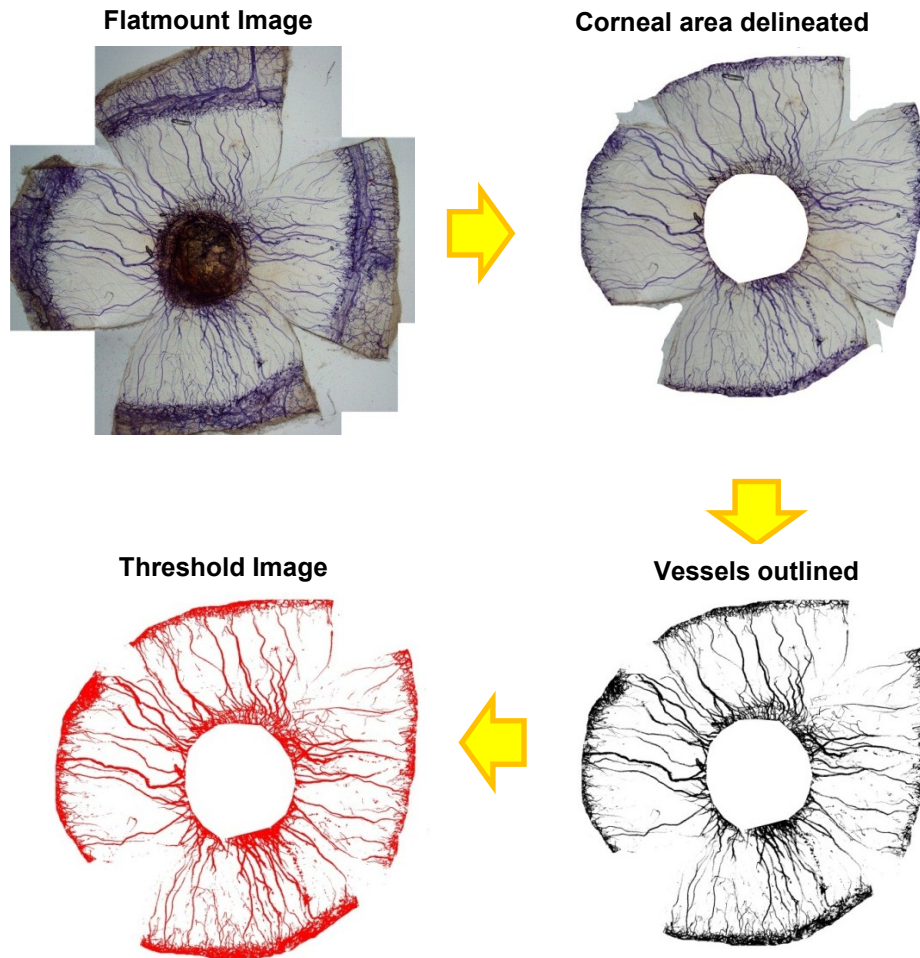


Figure 2-6 Quantification of corneal vessel area

Flatmounted rat corneas with vessels perfused with haematoxylin were imaged on an Olympus BX51 microscope. A montage image was generated using Adobe Photoshop. Image analysis was performed using ImageJ software. First the corneal area was delineated by removing the area beyond the limbal arcades. The image was converted to a RGB stack and all processing was performed on the green channel, as this channel had the maximum contrast. The file was converted to 8-bit and the vessels were outlined. The image was next thresholded and the “analyse particles” function applied to measure the vessel area. The cornea was outlined using the polygon function and the area measured. The percent of the cornea covered by vessels was then calculated.

millilitre of MCDB153 medium with 2.2 U/ml dispase I (Life Technologies, Carlsbad, CA, USA) for 1 hr at 37°C. The epithelial tissue was then gently detached from underlying tissue using forceps, washed in sterile BSS and placed in 500 µl 0.25% trypsin, 2.65 mM EDTA in BSS for 5 minutes. The tissue was gently disaggregated using two 21 gauge needles and 1 ml MCDB153 with 10% FBS, insulin transferrin sodium selenate supplement, 100 U/ml penicillin/ 100 µg/ml streptomycin, 5 ng/ml amphotericin, 5 ng/ml EGF, 10 ng/ml β-NGF, 200 ng/ml hydrocortisone and 0.03 pg/ml tri-iodothyronine (complete medium). The cells were washed with 10 ml complete medium and pelleted at 100 g for 5 minutes. The cells were resuspended in 100 µl complete medium and seeded on collagen IV and vitronectin coated aminosilicised pSi membranes in 24 well plates. The cells on the pSi were placed in an incubator at 37°C with 5% CO₂ in air for 1 hr to allow attachment, and then 1 ml of complete medium was added. The medium was replaced with fresh complete medium the following day then twice weekly. The cells were used at passage 1 and up to two donor rats were used per experiment.

2.5.2.b Antibody labelling of oral mucosal epithelial cells

Rat oral mucosal epithelial cells (OMECE) grown on porous silicon scaffolds were transferred to 96 well plates. The cells were fixed with 4% paraformaldehyde in PBS for 10 min at room temperature and permeabilised in 0.4% Triton X-100 in PBS for 5 min. 5% v/v goat serum (Life Technologies, Carlsbad, CA, USA) in PBS for 2 h was used to block non-specific binding. The cells were then incubated with primary antibodies diluted in PBS with 1% v/v goat serum as described in Table 2-7 for 1 hr at room temperature. Unbound antibody was washed off using PBS and a goat anti-mouse IgG Alexa Fluor[®] 488 secondary antibody diluted 1/500 in PBS was

incubated with the cells for 1 hr at room temperature in the dark. The nuclei of the cells were counterstained with 2 µg/ml Hoechst 33342 for 5 min. Where the protein of interest localised to the nucleus, cytoplasmic actin was stained with 1/200 Alexa Fluor 594 phalloidin (Life Technologies, Carlsbad, CA, USA). Excess stain was removed by washing with PBS four times, the cells were mounted in buffered glycerol and fluorescence imaged on an Olympus BX50 microscope.

Table 2-7 Primary antibody dilutions for labelling of rat OMEC

Primary antibody	Dilution
CK3/12 clone AE5	1/100
CK19 clone E6	1/100
P63 clone 4A4	1/100
ABCG2 clone 5D3	1/200

2.5.2.c Labelling rat OMEC with the cell tracker dye PKH26

Rat OMEC grown on pSi scaffolds were washed once with serum free medium followed by diluent C (from PKH cell labelling kit, Sigma-Aldrich, St Louis, MO, USA). One millilitre of diluent C was then added to the cells, followed by 1 ml of PKH26 dye solution (1×10^{-7} M). Cells were incubated in dye solution for 5 mins. The staining reaction was stopped by the addition of 2 ml of FBS for 1 min. The cells were then washed once with complete medium to remove unbound dye.

2.5.2.d *Surgical implantation of porous silicon materials into the rat eye*

Female Sprague-Dawley rats were anaesthetised using inhaled isoflurane. A drop of 0.5% proxymethacaine (Alcon, Fort Worth, TX) was placed on the right eye for two minutes to provide local anaesthesia. Incisions were made in the conjunctiva and a pocket was blunt dissected using scissors. pSi membranes were inserted into the pocket and the opening closed using 10-0 Ethilon monofilament nylon sutures (Ethicon, Piscataway, NJ, USA). The procedure was repeated so as to have an implant in the superior, inferior and temporal regions of the eye. 1% chloramphenicol ointment (Parke Davis, Caringbah, NSW, Australia) was placed on the eye and the eyelid sutured shut with a single suture for 24 h. The implanted eye was monitored under the operating microscope thrice weekly for two weeks and then once weekly. The implants were photographed weekly using an Olympus E-330 digital camera. The cells from the ocular surface were sampled using FTA paper (Millipore, Billerica, MA), as described in section 2.5.2.e. The animals were killed by an overdose of inhaled isoflurane eight weeks after implantation and the eyes were enucleated for histology.

2.5.2.e *Impression cytology using FTA paper*

Rats were anaesthetised with inhaled isoflurane and the tear film was absorbed using a surgical spear. A 2 mm disc of FTA paper was applied to the central cornea, using a forceps, and gently agitated in a circular motion to collect superficial cells. The FTA disc was then placed in a sterile PCR tube for analysis. The forceps was washed with 10 M NaOH, 1 M HCl and 70% ethyl alcohol between samplings to prevent contamination.

2.5.2.f *Induction of mild ocular surface disease by n-heptanol*

Female inbred Sprague-Dawley rats were anaesthetised using inhaled isoflurane in a glass chamber. Anaesthesia was maintained by administration of 2 l per minute isoflurane in oxygen delivered via a nose cone. Topical anaesthetic (1% topical amide eye drop) was applied to the right eye for two minutes. A sterile cotton swab was dipped in n-heptanol (Sigma-Aldrich, St. Louis, MO, USA) and gently placed on the central cornea. The swab was then run across the surface of the cornea in a spiral motion for 5 seconds. The eye was washed with sterile BSS, Chloromycetin ointment was applied and the eyelid was sutured shut. The eyelid suture was removed the following day and inflammation, blister response and neovascularization were monitored daily for a week. Impression cytology was performed weekly to confirm induction of OSD by the presence of conjunctival goblet cells on the corneal surface.

2.5.2.g *Impression cytology of the rat eye to confirm OSD*

Rats with n-heptanol-induced OSD were anaesthetised and a surgical spear was used to absorb excess liquid from the eye. A 2x2 mm piece of cellulose acetate membrane (Sigma-Aldrich, St. Louis, MO, USA) was then placed on the central cornea and held in place using a forceps. After 10-15 seconds the membrane was gently removed, taking care that the epithelial cells remained attached to it. The membranes were fixed to a glass slide using double sided tape and placed in 100% ethanol for 1 hr. The membranes were rehydrated by passing through 90% ethanol for 2 minutes followed by 70% ethanol for 2 minutes and distilled water for 2 minutes. The membranes were dipped in distilled water then placed in 1% periodic acid for 2 minutes followed by distilled water for 2 minutes, Schiff's reagent for 10 minutes, washed in tap water for

5 minutes then stained with haematoxylin and mounted in DePeX medium (Sigma-Aldrich, St. Louis, MO, USA).

2.5.2.h *Fixation, processing and embedding*

The enucleated eyes were fixed in 10% (v/v) buffered formalin for a minimum of 24 hours. The globes were dehydrated through 70% (v/v) ethanol, 80% (v/v) ethanol, 90% (v/v) ethanol, each for 1 h followed by 3 changes of 100% (v/v) ethanol for 30 min each. The globes were then left in 100% (v/v) chloroform overnight. The globes were placed in molten paraffin wax at 60°C for 45 min, then in fresh wax under vacuum for two 45 minute periods and embedded in fresh wax. The paraffin blocks were sectioned on a microtome; 5 mm sections were cut, mounted on chrome-alum subbed slides and air dried at 40°C before storage at room temperature.

2.5.2.i *Haematoxylin and eosin staining*

Paraffin-embedded sections were dewaxed by two consecutive 2 minute washes in 100% (v/v) xylene. They were rehydrated by 2 minute washes in 100% (v/v), 100% (v/v), 90% (v/v) and 70% (v/v) ethanol, and water. The sections were stained with modified Harris haematoxylin for 10 minutes, rinsed in water, dipped in acid alcohol for 2 seconds and rinsed in water again. Blue haematoxylin stain was developed by incubation in 0.05% (w/v) lithium carbonate for 2 minutes, then rinsed and counterstained with eosin for 2 minutes. Excess eosin stain was removed by washing with water for 5-7 minutes. The sections were dehydrated with three 30 second washes in 100% (v/v) ethanol, and two 1 minute washes in xylene then cover-slipped with DePeX mounting medium.

2.6 Statistical analyses

The statistical program IBM SPSS statistics 22 (IBM, Armonk, NY, USA) was used to perform all statistical analysis. Statistical analysis was performed with advice from a statistician, Dr. Miriam Keane, Department of Ophthalmology, Flinders University.

Data were first analysed for normality using the Shapiro-Wilk test with a p-value >0.05 indicating the data was normally distributed. As all data were found not to be normally distributed, non-parametric tests were used. Where two groups were being compared, the Mann-Whitney U test was used. If three or more groups were compared, the Kruskal-Wallis test was used. Comparisons between subsets of data were carried out using Mann-Whitney U tests with Bonferroni correction for multiple testing. The significance level (alpha) was set at 0.05.

CHAPTER 3 POROUS SILICON MATERIALS AS CARRIERS OF CELLS AND DRUGS TO THE EYE

3.1 Porous silicon as an ocular implant

Although porous silicon (pSi) was first discovered in the 1950's, little was known about its biocompatibility until the 1990's³⁶¹. Porous silicon supports the attachment and growth of a variety of mammalian cells *in vitro*^{370, 371, 391}. The biocompatibility of pSi *in vivo* has been demonstrated by subcutaneous implantation in guinea-pigs and implantation into the abdominal wall in rats^{363, 366}. In the context of the eye, a pSi membrane implanted under the rat conjunctiva slowly dissolves, but is still visible 8 weeks post implantation³⁹¹. The implant does not damage the surrounding tissue and does not cause inflammation or neovascularization, however a thin fibrous capsule forms around it³⁹¹. Eventually, pSi degrades into non-toxic silicic acid³⁶¹. The highly porous nature of pSi (Figure 3-1 A) gives it a large surface area to volume ratio³⁵⁹ which allows loading of a large amount of substances such as proteins⁴⁴⁶ and drugs³⁵¹. The size and shape of the pSi pores can be altered to mimic the structure of the limbal palisades of Vogt (Figure 3-1 B & C). Furthermore, self-reporting of drug release from multilayered pSi microparticles can be achieved, as the pSi changes colour as it degrades³⁶⁰. Being inorganic, pSi is also easily sterilised by autoclaving³⁹². These properties taken together suggest that pSi might make an excellent implant for the eye.

The overarching aim of this part of my study was to determine whether pSi materials could be used to transfer cells and drugs to the rat eye, with the view to creating an artificial stem cell niche for the treatment of ocular surface disease (OSD). Two pSi materials were tested: the first material was a freestanding pSi membrane, and the

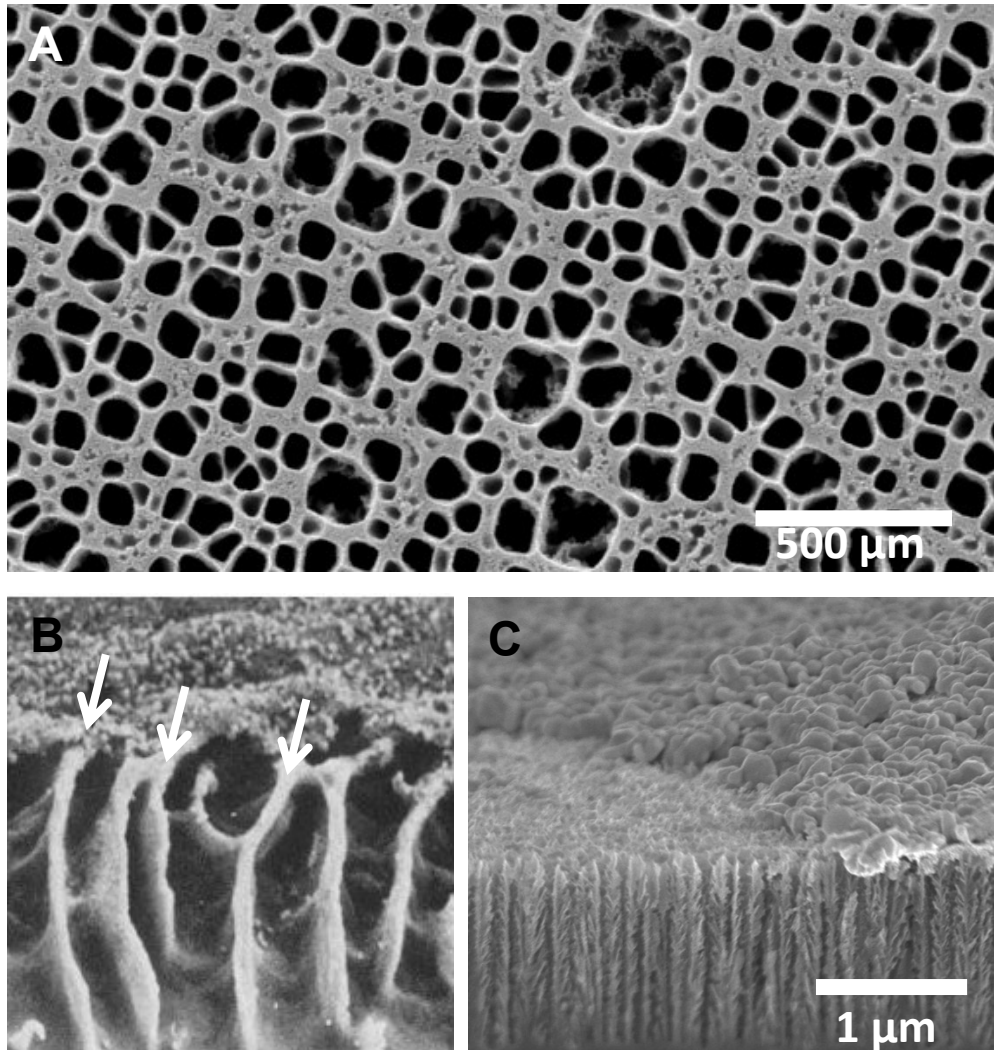


Figure 3-1 Porous silicon membranes

(A) Scanning electron micrograph (SEM) of a porous silicon membrane demonstrating its highly porous nature. Image courtesy Dr. Steven McInnes, University of South Australia. (B) SEM of the limbal palisades of Vogt from Gipson *et al* 1989¹⁴. The arrows points to the palisades of Vogt. (C) SEM of a pSi membrane, showing some similarities in structure to the palisades of Vogt.

second a composite prepared from a non-woven polymer fabric with pSi microparticles embedded in the fibres. Cell growth, drug loading and ocular biocompatibility of the two materials were assessed. Our hypothesis was that pSi materials coated with growth factors would support the growth of oral mucosal epithelial cells, including stem cells, and that the cells would migrate across the corneal surface after implantation under the rat conjunctiva. The following sections will present the results of these experiments and discuss the advantages and limitations of the two pSi materials.

3.2 Exploration of porous silicon membranes as a stem cell niche

3.2.1 Harvest and culture of oral mucosal epithelial cells from the rat

Oral mucosal epithelial cells might provide a suitable alternative to corneal epithelium, and oral mucosa itself is a source of stem cells. Oral mucosal tissue was surgically dissected from young (6-8 week old), male, inbred Sprague-Dawley rats, and enzymatically digested to yield a single cell suspension. The cells were grown on collagen IV-coated glass coverslips, in low calcium medium, to maintain the cells in an undifferentiated state, with growth factors to stimulate proliferation of the cells, as described in section (section 2.5.2.a).

Oral mucosal epithelial cells (OMECS) proliferated to form colonies over a period of 7 days (Figure 3-2 A). The colonies were approximately circular with a cobblestone appearance, and contained densely packed cuboidal cells (Figure 3-2 B). Cells on the borders of the colonies appeared to be more flattened. On further culture, the cells

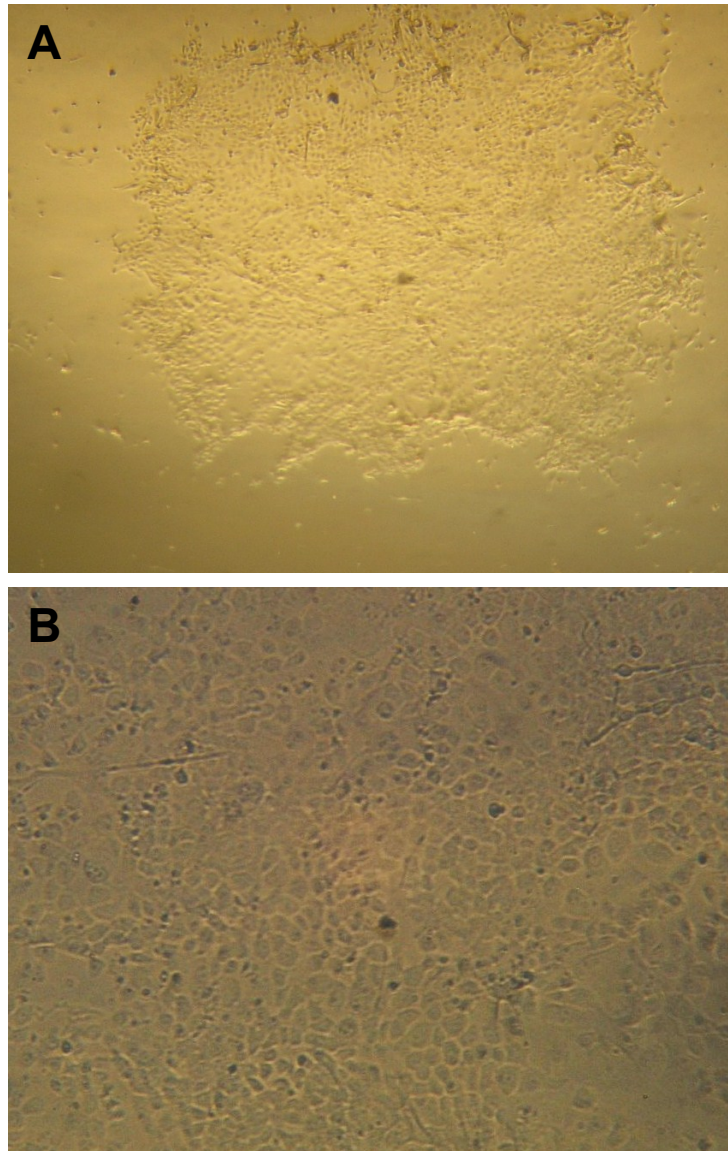


Figure 3-2 Rat oral mucosal epithelial cells grown on collagen IV coated tissue culture plates

Oral mucosal tissue was harvested from young (6-8 week old) male inbred Sprague-Dawley rats, and enzymatically disassociated to yield a single cell suspension. The cells were seeded on collagen coated tissue culture plates, and grown for 7 days. **(A)** Rat oral mucosal epithelial cells proliferated to form round colonies (original magnification 100X). **(B)** The centre of OMEC colonies contained densely packed cuboidal cells (original magnification 200X). Images captured at the inverted light microscope.

did not form a stratified epithelium, as the superficial cells detached from underlying cells.

3.2.2 Oral mucosal epithelial cells grown on collagen IV coated pSi express corneal epithelial cell markers

OMECS were seeded on collagen IV coated porous silicon membranes and allowed to grow for 7 days. The cells were fixed and probed with antibodies raised against the corneal epithelial cell marker CK3/12 and the basal epithelial cell marker CK19. The cytokeratins are found in the intermediate filaments of the cytoskeleton, and were expected to be expressed in the cytoplasm. Strong cytoplasmic expression of CK3/12 was observed in the OMECS grown on collagen IV coated pSi membranes (Figure 3-3). At higher magnifications (40X objective), the CK3/12 antibodies appeared to label thin fibrils, an appearance consistent with CK3/12 being an intermediate filament protein⁶⁶. Labelling for CK19 was not as intense as CK3/12 labelling. Weak labelling was observed in a large proportion of cells (Figure 3-3). A few cells showed more intense labelling. In some cells, intense nuclear labelling accompanied the cytoplasmic labelling (Figure 3-3). CK19 might be present in the nucleolus, or structural elements of the nucleus in these cells. The expression of corneal epithelial cell markers in the OMECS highlights the similarities between oral mucosal epithelium and corneal epithelium. Rat OMECS might thus be considered near-corneal epithelial equivalents, however a population of stem cells within the OMEC population would be required for long-term reconstruction of the corneal epithelium in OSD. In the next section, the pSi membranes were coated with factors with the view to recreating a niche environment for stem cells.

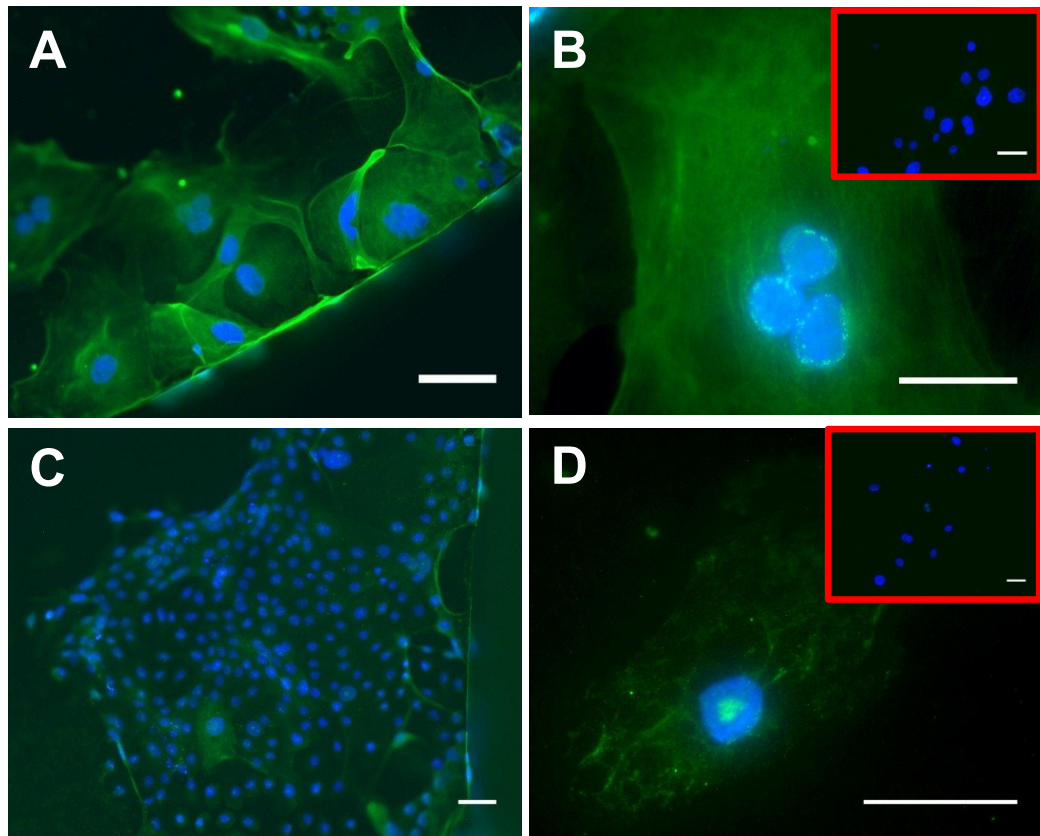


Figure 3-3 Oral mucosal epithelial cells grown on porous silicon membranes express corneal epithelial cell markers

Rat oral mucosal epithelial cells (OMECS) were seeded on porous silicon membranes, and allowed to grow for 7 days. Cells were labelled for the cytoskeletal proteins cytokeratin (CK) 3/12, expressed by superficial corneal epithelial cells, and CK19, expressed by basal epithelial cells, using monoclonal antibodies. **(A) and (B)** CK3 expression in rat OMECS. CK3/12 is normally expressed by differentiated corneal epithelial cells. **(C) and (D)** CK19 expression in rat OMECS. Inserts show an isotype matched negative control. Scale bars 50 μm , insert scale bar 10 μm . Nuclei stained with Hoechst 33342 dye.

3.2.3 Characterization of OMECs grown on pSi scaffolds coated with collagen IV and vitronectin

The effect of coating pSi membrane scaffolds with collagen IV, vitronectin, or a combination of the two, on expression of cytokeratins and putative stem cell markers in adherent OMECs was investigated. Collagen IV is a major component of the limbal epithelial basement membrane, and has been used to enrich stem cells from the limbus⁴⁴⁷ and oral mucosa⁴⁴⁸. Vitronectin is an extracellular matrix protein, which is expressed at the limbus⁷⁷, and has been shown to support corneal epithelial cell migration and proliferation^{449, 450}. Coating pSi membranes with collagen IV and vitronectin might create a niche environment to maintain stem cells.

Porous silicon membranes were coated with 10 $\mu\text{g}/\text{cm}^2$ collagen IV, 1 $\mu\text{g}/\text{cm}^2$ vitronectin or a mixture of the two. OMECs were seeded on the scaffolds and allowed to grow for 7 days. The cells were fixed and probed with antibodies raised against CK3/12, CK19, p63 and ABCG2. CK3/12 is expressed by differentiated corneal epithelial cells^{66, 73}, whereas CK19 is expressed by basal epithelial cells of the peripheral cornea⁶⁶. p63 is a nuclear transcription factor, expressed by transient amplifying cells⁴⁶. ABCG2 is a membrane bound transporter protein, that is associated with the side population cells, which are able to efflux Hoechst dye^{53, 54}. High levels of ABCG2 have been found in a number of stem cells, making it a putative stem cell marker⁵².

CK3/12, a corneal epithelial differentiation marker, was expressed by OMECs grown on pSi membranes, regardless of the protein coating. However, the expression was variable, with some cells expressing the marker strongly while others showed either

weak, or no expression. On collagen IV-coated pSi membranes, some colonies of OMECs completely lacked CK3/12, while others showed strong expression (Figure 3-4 A & B). On vitronectin or collagen IV plus vitronectin coated pSi, the OMECs displayed expression of CK3/12 at the periphery of the colonies, with little or no expression in the centre (Figure 3-5 A, Figure 3-6 A). This could indicate that cells at the periphery had undergone more replications, and had differentiated more than the cells at the centre of the colonies.

The expression of CK19, a basal epithelial cell marker⁶⁶, was uniformly weak across the various coatings. OMECs grown on collagen IV displayed patchy, cytoplasmic labelling, with some cells displaying strong intranuclear labelling (Figure 3-4 C). Vitronectin coated materials displayed a uniform, but weak, cytoplasmic expression of CK19 (Figure 3-5 B, Figure 3-6 B).

The nuclear transcription factor p63, which labels transient amplifying cells (TACs), was expressed in a large proportion of OMECs grown on collagen IV, vitronectin, and collagen IV plus vitronectin coated pSi membranes (Figure 3-4 D, Figure 3-5 C, Figure 3-6 C). Strong nuclear expression of the marker was observed, with no observable differences related to growth of the cells on different protein substrates. High levels of expression of p63 indicated that a large proportion of the cultured OMECs had some proliferative potential.

A small proportion of OMECs expressed the putative stem cell marker ABCG2. Cytoplasmic expression of ABCG2 was observed in OMECs grown on all of the coatings under investigation (Figure 3-4 E, Figure 3-5 D, Figure 3-6 D). ABCG2 expression might indicate the presence of putative stem cells in the OMECs.

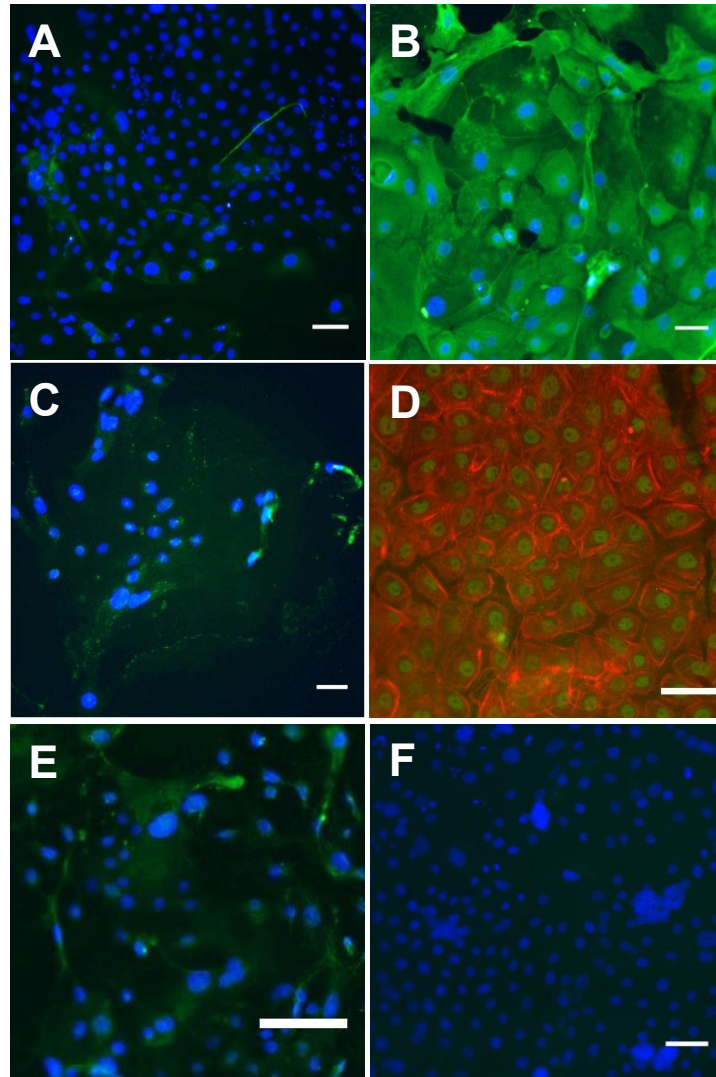


Figure 3-4 Expression of epithelial and putative stem cell markers in rat oral mucosal epithelial cells grown on collagen IV coated pSi membranes

Rat oral mucosal epithelial cells (OMECS), 7 days after seeding on collagen IV coated, porous silicon scaffolds. **(A)** and **(B)** Differential expression of CK3/12 (green). Some colonies exhibited strong expression of CK3/12 while others displayed little or no expression. **(C)** Expression of CK19 (green) was low. **(D)** Nuclear expression of p63 (green) was observed in a large proportion of OMECS. Actin filaments labelled with Alexa Fluor 594 phalloidin (red). **(E)** A small proportion of OMECS expressed ABCG2 (green). **(F)** Isotype matched negative control antibody. Nuclei stained with Hoechst 33342. Scale bars 50 μm .

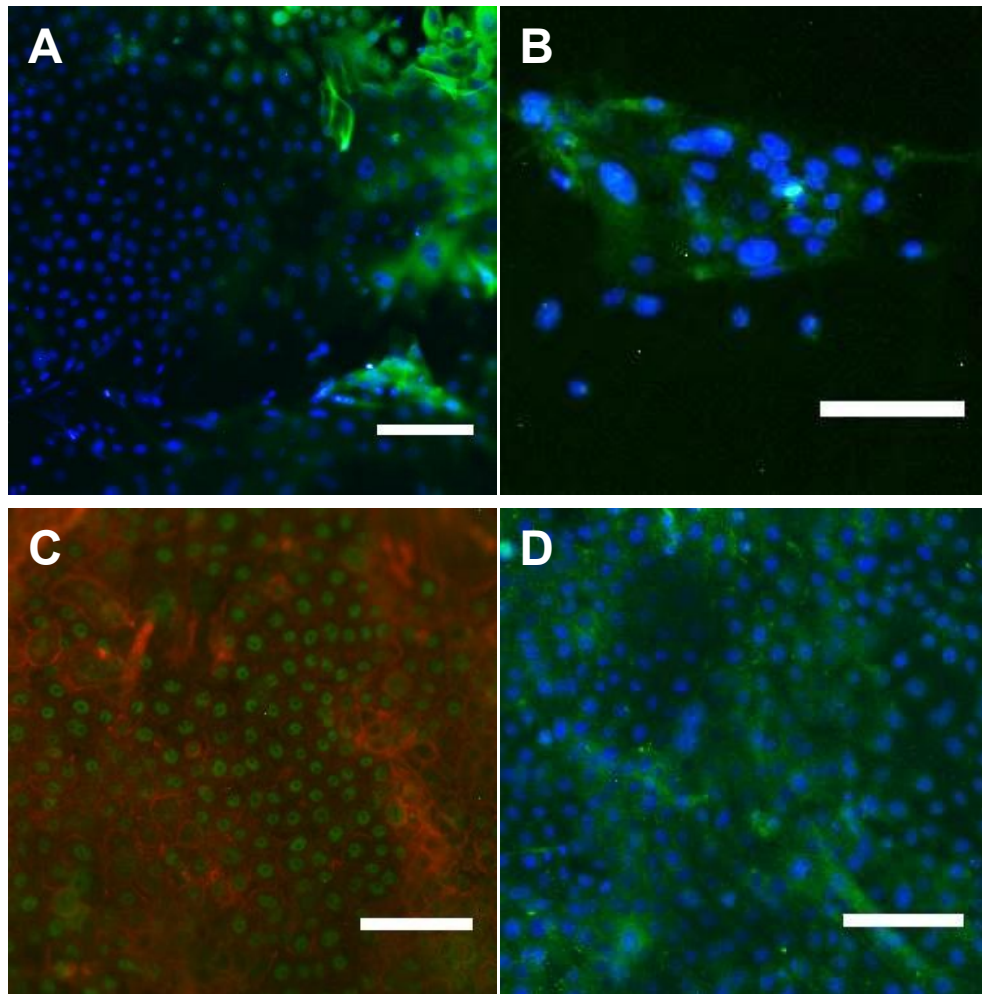


Figure 3-5 Expression of epithelial and putative stem cell markers in rat oral mucosal epithelial cells grown on vitronectin coated membranes

Rat oral mucosal epithelial cells (OMECS), 7 days after seeding on vitronectin coated, porous silicon scaffolds. **(A)** Expression of CK3/12 was variable. Some cells expressed CK3/12 strongly, while others lacked cytoplasmic expression. **(B)** Weak expression of CK19 was observed in OMECS. **(C)** OMECS expressed the nuclear transcription factor p63 (green). Actin filaments were stained with Alexa Fluor 594 phalloidin (red). **(D)** The putative stem cell marker ABCG2 was weakly expressed. Nuclei stained with Hoechst 33342. Scale bars 50 μ m.

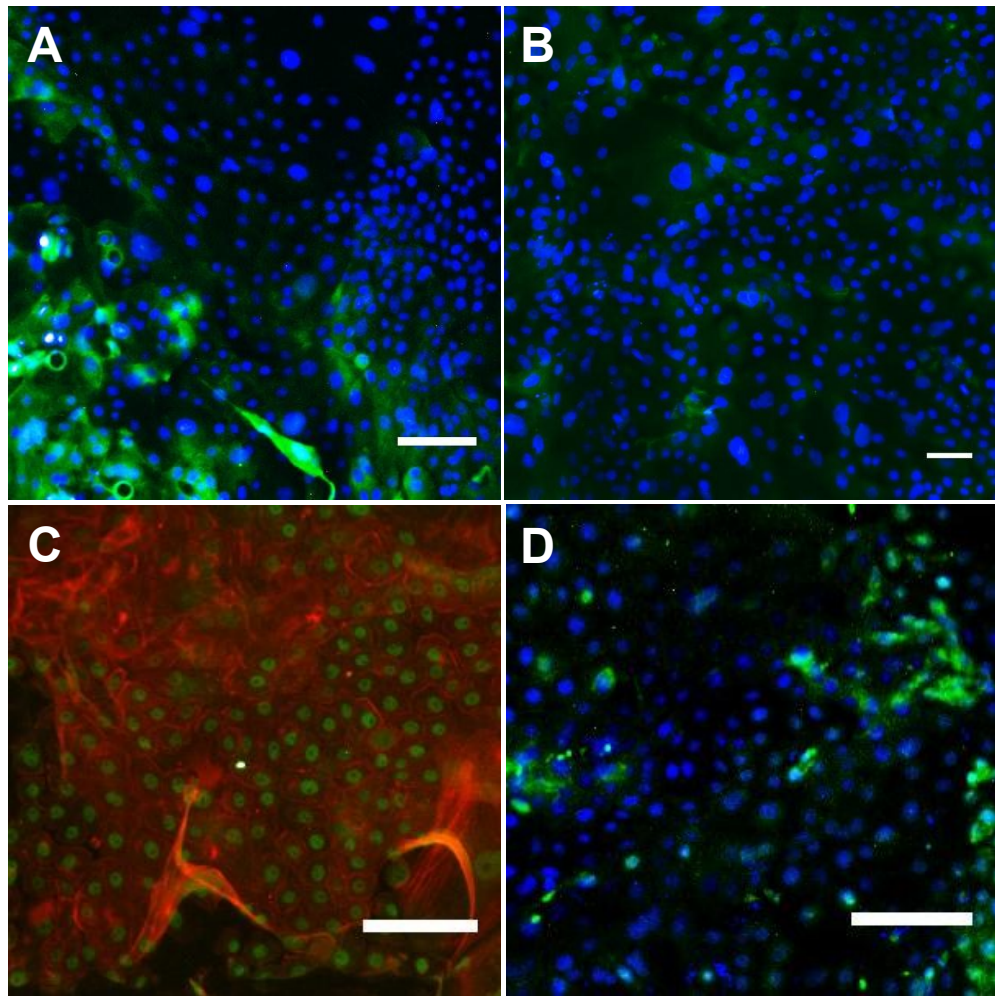


Figure 3-6 Expression of epithelial and putative stem cell markers in rat oral mucosal epithelial cells grown on collagen IV plus vitronectin coated pSi

Rat oral mucosal epithelial cells (OMECS), 7 days after seeding on collagen IV plus vitronectin coated, porous silicon scaffolds. **(A)** The expression of CK3/12 was variable, with patches of cells strongly expressing the marker, while other cells did not express it. **(B)** The basal epithelial cell marker CK19 was weakly expressed in some OMECS. **(C)** A majority of OMECS expressed p63 in their nuclei. **(D)** A small proportion of OMECS expressed the putative stem cell marker ABCG2. Nuclei stained with Hoechst 33342. Scale bars 50 μm .

OMECs grown on pSi membranes consisted mostly of p63 expressing transient amplifying cells. Differentiated cells expressing CK3/12 were also observed. A small proportion of cells expressed the putative stem cell marker ABCG2. These cells were potentially stem cells.

The expression of markers in OMECs grown on pSi membranes with collagen and vitronectin coatings is summarised in Table 3-1. There was no significant difference in expression of epithelial cell or putative stem cell markers between the coatings tested, indicating that both collagen IV and vitronectin could support the growth of OMECs on pSi membranes.

Table 3-1 Summary of cytokeratin profile and putative stem cell marker expression in OMECs grown on pSi membranes

Group	Marker expressed			
	CK 3/12	CK 19	p63	ABCG2
Collagen IV	-/+++	+ weak	+++	-/+
Vitronectin	-/++	+ weak	+++	-/+
Collagen IV + Vitronectin	-/++	+ weak	+++	-/++

- No expression + expressed in some cells ++ expressed in a few cells +++ expressed in a majority of cells.

3.2.4 Stability and biocompatibility of pSi membranes *in vivo*

Rat OMECs were successfully grown on pSi membranes and expressed corneal epithelial, transient amplifying cell and putative stem cell markers. Next, the ability of the cells to migrate off the pSi scaffold on to the ocular surface was assessed. OMECs were harvested from young male inbred Sprague-Dawley rats and cultured

on pSi scaffolds, coated with collagen IV or vitronectin for 7 days. Collagen IV is a major constituent of epithelial basement membranes⁴⁵¹ and promotes migration of corneal epithelial cells⁴⁵². Furthermore, collagen IV is expressed in the limbus but not in the central cornea⁷⁹. Migration of cells off the pSi scaffold onto the ocular surface is desirable for the treatment of ocular surface disease. Vitronectin is expressed at the limbus, and is thought to maintain corneal epithelial stem cells⁴⁵⁰.

As the pSi is opaque, the cells could not be visualised by microscopy. However, the presence of cells on the pSi distorted the surface of the pSi, making visual inspection possible. The presence of cells on the surface of the pSi was confirmed visually before implantation into animals. Three pieces of pSi membrane, measuring 2 x 2 mm each, were implanted under the conjunctiva of female inbred Sprague-Dawley rats. An incision in the conjunctiva was used to blunt-dissect a pocket beneath the conjunctiva. The pSi membranes carrying cells were carefully placed into the pockets, with the side carrying cells facing anteriorly. The pocket was closed with 10-0 nylon sutures. The rats were observed under the operating microscope weekly for 8 weeks.

The pSi scaffold was clearly visible under the conjunctiva immediately after implantation (Figure 3-7 A). Implantation of the pSi scaffold caused mild inflammation (redness) up to 2 week post-implant, and neovascularization. Two weeks later, the pSi scaffold was still visible. New vessels had grown in the vicinity of the implant, and appeared denser around the sutures (Figure 3-7 B). Four weeks post-implant, no residual inflammation was apparent. The pSi scaffold had undergone degradation, as evidenced by the change in colour of the implant from black to brown (Figure 3-7 C). The implant remained visible at the operating

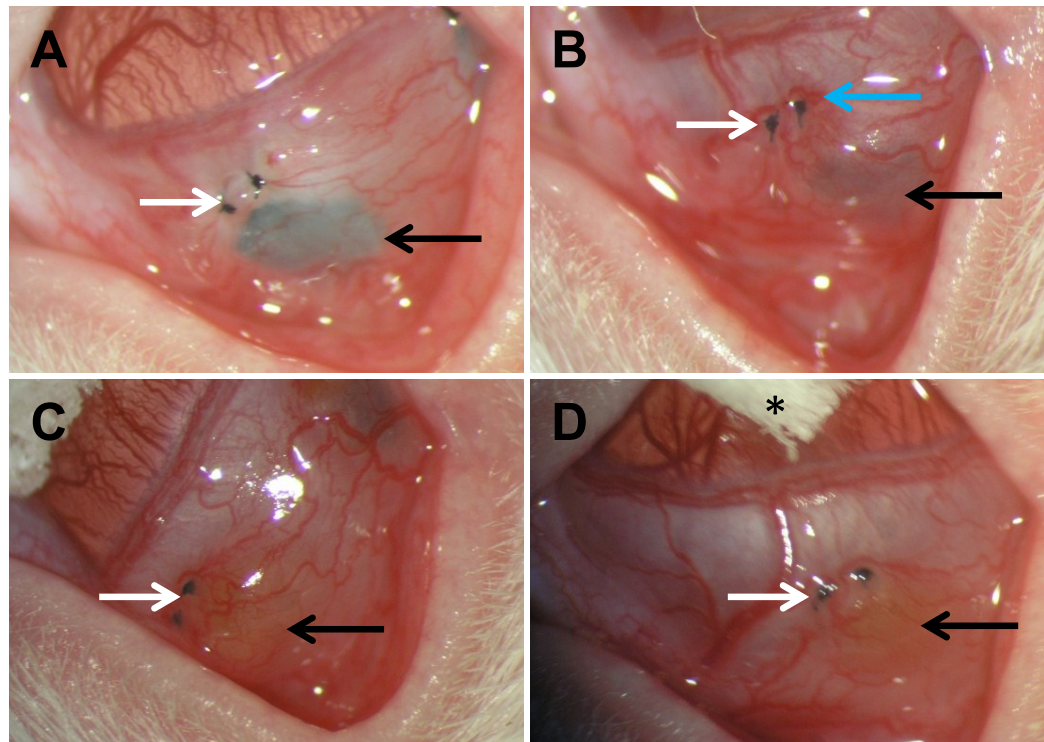


Figure 3-7 Subconjunctival implantation of pSi scaffolds carrying ex vivo expanded rat oral mucosal epithelial cells

pSi scaffolds carrying male rat oral mucosal epithelial cells were implanted under the conjunctiva of female inbred Sprague-Dawley rats. **(A)** The pSi (black arrow), and the sutures (white arrow), were visible under the conjunctiva, one day after implantation. **(B)** At 2 weeks post implantation, signs of degradation were apparent, as the pSi changed colour. There was also mild inflammation and neovascularization. The vessels appeared to be reaching the sutures (blue arrow). **(C)** Four weeks post implantation, the pSi scaffold had degraded further. Little or no inflammation was apparent, however the blood vessels persisted. **(D)** Eight weeks after implantation the pSi scaffold was still visible. An ophthalmic spear (asterisk) is visible at the top of image D. Images captured at the operating microscope.

microscope up to 8 weeks post-implant, however extensive degradation was apparent (Figure 3-7 D). The vasculature around the site of the implant had undergone remodelling, with a number of vessels regressing. A network of vessels had formed around the implant site, with larger vessels around the sutures (Figure 3-7 D).

In summary, pSi membranes carrying OMECs were successfully implanted under the conjunctiva in rats. The implants were well tolerated and did not cause prolonged inflammation or extensive neovascularization. However, the rate of degradation of the pSi membrane was rapid. This was of concern because the goal was to generate a long-term artificial stem cell niche.

3.2.5 Detection of transplanted cells on the ocular surface

Porous silicon membranes carrying OMECs were implanted under the conjunctiva of rats, as described in the previous section. The next experiment was performed to detect if the transplanted cells had migrated across the ocular surface. An initial experiment was performed with male OMECs on pSi scaffolds implanted under the conjunctiva of 2 female rats. Weekly impression cytology samples from the central cornea and the conjunctiva were taken with FTA paper. The presence of the male specific gene, sex determining region Y (*sry*) in the samples, which would indicate presence of transplanted cells^{97, 453}, was detected by PCR for genomic DNA.

Amplification of *sry* from the samples should yield a product of 168 bp. Samples from the female rat corneas and conjunctivas taken 1 to 8 weeks post implantation of male cells were analysed. In rat one, a band corresponding to the expected size for *sry* was observed, in the corneal samples, from 1-4 weeks post-implantation

(Figure 3-8). A positive result in the conjunctival samples from rat one was also obtained in weeks 2, 5 and 6 post-implant. Detection of *sry* in rat two was more variable, with a band of the correct size amplified from the cornea, 2, 3 and 6 weeks post implant, and in the sample collected on the day of implant from the conjunctiva. These results suggested that the transplanted OMECs were able to migrate off the pSi scaffold on to the corneal surface. However, the PCR reaction used to amplify *sry* also amplified a large number of spurious bands, as can be seen from Figure 3-8. The PCR reaction employed 65 cycles of amplification, in order to maximise the sensitivity of detection. The large number of amplification cycles generated misprimed artefacts. In order to overcome this issue, a new PCR protocol with increased specificity and sensitivity was developed.

3.2.6 Novel *sry* PCR protocol for increased specificity and sensitivity

Detection of a small amount of male DNA in the presence of female DNA required a large number of rounds of amplification. This resulted in the presence of artefacts, which reduced confidence that the band previously amplified was specific for *sry*. Furthermore, in cases where no bands were observed, for example, in Figure 3-8 lane 8, it was not possible to determine whether no male DNA was present in the sample or whether there was no DNA at all on the FTA paper, that is, whether there had been a technical failure in collection of the sample.

A nested PCR protocol was employed to overcome these problems. The first amplification was a multiplex reaction, which amplified the male specific gene *sry* and the housekeeper gene acidic ribosomal phosphoprotein (*arbp*). Amplification of the housekeeper gene confirmed that the samples contained DNA (that is, cells had

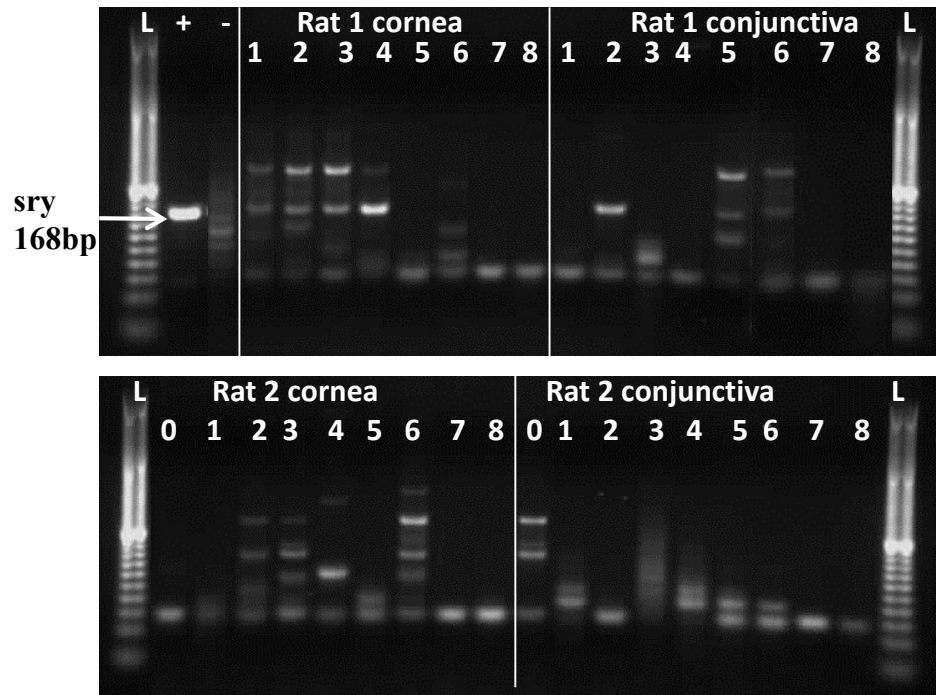


Figure 3-8 Detection of transplanted cell on the rat ocular surface

Rat oral mucosal epithelial cells, harvested from a male inbred Sprague-Dawley rat, were grown on pSi scaffolds, and transferred to the eyes of two female, inbred Sprague-Dawley rats. Cell samples were taken from the central cornea and the conjunctiva, weekly, for 8 weeks, using FTA paper. The samples were analysed by PCR for the presence of transplanted male genomic DNA. Male rat genomic DNA was used as a positive control (+), the negative control (-) was a blank FTA paper disc. Bands corresponding to the expected size for the male specific gene, *sry* (168 bp), were detected on the cornea of rat one up to 4 weeks post implant. Indicative of the presence of transplanted male cells. A large number of spurious bands were observed, making accurate prediction of cell transfer difficult. The 20 bp ladder was run in the lanes marked L. The numbers 0-8 indicate that the sample was taken 0-8 weeks post-implantation.

been collected on the FTA paper), while amplification of *sry* would indicate that cells of donor origin had been collected. Samples collected from female rat corneas amplified only a band corresponding to *arbp*, while in samples collected from a male rat eye, a strong band corresponding to the expected size for *sry*, and a weak band corresponding to the size of *arbp* were observed (Figure 3-9 A). When there was a large amount of male gDNA, *sry* was easily detected in the first PCR reaction. However, in the case of samples collected from a female rat eye with a few transplanted male cells, a small amount of male gDNA would be diluted by a large amount of female gDNA. To replicate this condition, a cell sample was taken from a female rat and spiked with 8 pg of male gDNA, corresponding to one cell equivalent of gDNA. A band corresponding to the expected size for *arbp* was observed with this sample, but *sry* was not detected in the first round of PCR.

A second round of amplification was then performed using nested primers for *sry*. The second round of amplification greatly increased the sensitivity of detection of *sry*, while maintaining specificity. Eight picograms of male gDNA added to a cell sample taken from a female rat eye yielded a single band corresponding to the expected size (168 bp) for *sry* (Figure 3-9 B). In the absence of male gDNA, no spurious bands were amplified from female gDNA. These data suggest that the nested *sry* PCR was sensitive enough to detect a single transplanted male cell in the presence of large numbers female cells, and that it specifically amplified rat genomic *sry*. The primers were designed to be specific for rat *sry* and did not amplify *SRY* from male human gDNA (data not shown).

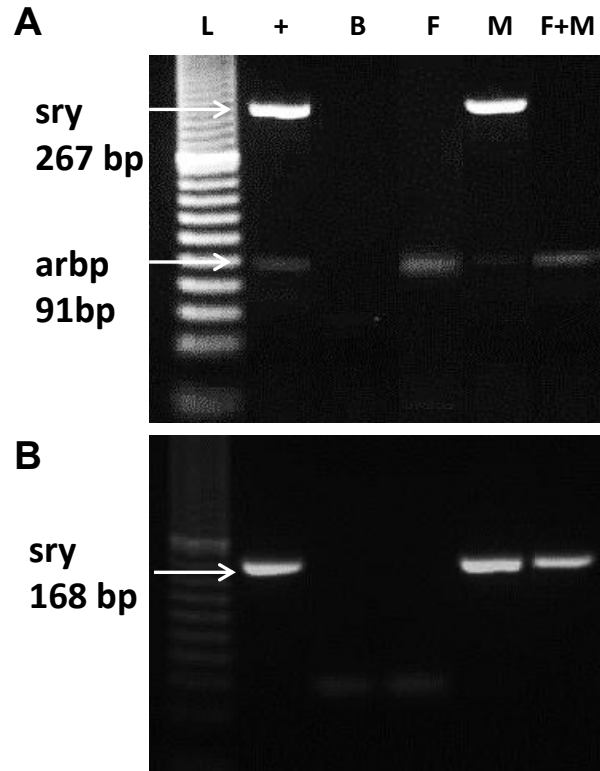


Figure 3-9 Multiplex nested PCR for improved detection of transplanted male cells

A two-step PCR protocol was developed for detection of male DNA in the presence of female DNA, and confirmation of the presence of any DNA on the FTA paper samples. **(A)** The first round of amplification was a multiplex PCR which amplified the male specific gene *sry* and the housekeeper gene *arbp*. In the presence of a large amount of male DNA (+, M), *sry* was detected. However, small amounts of male DNA (F+M) or female DNA (F) did not produce a band. Detection of *arbp* confirmed the presence of DNA on the FTA disc. **(B)** The products from the first round of PCR were amplified with nested primers. This allowed for sensitive detection of male DNA in the presence of female DNA. L = 20 base pair ladder, + = male rat gDNA, B = blank FTA disc, F = FTA disc from a female rat eye, M = FTA disc from a male rat eye, M+F = FTA disc from a female rat eye with male gDNA.

3.2.6.a *Detection of transplanted male cells using the novel sry PCR*

OMECs harvested from male inbred Sprague-Dawley rats were grown on pSi membranes coated with collagen IV, vitronectin or collagen IV plus vitronectin, for 7 days, and implanted under the conjunctiva of 4, 4 and 3 female rats respectively. The implants were observed under the operating microscope for 8 weeks and cell samples were taken from the central cornea as well as the conjunctiva weekly, using FTA paper. The cells samples on the FTA paper were analysed for the presence of transplanted cells using the novel nested PCR protocol.

Only a band corresponding to arbp was obtained from female samples, while male samples yielded a band corresponding to sry (Figure 3-10). No bands were amplified from either a water control or a blank FTA disc. A band corresponding to the expected size for arbp was amplified in 58% of the corneal samples and 46% of the conjunctival samples (Figure 3-11). This indicated that approximately 40% of the FTA paper lifts failed to collect cells from the ocular surface. *sry* was not amplified in the first round of amplification in any of the samples. The second round of amplification with nested primers did not amplify a band corresponding to *sry* in any of the samples tested. This indicated that the transplanted cells were not detected from the central corneal surface post-implantation.

In summary, pSi membranes carrying OMECs were implanted into the eyes of normal rats, with an intact corneal epithelium. No migration of transplanted male cells was able to be detected. However, the central cornea was normal, with the epithelium being regenerated from the limbus. Under these circumstances, the

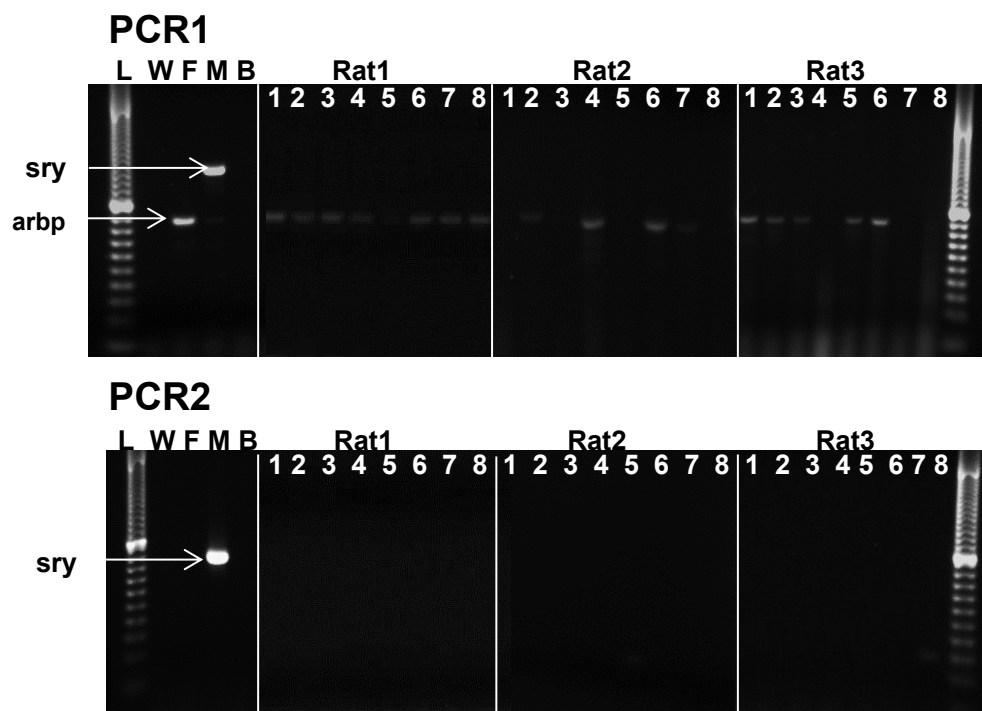


Figure 3-10 Detection of transplanted male OMECs on the cornea of female rats

Male OMECs were transplanted, on pSi scaffolds, under the conjunctiva of 11 female inbred Sprague-Dawley rats. A two-step PCR protocol was used to detect the presence of male specific DNA in samples collected from the corneas of the female rats. A representative gel showing the result from three rats is shown. The housekeeper gene *arbp* was amplified from most of the samples, which indicated that the samples contained DNA. However, the male specific *sry* gene was not amplified in any of the samples. L = 20 base pair ladder, W = water control, F = female rat gDNA, M = male rat gDNA, B = blank FTA disc, C = collagen coated pSi, V= vitronectin coated pSi, C+V = collagen and vitronectin coated pSi, 1-8 = sample taken 1-8 weeks after transplantation. Rat 1, 2, 3, implanted with OMECs grown on pSi membranes coated with collagen IV plus vitronectin, vitronectin and collagen IV respectively.

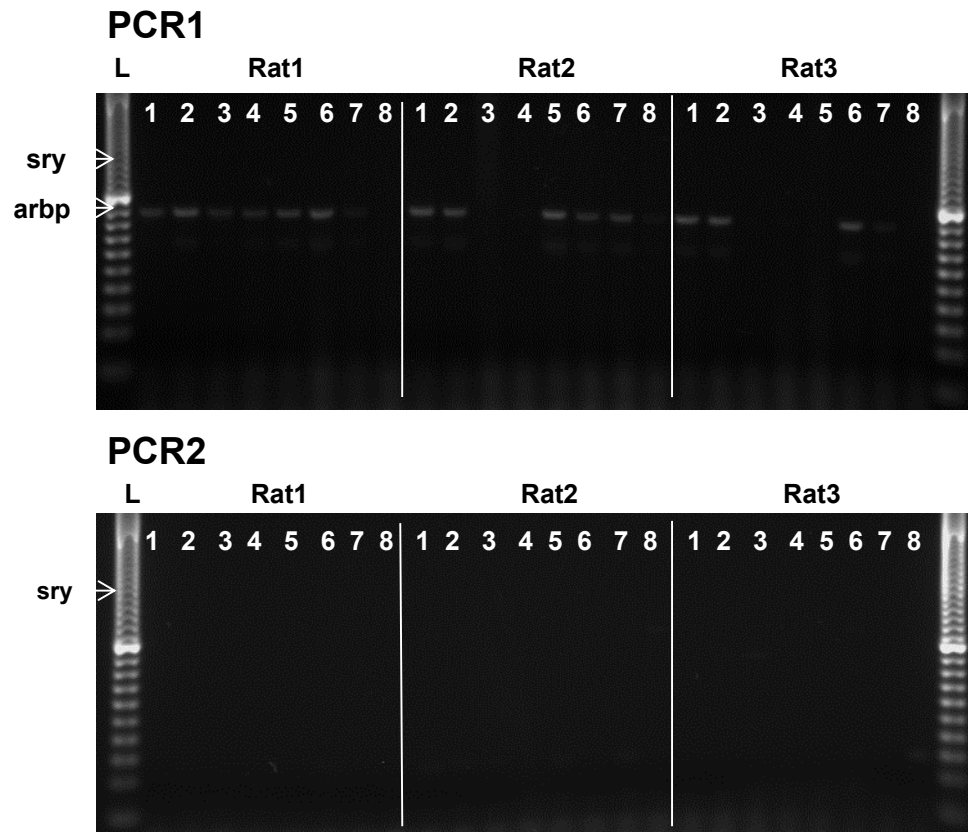


Figure 3-11 Detection of transplanted male OMECs on the conjunctiva of female rats

Male OMECs were transplanted, on pSi scaffolds, under the conjunctiva of 13 female inbred Sprague-Dawley rats. A two-step PCR protocol was used to detect the presence of male specific DNA in samples collected from the conjunctiva of the female rats. A representative gel showing the result from three rats is shown. The housekeeper gene *arbp* was amplified from most of the samples, which indicated that the samples contained DNA. However, the male specific *sry* gene was not amplified in any of the samples. L = 20 base pair ladder, 1-8 = sample taken 1-8 weeks after transplantation. Rat 1, 2, 3, implanted with OMECs grown on pSi membranes coated with collagen IV plus vitronectin, vitronectin and collagen IV respectively.

implanted OMECs might not have received any stimulus to migrate across the corneal surface.

3.2.7 Induction of ocular surface disease prior to cell transplantation

OMECs transplanted under the conjunctiva of the rat eye may not have received adequate stimuli to migrate across the surface of a normal cornea. Damage to the corneal epithelium might induce migration of peripheral cells to repair the injury. Thus, n-heptanol was used to debride the corneal epithelium, to induce ocular surface disease. Cell samples from the corneal surface were collected on nitrocellulose membranes, and periodic acid Schiff (PAS)-haematoxylin staining was used to characterise the cells.

Impression cytology from normal rat corneas revealed large, tightly packed, hexagonal cells with small nuclei (Figure 3-12). The cells appeared purple due to haematoxylin staining. Normal conjunctival cells had smaller densely stained nuclei, which appeared in clusters. Pink PAS staining was present in the mucin-producing goblet cells.

Impression cytology and PAS-haematoxylin staining were performed on rat corneas that had been debrided with n-heptanol. Samples taken from the central cornea of these rats showed large flattened epithelial cells. However, clusters of densely-stained nuclei, and positive PAS staining were also observed (Figure 3-12 C & D). These findings were indicative of the presence of goblet cells, which are normally restricted to the conjunctiva. PAS-positive goblet cells were observed up to 4 weeks post-debridement. It was concluded that ocular surface disease had successfully been

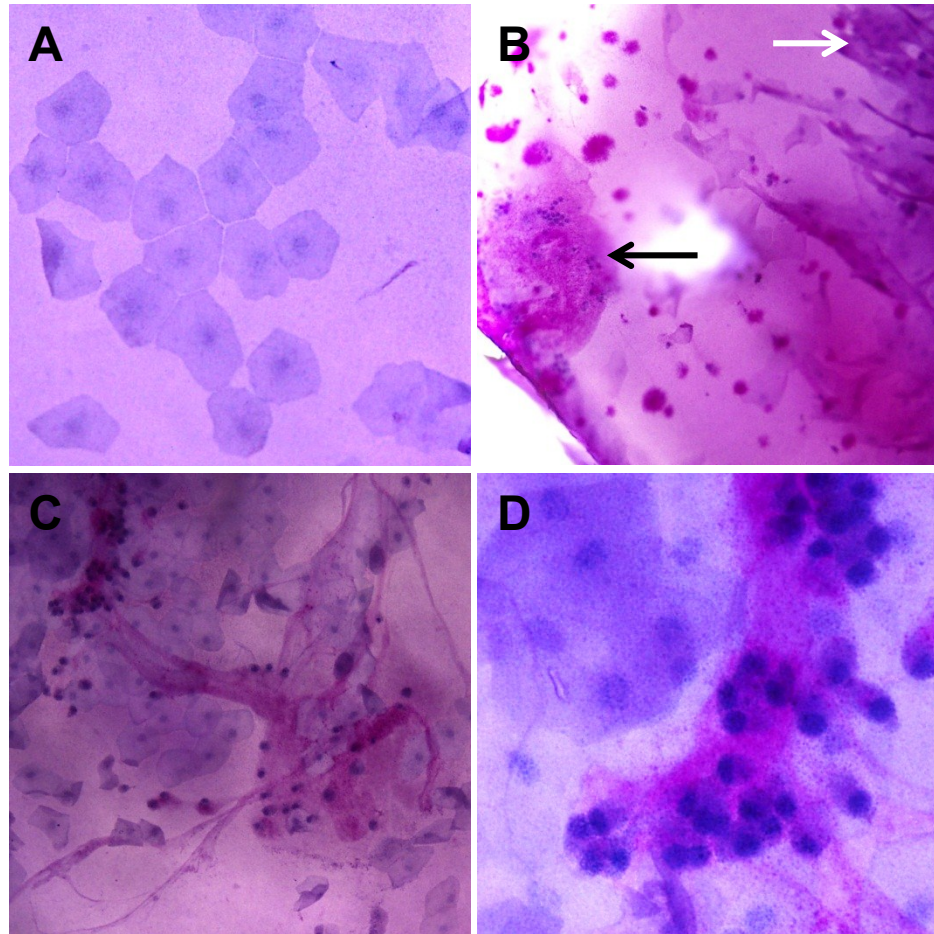


Figure 3-12 Impression cytology to confirm induction of ocular surface disease

Cells were lifted from the surface of rat eyes using nitrocellulose membranes. Haematoxylin periodic acid-Schiff (PAS) staining was then performed on the lifts

(A) Nuclei from epithelial cells from normal rat corneas were stained with haematoxylin, but no pink PAS staining was observed. Superficial corneal epithelial cells were large and flattened. **(B)** A sample from the corneo-conjunctival border showing flattened corneal epithelial cells (white arrow) and PAS positive, conjunctival cells (black arrow), indicating the presence of mucins secreted by goblet cells. **(C)** and **(D)** Samples from the corneas of n-heptanol treated rats. PAS positive cells were observed amongst the corneal epithelial cells, confirming the presence of conjunctival goblet cells, indicative of

induced in these rats, as evidenced by the conjunctivization of the corneal epithelium.

3.2.7.a *Implantation of pSi scaffolds carrying OMECs in h-heptanol debrided rat eyes*

OMECs from male rats, grown on pSi scaffolds coated with vitronectin, were implanted under the conjunctiva of female rats 4 weeks after debridement with n-heptanol. The implants were observed at the operating microscope for 8 weeks and weekly cell samples were taken from the cornea and conjunctiva using FTA paper.

The cell samples were analysed using the novel *sry* PCR protocol. A band corresponding to the expected size for arbp was detected in 17/24 (70%) samples (Figure 3-13). A second round of amplification with nested PCR was used to increase the sensitivity of detection of *sry*. However, it was not detected in any of the samples (Figure 3-13).

These data suggest that induction of ocular surface disease in rats prior to implantation of OMECs on pSi scaffolds did not induce detectable migration of the cells across the ocular surface, as measured by PCR. The fate of the OMECs after implantation under the rat conjunctiva was further investigated by staining the cells with a cell tracker dye.

3.2.8 Fate of the transplanted oral mucosal epithelial cells

In order to further investigate the fate of the transplanted OMECs, cells were labelled with the cell tracker dye PKH26 prior to transplantation. PKH26 is a fluorescent dye

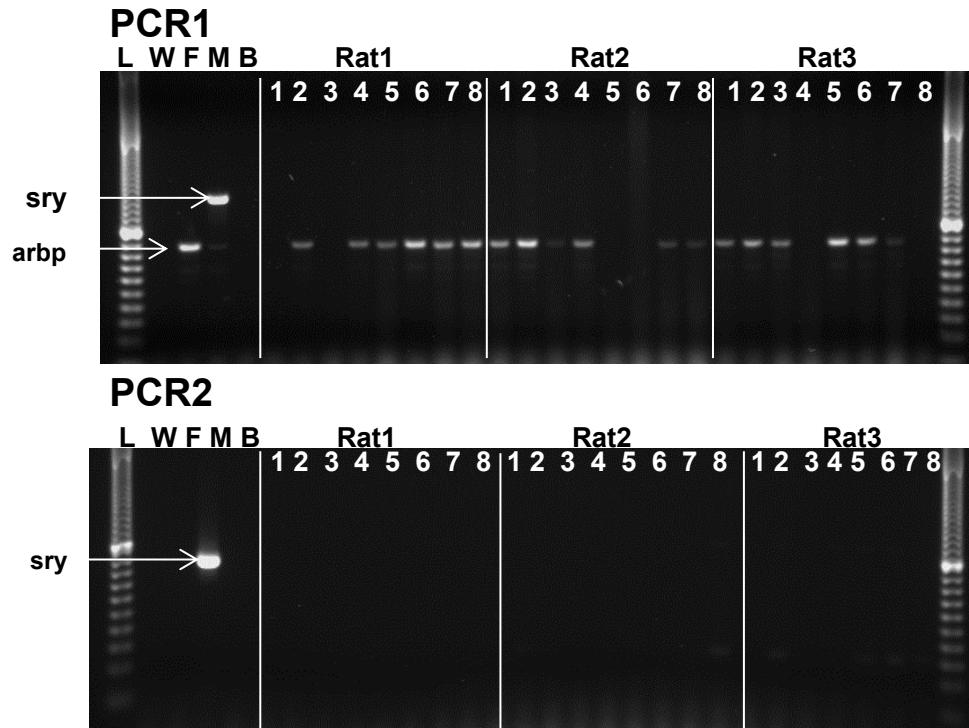


Figure 3-13 Detection of transplanted male OMECs on the corneas of female rats with induced ocular surface disease

The corneas of 3 female inbred Sprague-Dawley rats were debrided with n-heptanol to induce ocular surface disease (OSD). Induction of OSD was confirmed by the detection of goblet cells on the corneal surface. Male OMECs on pSi scaffolds were implanted under the conjunctiva of the female rats. Weekly cell samples were taken from the cornea using FTA paper. The presence of transplanted male cells was detected by PCR for the male specific *sry* gene. No male cells were detected on the surface of the corneas of the 3 female rats. L = 20 base pair ladder, W = water control, F = female rat gDNA, M = male rat gDNA, B = blank FTA disc, 1-8 = sample taken x weeks after transplantation.

with a long aliphatic tail, and is incorporated and retained by the cell membrane. PKH26 is extremely stable, allowing cell tracking *in vivo*, however it is divided equally between daughter cells during cell division, resulting in dilution of the fluorescent signal. OMECs grown on pSi membranes readily took up the PKH26 dye, resulting in patchy cytoplasmic labelling (Figure 3-14).

PKH26 labelled OMECs on pSi membranes coated with collagen IV were implanted under the conjunctiva of rats, and monitored for up to 8 weeks. At 1, 2, 4 and 8 weeks post implantation, the rats were euthanised and the corneas with a scleral rim containing the implants were flatmounted for microscopic observation. At 1, 2 and 4 weeks post-implantation, distinct red fluorescence was detected in the flatmounted corneas (Figure 3-15). At higher magnification it was apparent that the fluorescence localised to the cytoplasm of cells, not the nuclei (Figure 3-15), as expected. The labelled OMECs remained on the pSi scaffolds up to two weeks post-implant (Figure 3-16). However, small patches of red fluorescence were observed outside the borders of the pSi implants. At 8 weeks post-implant the fluorescence was more diffuse, making it difficult to image. However, it was noted that there was distinct red fluorescence around one of the sutures, which might be indicative of cell migration. No fluorescence was detected in the central cornea at any time point. These data suggest that the OMECs had not migrated across the surface of the cornea, to a detectable extent, even in the presence of OSD.

In summary, rat OMECs were successfully cultured on pSi membranes coated with collagen IV, vitronectin or collagen IV plus vitronectin, and expressed the corneal epithelial marker CK3/12, the TAC marker p63 and the putative stem cell marker ABCG2. Implantation of pSi membranes carrying OMECs under the conjunctiva of

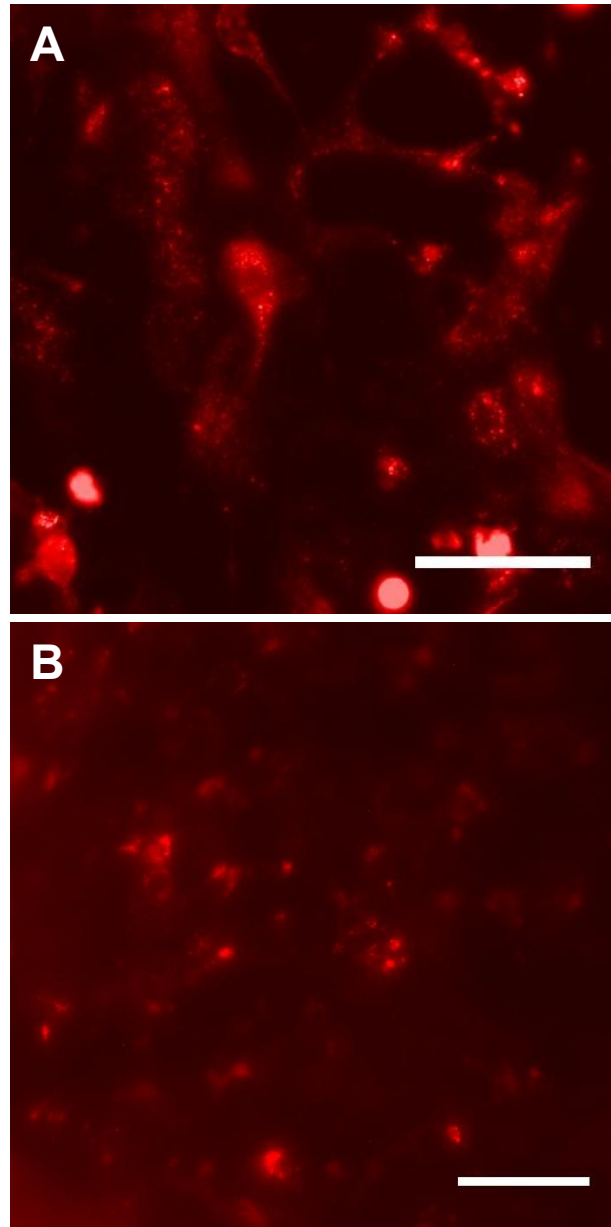


Figure 3-14 Labelling OMECs with the cell tracker dye PKH26 *in vitro*

(A) OMECs were grown on collagen IV coated cell culture plates for 7 days before labelling with PKH26. The lipophilic dye is taken up by the cell membrane resulting in red fluorescence of the cells. Scale bar 10 μm .

(B) OMECs were grown on collagen IV coated pSi scaffolds and labelled with PKH26 before subconjunctival implantation in rats. The labelled cells were detected in corneal flatmounts at 7 days post implant. Scale bar 50 μm .

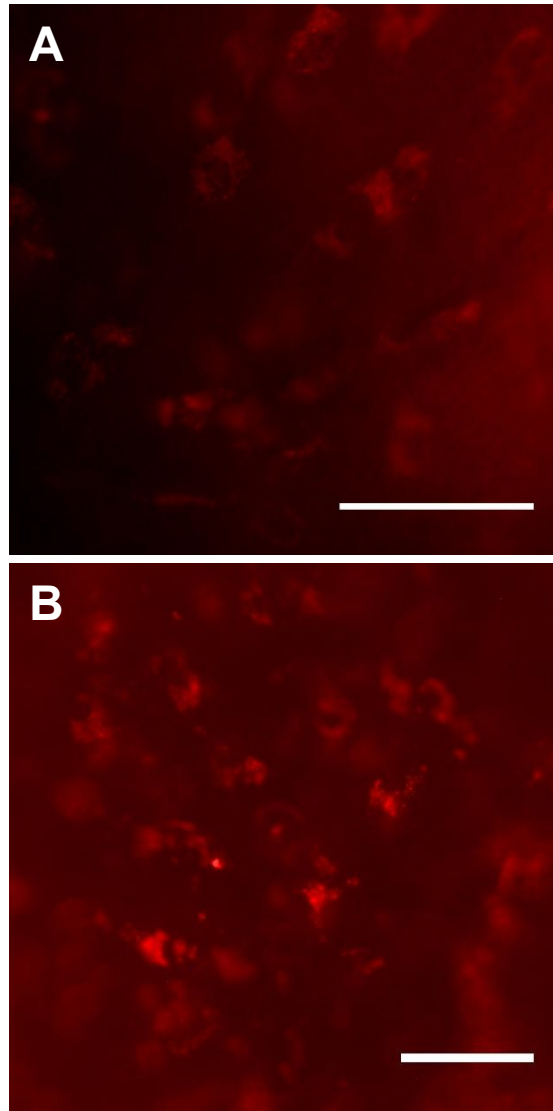


Figure 3-15 Detection of PKH26 labelled OMECs after transplantation under the rat conjunctiva

PKH26 labelled OMECs on pSi membranes coated with collagen IV were implanted under the conjunctiva of 4 inbred Sprague-Dawley rats. Corneas with a scleral rim were harvested and flatmounted at: **(A)** 14 days; and **(B)** 28 days post implant. Labelled cells were visualised by fluorescence microscopy. Scale bars 50 μm .

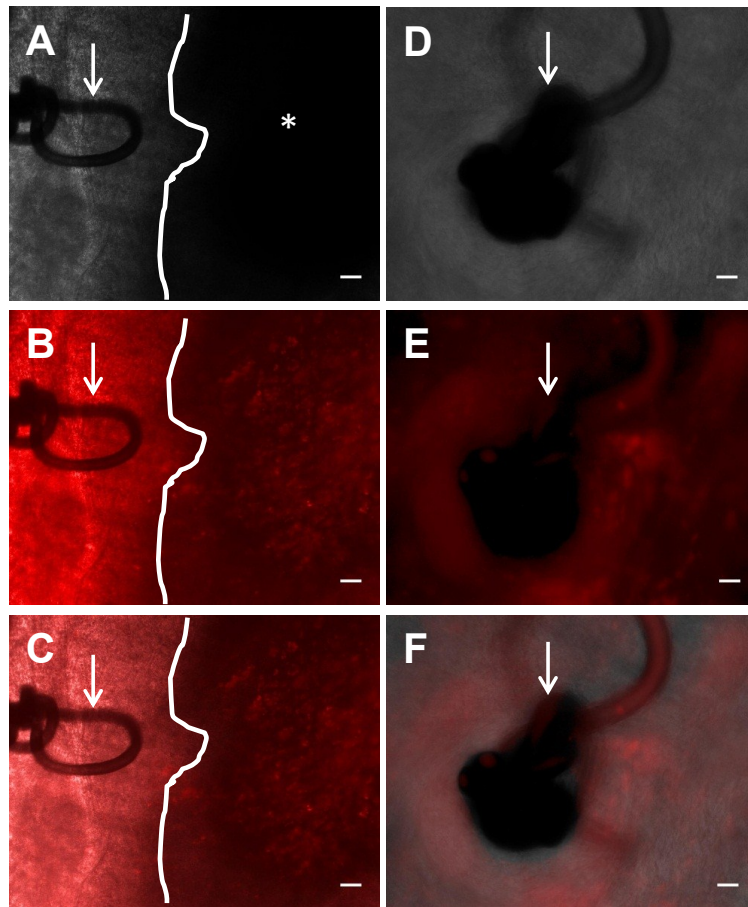


Figure 3-16 Migration of PKH26 labelled OMECs after implantation under the rat conjunctiva

PKH26 labelled OMECs on pSi membranes coated with collagen IV were implanted under the conjunctiva of 4 inbred Sprague-Dawley rats.

(A) Brightfield, (B) fluorescence (PKH26) and (C) merged images of PKH26 labelled OMECs 2 weeks post implant. (D) Brightfield, (E) fluorescence (PKH26) and (F) merged images of OMECs 8 weeks post implant. Sutures (white arrows) are visible in each image. At two weeks post implant, the majority of PKH26 labelling was observed on the pSi particle (asterisk). Fluorescence was detected around the suture at 8 weeks post implant. This was indicative of migration of labelled cells from the pSi scaffolds. The edge of the pSi particle is highlighted by the white lines in images A-C. Scale bars 50 μm .

rats did not cause significant inflammation or neovascularization. However, transplanted OMECs did not migrate across the ocular surface to the central cornea, to any significant extent, either in normal eyes, or in eyes in which OSD had been induced prior to implantation. Furthermore, the pSi membranes degraded rapidly over the course of 8 weeks. It was concluded that a more stable scaffold might be more appropriate for the development of an artificial stem cell niche, rather than the pSi membranes used up until this point.

3.3 Porous silicon polymer composite materials

Although pSi has a number of properties that might theoretically make it an excellent ocular implant, it does have drawbacks. Porous silicon membranes are rigid and possess sharp edges. Although subconjunctival implantation of pSi membranes did not cause damage to surrounding tissue, there is the potential that large implants with sharp edges might cause discomfort when implanted in humans.

Furthermore, as described in section 3.2.8, pSi membranes proved unsuitable for development of a limbal stem cells niche, because the material degraded too rapidly. Composites of pSi with soft polymers such as poly-caprolactone might overcome some of the problems of pSi membranes⁴²². We considered that incorporation of pSi microparticles into flexible polymer fabrics might make surgical implantation easier, and the sharp edges of the pSi would be covered with soft polymer. However, complete encapsulation of the pSi particles would make drug loading into the material difficult. Thus, a novel composite, pressed pSi-PCL was developed. This material consisted of a non-woven fabric of poly-caprolactone with pSi

microparticles, of two sizes (<40 μM and 150-250 μM), partially embedded in the fibres (Figure 3-17).

In this section, transfer of a model drug, fluorescein diacetate (FDA) to cells grown on composite material was assessed, the effect of loading a model growth factor mixture (foetal bovine serum) on cell attachment and growth *in vitro* was investigated, a mixture of recombinant biologic agents, comprising epidermal growth factor (EGF), insulin and transferrin was loaded in the material and their effect on cell proliferation assayed *in vitro*, and implantation of the material beneath the conjunctiva of rats, at the limbus, was performed to assess biocompatibility.

3.3.1 Transfer of small molecule drugs to cells grown on pSi-PCL composite materials

The feasibility of transferring drugs from the pSi composite material into cells was first assessed. FDA was used as a model small drug. FDA has a molecular weight of 416 Daltons, is in itself non-fluorescent, and is readily taken up by cells⁴⁵⁴. In living cells, intracellular esterase activity converts FDA to the fluorescent product fluorescein, which is retained within the cytoplasm of living cells with intact cell membranes^{454, 455}. The FDA thus serves a dual purpose, demonstrating the transfer of a model small molecule drug to cells, as well as the viability of those cells.

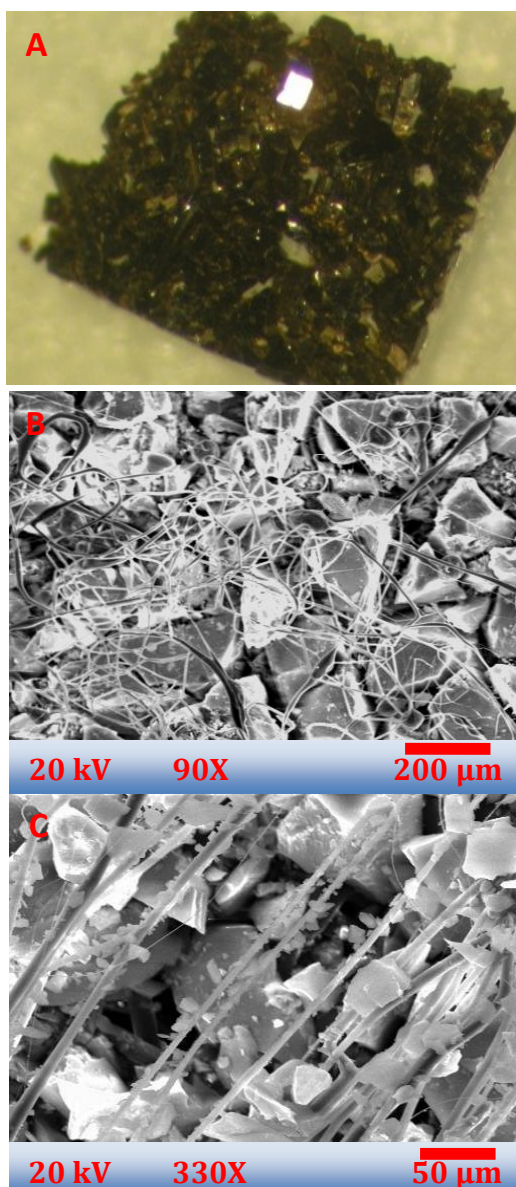


Figure 3-17 Pressed pSi-PCL composite materials

Images of the pressed pSi-PCL composite materials. **(A)** Photograph of pressed pSi-PCL material with 150-250 μm pSi particles. **(B)** Scanning electron micrograph of the pSi-PCL composite material with 150-250 μm pSi particles. The larger particles are entangled within the polymer mesh. Scale bar 200 μm . **(C)** SEM image of the pSi-PCL composite material with <40 μm particles. The small pSi particles are intimately associated with the polymer fibres. Scale bar 50 μm . Images provided by Prof. Jeffery Coffey, Texas Christian University.

3.3.1.a *Effect of pSi particle size on transfer of drugs*

Porous silicon nanoparticles were prepared with particle sizes of $<40\ \mu\text{m}$ and 150-250 μm and loaded with FDA. Two kinds of pressed pSi-PCL composite materials were prepared, one with the small ($<40\ \mu\text{m}$) particles, and the other with the large (150-250 μm) particles. Composite materials prepared with unloaded pSi particles (no FDA) were used as controls. The small pSi particles were closely associated with the polymer fibres while the larger pSi particles were entangled within the polymer mesh (Figure 3-17). The larger pSi particles had a greater drug loading capacity, as their greater volume translated to a larger surface area for drug adsorption.

Human lens epithelial cells (designated SRA01/04) were seeded on FDA loaded and unloaded pSi-PCL composite materials with either small or large pSi particles, and allowed to attach for 6 hours before labelling the nuclei with Hoechst 33342 dye. FDA transfer to the cells was assessed by fluorescence microscopy. Six hours after seeding, cells were observed to be attached to all of the materials. Green fluorescence was observed in the cytoplasm of cells on the FDA-loaded materials, indicating the cells were viable. Cells seeded on composite material with larger (150-250 μm) particles appeared to fluoresce more brightly than those on composite with smaller pSi particles (Figure 3-18 B & D), indicating greater FDA transfer from large pSi particles.

Five representative images were analysed in ImageJ to determine the mean fluorescence intensity. The mean fluorescence intensity of cells growing on composite material with large pSi particles was significantly higher than those growing on material with small pSi particles, $p=0.008$ (Figure 3-20 A). No

fluorescence was observed from cells seeded on unloaded composite material (Figure 3-18 A).

3.3.1.b *Effect of position of the cells on composite materials*

Porous silicon particles tended to be unevenly distributed on the polymer fibres, irrespective of particle size. This gave rise to areas with a large number of pSi particles and other areas with few or no pSi particles. In contrast, cells were evenly distributed on the materials and grew on the PCL fibres as well as on the pSi particles. Cells growing on or near the pSi particles appeared to fluoresce more brightly than cells more distant to particles (Figure 3-19). This was observed irrespective of the size of the particles. The fluorescence of cells growing near and far from pSi particles was quantified using ImageJ. The cells were selected using the polygon selection tool and fluorescence measured, and then the total corrected cell fluorescence was obtained by subtracting the background fluorescence. Mean corrected cell fluorescence (MCCF) was calculated for cells growing near or far from the pSi particles. At least 10 cells were counted per image. The MCCF of cells growing on or near pSi particles was significantly higher on both larger and smaller pSi-PCL materials, $p < 0.001$ (Figure 3-20 B). The MCCF of cells growing on or near larger particles was significantly higher than those growing on or near smaller pSi particles, $p < 0.001$.

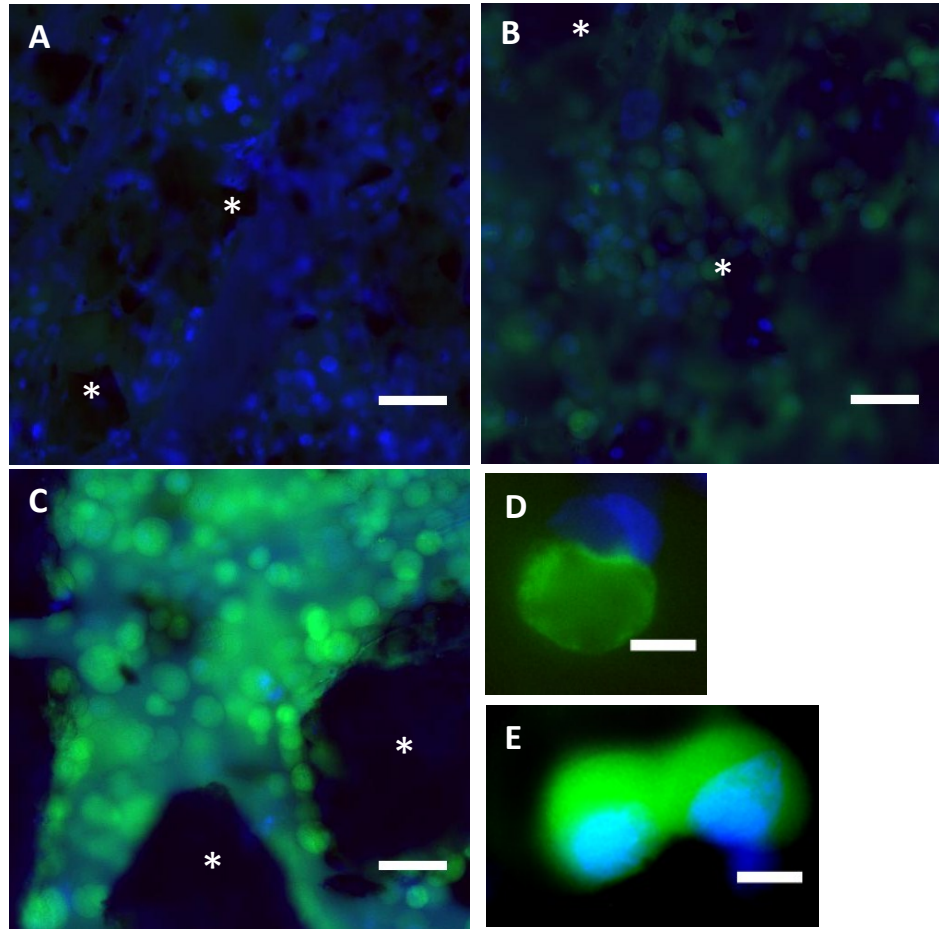


Figure 3-18 FDA uptake by SRA01/04 cells attached to pressed pSi-PCL composite materials

Images of SRA01/04 cells 6 h after seeding on pSi-PCL composite materials loaded with FDA. pSi particles were observed as dark masses in the images (asterisk). **(A)** Unloaded composite with $<40\ \mu\text{m}$ pSi particles (small); **(B)** FDA-loaded composite with $<40\ \mu\text{m}$ pSi particles showing fluorescent cells; **(C)** FDA-loaded composite with $150\text{-}250\ \mu\text{m}$ pSi particles (large); **(D)** Magnified section of panel B; **(E)** Magnified section of panel C. More brightly fluorescent cells were observed in FDA loaded composite material with large pSi particles than with composite material with small pSi particles. Cell nuclei stained with Hoechst 33342 (blue), cell cytoplasm stained with fluorescein (green), scale bars panel A, B, C $50\ \mu\text{m}$, panel D, E $10\ \mu\text{m}$.

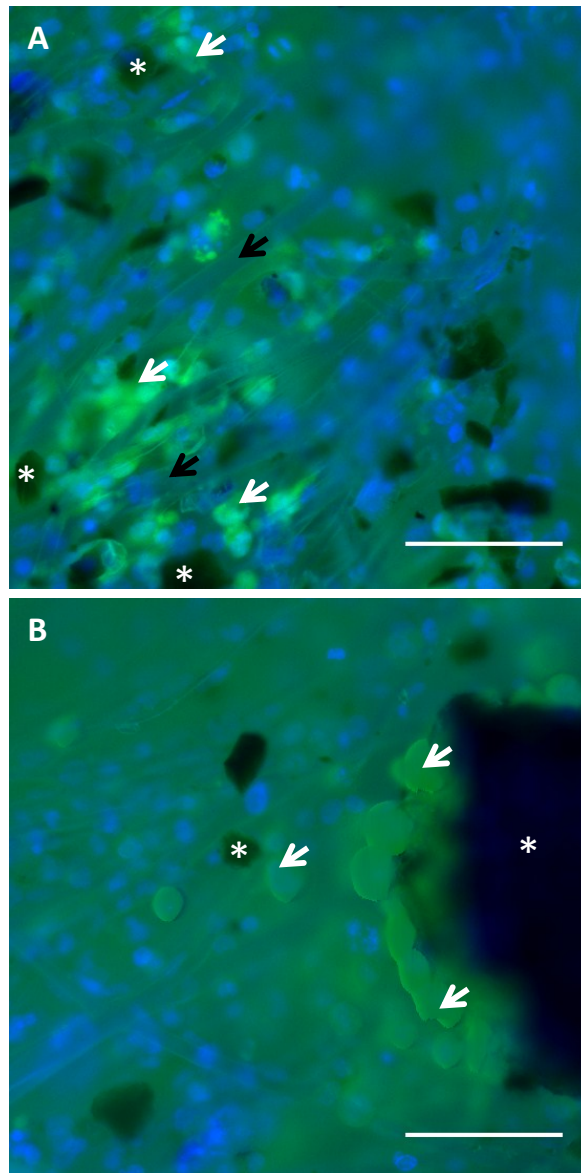


Figure 3-19 Increased fluorescence on or near pSi particles

Images of SRA01/04 cells 6 h after seeding on FDA loaded pSi-PCL composite materials, consisting of pSi particles (asterisks) embedded in polymer fibers (black arrows). **(A)** FDA-loaded composite with $<40\ \mu\text{m}$ pSi particles; **(B)** FDA-loaded composite with $150\text{-}250\ \mu\text{m}$ pSi particles. Brighter fluorescence was observed in cells on or near pSi particles (white arrows). Cell nuclei stained with Hoechst 33342 (blue), cell cytoplasm stained with fluorescein (green), scale bar $100\ \mu\text{m}$.

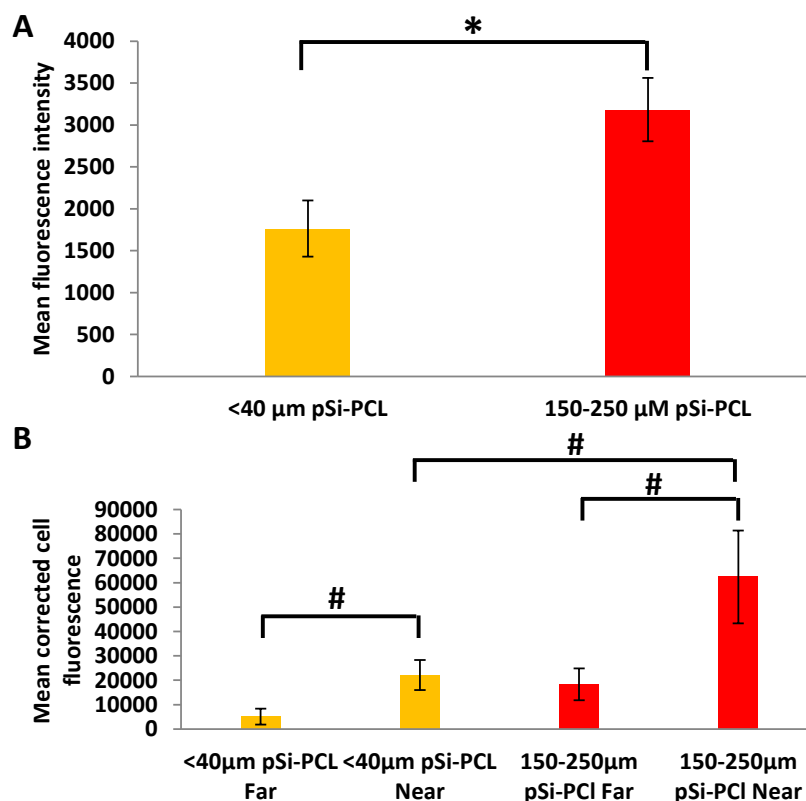


Figure 3-20 Quantification of fluorescence from cells seeded on FDA loaded pSi-PCL composites

The fluorescence from SRA01/04 cells seeded on FDA loaded pSi-PCL was quantified using ImageJ software. The total fluorescence in the green channel (fluorescein) was measured in 5 images and the average was plotted as the mean fluorescence intensity. Cells near or far from pSi particles were selected and the total cell fluorescence was calculated. Cells were considered to be far from particles if they were at least 1x the particle diameter away from large particles or at least 3x the particle diameter away from small particles. The corrected fluorescence was obtained by subtracting background readings. The values were averaged to give the mean corrected cell fluorescence (MCCF). A minimum of 10 cells were counted per image. **(A)** Cells seeded on material with larger pSi particles showed higher mean fluorescence * $p=0.008$. **(B)** Cells growing in the vicinity of pSi particles had a higher MCCF compared to cells growing further away. This was observed irrespective of the size of pSi particles. Cell fluorescence was higher on pSi-PCL with larger pSi particles, # $p<0.001$. Histogram bars represent mean fluorescence intensity \pm standard deviation.

3.3.2 Transfer of biologics to cells grown on pSi-PCL composite material

The pSi particles in the pressed pSi-PCL composite materials remain partially exposed, allowing loading of drugs after fabrication of the materials. This is particularly important for loading of “biologics”, which would lose activity when exposed to the high temperatures and solvents used during composite fabrication. First, the effect of coating the material with a model growth factor, foetal bovine serum (FBS), was assessed. Then, a mixture of biologic growth factors, recombinant epidermal growth factor, insulin and transferrin (EGF-ITS) was loaded in the composite materials and its effect on proliferation of BALB/c 3T3 cells assayed.

3.3.2.a *Effect of FBS coating on cell growth on pSi-PCL composite materials*

pSi-PCL composite materials were prepared with two sizes of pSi particles, <40 μm and 150-250 μm . SRA01/04 cells were seeded on the materials and allowed to grow for 24 h. The cell nuclei were labelled with Hoechst 33342 dye. Cell attachment and growth on uncoated materials was poor (Figure 3-21 A & C). Coating of the materials with FBS greatly enhanced cell attachment (Table 3-2). A statistically significant difference in cell numbers was observed between the uncoated and coated materials, regardless of pSi particle size ($p=0.009$). No difference was observed in the number of cells attached to materials with small or large pSi particles ($p=0.47$). The cells colonised the polymer fibres as well as the pSi particles (Figure 3-21).

Table 3-2 Cell growth on FBS coated psi-PCL

Hoechst33342 stained SRA01/04 cells grown on coated and uncoated pSi-PCL materials for 24 h were imaged. The number of cells in each image was enumerated by counting the nuclei. Five representative images were counted from each sample.

Material	Average cell count (\pmSD), n=5	Significance
Uncoated pSi-PCL with <40 μ m pSi	84 (\pm 37)	p=0.009*
FBS-coated pSi-PCL with <40 μ m pSi	642 (\pm 39)	
Uncoated pSi-PCL with 150-250 μ m pSi	78 (\pm 27)	p=0.009*
FBS-coated pSi-PCL with 150-250 μ m pSi	650 (\pm 16)	

*Mann-Whitney U test

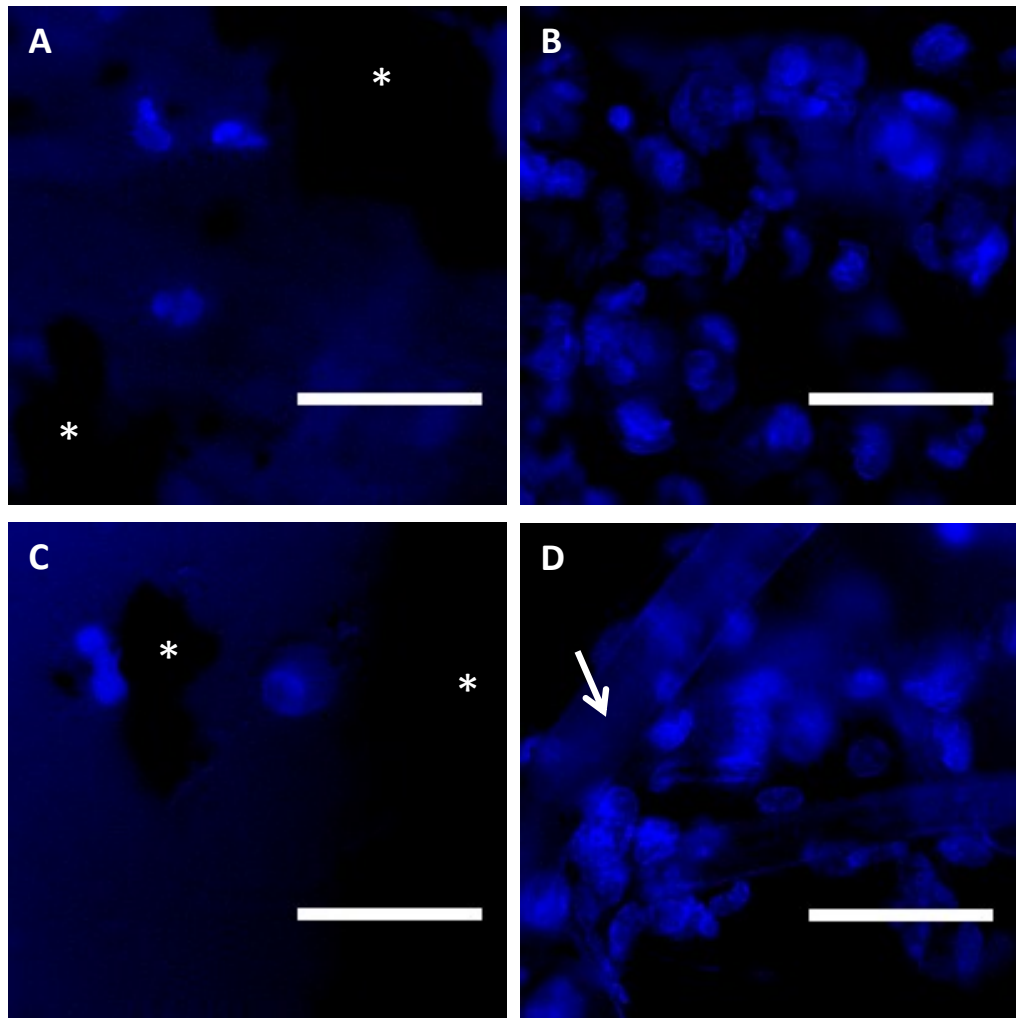


Figure 3-21 Growth of SRA01/04 cells on FBS coated and uncoated pSi-PCL composite materials

Images of Hoechst 33342 stained SRA01/04 cells 24 h after seeding on pSi-PCL composite materials. **(A)** Uncoated pSi-PCL with $<40 \mu\text{m}$ pSi **(B)** FBS-coated pSi-PCL with $<40 \mu\text{m}$ pSi **(C)** uncoated pSi-PCL with $150\text{-}250 \mu\text{m}$ pSi **(D)** FBS-coated pSi-PCL with $150\text{-}250 \mu\text{m}$ pSi. Minimal cell attachment and growth was observed on uncoated materials. Cells adhered to and grew on FBS coated materials. Cells were observed on the pSi particles (asterisks) as well as the polymer fibers (arrow). The size of the pSi particles in the composite material did not appear to influence cell attachment. Cell nuclei stained with Hoechst 33342 (blue), scale bar $50 \mu\text{m}$.

3.3.2.b *Loading and release of biologic growth factors from composite materials post-fabrication*

A mixture of epidermal growth factor, insulin, transferrin and sodium selenite (EGF-ITS) was loaded into the pSi-PCL composite materials post-fabrication by passive adsorption. This combination of biologics is known to induce proliferation in serum-deprived murine BALB/c 3T3 fibroblast cells^{444, 445}. BALB/c 3T3 cells seeded on biologic-loaded and washed material, or on unloaded composite material with biologics added to the medium, showed significantly more proliferation than cells grown on unloaded composite material (Figure 3-22 A). Cells seeded on polymer without pSi but pre-incubated with biologics did not show increased proliferation, indicating the biologics were loaded into the pSi particles.

The release of biologics loaded in composite materials into cell culture medium was demonstrated by the functional effect on proliferation of serum-deprived BALB/c 3T3 cells *in vitro*. The release was monitored over 6 days with samples taken on day one, day two and a third sample consisting of release from days three to six inclusive. DMEM conditioned by incubation of EGF-ITS loaded pSi-PCL composite materials was able to induce proliferation in BALB/c 3T3 cells (Figure 3-22 B), in comparison to medium conditioned with unloaded pSi-PCL. Samples taken on day one of the release elicited the largest proliferative response, indicating a large amount of the loaded EGF-ITS had been released on day one. However, samples collected between days 3-6 also induced cell proliferation. Taken together these data suggest a burst release of EGF-ITS, followed by a slow release as the pSi dissolved.

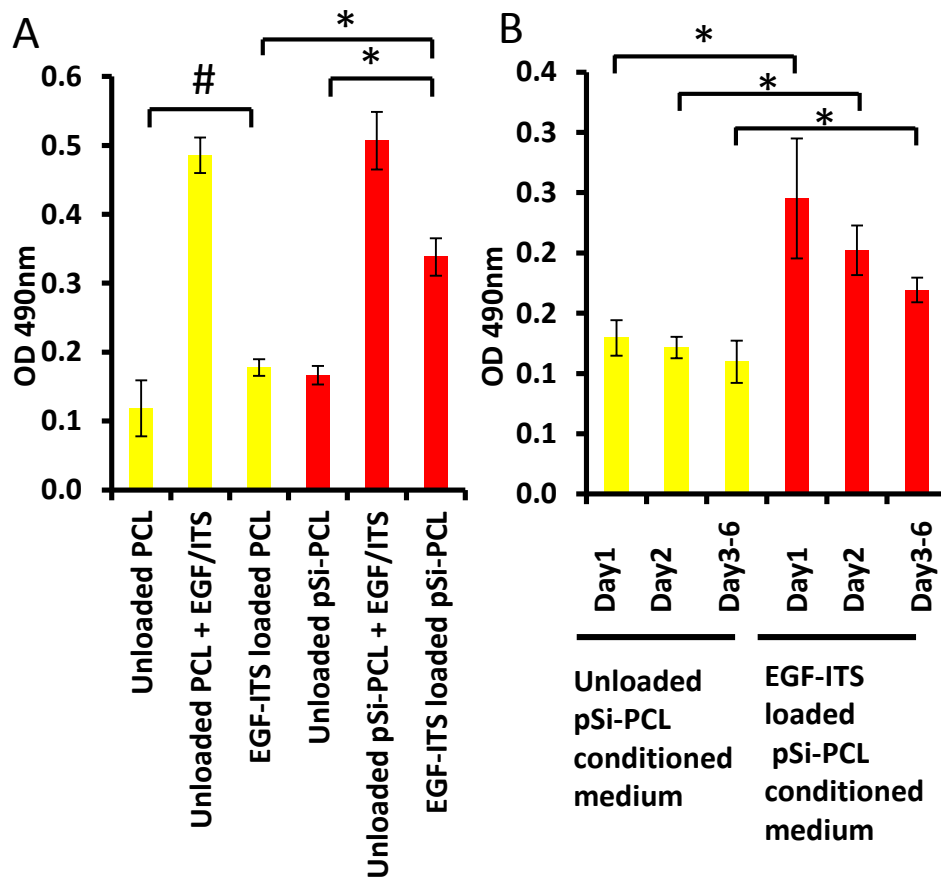


Figure 3-22 EGF-ITS loaded pSi-PCL materials induce proliferation in BALBc/3T3 cells

(A) Proliferation of BALBc/3T3 cells 48 h after seeding on pSi-PCL composite materials or PCL fibres loaded with EGF-ITS. Cells seeded on EGF-ITS loaded pSi-PCL showed significantly more proliferation than on unloaded composite material and loaded PCL * $p < 0.01$. Cells seeded on EGF-ITS loaded PCL did not proliferate more than cells loaded on unloaded PCL # $p = 0.095$. **(B)** Proliferation of BALBc/3T3 cells in response to medium incubated with EGF-ITS loaded pSi-PCL composite material. EGF-ITS loaded in pSi-PCL composite materials was released into cell culture medium. Medium conditioned with EGF-ITS loaded pSi-PCL composite material induced proliferation of cells compared to medium conditioned with unloaded pSi-PCL * $p < 0.01$.

3.3.3 Biocompatibility of pSi-PCL composite material in the rat eye

If the pSi-PCL composite materials are to be of use as ocular implants, they must be biocompatible. Ocular biocompatibility of the composite materials was tested in three rats by implantation of 2 x 2 mm pieces under the conjunctiva (Figure 3-23). The flexibility of the composite material allowed ready implantation. Animals were monitored for signs of infection, inflammation and neovascularization, daily at the operating microscope for a week after implantation and thrice weekly thereafter for a further 7 weeks. No signs of pain or distress were evident after implantation of the materials, however mild inflammation at the implant site (redness) was observed under the operating microscope. The inflammation resolved over the first 7 days and no further inflammation was observed up to 8 weeks post implant. Some neovascularization was observed around the implant site. It was noted that vessels grew towards and encircled the sutures. Porous silicon particles were visible immediately after implantation but disappointingly, had completely dissolved at 8 weeks (Figure 3-24).

The animals were euthanised and their eyes were collected 8 weeks post implant for histological analysis. A foreign body response mediated by macrophages and foreign body-type giant cells was observed by light microscopy (Figure 3-24 C & D). The inflammatory response to the implanted material was similar to that mounted against the sutures (Figure 3-24 E). The implant was surrounded by an incomplete fibrous capsule. Overall, the implants appeared to be well tolerated by the animals and did not cause significant ongoing inflammation, neovascularization or a specific lymphocyte-mediated response. However, the magnitude of the response to the

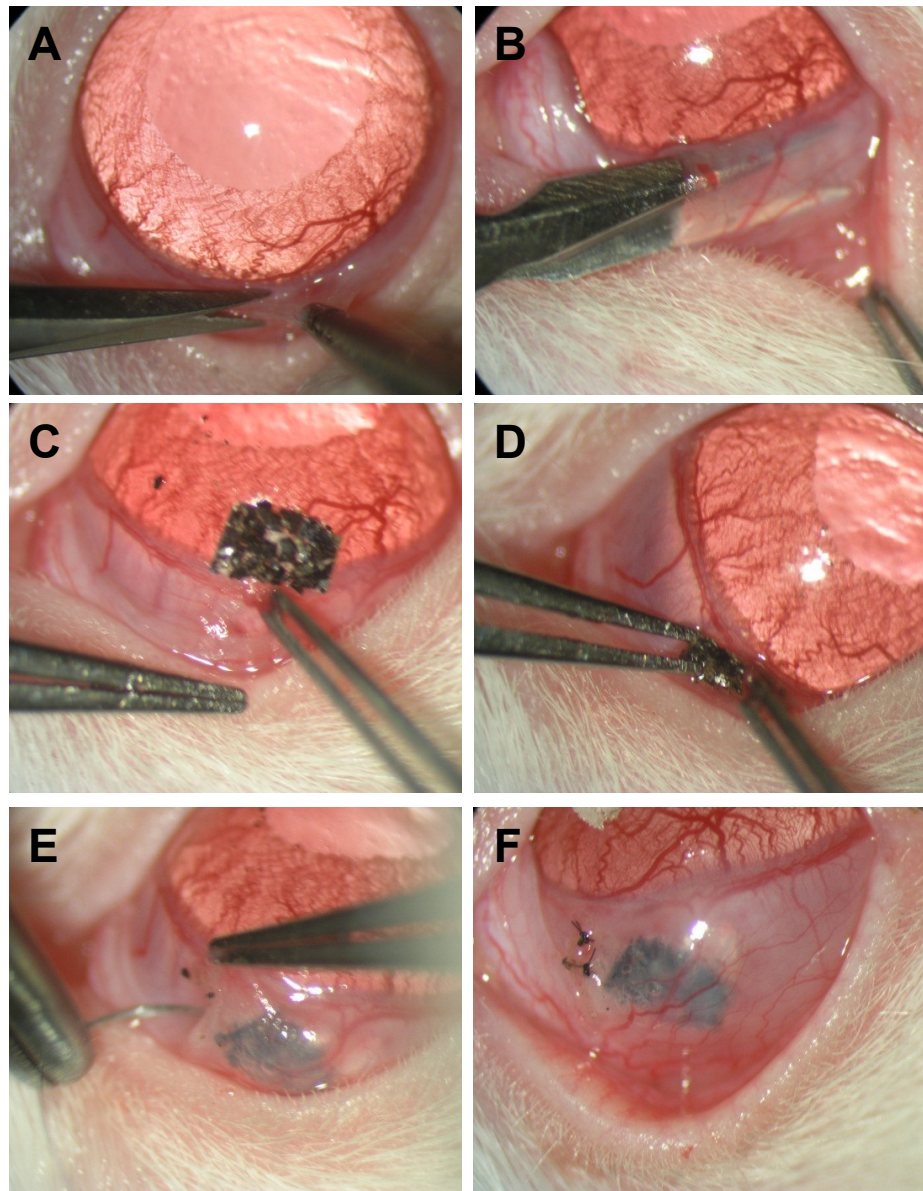


Figure 3-23 Subconjunctival implantation of pSi-PCL composite materials

(A) The conjunctiva was lifted and a small incision made with dissecting scissors. (B) A pocket was created under the conjunctiva, by blunt dissection, using scissors. (C) The implant was placed on the surface of the eye, and the conjunctival pocket opened. (D) The implant was carefully maneuvered into the conjunctival pocket. (E) The conjunctival pocket was closed using 10-0 monofilament sutures. (F) pSi-PCL implanted under the conjunctiva of the rat eye. Images were taken at the operating microscope.

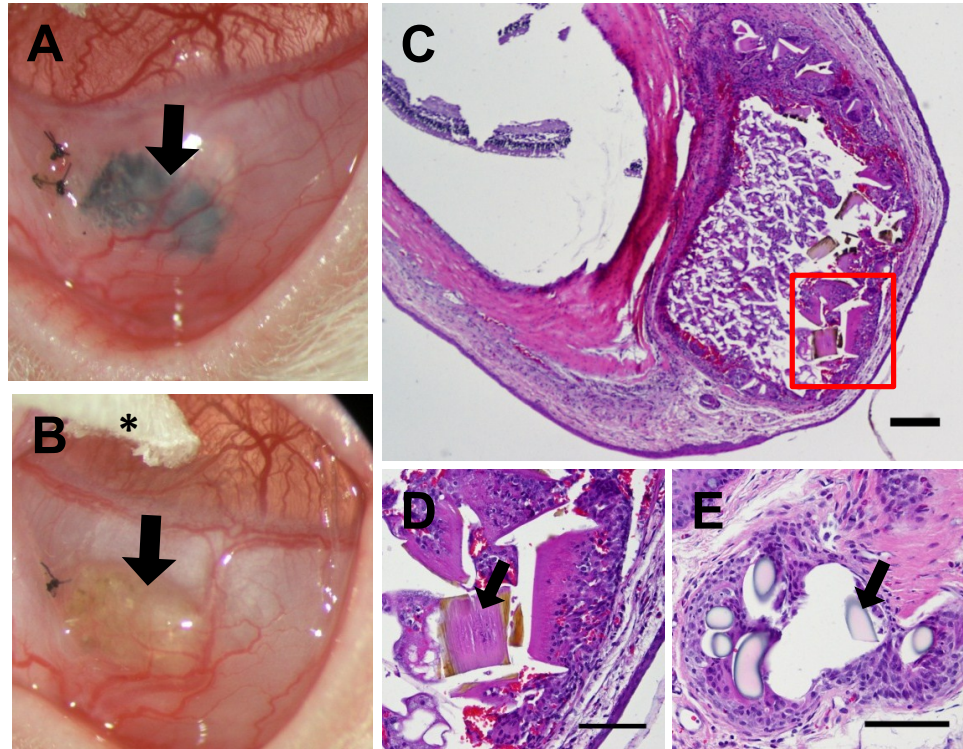


Figure 3-24 Biocompatibility of the pSi-PCL composite materials *in vivo*

(A) & (B) Pressed pSi-PCL composite material implanted under the rat conjunctiva, immediately after implant and 8 weeks post implant respectively. Arrows mark the implants. The pSi particles were visible immediately after implantation but had completely dissolved at 8 weeks. A gauze swab is visible in the top left corner of image B (asterisk). (C) Haematoxylin & eosin stained section of a representative eye 8 weeks post-implantation, depicted a foreign body response, mediated by macrophages and foreign body-type giant cells. (D) Magnified view of the area delineated by the red box in (C), part of the implant is still visible (arrow). (E) Inflammatory response to the suture (arrow) was similar to the foreign body response against the implant. Although a lymphocyte-mediated response was not observed, the intensity of the foreign-body type response to the materials was of concern. Scale bars (C) 200 μm , (D) & (E) 100 μm .

materials was greater than that mounted to the sutures, with a substantial infiltrate of macrophages and giant cells.

In summary, novel pressed pSi-PCL composite materials were prepared. The materials could be loaded with drugs including biologics. The loaded drugs were released in an active form and had a functional effect on cells grown on the composite materials. The composites were implanted under the conjunctiva of rats. At 8 weeks post-implantation the pSi particles had dissolved, however the polymer fabric remained visible. Histological examination revealed that there was a foreign body type inflammatory response, consisting of histiocytes and giant cells. The magnitude of the response was larger than that observed against pSi membranes, and will be of concern if the materials are used to construct an artificial stem cell niche.

3.4 Discussion

The overarching aim of this section of the work was to explore the suitability of different scaffolds for the transfer of epithelial cells to the eye, with the view to create an artificial stem cell niche for the treatment of ocular surface disease. Two porous silicon materials, pSi membranes and pSi-PCL composite materials, were investigated. First, rat OMECs were grown on pSi membranes coated with collagen IV and vitronectin. The OMECs expressed corneal epithelial cell and putative stem cell markers. However, these cells grown on pSi membranes failed to migrate across the ocular surface when implanted under the conjunctiva of rats. The pSi membranes degraded rapidly *in vivo*, and thus pSi-PCL composite materials, which were longer-lived, were investigated. The pSi-PCL composite materials could be loaded with drugs including “biologics”. The drugs were released in an active form and exerted a

functional effect on cells grown on the composites. However, the composite materials elicited a more pronounced inflammatory response on implantation under the rat conjunctiva than had the pSi membranes.

Porous silicon materials have a number of properties that make them amenable for use as an ophthalmic implant for the transfer of cells and drugs to the eye. Porous silicon is first and foremost biocompatible^{363, 366, 391}. It is a versatile material that can be fabricated into films, membranes, micro- or nano-particles, and composite materials, which allows tuning of the properties to suite the application³⁵⁴. It is easily sterilised, minimizing the risk of infection. The size and shape of the pores can be altered³⁶⁰, a property that could be used to better mimic the stem cell niche architecture. Porous silicon materials support the growth of a wide variety of mammalian cells^{368, 369, 391}, and can be loaded with drugs^{364, 381, 456, 457}, including biologics^{350, 458-460}. This property is particularly important as an artificial stem cell niche might need to be loaded with factors that maintain stem cells.

3.4.1 Scaffolds to transfer stem cells to the eye for ocular surface regeneration

Amniotic membrane is the current scaffold of choice for the transfer of epithelial cell to the eye, for the treatment of limbal stem cell dysfunction (LCSF) in humans. Amniotic membrane does support epithelial cells, and has anti-inflammatory⁴⁶¹ and anti-neovascular⁴⁶² properties. Tsai *et al* expanded autologous limbal tissue from the contralateral eye of six patients with LCSF, on amniotic membranes. Transplantation of the membranes carrying cells in the diseased eye led to complete re-epithelialization and improvement of visual acuity in all cases¹⁴⁴. Koizumi *et al* used allogeneic limbal tissue cultivated on amniotic membrane to treat ocular surface

disease in 13 eyes of 11 patients. Six months post-graft, visual acuity was improved by two or more lines in 10 of the 13 eyes, although epithelial rejection was observed in the remaining eyes¹⁰². Basu *et al* published two large retrospective studies of patients with unilateral (n=50) or bilateral (n=28) LCSD, treated with autologous or allogeneic limbal cells, respectively. Thirty three of 50 patients treated with autologous cells maintained a stable corneal surface, and visual acuity was improved by two or more lines in 38 patients¹⁵¹. In the group receiving allogeneic limbal cells, 20 of 28 eyes had re-epithelialised, and 19 eyes demonstrated an improvement in visual acuity, however penetrating keratoplasty was required in 13 eyes⁴⁶³. Amniotic membrane does have some disadvantages: it is translucent, rather than transparent, and being biologically sourced, poses the risk of transmission of infectious agents. Infections following transplantation of amniotic membrane have been reported, with the majority of cases being attributed to Gram-positive bacteria⁴⁶⁴.

A number of materials are under investigation as possible alternatives to amniotic membrane. Culture of human corneal epithelial cells has been demonstrated on a wide range of materials *in vitro*. Human corneal epithelial cells have been grown on silk fibroin¹⁸⁴, a protein extracted from the cocoons of the silk worm. Human and rabbit primary limbal explants were successfully cultured on silk fibroin matrices, and developed into stratified epithelium expressing the progenitor cell marker Δ Np63, and the corneal epithelial cell marker CK3/12⁴⁶⁵. Human hair keratin is another material derived from a natural source. Corneal epithelial cells have been successfully grown on keratin films⁴⁶⁶, however it was found that the films were difficult to implant in porcine eyes *ex vivo*, due to difficulty placing the sutures⁴⁶⁷.

Non biological substrates have also been investigated as an alternative to amniotic membrane. Corneal epithelial cells have been cultured *in vitro* on completely artificial substrates such as polymethylacrylate^{190, 191}, hydroxyethyl-methyl acrylate¹⁹², polylactide¹⁸⁹ and poly(ϵ -caprolactone)¹⁸⁸. Electrospun polycaprolactone scaffolds have been shown to support the growth of rabbit conjunctival epithelial cells, which formed a stratified epithelial layer expressing conjunctival markers, when implanted into SCID mice¹⁸⁷.

Besides amniotic membrane, two materials have been employed for the transfer of cells to the human eye *in vivo*. Rama *et al* cultivated autologous limbal epithelial cells from patients with unilateral LCSD on fibrin sheets, and transplanted the cells into the damaged eye¹⁷⁸. Re-epithelialization was observed in 14 of 18 patients, with improved visual acuity¹⁷⁸. In a larger follow-up study, 112 patients were treated, with 76% of the corneas re-epithelialised and stable ocular surfaces observed for up to 10 years¹⁷⁹. Limbal epithelial cells grown in medium with autologous serum have been shown to adhere to and proliferate on soft contact lenses, and to express CK3/12 and p63¹⁵². A study in three patients demonstrated transfer of the cells, grown on contact lenses, to the damaged ocular surface in patients with LCSD, resulting in a stable ocular surface and improved visual acuity¹⁵⁶.

Much of the research on scaffolds to transfer cells to the ocular surface has focused on delivery of the cells directly to the central cornea, with the scaffold acting like a bandage to cover the epithelial defect. Although this approach has resulted in some promising results, in cases with total LCSD, if stem cells are not transferred and maintained over a long period of time, the therapy will eventually fail.

An alternate approach is to replace the damaged stem cell niche with an artificial substrate carrying stem cells. The goal is to have a population of self-renewing stem cells in the niche. Daughter cells would migrate across the cornea and differentiate into mature corneal epithelial cells. This approach has been tested by others, using different scaffolds. In an attempt to recreate the limbal microenvironment, dual-layer silk fibroin membranes have been shown to support the culture of human epithelial and stromal cells¹⁸⁶. Three dimensional patterned polymer scaffolds have been developed to mimic the structure of the limbus. These scaffolds supported the growth of rabbit limbal epithelial cells⁴⁶⁸. In 2013, three dimensional porous silicon materials were fabricated to mimic the architecture of the palisades of Vogt. Coating the scaffold with fibronectin improved cell adhesion and migration, and the cells formed multilayered epithelium when implanted in the cornea *ex vivo*⁴⁶⁹.

The current study examined the possible use of pSi scaffolds carrying epithelial cells, implanted under the conjunctiva close to the limbus, for the treatment of ocular surface disease. pSi materials have a large drug loading capacity and can be loaded with macromolecular drugs. In the context of recreating the limbal stem cell niche, pSi scaffolds were loaded with collagen IV and vitronectin, which have been shown to be expressed at the limbus but not to a significant extent in the central cornea⁷⁷. pSi membranes coated with vitronectin or collagen IV supported the growth of oral mucosal epithelial cells, containing a small population of putative stem cells.

3.4.2 Source of stem cells

In the case of unilateral disease, limbal stem cells can be harvested from the contralateral eye. However, if too much limbal tissue is harvested, there is a risk of

inducing disease in the normal eye⁸⁶. Furthermore, this is not an option in LCSD caused by a genetic condition such as aniridia, or by Stevens-Johnson syndrome. This forces the transplantation of allogeneic tissue from cadaveric donors, and such grafts usually require long-term systemic immunosuppression^{94, 470}. Cadaveric tissue is generally obtained from older donors, which may be of concern, as the colony forming efficiency of limbal epithelial cells is reduced after the age of sixty³⁴.

Alternate autologous sources of stem cells for corneal surface reconstruction are currently being investigated. Corneal epithelial equivalents have been harvested from oral mucosa, conjunctiva, skin, dental pulp, hair follicles, and nasal mucosa. Induced pluripotent stem cells and embryonic stem cells have also been investigated^{132, 471}. However, the best results have been obtained using oral mucosal epithelium. The advantages of using oral mucosa are manifold. Normal human oral mucosal epithelium, like corneal epithelium, is non-keratinised. It is an easily-accessible tissue to biopsy and is a source of adult stem cells. *Ex vivo* expanded oral mucosal cells have been used clinically for the treatment of LCSD. Initial studies demonstrated that cultured autologous oral mucosal epithelial cells can be transferred to the eye, in humans, on amniotic membranes (n=6)¹¹³, or as freestanding epithelial sheets generated by detachment from a temperature responsive gel (n=4)¹⁰⁷, resulting in complete re-epithelialization of the corneal surface. The Kinoshita group has published long-term results demonstrating complete re-epithelialization in 19 eyes in 17 patients, with 53% of patients showing an improvement in visual acuity at 36 months¹¹⁴. A larger study with 46 eyes in 40 patients yielded similar results, with 15 of 31 (48%) of patients with vision loss recording improved visual acuity⁴⁷². These results have been replicated by Satake *et al*, who showed that 53% of patients had a

stable ocular surface 3 years after an oral mucosal cell graft (n=40 eyes in 36 patients)¹¹⁵.

Oral mucosal epithelial cells have previously been isolated from the rat, and grown on temperature responsive culture dishes, with 3T3 feeder cells¹⁰⁹. Oral mucosal tissue was successfully isolated from young male (6-8 week old) inbred Sprague-Dawley rats. The epithelium was separated after dispase treatment, and a single cell suspension generated by trypsin digestion and gentle mechanical disaggregation. Tissue from young rats (6-8 weeks old) yielded more colonies than tissue from rats over 12 weeks old, which is in keeping with observations in the human³⁴. Colonies of oral mucosal epithelial cells readily grew on porous silicon coated with collagen IV or vitronectin. The cells were grown in low calcium medium to prevent differentiation⁴⁷³. Airlifting the cells was also avoided to maintain the cells in an undifferentiated state, preventing stratification into a multi-layered epithelial cell sheet¹⁴⁶. The cells expressed epithelial cell markers, as well as progenitor cell markers, which will be discussed further below.

3.4.3 Characterization of OMECs on pSi scaffolds

There are currently no unambiguous markers for corneal epithelial stem cells. Identification of putative stem cells and their progeny relies on using a combination of markers for both undifferentiated and differentiated cells. Differentiation markers are used for TACs and terminally differentiated cells, while other markers label progenitor and putative stem cells. Rat oral mucosal epithelial cells grown on pSi scaffolds were probed with antibodies raised against CK3/12, a marker of mature corneal epithelial cells⁶⁶, CK19, a basal epithelial cell marker⁶⁶, p63, a transient

amplifying cell marker⁴⁶ and ABCG2, which has been shown to be highly expressed in a number of stem cells⁵².

CK3/12 is expressed by mature human corneal epithelial cells⁶⁵, and is not expressed in the basal cells of the limbus¹⁸. CK3/12 expression can be detected in human corneal epithelium, but is lacking in other epithelial tissue⁶⁵. A similar pattern of CK3/12 expression has been observed in the guinea pig⁷³ and mouse⁴⁷⁴. Here, we found that rat OMECs had varying levels of CK3/12 expression, with some cells showing strong expression, while others had either low or no expression. This would indicate that the OMECs consisted of a heterogeneous population of cells, in varying degrees of differentiation.

CK19 is a basal epithelial cell marker. In both mouse and humans, CK19 has been shown to be expressed in the stem cells of the skin⁷². In the human eye, expression of CK19 has been demonstrated in the basal cells in the periphery of the cornea, but expression is lacking in the central cornea⁶⁶. The rat OMECs expressed low levels of CK19. An interesting expression pattern was observed in some cells, with strong nuclear expression along with cytoplasmic expression. As the cytokeratins are intermediate filament proteins, expression would be expected in the cytoskeleton.

The transcription factor p63 has been shown to be expressed in human keratinocyte stem cells¹⁹. In human corneas p63 expression has been shown to localise to basal epithelial cells, with higher expression in the limbal region⁴⁶. p63 is thought to label transient amplifying cells but not stem cells. A majority of rat oral mucosal epithelial cells grown on pSi scaffolds had strong nuclear expression of p63, indicating that the OMECs maintained proliferative potential when cultured on pSi scaffolds.

The most widely used marker for putative corneal epithelial stem cells is ABCG2, which is a cell membrane bound transporter protein⁴⁷⁵. ABCG2 is associated with the side population phenotype, of cells that efflux Hoechst 33342 dye. High expression of ABCG2 has been demonstrated in a number of stem cells^{52, 53}. A side population phenotype has been associated with limbal epithelial cells⁵⁷; such cells express high levels of ABCG2 and have a higher colony forming efficiency than ABCG2 negative cells⁵⁹. ABCG2 mRNA expression has been detected in both limbal and oral mucosal epithelial cell cultures derived from human tissue¹¹⁹. In this study, a small proportion of rat OMECs grown on pSi scaffolds expressed ABCG2, indicative of the presence of a small number of putative stem cells. A number of other markers have been used for the characterization of limbal and oral mucosal epithelial cells, some of which are outlined in Table 5-1.

In summary, rat OMEC cultured on pSi scaffolds consisted of a heterogeneous population of cells containing some differentiated cells that expressed CK3/12, a large number of p63-positive transient amplifying cells, and a small number of putative stem cells that expressed ABCG2. This is the ideal mixture of cells for transplantation to the eye for the treatment of ocular surface disease. The presence of stem cells provides a source of renewal for the corneal epithelium, while transient amplifying cells can rapidly proliferate, migrate and undergo differentiation to yield mature corneal epithelial cells.

3.4.4 Fate of OMECs after transplantation to the rat eye

Oral mucosal epithelial cells were grown on pSi scaffolds, and implanted under the conjunctiva of female rat eyes. Cell samples taken from the central cornea and the

conjunctiva around the implant site were analysed by PCR for the presence of transplanted cells. Transplanted male cells that had migrated over the ocular surface would be detected in the cell lifts by amplifying the male specific gene *sry*, by PCR. This approach has been used previously for the detection of transplanted tissue in the heart⁴⁵³. *sry* PCR has also been used in our laboratory to monitor the survival of donor cells on the surface of the rat eye following limbal grafts⁹⁷.

In the experiments reported here, no transplanted male cells were detected from the central cornea or the conjunctiva around the implant site, by PCR. The PCR was designed to maximise sensitivity without compromising specificity: *sry* could be amplified from 8 pg of male gDNA in the presence of female cells. This is equivalent to detection of a single male cell. However, it must be noted that no DNA was detectable in a significant percentage of cell samples (up to 50%). This indicated a significant technical failure rate in the collection of DNA from the ocular surface.

The failure to detect transplanted male cells may be attributed to a number of factors including the placement of the pSi scaffolds. Although every effort was made to place the implants carrying OMECs as close to the limbus as possible, they were not at the limbus. Furthermore, the cells might not have migrated to the central cornea in the timeframe of the experiment. Under normal conditions, corneal epithelial cells migrate from the periphery to the centre of the cornea in 7 to 10 days^{25, 43}, and even faster during wound healing⁴⁷⁶. The length of the current study was 8 weeks, which should have provided sufficient time for the cells to migrate to the central cornea.

Under normal conditions, with a normal corneal epithelium, the transplanted cells might not have migrated over the corneal surface. To test this possibility, ocular

surface disease was induced in rats prior to implantation of cells. A characteristic feature of OSD is conjunctivization of the corneal epithelium. Impression cytology from the central cornea of rats that had their corneas debrided with n-heptanol revealed the presence of PAS-positive goblet cells, indicative of OSD. However, transplanted OMECs were still not detected on the central corneas of rats with OSD, which suggests that induction of OSD did not stimulate OMEC cell migration.

The cells sampled using FTA paper were superficial epithelial cells and it is possible that the transplanted cells had not migrated to the surface of the cornea (Figure 1-5). To test for this possibility, rat OMECs were labelled with the fluorescent dye PKH26, in order to track the cells visually *in vivo*, as has been demonstrated previously⁴⁷⁷. Labelled cells were detected in corneal flatmounts up to 8 weeks post-implantation, by fluorescence microscopy. However, the majority of labelled cells remained on the pSi scaffold 2 weeks post-implantation. Some cells were detected in the tissue surrounding the implant at later time points, but the cells did not migrate onto the corneal surface. This is in contrast to experiments conducted by Low *et al*, who showed that human limbal epithelial cells migrated off pSi implants one week post-implantation under the rat conjunctiva³⁹¹. These experiments used rat collagen I coating on pSi scaffolds, while the current study used collagen IV and vitronectin. Differences in the coatings might explain the observed difference in cell migration.

3.4.5 Degradation of the pSi scaffold

Freshly etched porous silicon without any surface modifications degrades over the course of a few hours in aqueous solution³⁸⁷. For a porous silicon scaffold to be of use as an artificial stem cell niche, it will need to maintain its structure in the longer

term. Oxidation stabilises pSi, preventing rapid degradation^{375, 376}. Oxidised pSi membranes implanted in rat eyes were exposed to OMECs in cell culture medium for one week, followed by subconjunctival implantation under the conjunctiva in rats for up to 8 weeks. Visual signs of degradation (change in colour from black to brown) were apparent in the materials as early as 4 weeks after implantation. The materials had not dissolved completely by 8 weeks post implant, but had undergone a significant degree of degradation. Porous silicon degrades to silicic acid^{361, 372}, which in turn may lead to local toxicity. The degradation rate of the porous silicon membranes was not acceptable for its use as a scaffold to recreate a niche for stem cells. As noted above, an artificial stem cell niche would need to be stable over a period of weeks to even years, to maintain a stem cell reservoir to renew the corneal epithelium. To address this issue we moved to the use of pSi composite materials.

3.4.6 Porous silicon polycaprolactone composite materials as ophthalmic implants

Composite materials prepared with porous silicon and soft polymers such as polycaprolactone have significant advantages over the individual component materials. The polymer lends flexibility to the ridged pSi, making manipulation and implantation easier. Importantly, PCL also degrades more slowly than pSi *in vivo*. For example, PCL capsules degraded over the course of 2-3 years when implanted subcutaneously in the rat⁴⁰⁹. This would make the composite materials longer lived than pSi membranes. The biocompatibility of PCL in the eye has been evaluated: PCL sheets remained stable after implantation in rabbit eyes for up to 9 months, without adverse effects on the ocular tissue⁴⁷⁸. Addition of pSi particles to the polymer allows loading of a large amount of drugs, including biologics. We

considered that a pSi-PCL composite material might potentially be used as an artificial stem cell niche for the transfer of cells to the eye for the treatment of ocular surface disease.

A novel composite material of pSi and PCL was thus formulated. The PCL was electrospun into a non-woven fabric, and pSi microparticles were partially embedded into the pSi fibres. A composite material of pSi and PCL, with the pSi particles completely encapsulated in the PCL fibres, was previously investigated in our laboratory, and was shown to support the growth of human lens epithelial cells⁴²². The advantage of the novel material described herein, is that it can be loaded with drugs *after* fabrication. This is particularly important in the context of recreating an artificial stem cell niche, as biologics such as collagen and vitronectin which support the growth of epithelial cells, will otherwise be destroyed during the composite fabrication process.

3.4.6.a *Drug loading in the pSi-PCL composite materials*

In order to function as an artificial stem cell niche, a pSi-PCL composite material will need to be loaded with factors to support the growth of stem cells. The feasibility of drug loading in the material was thus evaluated.

Firstly, the loading of a model small molecule drug, fluorescein diacetate (FDA), was examined. The ability of the composite material to release the FDA was assessed by seeding lens epithelial cells on FDA loaded materials. Lens epithelial cells grown on the FDA loaded material demonstrated green fluorescence, indicating that the FDA was released from the materials and converted to fluorescein. An added advantage of

this assay was the demonstration that the cells grown on the materials were viable. This result opens up the possibility of the composite materials being used for the delivery of drugs to the eye. Decrease of intraocular pressure has been demonstrated in rabbits after implantation of a polycaprolactone scaffold loaded with dorzolamide⁴⁷⁹. A pSi-PCL composite material with a large drug loading capacity could be of use for such an application.

The loading of macromolecule “biologics” into composites was also investigated. A mixture of recombinant epidermal growth factor, insulin, transferrin and selenium sulphate (EGF-ITS), which induces cell proliferation in the absence of serum, was tested. Such a cocktail of specific, recombinant biologics might reduce reliance on foetal calf serum for the growth of OMECs, as FCS poses regulatory concerns associated with the transmission of infectious agents such as prions. The release of the biologics in an active form was assayed using BALBc/3T3 cell proliferation. The cells did not proliferate in serum-free medium when seeded on either unloaded pSi-PCL composites or PCL alone loaded with the growth factors. However, cells seeded on pSi-PCL composite materials loaded with EFG-ITS, in serum-free medium, proliferated. This experiment demonstrated that factors loaded in the composite materials were taken up by adherent cells. It also demonstrated the importance of the pSi on the composite materials, as no proliferation was observed in cells seeded on “loaded” PCL, indicating that only pSi-PCL composite materials could be loaded with the biologics post-fabrication and that the biologics had in fact loaded in the pSi particles. These experiments demonstrated the feasibility of loading the pSi-PCL composite materials with factors to help in the re-creation of a niche that might

sustain the growth of stem cells. The next step was to confirm the biocompatibility of the materials in the rat eye.

3.4.6.b *Biocompatibility of pSi-PCL composite material in the rat eye*

Haematoxylin and eosin stained sections of rat eyes containing pSi-PCL composite material 8 weeks post-implant showed a foreign body-type inflammatory response, similar in kind to that directed to the sutures. However the magnitude of the response to the implant was greater. Larger numbers of infiltrating cells were observed, both in and around the implant, and the implant itself was surrounded by an incomplete fibrous capsule. This was unexpected, taking into consideration that both the pSi and PCL are generally well tolerated *in vivo*. PCL has demonstrated good biocompatibility in the rabbit eye, with no inflammation, morphogenic changes or fibrosis noted after 6 months of implantation⁴⁷⁸. pSi scaffolds implanted under the rat eye did not cause an accumulation of inflammatory cells³⁹¹. Previous work in our laboratory with a different pSi-PCL composite material showed implantation under the rat conjunctiva resulted in a histiocytic foreign body-type granulomatous response, similar to that mounted against the sutures⁴²². The difference between the two materials was that in the new composites described here, the pSi microparticles were partially exposed, whereas they were completely encapsulated in the old materials. The presence of both pSi and PCL on the surface of the material might have caused the more pronounced infiltration of inflammatory cells. It must be noted that there was no lymphocyte-mediated response to the pSi-PCL materials. No overt signs of inflammation were observed macroscopically after 7 days of implantation. However, the degree of infiltration of macrophages and histiocytoid giant cells observed at end-point histology was troubling.

3.5 Conclusions

Two porous silicon materials were investigated for the transfer of cells and drugs to the rat eye. Porous silicon membranes coated with collagen and vitronectin supported the growth of rat oral mucosal epithelial cells. The rat OMECs expressed corneal epithelial and putative stem cell markers. However, OMECs grown on pSi membranes did not migrate across the surface of the rat eye when implanted under the conjunctiva. The pSi membranes demonstrated good biocompatibility, but dissolved rapidly. Longer-lived pSi-PCL composite materials were then tested. The composite materials could be loaded with drugs including biologics, which were released in an active form and had a functional effect on cells. However, implantation of the composite materials under the conjunctiva in rats elicited a foreign body-type inflammatory response. The magnitude of the response was of some concern. Porous silicon poly-(ϵ -caprolactone) composites offer advantages over the individual components, but improved biocompatibility is required to recreate an artificial stem cell niche for the treatment of ocular surface disease.

This study demonstrated that rat oral mucosa is a good source of epithelial cells, including putative stem cells. OSD was successfully induced in rats, providing a robust model for testing future cell therapies. However, transplanted cells must be able to migrate over the ocular surface after induction of OSD and this was not observed in the experiments described here.

CHAPTER 4 VEGF-B ANTAGONISM IN CORNEAL NEOVASCULARIZATION

VEGF-B is a member of the vascular endothelial growth factor family, and has structural similarities to VEGF-A and PlGF²³⁷. Unlike other members of the VEGF family, VEGF-B does not behave as a pro-angiogenic factor. It is the only member of the VEGF family that does not induce angiogenesis, lymphangiogenesis or vessel permeability^{248, 249}. Recent evidence suggests that VEGF-B is more of a survival than a growth factor^{257, 480}, and has a role in lipid transport²⁷⁶. VEGF-B is a potent survival factor for vascular endothelial cells, pericytes and smooth muscle cells²⁵⁷. VEGF-B deficiency leads to increased apoptosis of endothelial and smooth muscle cells and poorer survival of blood vessels²⁵⁷. Furthermore, VEGF-B expression has been found to augment pathological neovessel formation in models of choroidal and retinal neovascularization²⁵⁸. VEGF-B also appears to be a survival factor for different types of neurons including brain cortical neurons^{272, 273}, retinal neurons²⁷³ and motor neurons in the spinal cord²⁷¹. Taken together, these data suggest that VEGF-B is a potential target for therapy directed at existing vasculature. However, targeting VEGF-B may risk damaging neurons.

As VEGF-B appears to be a survival factor for a large range of cells including neurons, *targeted* delivery of an anti-VEGF-B drug to the cornea may be essential, to ameliorate corneal neovascularization. The cornea is accessible and topical delivery in the form of eye drops is possible. In contrast, delivery of agents to the retina necessitates intravitreal injection. Topical delivery to the cornea in the form of eye drops might prevent unwanted systemic side effects. Furthermore, eye drops can be

relatively easily self-administered. Targeted delivery to the cornea can also be achieved by subconjunctival injection.

Antibodies are important therapeutic agents and serve as molecular traps or targeting agents. Antibodies are, however, too large for effective topical delivery to the cornea^{443, 481} and have the potential to be immunogenic and elicit unwanted release of cytokines mediated by the Fc region of the immunoglobulin tail^{482, 483}. Genetically engineered antibody fragments maintain the antigen binding specificity of the parent antibody but lack some of the undesirable properties of the latter, such as poor tissue penetration, long half-life in blood and activation of the effector arm of the immune system. As proof of principle for local administration, a topically delivered antibody fragment to TNF α has been shown to inhibit development of laser-induced choroidal neovascularization in a monkey model⁴⁸⁴.

The aim of this work was to engineer an antibody fragment which binds to VEGF-B, and to test the effect of topical and subconjunctival injection of the scFv on growing and especially on established vessels, in a rat model of corneal neovascularization. We hypothesised that the anti-VEGF-B scFv, delivered locally to the cornea, would cause regression of established corneal vessels.

4.1 Generation and characterization of an anti-VEGF-B scFv

4.1.1 The 2H10 hybridoma

The 2H10 hybridoma secretes an antibody with specificity for human, mouse and rat VEGF-B⁴⁸⁵ (Appendix C.1). cDNA from this hybridoma was a gift from Dr. Pierre Scotney and Dr. Andrew Nash (CSL Ltd. & Melbourne University). An antibody

fragment in the scFv format was engineered from 2H10. The first step in this process was the amplification of the variable region genes from hybridoma cDNA.

4.1.2 Amplification of the V_L and V_H and production of a scFv gene

A scFv consists of a variable light chain (V_L) and variable heavy chain (V_H) joined together by a peptide linker. The V_L and V_H of the 2H10 hybridoma were successfully amplified from 2H10 hybridoma cDNA using custom-designed primers (Table 2-1). The expected product sizes for the V_L and the V_H were 387 bp and 407 bp respectively. The products amplified corresponded to the expected sizes (Figure 4-1). The primers added nucleotides encoding the linker region to the 3' end of the V_L and 5' end of the V_H respectively. The primers also had complementary regions which allowed for splicing together the V_L and V_H. A scFv gene was generated from the V_L and V_H of the 2H10 hybridoma using an assembly PCR protocol (section 2.2.4). The expected size of the assembly PCR product was 771 bp, and the predominant band ran slightly below the 800 bp marker (Figure 4-1). The anti-VEGF-B scFv gene was then cloned into a bacterial expression vector.

4.1.3 Cloning of the anti-VEGF-B scFv in *E.coli*

4.1.3.a Restriction endonuclease digestion with *Sfi*I

The assembly PCR product from the 2H10 hybridoma and the pHB400 bacterial expression vector was digested with the restriction endonuclease *Sfi*I. Initially a 4 h digestion was used which was insufficient for complete digestion of the plasmid (Figure 4-2). Subsequently, both the plasmid and the scFv were digested overnight with *sfi*I as described in section 2.2.6 (Figure 4-2). The vector region of the plasmid (~4800 bp) (Figure 2-1) was gel purified and *Sfi*I digested insert (scFv) was PCR

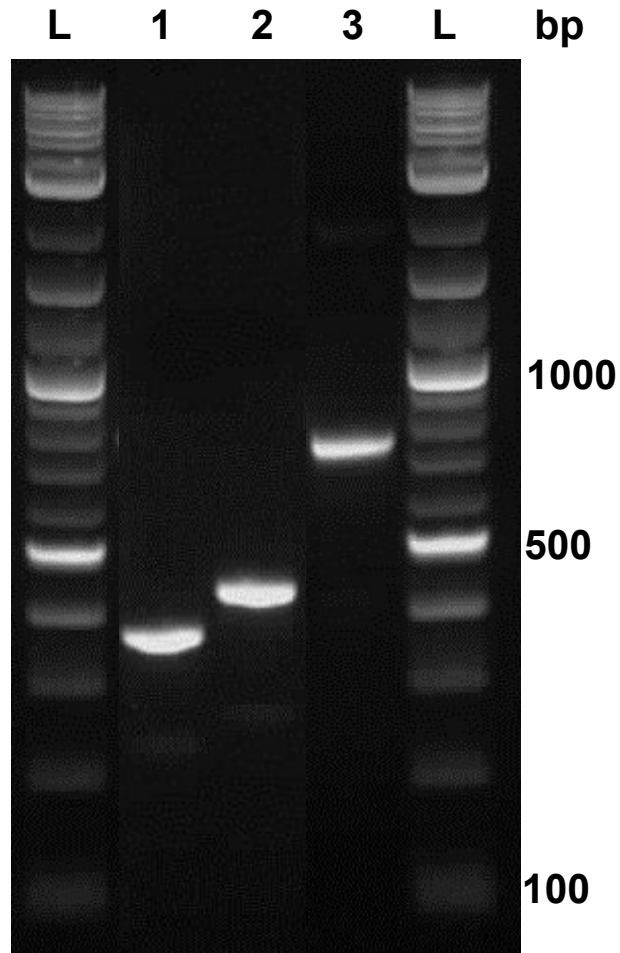


Figure 4-1 Generation of an anti-VEGF-B scFv gene from the 2H10 hybridoma

The V_L (lane1) and V_H (lane2) regions were amplified from 2H10 hybridoma cDNA. The primers used to amplify the V_L and V_H added complementary DNA encoding a linker region, allowing assembly of the scFv gene (lane3) by splice by overlap extension (SOE) PCR. The expected product sizes for the V_L, V_H and SOE product were 387, 407 and 771 bp respectively. The observed bands corresponded to the expected product sizes. Five hundred nanograms of the 2Log ladder size marker was run in the lanes marked L. Fragment lengths are represented in base pairs.

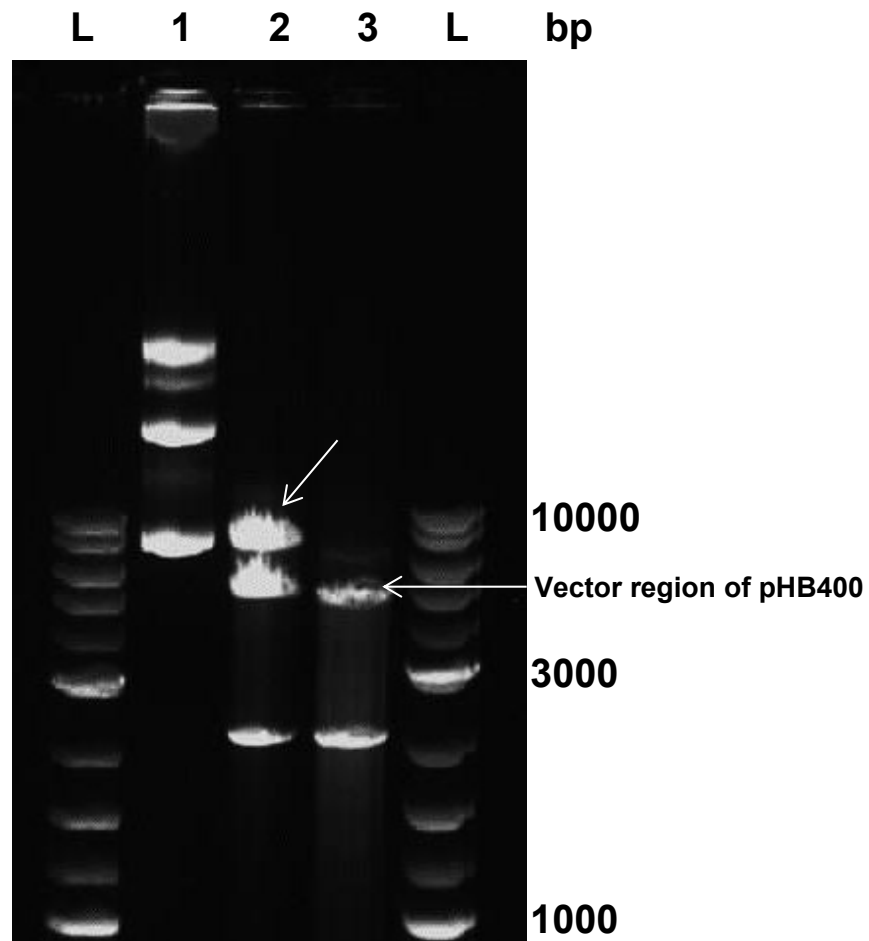


Figure 4-2 SfiI digestion of plasmid pHB400

The plasmid pHB400 (lane1) was digested with SfiI for 4h (lane2) or overnight (lane3). Incomplete digestion was observed at 4 hours as evidenced by the presence of a band corresponding to uncut plasmid (white arrow). Overnight digestion was required to minimise uncut plasmid. Five hundred nanograms of the 2Log ladder size marker was run in the lanes marked L.

purified using the QIAquick gel extraction kit and the PCR purification kit respectively (Qiagen, Valencia, CA, USA). The scFv gene was next ligated into a bacterial expression plasmid.

4.1.3.b *Ligation of scFv into the bacterial expression plasmid pHB400*

Overnight ligation reactions were carried out using T4 DNA ligase (section 2.2.7). Two sets of ligation controls were included. The first contained plasmid but no ligase and no insert and the second plasmid and ligase but no insert. Insert to vector molar ratios of 1:1 and 2:1 were used.

The ligation reactions were precipitated and washed twice with ethanol to remove protein and salts, to increase the efficiency of the subsequent electroporations. The precipitated DNA was dissolved in a small amount of ddH₂O and an aliquot was separated on a 0.8% agarose gel to visualise the results of the ligation reactions (Figure 4-3). The anti-VEGF-B scFv was successfully ligated into pHB400, as evidenced by observation of bands not corresponding to the size uncut or single cut pHB400 (Figure 4-3). The pHB400 vector carrying the anti-VEGF-B scFv was then used to transform electrocompetent *E.coli*.

4.1.3.c *Transfection of E.coli HB2151 with plasmid containing the anti-VEGF-B scFv*

Electrocompetent *E.coli* HB2151 cells were generated as described in section 2.3.1. The cells were transfected with pHB400 containing the anti-VEGF-B scFv, as well as ligation controls, as described in section 2.3.2. pHB400 contains the CAT gene

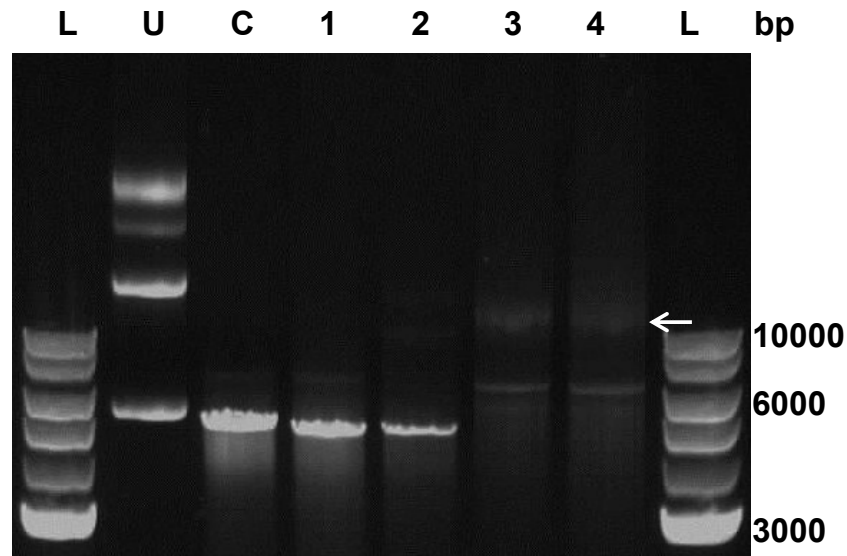


Figure 4-3 Ligation of the anti-VEGF-B scFv into pHB400

The 2H10 scFv gene was ligated into the plasmid pHB400 using T4 DNA ligase. Fragment sizes are represented in base pairs.

Lanes:

L – 2Log ladder size marker

U – Purified undigested pHB400

C – Purified SfiI digested pHB400

1 – SfiI digested pHB400 + ligation buffer (control reaction)

2 – SfiI digested pHB400 + ligation buffer and T4 DNA ligase (control reaction)

3 – SfiI digested pHB400 + ligation buffer, T4 DNA ligase and SfiI digested 2H10 scFv (1:1 molar ratio)

4 – SfiI digested pHB400 + ligation buffer, T4 DNA ligase and SfiI digested 2H10 scFv (1:3 molar ratio)

No ligation was observed in the reaction containing cut plasmid with ligation buffer (1) or plasmid with ligation buffer and T4 DNA ligase (2). Two molar ratios of plasmid to insert were tested. Ligation was observed in both reactions as evidenced by the presence of faint bands that did not correspond to either uncut or cut plasmid (arrow).

which confers resistance to the antibiotic chloramphenicol, allowing transfected cells to grow on chloramphenicol containing medium.

Cells electroporated with SfiI digested pHB400 yielded very few colonies, indicating low levels of uncut plasmid. Cells transformed with religated plasmid showed a large number of colonies, confirming activity of the ligation reactions. Cells transformed with scFv containing plasmid generated a large number of colonies (Table 4-1).

The colonies of *E.coli* HB2151 cells grown on chloramphenicol-containing medium should have had an intact plasmid carrying the CAT gene. However, the colonies still needed to be screened for expression of the anti-VEGF-B scFv.

Table 4-1 Electroporation of 2H10 scFv in pHB400 into *E. coli* HB2151

Sample	Time Constant (ms)	Number of colonies
SfiI digested pHB400	4.1	3
SfiI digested pHB400 + ligase	3.9	TNTC
SfiI digested pHB400 + ligase + scFv 1:1	3.8	TNTC
SfiI digested pHB400 + ligase + scFv 1:2	3.9	TNTC

ms=milliseconds TNTC – too numerous to count

4.1.4 Screening 2H10 scFv transfected clones

Transfection of E.coli HB2151 cells with plasmids containing the 2H10 scFv yielded a large number of colonies. The colonies were first screened by colony blot for the expression of His-tagged recombinant protein and then crude bacterial extracts were screened for binding to rhVEGF-B by ELISA.

4.1.4.a *Colony blot to detect recombinant protein in transfected HB2151 colonies*

The colonies were picked and transferred on to grid plates with medium containing chloramphenicol, to maintain the selective pressure on cells to retain the plasmid. Colonies were grown overnight, transferred to nitrocellulose membranes and placed on agar plates containing 1mM isopropyl β -D-1-thiogalactopyranoside (IPTG), which induces production of recombinant protein, for 24 hours. The membranes were removed from the plates and the cells lysed to allow binding of proteins to the nitrocellulose membranes. The membranes were probed with an anti-polyhistidine antibody. The His-tag is only expressed in colonies that contain a scFv gene that is in the correct phase throughout.

A total of 200 colonies were screened for recombinant protein expression. Seventy eight colonies showed expression of the His tag, of which 40 showed strong expression (Figure 4-4). The remainder of the colonies likely did not express His-tagged scFv. The colonies that displayed expression of the His-tag were then further screened for binding to human VEGF-B by ELISA.

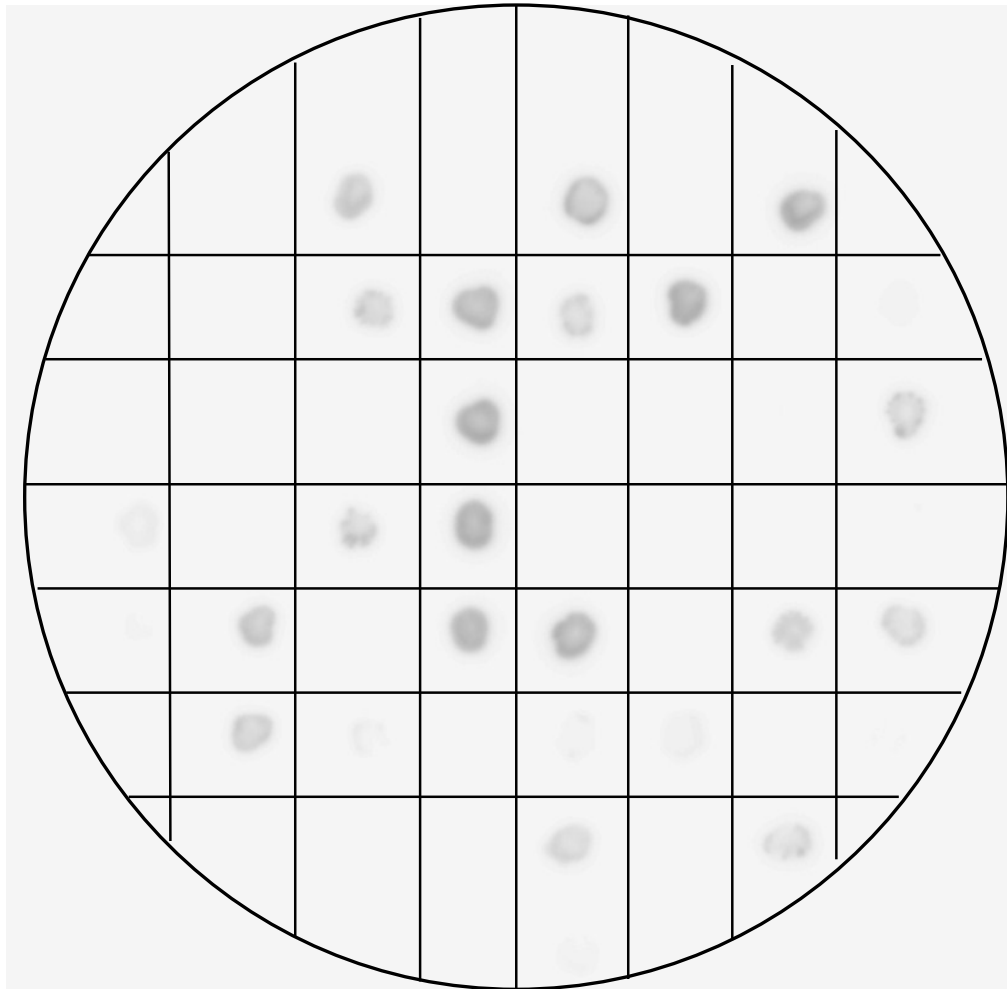


Figure 4-4 Colony blot showing recombinant protein expression in 2H10 scFv clones

Clones of cells transfected with scFv constructs were picked and plated in a grid pattern on replica plates. Colonies from one plate were transferred to nitrocellulose discs and recombinant protein production was induced by addition of IPTG. Presence of recombinant protein was detected by probing with an anti-polyhistidine antibody. A representative membrane containing protein from 50 colonies is shown above. Colonies strongly expressing recombinant appear darker than colonies with intermediate or low expression. A similar pattern of expression was observed with the remaining colonies containing 2H10 scFv.

4.1.4.b *Detection of binding of scFv containing bacterial lysates to VEGF-B*

Bacterial lysates were prepared from *E.coli* producing scFv as described in section 2.3.5. The lysates were assayed for anti-VEGF-B activity using a direct ELISA as described in section 2.2.12. A strong positive signal was obtained with anti-VEGF-B scFv lysate (Figure 4-5), indicating binding to human VEGF-B. Bacterial lysate containing control scFvs with specificity for human VEGF-A⁴⁸⁶ and *Acanthamoeba*⁴⁸⁷ returned negligible readings. The level of scFv expressed from different colonies was variable, which might have had an effect on the binding to VEGF-B. The binding of the scFv produced from different colonies to human VEGF-B was thus assessed by ELISA.

4.1.4.c *Comparison of binding of anti-VEGF-B scFv clones to VEGF-B*

Bacterial extracts were prepared from the 31 highest expressing clones in the colony blot. The extracts were assayed for binding to VEGF-B by direct ELISA. Bacterial extract from pHB400 (empty vector) transfected cells was used as a control. All clones showed binding to VEGF-B when compared to the control. The binding observed varied between clones. The binding was thus normalised to total protein (Figure 4-6). Clone 4.2 and 4.19 displayed the highest binding after normalisation. The higher binding might have been the result either of higher concentration of scFv or by higher affinity of the scFv clone for VEGF-B. The observed differences in the binding of different anti-VEGF-b scFv clones might stem from mutations introduced during the cloning. To further investigate this, a selection of clones was sequenced.

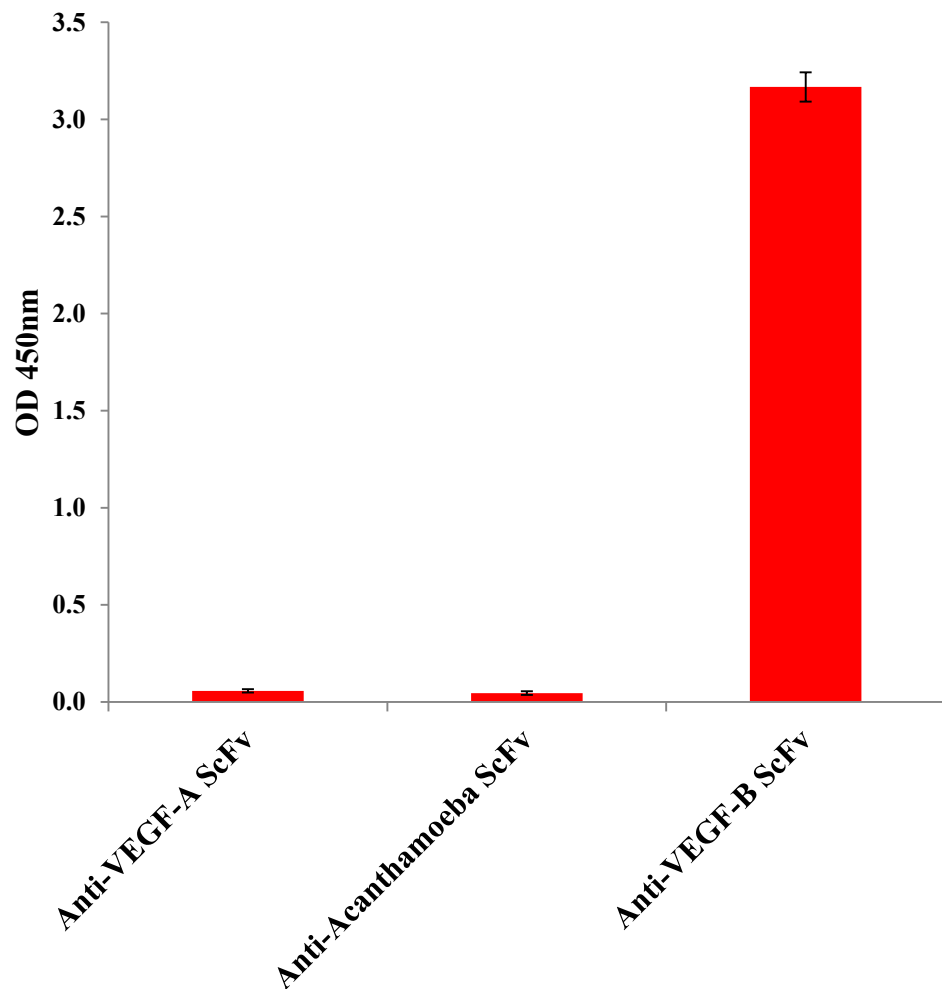


Figure 4-5 Binding of anti-VEGF-B scFv bacterial lysates to human VEGF-B

A direct ELISA was used to assay binding of scFvs present in bacterial lysates to human VEGF-B. The anti-VEGF-B scFv demonstrated strong binding to VEGF-B. Anti-VEGF-A or anti-Acanthamoeba scFvs did not bind to VEGF-B. The bars represent the mean OD_{450nm} of three technical replicates and the error bars represent standard deviation.

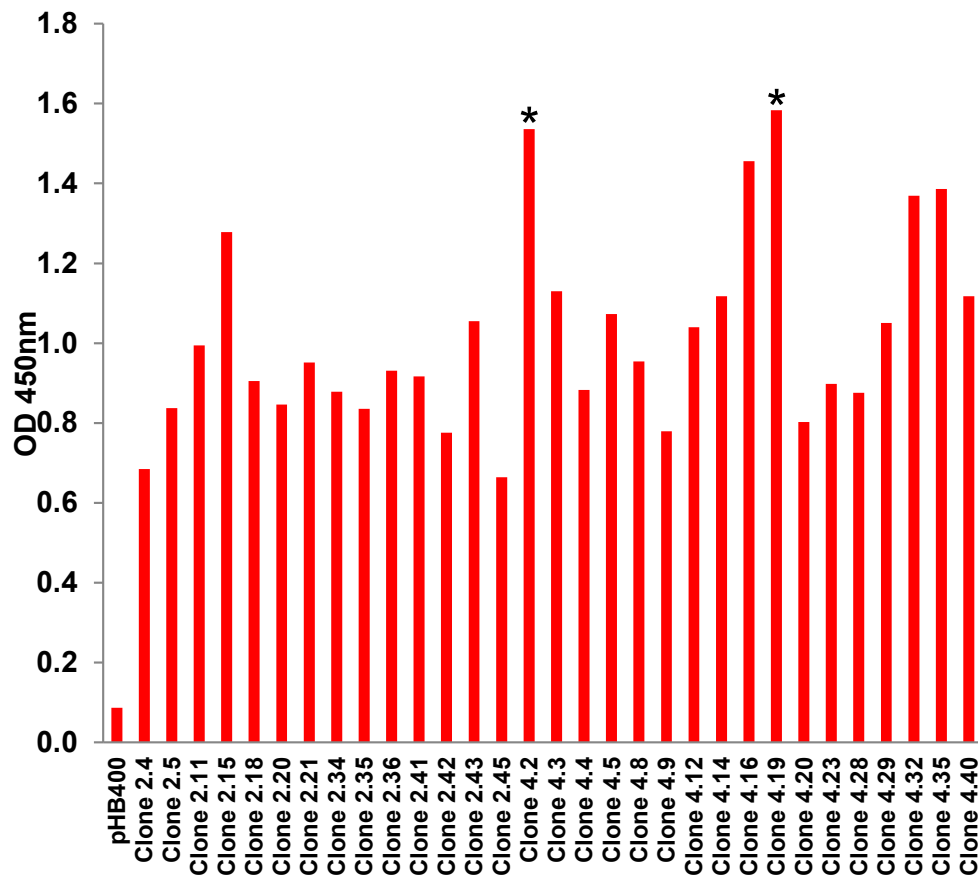


Figure 4-6 Comparison of binding of anti-VEGF-B scFv clones to VEGF-B

Thirty one 2H10 scFv clones which showed high expression by colony blot were screened for binding to VEGF-B by direct ELISA. The results were normalised to total protein. Clones 4.2 and 4.19 (*) showed the highest binding to VEGF-B. This may have been due to higher affinity or higher production of scFv. The bars represent the absorbance at 450 nanometers.

4.1.4.d *Sequencing of anti-VEGF-B scFv clones*

A total of 8 2H10 scFv clones were sequenced with the primers Scfor, Scback, SeqVLfor and SeqVHback as described in section 2.2.14. Clones with high, medium and low expression in the ELISA were chosen for sequencing to investigate whether the differences were caused by mutations. Good quality sequence was obtained from all clones. The sequence from each of the primers was assembled into a contig for each of the clones. Each residue of the scFv was covered by at least two sequencing reads. The contigs were then aligned to the known sequence of the 2H10 V_L and V_H (Figure 4-7).

Each of the 8 clones sequenced had an identical V_L and V_H. Each one contained a linker region comprising 4 x G₄S repeats which joined the V_L and V_H, and a 6 x histidine tag following the carboxyl terminal of the V_H. There was a single nucleotide difference in the sequence of the scFv and the hybridoma cDNA (Figure 4-7). This change was introduced by the primer (2H10V_Hback) and led to an amino acid change from an arginine to a serine at the last residue of the V_H. Although this was a non-conserved amino acid change, it was present in the framework region of the V_H. This change did not appear to affect the folding of the protein adversely, as the resultant scFv maintained binding to human VEGF-B.

Since no differences in sequence were detected amongst the anti-VEGF-B scFv clones, one of the clones (clone 4.2), which consistently demonstrated higher readings in the VEGF-B ELISA, was selected for further work. The scale of the bacterial cultures was increased to produce more scFv, and the scFv was purified from the bacterial lysate by immobilised metal ion chromatography.

2H10 S _c Fv	GGCCCAGCCGGCCATGGCGGACTACAAAGAGATCCAGATGACCCAGACCACCTCCAGCCT	60
2H10 V _L	-----GAGATCCAGATGACCCAGACCACCTCCAGCCT	32
2H10 V _H	-----	0
2H10 s _c Fv	GAGCGCCAGCCTGGGCGACAGAGTGACCATCAGCTGCCGGGCCAGCCAGGACATCAGCAA	120
2H10 V _L	GAGCGCCAGCCTGGGCGACAGAGTGACCATCAGCTGCCGGGCCAGCCAGGACATCAGCAA	92
2H10 V _H	-----	0
2H10 s _c Fv	CTTTCTGAACTGGTATCAGCAGAAACCCGACGGCACCGTGAAGCTGCTGATCTACTACAC	180
2H10 V _L	CTTTCTGAACTGGTATCAGCAGAAACCCGACGGCACCGTGAAGCTGCTGATCTACTACAC	152
2H10 V _H	-----	0
2H10 S _c Fv	CAGCACCTGCACAGCGGCGTGCCAGCCGGTTTAGCGGCAGCGGCTCCGGCACCGACTA	240
2H10 V _L	CAGCACCTGCACAGCGGCGTGCCAGCCGGTTTAGCGGCAGCGGCTCCGGCACCGACTA	212
2H10 V _H	-----	0
2H10 S _c Fv	CAGCCTGACCATCTCCAACCTGGAACAGGAAGATATTGCCACCTACTTTTGCCAGCAGGG	300
2H10 V _L	CAGCCTGACCATCTCCAACCTGGAACAGGAAGATATTGCCACCTACTTTTGCCAGCAGGG	272
2H10 V _H	-----	0
2H10 s _c Fv	CAAGACACTGCCCCACCTTTGGCGGCGGAACAAAGCTGGAATCAAGAGGGTGGTGG	360
2H10 V _L	CAAGACACTGCCCCACCTTTGGCGGCGGAACAAAGCTGGAATCAAGAGG-----	324
2H10 V _H	-----	0
2H10 s _c Fv	<u>TGGTTCTGGTGGTGGTGGTTCTGGCGGCGGCGGCTCCGGTGGTGGTGGATCCAGGTGCA</u>	420
2H10 V _L	-----	-
2H10 V _H	-----CAGGTGCA	8
2H10 s _c Fv	GCTGCAGCAGCCCGCACCCGAGCTGGTGAAGCCTGGCGCCTCCGTGAAACTGTCTGCAA	480
2H10 V _L	-----	-
2H10 V _H	GCTGCAGCAGCCCGCACCCGAGCTGGTGAAGCCTGGCGCCTCCGTGAAACTGTCTGCAA	68
2H10 s _c Fv	GGCCTCCGGCTACACCTTACCAGGCTTTTGGATCCACTGGGTGAAACAGAGACCAGGACA	540
2H10 V _L	-----	-
2H10 V _H	GGCCTCCGGCTACACCTTACCAGGCTTTTGGATCCACTGGGTGAAACAGAGACCAGGACA	128
2H10 s _c Fv	GGGCCTGGAATGGATCGGCCACATCAACCCGGCAACGGCGGCACCAACTACAACGAGAA	600
2H10 V _L	-----	-
2H10 V _H	GGGCCTGGAATGGATCGGCCACATCAACCCGGCAACGGCGGCACCAACTACAACGAGAA	188
2H10 s _c Fv	GTTCAAGCGGATGGCCACCCTGACCGTGGACAAGAGCAGCAGCACCCTACATGCAGCT	660
2H10 V _L	-----	-
2H10 V _H	GTTCAAGCGGATGGCCACCCTGACCGTGGACAAGAGCAGCAGCACCCTACATGCAGCT	248
2H10 s _c Fv	GTCCAGCCTGACCAGCGAGGACAGCGCCGTGACTACTGCGCCCGCAGCTACAGCAACTA	720
2H10 V _L	-----	-
2H10 V _H	GTCCAGCCTGACCAGCGAGGACAGCGCCGTGACTACTGCGCCCGCAGCTACAGCAACTA	308
2H10 s _c Fv	CGTGGCGGCCATGGACTACTGGGCCAGGGCACCAGCGTGACCGTGCCAGGGCCTCGGG	780
2H10 V _L	-----	-
2H10 V _H	CGTGGCGGCCATGGACTACTGGGCCAGGGCACCAGCGTGACCGTGCCAGGGCCTCGGG	360
2H10 s _c Fv	GGCCGAT CACCATCATCACCATCAT	807
2H10 V _L	-----	-
2H10 V _H	-----	-

Figure 4-7 Sequence of the anti-VEGF-B scFv

The sequence of the anti-VEGF-B scFv (2H10) aligned to the known sequence of the V_L and V_H regions of the 2H10 hybridoma, showing the linker region (underlined) and the histidine tag (bold, black box). The sequence of the 2H10 scFv was identical to the expected sequence of the V_L and V_H except for one mismatched base shown in bold red text (red box).

4.1.5 Purification of anti-VEGF-B scFv

Anti-VEGF-B scFv was purified from bacterial lysates using IMAC on a BiologicLP chromatography system. A large amount of protein was eluted from the column in a single peak (Figure 4-8). No protein was eluted with either 20 mM or 30 mM imidazole washes, indicating minimal binding of non-specific proteins. Aliquots of the purified anti-VEGF-B scFv and crude bacterial extract were separated on a polyacrylamide gel (Figure 4-9). A large number of bands were observed with crude bacterial extract confirming the heterogeneous nature of the sample. The purified scFv contained predominantly a single band that ran slightly above the 25 kDa marker. This corresponded well to the expected size of the scFv (28 kDa). The final concentration of purified dialysed anti-VEGF-B scFv ranged from 0.6-0.8 mg/ml, in different batches. The binding of the purified scFv to human VEGF-B was assessed to confirm that the anti-VEGF-B scFv maintained its binding specificity after the purification process.

4.1.6 Binding of purified anti-VEGF-B scFv to VEGF-B

The binding affinity of purified anti-VEGF-B scFv for human VEGF-B was assayed. A dilution range of the scFv covering six orders of magnitude from 7 µg/ml to 7 pg/ml was tested. Binding to VEGF-B was maintained over the entire range of dilutions, demonstrated by absorbance readings above background in the direct ELISA (Figure 4-10). ScFvs with specificity for human VEGF-A and *Acanthamoeba*, respectively, were included as controls. The control scFvs did not display binding to human VEGF-B.

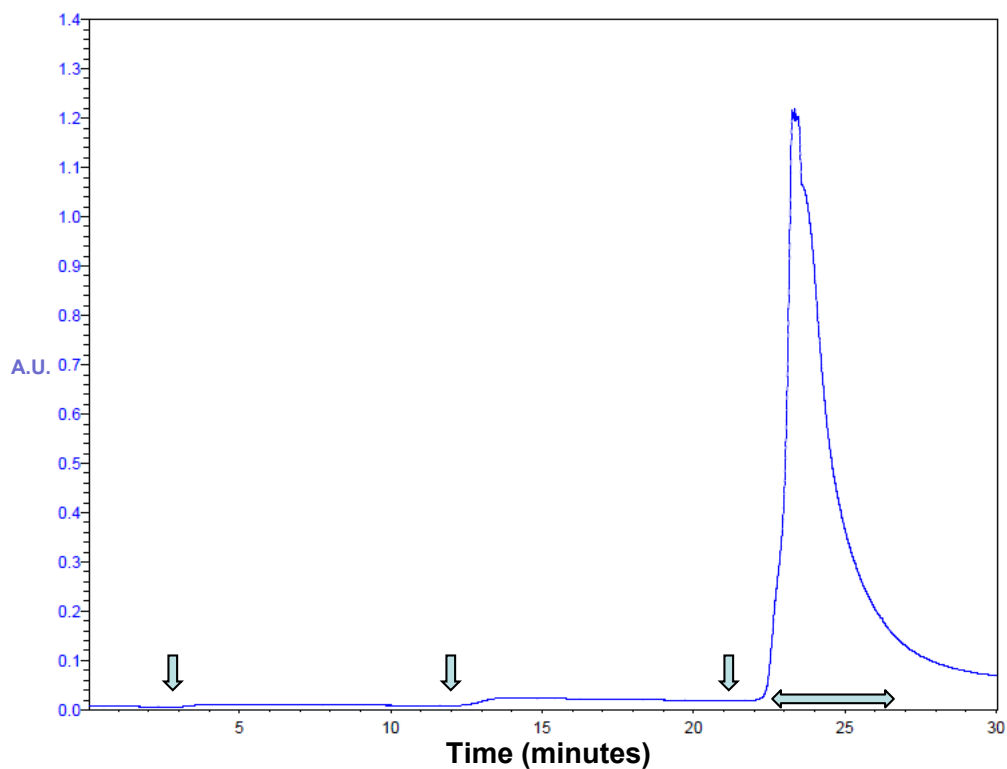


Figure 4-8 Purification of anti-VEGF-B scFv by immobilised metal ion chromatography

Anti-VEGF-B scFv was purified from bacterial lysate using IMAC on a Biologic LP chromatography system. The protein elution was detected by absorbance at 280 nm. The arrows indicate flow through of wash buffer containing 20 mM imidazole, wash buffer with 30 mM imidazole and elution buffer with 250 mM imidazole respectively. No protein was eluted off the column after washing with 20 mM or 30 mM imidazole wash buffers. Protein was eluted off the column in a single peak after the addition of buffer with 250 mM imidazole (double headed arrow). A.U. = absorbance units.

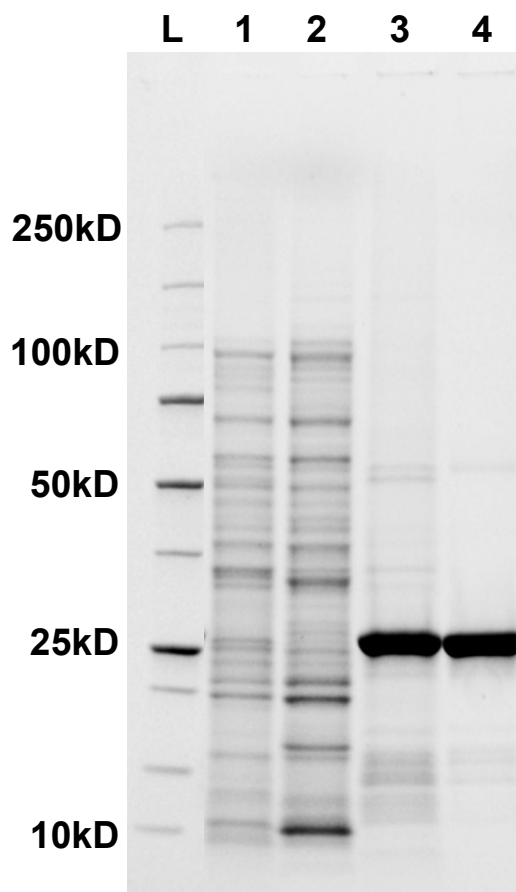


Figure 4-9 Visualization of the purity of the purified VEGF-B scFv after IMAC

Anti-VEGF-B scFv was purified from bacterial lysate using IMAC on a Biologic LP chromatography system. Aliquots of the crude bacterial lysate (lane 1), flowthrough from the IMAC column (lane 2), purified pooled fractions (lane 3) and purified dialysed scFv (lane 4) were separated on a 4-20% polyacrylamide gel. The crude bacterial extract as well as the column flowthrough showed a large number of bands indicating presence of mixture of proteins. IMAC purification led to the presence of a major band around 25 kDa, which was the expected size of the VEGF-B scFv. Five micrograms of protein was loaded in each lane and 5 μ l of Precision Plus Protein™ unstained standard (BioRad) was run in lane L.

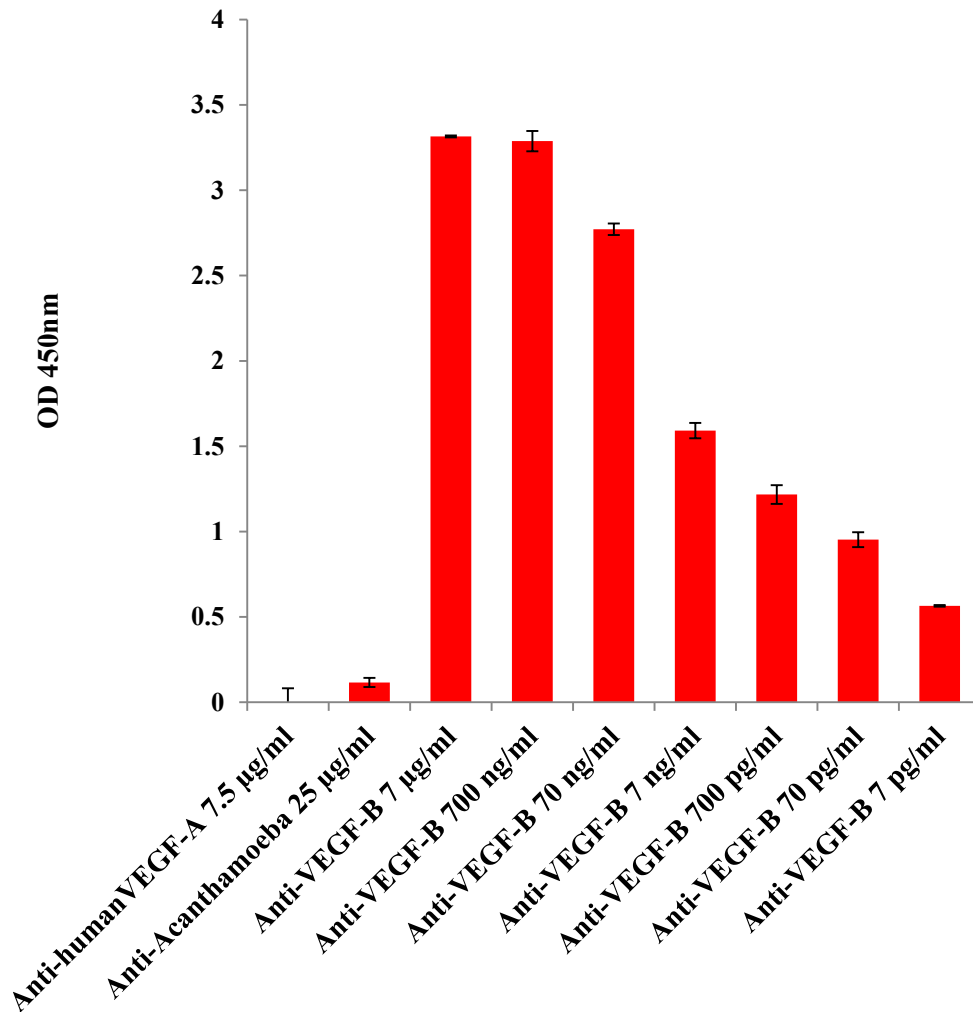


Figure 4-10 Binding of purified bacterial produced anti-VEGF-B scFv to human VEGF-B

Anti-VEGF-B and control scFvs (anti-VEGF-A and anti-*acanthamoeba*) were expressed in *E.coli*. Recombinant scFv was purified from bacterial lysates by IMAC, and pooled fractions were dialysed against PBS. Purified anti-VEGF-B scFv was diluted from 7 µg/ml to 7 pg/ml and binding to human VEGF-B was assayed by a direct ELISA. Binding above background levels was observed at each dilution tested. The control scFvs did not bind to rhVEGF-B. The bars represent the mean OD_{450nm} of three technical replicates and the error bars represent standard deviation.

In summary, an anti-VEGF-B scFv was successfully engineered from a hybridoma which secreted an antibody with specificity for human, mouse and rat VEGF-B. The scFv gene was cloned into a plasmid vector, expressed in *E.coli*, and purified by IMAC. Bacterially-expressed anti-VEGF-B scFv maintained binding to human VEGF-B, and was able to be produced in milligram amounts. However, bacterial expression of proteins is associated with the presence of large amounts of endotoxin. Hence, the scFv produced in *E.coli* was used for *in vitro* experiments only. For *in vivo* work, scFv was codon-optimised and expressed in a mammalian expression system at CSL Ltd. In the next section, characterization of the anti-VEGF-B scFv produced in mammalian cells is described.

4.2 Characterization of anti-VEGF-B scFv produced in mammalian cells

Anti-VEGF-B scFv was codon-optimised and produced in mammalian cell culture at CSL Ltd. Victoria, Australia. The binding of the scFv and the parental antibody were characterised at CSL Ltd. as described in Appendix C. ScFv was purified and dialysed against PBS. A concentrated solution of scFv at 10.4 mg/ml was transported to Flinders University by refrigerated freight, and stored at 4°C upon arrival. All animal experiments were carried out using scFv produced in mammalian cells, to minimise the amount of endotoxin. The levels of endotoxin in the scFv solution as estimated by Limulus amoebocyte lysate assay (Associates of Cape Cod, East Falmouth, MA, USA) were less than 3 EU/ml. The binding and stability of the anti-VEGF-B scFv produced at CSL Ltd. was further characterised at Flinders University as follows.

4.2.1 Binding of anti-VEGF-B scFv to human VEGF-B and VEGF-A

Binding of the codon-optimised anti-VEGF-B scFv to human VEGF-B was assayed by direct ELISA as described in section 2.2.12. Tenfold serial dilutions of anti-VEGF-B scFv from 100 µg/ml to 100 pg/ml were tested. The scFv produced in mammalian cells showed binding to human VEGF-B above concentrations of 10 ng/ml (Figure 4-11). The binding of the scFv to human VEGF-B was thus confirmed.

Next the specificity of the anti-VEGF-B scFv was evaluated by assessing binding to human VEGF-A. A sandwich ELISA that immobilised human VEGF-A to the assay plate via an anti-VEGF-A antibody was used. ScFv sample was then applied and bound scFv was detected through its His-tag. The anti-VEGF-B scFv did not demonstrate binding to human VEGF-A at the concentrations tested (Figure 4-11).

4.2.2 Stability of the anti-VEGF-B scFv

ScFv prepared at CSL Ltd. was shipped to Flinders University and stored for extended periods of time before use for *in vivo* experiments. The stability of the scFv upon storage was ascertained to confirm its activity before using in animal experiments.

Long term storage of the anti-VEGF-B scFv was tested by assaying binding to human VEGF-B by ELISA, immediately after production, and after 20 months at 4°C. ScFv was handled using aseptic techniques to minimise the chance of contamination. Anti-VEGF-B scFv displayed a similar degree of binding to human VEGF-B before and after the storage period (Figure 4-12). We concluded that

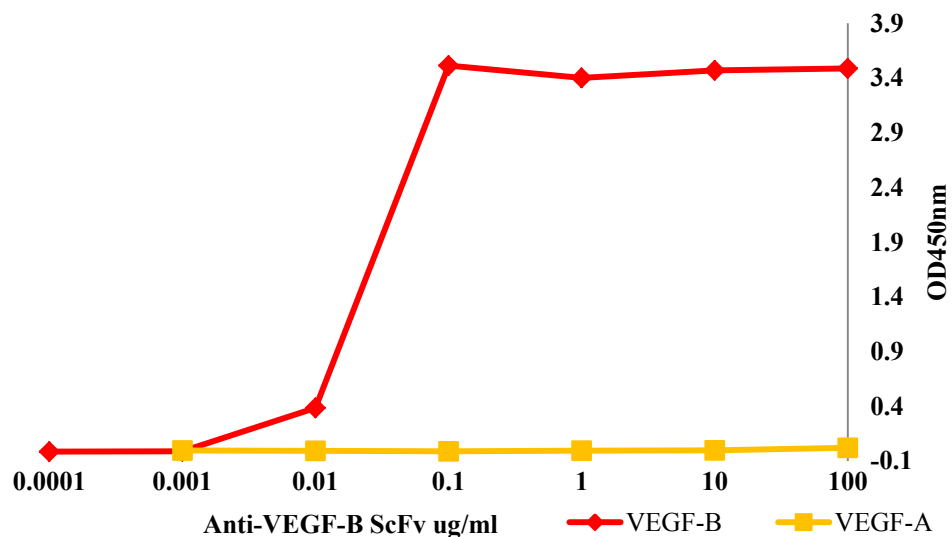


Figure 4-11 Binding of mammalian cell-produced 2H10 scFv to human VEGF-B and VEGF-A

Anti-VEGF-B scFv was produced in a mammalian expression system at CSL Ltd. ScFv was diluted from 100 $\mu\text{g/ml}$ to 100 pg/ml and its binding to human VEGF-B was assayed by direct ELISA. Strong binding was observed up to 100 ng/ml scFv and binding above background was observed down to 10 ng/ml scFv. The binding of the scFv to human VEGF-A was assayed by sandwich ELISA. The 2H10 scFv did not bind to human VEGF-A. The absorbance at 450 nanometers is plotted on the y-axis against the concentration of anti-VEGF-B scFv on the x-axis.

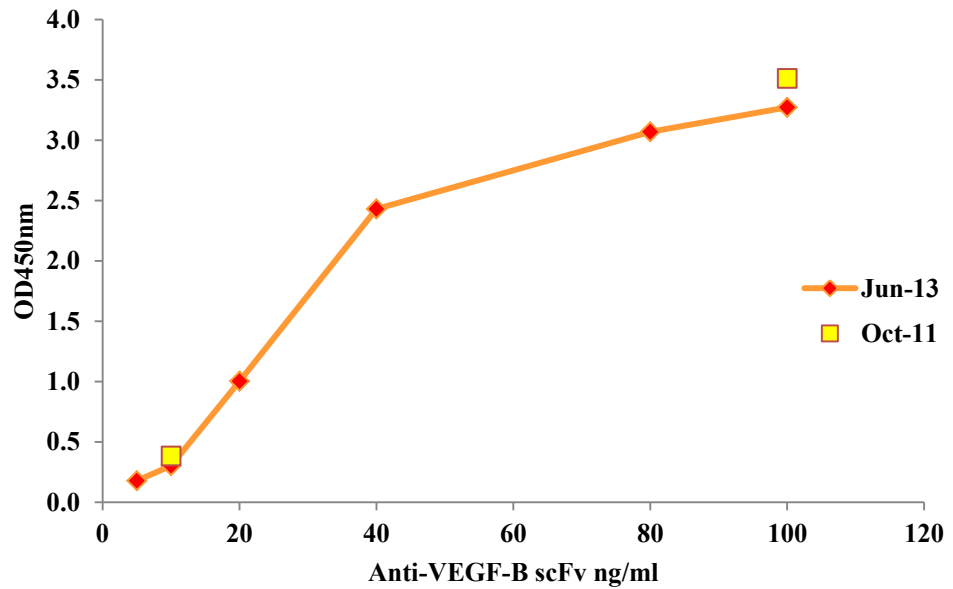


Figure 4-12 Stability of the anti-VEGF-B scFv

Anti-VEGF-B scFv produced in mammalian cells was assayed for binding to human VEGF-B by direct ELISA, and then stored at 4°C for 20 months before its binding was retested. The binding activity of the scFv was maintained during the storage period. The absorbance at 450 nanometers is plotted on the y-axis against the concentration of anti-VEGF-B scFv on the x-axis.

storage over 20 months did not adversely affect the binding of the anti-VEGF-B scFv to human VEGF-B.

4.2.3 Binding of the anti-VEGF-B scFv to human VEGF-B after formulation as an eye drop

Next the binding characteristics of the scFv upon formulation as an eye drop for topical delivery was assessed. The anti-VEGF-B scFv was formulated as an eye drop for topical delivery. The eye drop base contained an agent to increase the viscosity of the solution so that it remained on the corneal surface for a longer time, as well as a penetration enhancer to facilitate passage of the scFv into the cornea⁴⁴³ (Appendix B.13). A direct ELISA was performed on the eye drop solution to confirm that the anti-VEGF-B scFv maintained binding activity after formulation as an eye drop. Anti-VEGF-B eye drops demonstrated strong binding to human VEGF-B by ELISA (Figure 4-13). The eye drop solution was then stored for 3 months at 4°C before re-testing its binding to VEGF-B. The anti-VEGF-B scFv formulated as an eye drop maintained binding to human VEGF-B after 3 months of storage (Figure 4-13).

In summary, the anti-VEGF-B scFv produced in mammalian cells demonstrated binding to human VEGF-B by ELISA. The binding of the scFv and the parental mAb to human VEGF-B were assessed by surface plasmon resonance. The scFv had similar binding characteristics to the mAb, but the kinetics of the binding differed. The scFv blocked the functional effects of VEGF-B in a cell based assay. The binding of the scFv was maintained after 20 months of storage and after being formulated as eye drops, and the scFv had low levels of endotoxin.

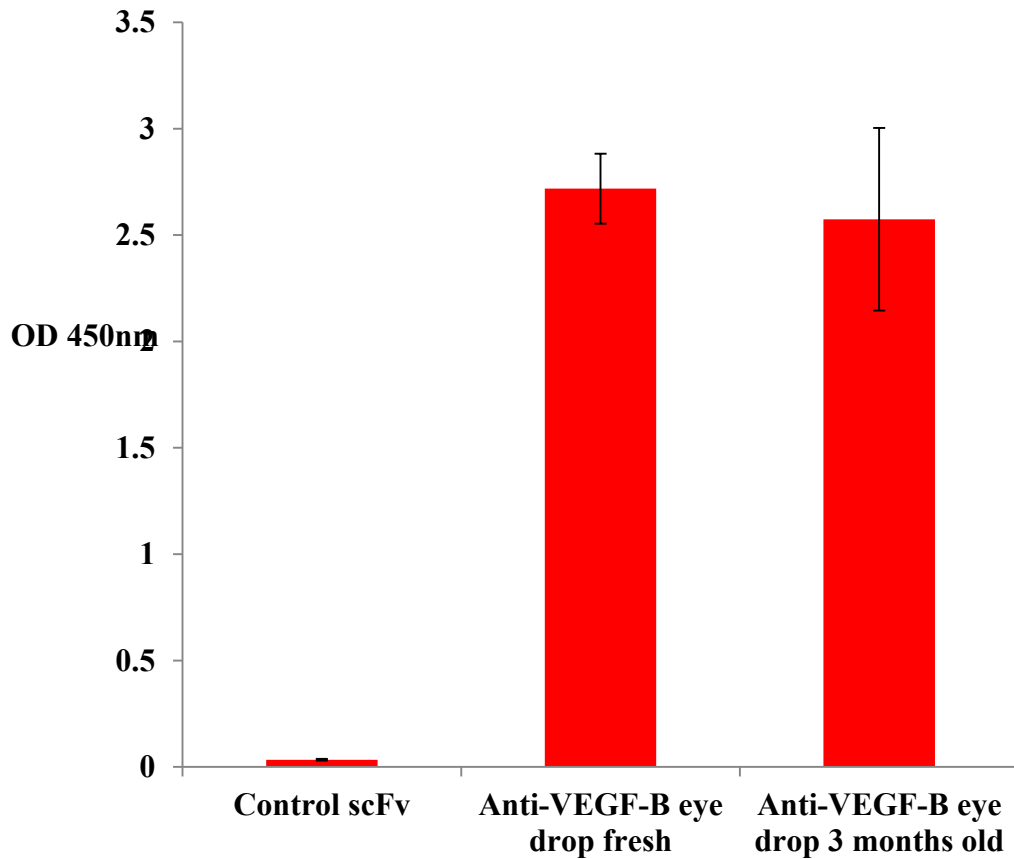


Figure 4-13 Maintenance of anti-VEGF scFv activity after formulation into eye drops

Anti-VEGF-B scFv was formulated into eye drops, which contained 1.5% hypromellose, a viscosity enhancer, and 1% capric acid, a penetration agent. Binding of the eye drops to human VEGF-B was assayed by direct ELISA. Freshly prepared eye drops maintained binding to human VEGF-B. The eye drops were then stored at 4°C for 3 months and binding retested. The eye drops maintained binding to human VEGF-B. The bars represent mean the mean optical density at 450 nanometers, of three technical replicates, and the error bars represent the standard deviation.

4.3 Anti neovascular activity of VEGF-B scFv in a rat model of corneal neovascularization

The effect of the scFv on growing and established vessels was then assessed in a rat model of corneal neovascularization. Corneal neovascularization was induced in Sprague-Dawley rats by superficial cautery using a silver nitrate applicator (section 2.5.1.a). Care was taken to position the applicator at the centre of the cornea, and to keep the size of the injury consistent between animals. The cautery caused corneal oedema and a mild blister response at the site of injury. Neovascularization was apparent at the limbal arcades 3-4 days post cautery and the vessels reached the site of cautery within 7-10 days. The vessels then anastomosed to form a vascular network by 14 days. Anti-VEGF-B scFv therapy was administered either immediately after induction of neovascularization to determine its effects on growing vessels, or the vessels were allowed to establish before treatment was started.

4.3.1 Effect of topical anti-VEGF-B therapy on developing vessels

Anti-VEGF-B scFv therapy was started the day after cautery to test the effect on developing vessels. A 5 µl eye drop was applied at 2 hour intervals 5 times per day. After the last eye drop of the day, polyvisc ointment was applied to maintain the scFv on the corneal surface overnight. Initial experiments examined the effect of 7 days of therapy.

Figure 4-14 shows representative flatmounts from control scFv and anti-VEGF-B scFv treated rats. The cauterised area is visible as a brown spot in the centre of the cornea. The corneal vessels were stained with haematoxylin. At day 8 post cautery vessels had infiltrated the cornea and were approximately halfway between the

limbus and the cauterised site (Figure 4-14). The percentage of the cornea covered by vessels was quantified as described in section 2.5.1.f. There was no significant difference in the corneal vessel area between rats treated with the control scFv and rats treated with the anti-VEGF-B scFv (Figure 4-15, $p=0.59$).

Next, a longer treatment regimen was tested. Corneal cautery was performed as above. Treatment commenced the day after cautery and consisted of 5 x 5 μ l eye drops per day for 14 days. The corneal vessels were stained 15 days post cautery and quantified as above. The longer treatment period allowed the vessels to grow further into the cornea, and by day 15 the vessels had reached the site of cautery (Figure 4-16). The degree of neovascularization did not appear to be different in untreated, control scFv treated, and anti-VEGF-B scFv treated animals, with all animals showing an even infiltration of densely packed vessels. Quantification of corneal vessel area revealed that there was no significant difference in the percentage of the cornea covered by vessels between the groups (Figure 4-17, $p=0.46$).

These results indicated that topical delivery of the anti-VEGF-B scFv had no effect on the growth of new corneal vessels in response to silver nitrate cautery. The result was not surprising, as VEGF-B is not a growth factor for developing vessels. As VEGF-B is known to be more of a survival factor for endothelial cells, the effect of topical therapy on more established vessels was next tested.

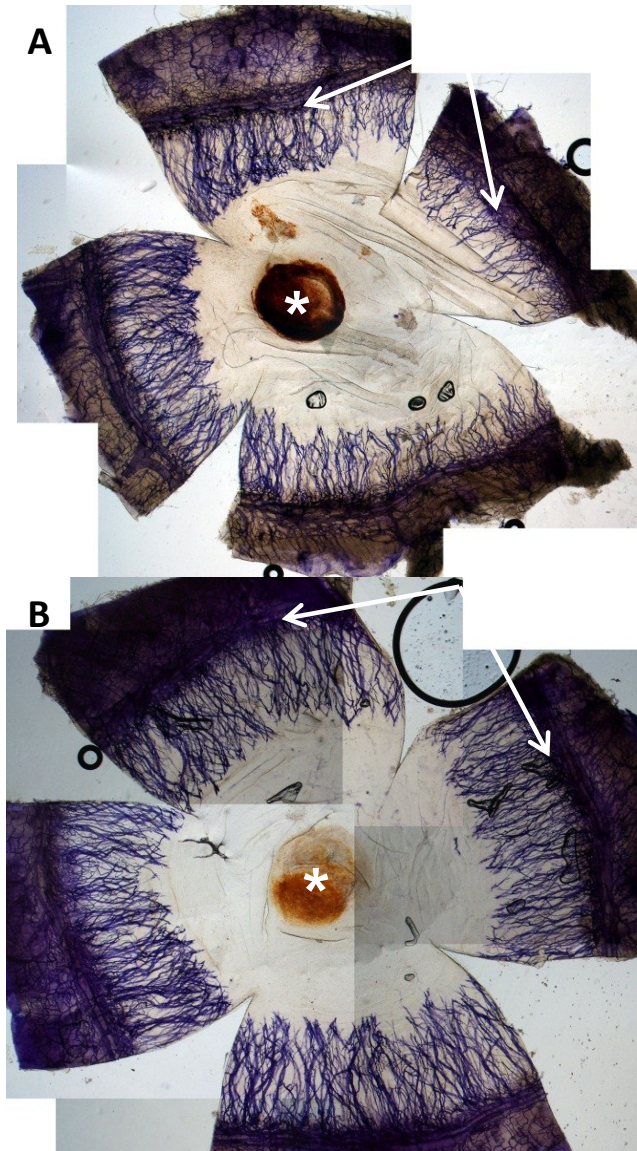


Figure 4-14 Representative images of haematoxylin perfused corneal flatmounts from rats treated for 7 days immediately after cautery

Corneal cautery was induced in Sprague-Dawley rats. Rats were treated with anti-VEGF-B or control scFv for 7 days. At the end of the treatment, the vasculature of the rat was perfused with haematoxylin. The eyes were removed and corneas dissected out and flatmounted. **(A)** Control scFv and **(B)** anti-VEGF-B scFv treated rats showed infiltration of vessels into the cornea. The vessels had penetrated halfway to the site of cautery in 7 days. The cautery site is marked with an asterisk, the limbal arcades are marked with white arrows. Neovessels in the cornea have been stained purple with haematoxylin. Air bubbles are visible in the top right corner of each image.

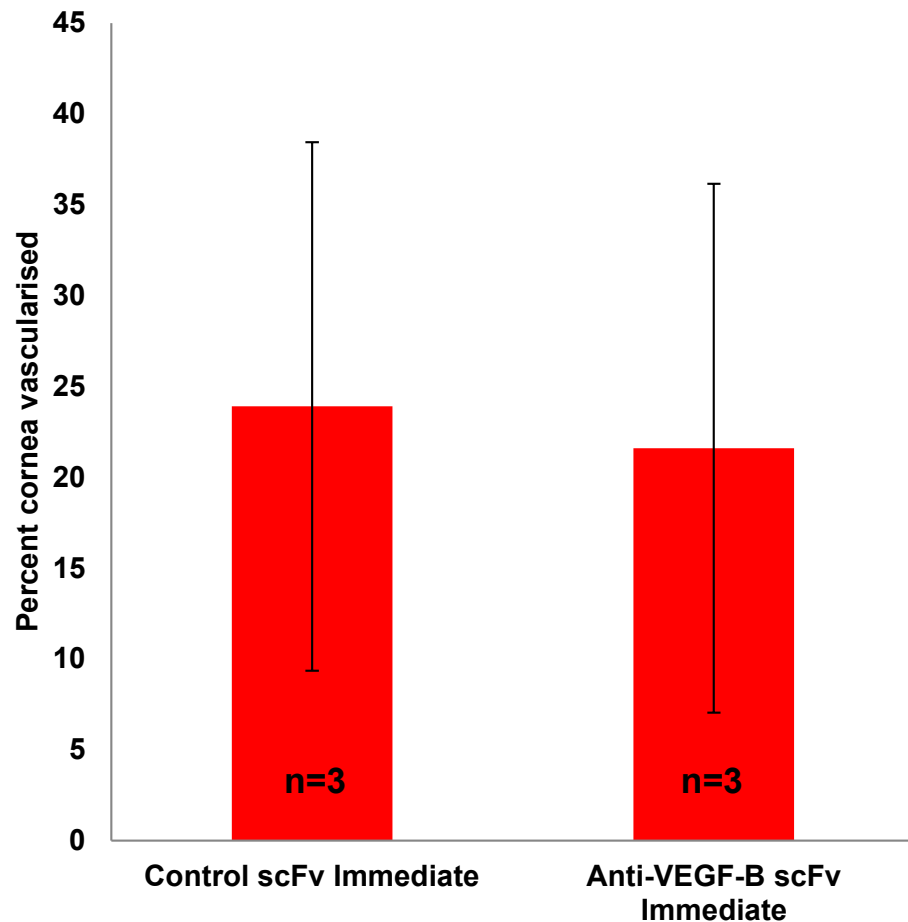


Figure 4-15 Effect of 7 days of topical scFv treatment on developing corneal vessels in a rat model of corneal neovascularization

Corneal neovascularization was induced in inbred Sprague-Dawley rats by silver nitrate cautery. Treatment with scFv eye drops was commenced the day after cautery. Eye drops were delivered at 2 hour intervals 5 times a day for 7 days. The corneal vessels were perfused with haematoxylin and the percentage of the cornea covered by vessels was quantified. The corneal vessel area was not different between anti-VEGF-B and control scFv treated animals $p=0.58$ (Kruskal–Wallis test). The bars represent the mean corneal vessel area of three biological replicates, and the error bars represent the standard deviation. n = number of rats in each group.

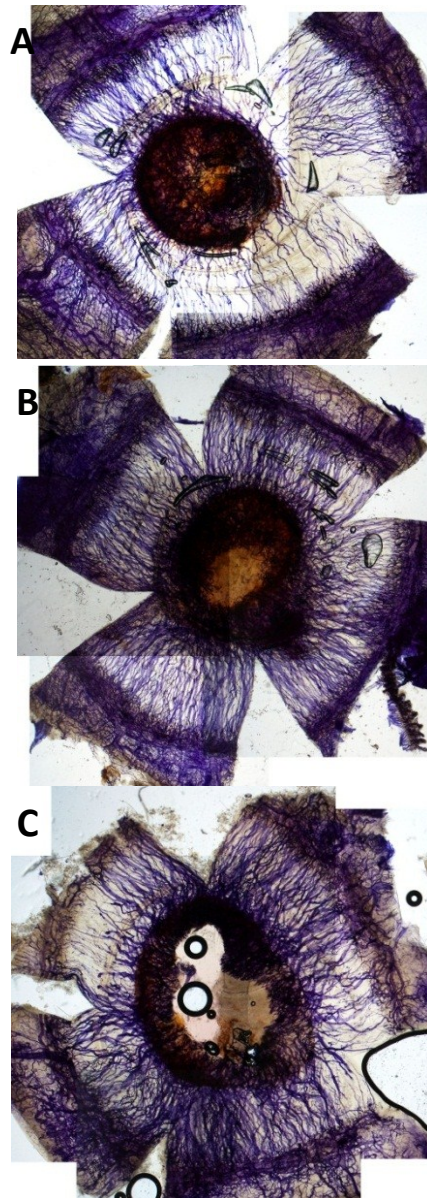


Figure 4-16 Representative images of haematoxylin perfused corneal flatmounts from rats treated for 14 days immediately after cautery

Corneal cautery was induced in Sprague-Dawley rats. The rats were then treated with anti-VEGF-scFv or control for 14 days. At the end of the treatment the vasculature of the rat was perfused with haematoxylin. The eyes were removed and corneas dissected out and flatmounted. **(A)** Untreated **(B)** Control scFv and **(C)** anti-VEGF-B scFv treated rats showed infiltration of vessels into the cornea. By day 14 the vessels had reached the site of cautery. No difference in corneal vessel area was observed amongst the groups. The cautery site is marked by an asterisk.

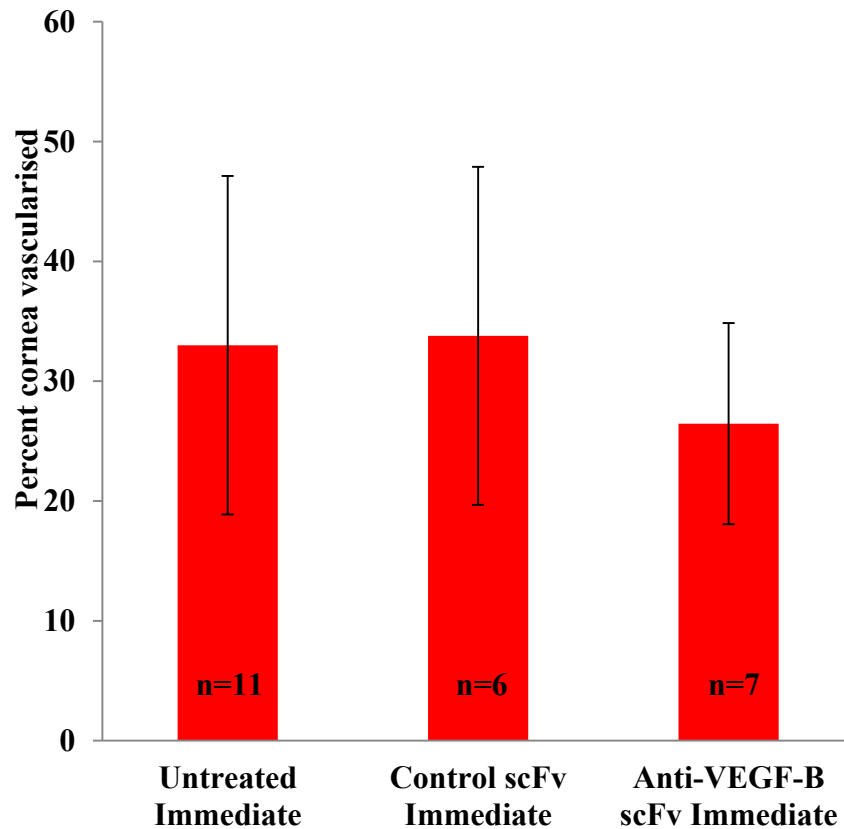


Figure 4-17 Effect of 14 days of topical scFv treatment on developing corneal vessels in a rat model of corneal neovascularization

Corneal neovascularization was induced in inbred Sprague-Dawley rats by silver nitrate cautery. Treatment with scFv eye drops was commenced one day after cautery. Eye drops were delivered at 2 hour intervals, 5 times a day for 14 days. The corneal vessels were perfused with haematoxylin and the percentage of the cornea covered by vessels was quantified. No significant difference in corneal vessel area between treatment and control groups was observed $p=0.46$ (Kruskal-Wallis test). The bars represent the mean corneal vessel area of biological replicates, and the error bars represent the standard deviation. n = number of rats in each group.

4.3.2 Effect of topical anti-VEGF-B scFv treatment on established vessels

VEGF-B is a survival factor for blood vessels²⁵⁷. We next aimed to test the ability of the anti-VEGF-B scFv to cause regression of *established* vessels. In order to do this, treatment was not commenced immediately after cautery, but vessels were allowed to grow into the central cornea before treating with the anti-VEGF-B scFv.

In the first instance vessels were allowed to grow into the cornea for 7 days and treatment was commenced on day 8 following cautery. Five x 5 µl eye drops were administered per day for 7 days. At euthanasia of the rats, vessels were stained with haematoxylin and the corneas flatmounted. By day 15 the vessels had reached the central cauterised area of the cornea (Figure 4-18). A uniform degree of vascularization was observed, with vessels growing more or less straight towards the site of cautery. The density of the vessels was similar between untreated, control scFv and anti-VEGF-B scFv treated eyes. There was no significant difference in the percent of the cornea covered by vessels amongst the treatment and control groups (Figure 4-19, p=0.83).

It was observed that corneal neovessels did not always reach the central cauterised area within 7 days post cautery. Fourteen days were required for the new vessels to develop completely to form a stable vascular network. In the next set of experiments, vessels were allowed to develop for 14 days after cautery was performed before initiation of anti-VEGF-B eye drops. The duration of therapy was increased to 14 days, and 5 x 5 µl eye drops were applied each day with polyvisc ointment applied

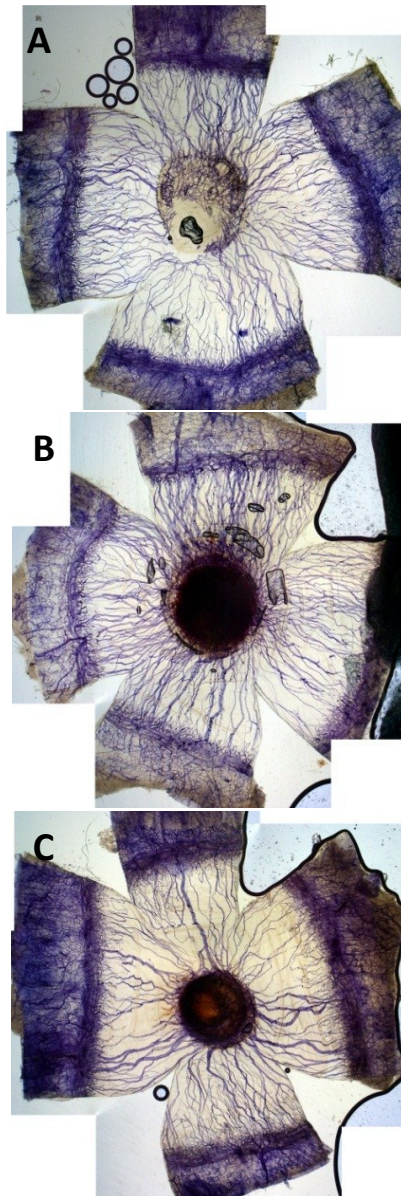


Figure 4-18 Representative images of haematoxylin perfused corneal flatmounts from rats treated for 7 days, beginning 7 days after cautery

Corneal cautery was induced in Sprague-Dawley rats. The vessels were allowed to establish for 7 days, after which 7 days of treatment with control or anti-VEGF-B scFv was applied. At the end of the treatment the vasculature of the rat was perfused with haematoxylin. The eyes were removed and corneas dissected out and flatmounted. (A) Untreated (B) Control scFv and (C) anti-VEGF-B scFv treated rats showed infiltration of vessels into the cornea. By day 14 the vessels had reached the site of cautery. No difference in corneal vessel area was observed amongst the groups.

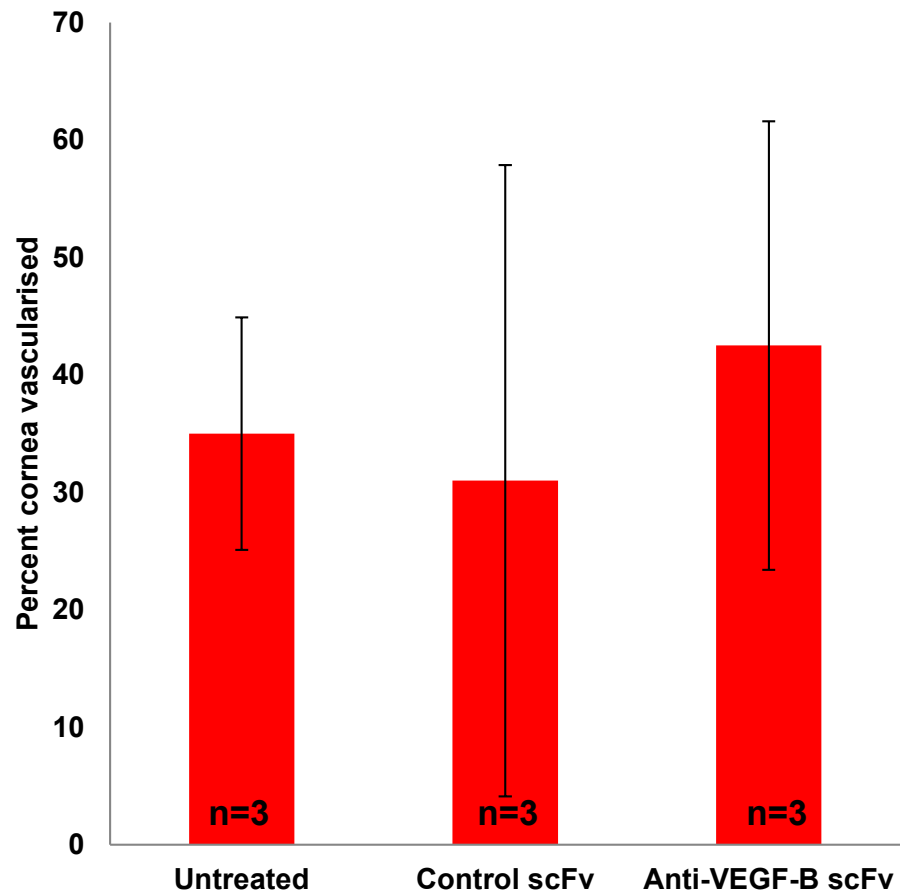


Figure 4-19 Effect of 7 days of topical scFv treatment on established corneal vessels in a rat model of corneal neovascularization

Corneal neovascularization was induced in inbred Sprague-Dawley rats by silver nitrate cautery. Treatment with scFv eye drops was commenced 7 days after cautery. Eye drops were delivered at 2 hour intervals 5 times a day for 7 days. At euthanasia, the corneal vessels were perfused with haematoxylin and the percentage of the cornea covered by vessels was quantified. No significant difference between treatment and control groups was observed $p=0.82$ (Kruskal-Wallis test). The bars represent the mean corneal vessel area of three biological replicates, and the error bars represent the standard deviation. n = number of rats in each group.

after the last drop on each day. The vessels were stained with haematoxylin and the corneas flatmounted.

After establishment of the vascular networks by day 14, some vessels began to regress regardless of treatment. Vessels covered a significantly larger proportion of the eyes of untreated animals at day 15 than day 29 (Figure 4-20). Regression of some of the vessels led to a heterogeneity in the density of the corneal vessels, with some areas containing more patent vessels while others had poorly perfused vessels (Figure 4-21). However, there was no significant difference in the area of the cornea covered by vessels in the anti-VEGF-B scFv treated and control rat eyes (Figure 4-22, $p=0.87$).

These results indicated that topically applied anti-VEGF-scFv had no effect on established corneal vessels. This result was unexpected in the light of VEGF-B being a potent survival factor for endothelial cells. However, during the course of these experiments an interesting observation about neovascularization in male and female rats was made.

4.3.3 Differences in the degree of neovascularization between males and females

Corneal neovascularization was induced in male and female Sprague-Dawley rats by silver nitrate cautery. In the days following cautery, it was noted that male rats developed darker blisters than females (Figure 4-23). Males generally developed dark brown or black blisters while females had light brown blisters. Male rats also developed more oedema and robust neovascularization. To investigate this further,

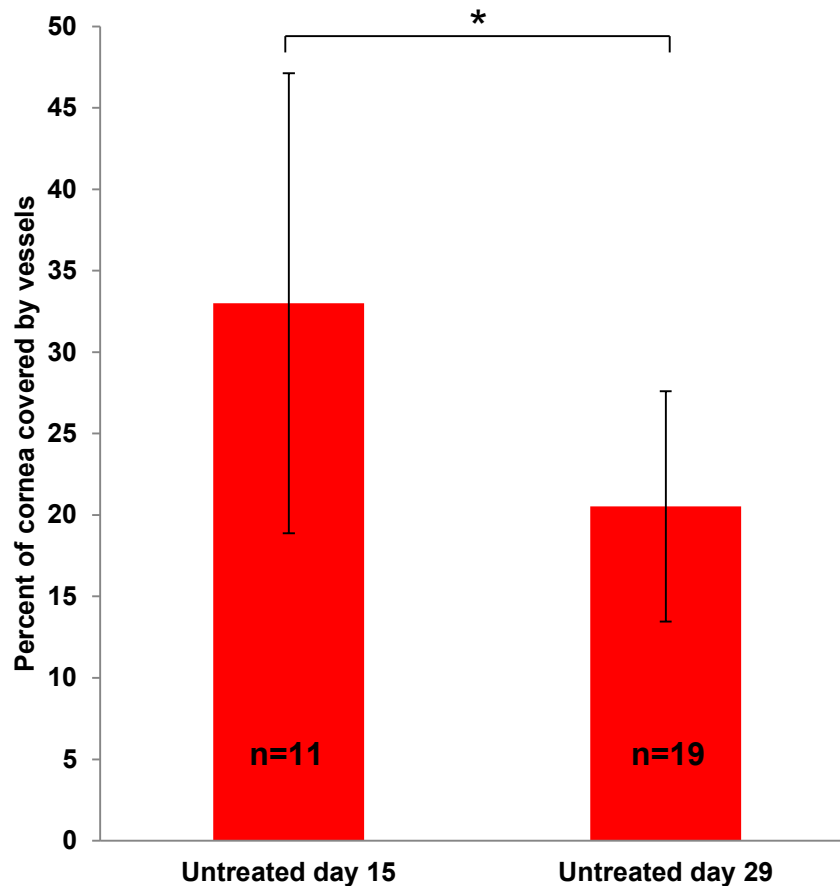


Figure 4-20 Comparison of corneal neovascularization in untreated rats 15 and 29 days after cautery

Corneal neovascularization was induced in inbred Sprague-Dawley rats by silver nitrate cautery. Vessels were allowed to develop for 15 and 29 days respectively, without any intervention. The vessels were stained with haematoxylin and the corneas flatmounted. The percent of the cornea covered by vessels was quantified. Vessels reached the central cauterised area between days 7-10 and formed a vascular network by day 14. Some vessels then spontaneously began to regress while others remained patent. There were significantly more vessels in the corneas of rats at day 15 than day 29 * $p=0.002$. The bars represent the mean corneal vessel area of biological replicates, and the error bars represent the standard deviation. n = number of rats in each group.

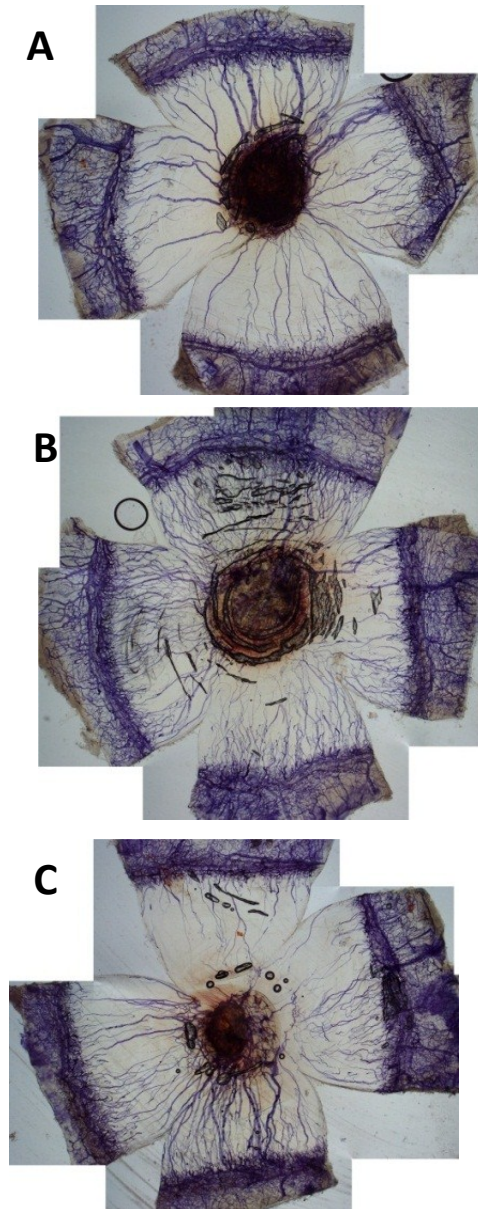


Figure 4-21 Representative images of haematoxylin perfused corneal flatmounts from rats treated for 14 days beginning 14 days after cautery

Corneal cautery was induced in Sprague-Dawley rats. The vessels were allowed to establish for 14 days, after which 14 days of treatment with control or anti-VEGF-B scFv was applied. At the end of the treatment the vasculature of the rats was perfused with haematoxylin. The eyes were removed and corneas dissected out and flatmounted. **(A)** Untreated **(B)** control scFv and **(C)** anti-VEGF-B scFv treated rats showed infiltration of vessels into the cornea. By day 28 the vessels had reached the site of cautery and anastomosed. No difference in corneal vessel area was observed amongst the groups.

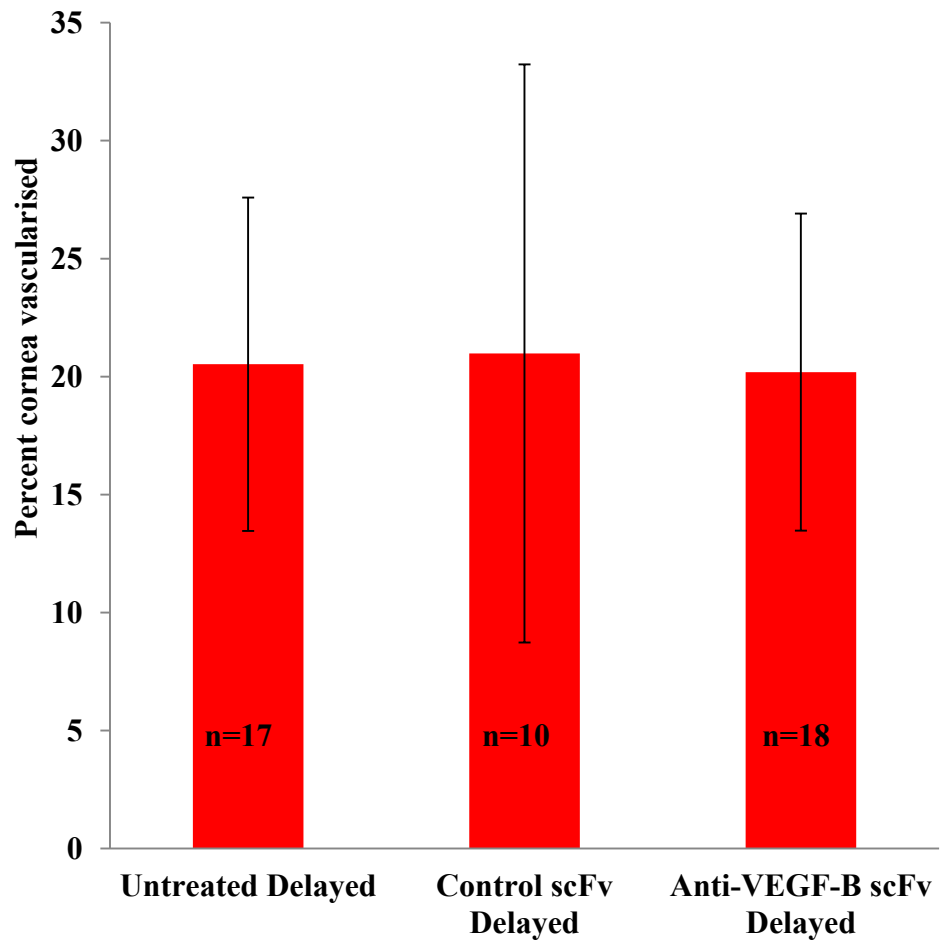


Figure 4-22 Effect of 14 days of topical scFv treatment on established corneal vessels in a rat model of corneal neovascularization

Corneal neovascularization was induced in inbred Sprague-Dawley rats by silver nitrate cautery. Treatment with scFv eye drops was commenced 14 days after cautery. Eye drops were delivered at 2 hour intervals, 5 times a day for 14 days. The corneal vessels were perfused with haematoxylin and the percentage of the cornea covered by vessels was quantified. No significant difference between treatment and control groups was observed $p=0.86$ (Kruskal-Wallis test). The bars represent mean corneal vessel area of the biological replicates, and the error bars represent the standard deviation. n = number of rats in each group.

the data from sections 4.3.1 and 4.3.2 were reanalysed, separating out males and females.

As there were no significant differences between any of the treatment groups, data from all animals were first analysed together. The percent of the cornea covered by vessels in males was significantly higher than in females, either after immediate treatment or after delayed treatment for 14 days, $p=0.001$ and $p<0.001$ respectively (Figure 4-24). The difference between males and females was also observed when only data from the untreated animals were analysed. Again males showed significantly higher neovascularization than females, either after immediate treatment or delayed treatment for 14 days, $p=0.012$ and $p<0.001$ respectively (Figure 4.26).

In light of these differences between male and female rats, the data from sections 4.3.1 and 4.3.2 were separated into males and females and analysed separately. The effect of topical anti-VEGF-B scFv therapy on developing vessels was first assessed. There was no significant difference in the percent of the cornea covered by vessels between the anti-VEGF-B scFv and control groups in either male ($p=0.39$) or female ($p=0.42$) animals (Figure 4-25). However, in each group the males had more vessels.

The effect of topical anti-VEGF-B therapy on established vessels was next assessed as described previously. The males in each group had more vessels than the females. There was no significant difference in the percent of the cornea covered by vessels between the anti-VEGF-B scFv and control groups in either male or female animals (Figure 4-26).

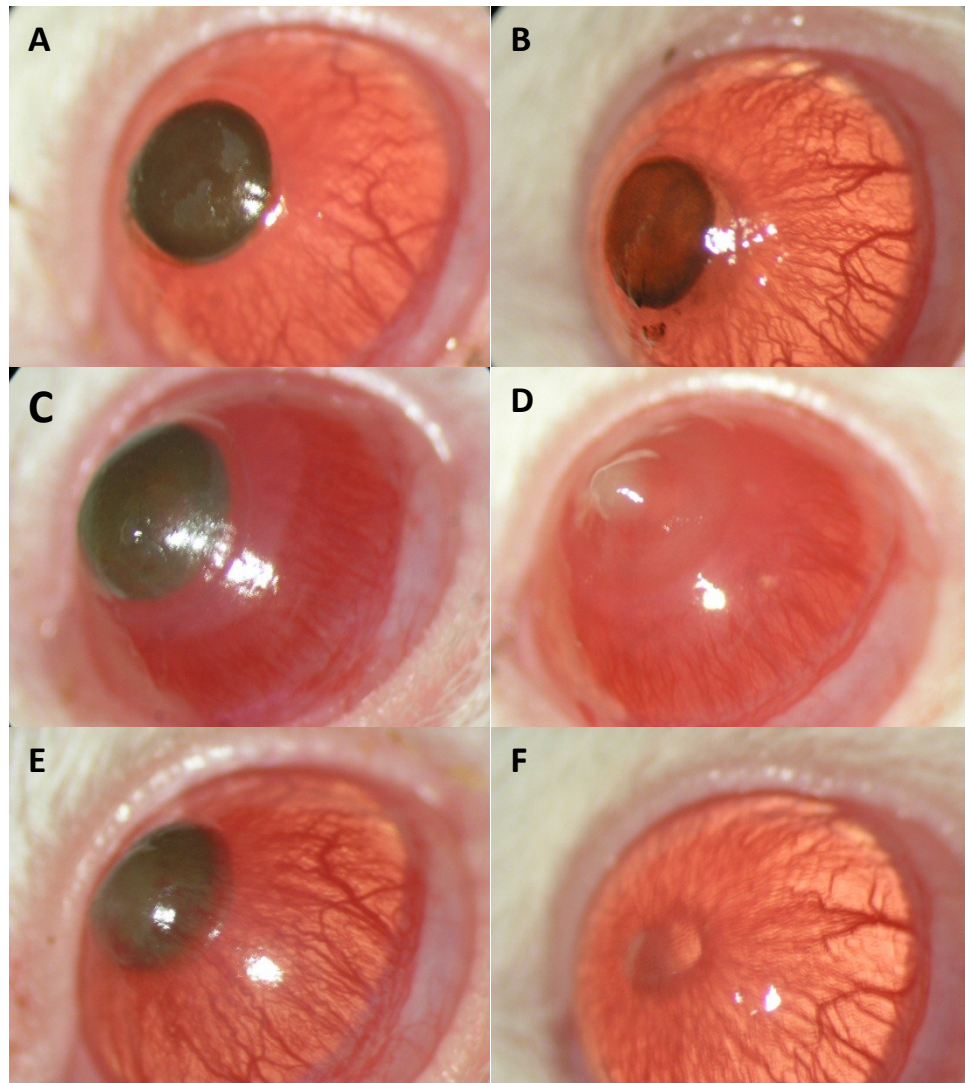


Figure 4-23 Representative images of male and female rat eyes following silver nitrate cautery

Eyes from male (**A, C, E**) and female (**B, D, F**) inbred Sprague-Dawley rats were photographed following silver nitrate cautery. The cauterised portion of the cornea was visible the day following cautery but was darker in males (**A**) when compared to females (**B**). Vessels were evident 7 days post cautery in both male (**C**) and female (**D**) eyes, however the cauterised portion was lighter in females. The vessels in the males appeared to be more densely infiltrating the cornea. The cornea was oedematous in both males and female rats. Fourteen days post corneal cautery, oedema had resolved in both male (**E**) and female (**F**) eyes.

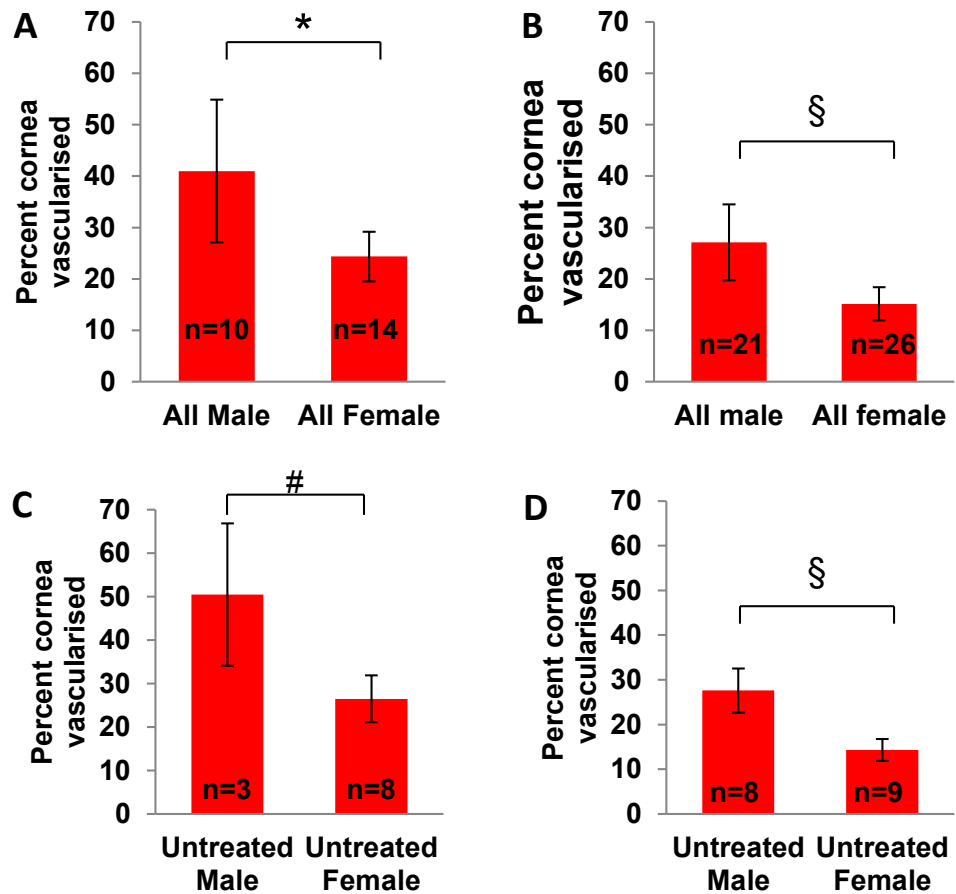


Figure 4-24 Differences in degree of corneal neovascularization between male and female rats

The degree of corneal neovascularization following silver nitrate cautery was compared in male and female Sprague-Dawley rats. Untreated, control scFv and anti-VEGF-B scFv treated animals, (A) treated immediately after cautery or (B) 14 days after cautery for 14 days were grouped together. Male rats showed significantly more corneal vessels than females in both immediate and delayed treatment groups. Males also showed significantly greater neovascularization when only the untreated animals were analysed after (C) immediate or (D) delayed treatment. * $p=0.001$ # $p=0.012$ § $p<0.001$. The bars represent the mean corneal vessel area in biological replicates, and the error bars represent the standard deviation. n = number of rats in each group.

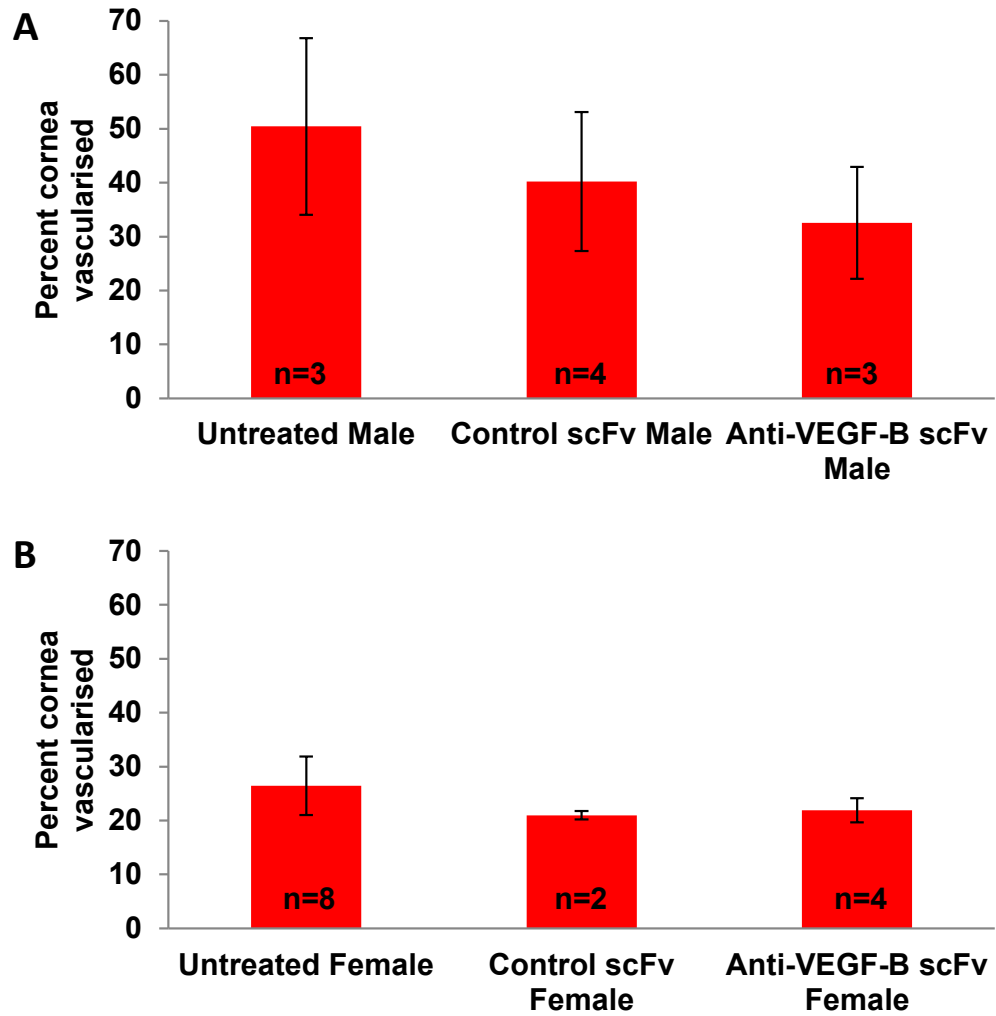


Figure 4-25 Effect of topical treatment with anti-VEGF-B scFv on developing vessels in male and female rats

The degree of corneal neovascularization following silver nitrate cautery was compared in **(A)** male and **(B)** female Sprague-Dawley rats treated immediately after cautery for 14 days. No significant differences were observed between anti-VEGF-B scFv treated and control groups in either males ($p=0.39$) or females ($p=0.42$). The bars represent the mean corneal vessel area in biological replicates, and the error bars represent the standard deviation. n = number of rats in each group.

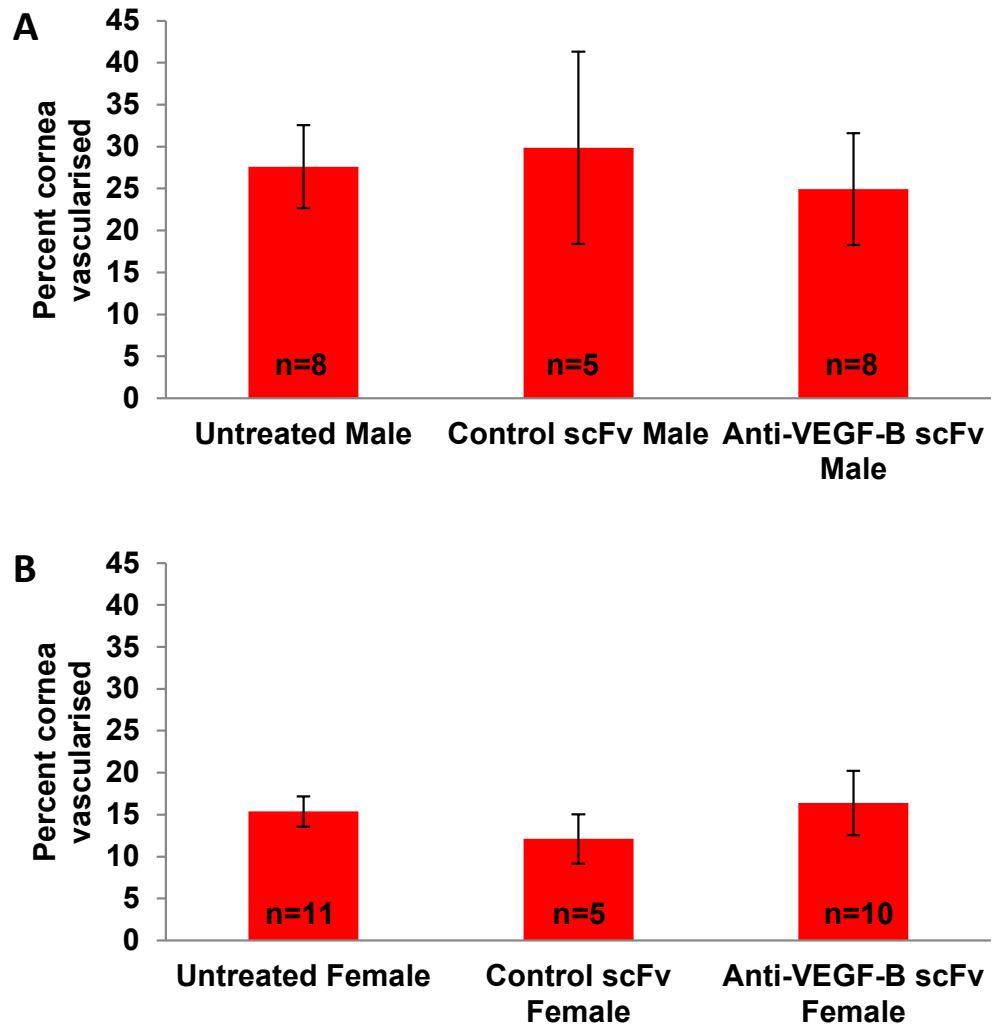


Figure 4-26 Effect of topical treatment with anti-VEGF-B scFv on established vessels in male and female rats

The degree of corneal neovascularization following silver nitrate cautery was compared in (A) male and (B) female Sprague-Dawley rats treated 14 days after cautery for 14 days. No significant differences were observed between anti-VEGF-B scFv treated and control groups in either males ($p=0.15$) or females ($p=0.08$). The bars represent the mean corneal vessel area in biological replicates, and the error bars represent the standard deviation. n = number of rats in each group.

In summary, a statistically significant difference in the neovascularization between male and female rats was observed. Male rats developed more vessels in response to corneal cautery than female rats. The anti-VEGF-B scFv did not have an effect on either growing or established vessels when delivered topically as an eye drop, in male or female rats analysed separately.

4.3.4 Effect of anti-VEGF-B scFv delivered by subconjunctival injection on established vessels

Topical delivery of the anti-VEGF-B scFv did not result in regression of vessels, and increasing the frequency of eye drops was not considered to be practical. We surmised that perhaps what was required was more sustained release of the scFv. To investigate this further, the topical anti-VEGF-B scFv treatment was supplemented with two subconjunctival injections of the scFv.

Subconjunctival injection is an alternate mode of delivery of drugs to the anterior segment. The effect of subconjunctival delivery of the anti-VEGF-B scFv on established vessels was assessed. Corneal cautery was induced in Sprague-Dawley rats as before. The vessels were allowed to establish a stable network for 14 days, following which anti-VEGF-B scFv was applied as eye drops 4 times daily at 2 hour intervals. The final eye drop of the day was formulated with a temperature sensitive gel, which was liquid at 4°C but formed a gel at body temperature. In addition on days 1 and 8 of treatment, scFv formulated with the temperature sensitive gel was delivered by subconjunctival injection, as described in section 2.5.1.c. At the end of the treatment regimen, the rats were euthanised and the vasculature was stained with haematoxylin and the corneas were flatmounted.

Figure 4-27 shows representative corneal flatmounts from an untreated rat, a rat treated with control scFv and an anti-VEGF-B scFv treated rat. In both groups, vessels had infiltrated the cornea, from the limbus, and reached the site of cautery. There was an even density of vessels over the surface of the cornea. The flatmounts from the rat treated with anti-VEGF-B scFv showed a prominent central blister. Some vessels spanned the limbus and the blister. However, a large proportion of the vessels did not extend all the way to the site of cautery.

The percent of the corneal area covered by vessels was then quantified. Animals treated with anti-VEGF-B scFv showed significantly less corneal area covered by vessels, $p < 0.001$ (Figure 4-28). There was no significant difference between untreated and control scFv treated animals, $p = 0.66$. The data were then separated into males and females. Male rats treated with anti-VEGF-B scFv showed significantly less corneal area covered with vessels than untreated or control scFv treated males, $p = 0.003$ and $p = 0.009$ respectively (Figure 4-29). There was no significant difference between untreated and control scFv treated males, $p = 0.53$. A similar result was observed in the females. Female rats treated with anti-VEGF-B scFv showed significantly less corneal area covered with vessels than untreated or control scFv treated males, $p = 0.006$ and $p = 0.048$ respectively (Figure 4-29). There was no significant difference between untreated and control scFv treated females, $p = 0.11$.

In summary, an anti-VEGF-B scFv was engineered from a hybridoma which secreted an antibody with specificity to human, mouse and rat VEGF-B. The scFv maintained the binding specificity of the parent antibody and was shown to block the biological effects of VEGF-B in a cell based assay. The effect of the scFv on developing and established vessels was assessed in a rat model of corneal neovascularization. The

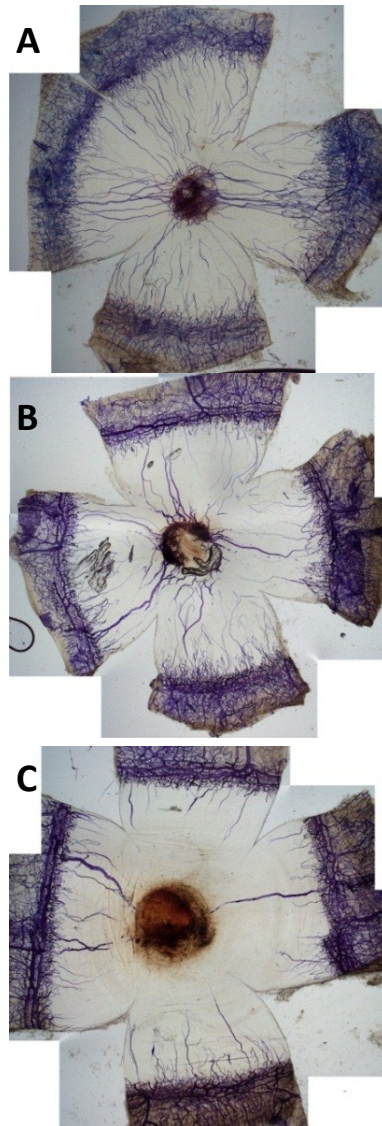


Figure 4-27 Representative images of haematoxylin perfused corneal flatmounts from rats treated with topical and subconjunctival scFv for 14 days beginning 14 days after cautery

Corneal cautery was induced in Sprague-Dawley rats. The vessels were allowed to establish for 14 days, after which 14 days of treatment with control or anti-VEGF-B scFv was applied. At the end of the treatment the vasculature of the rat was perfused with haematoxylin. The eyes were removed and corneas dissected out and flatmounted. (A) Untreated (B) Control scFv and (C) anti-VEGF-B scFv treated rats showed infiltration of vessels into the cornea. By day 28 the vessels had reached the site of cautery and anastomosed. Fewer vessels were observed in rats treated with VEGF-B scFv (panel C) compared to both control and untreated corneas.

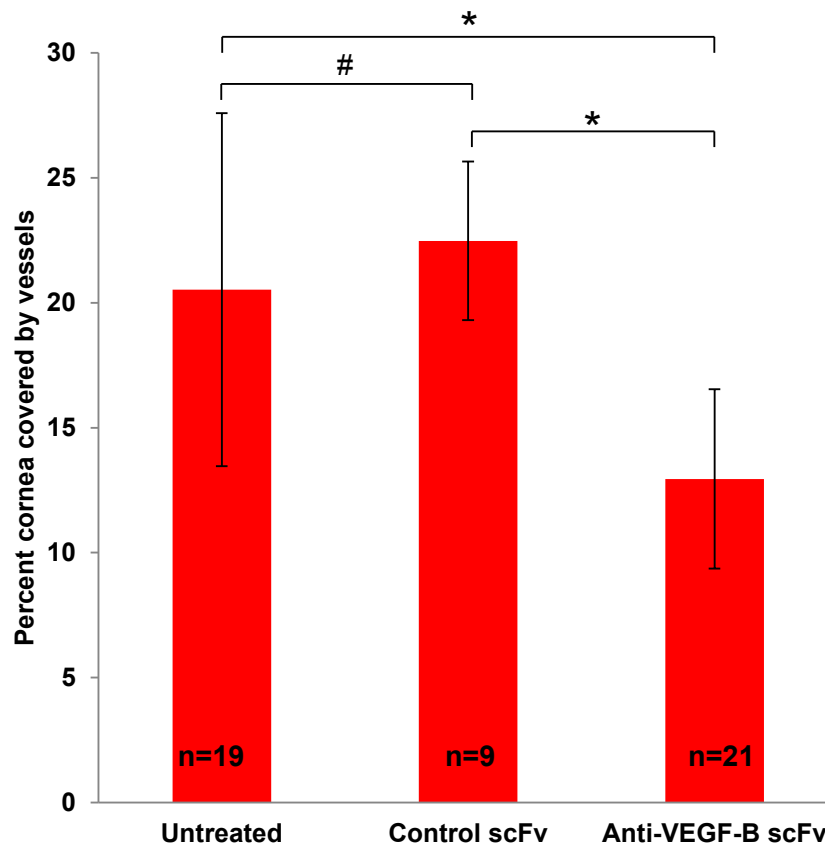


Figure 4-28 Effect of 14 days of topical scFv treatment combined with 2 subconjunctival scFv injections on corneal vessels in a rat model of corneal neovascularization

Corneal neovascularization was induced in inbred Sprague-Dawley rats by silver nitrate cautery. Treatment commenced 14 days after cautery. Eye drops were delivered at 2 hour intervals 5 times a day for 14 days. In addition, on days 1 and 8 of treatment scFv was delivered by subconjunctival injection. At euthanasia, the corneal vessels were perfused with haematoxylin and the percentage of the cornea covered by vessels was quantified. The percentage of cornea covered by vessels was significantly smaller in the anti-VEGF-B scFv treated group. * $p < 0.001$ # $p = 0.66$. The bars represent the mean corneal vessel area in biological replicates, and the error bars represent the standard deviation. n = number of rats in each group.

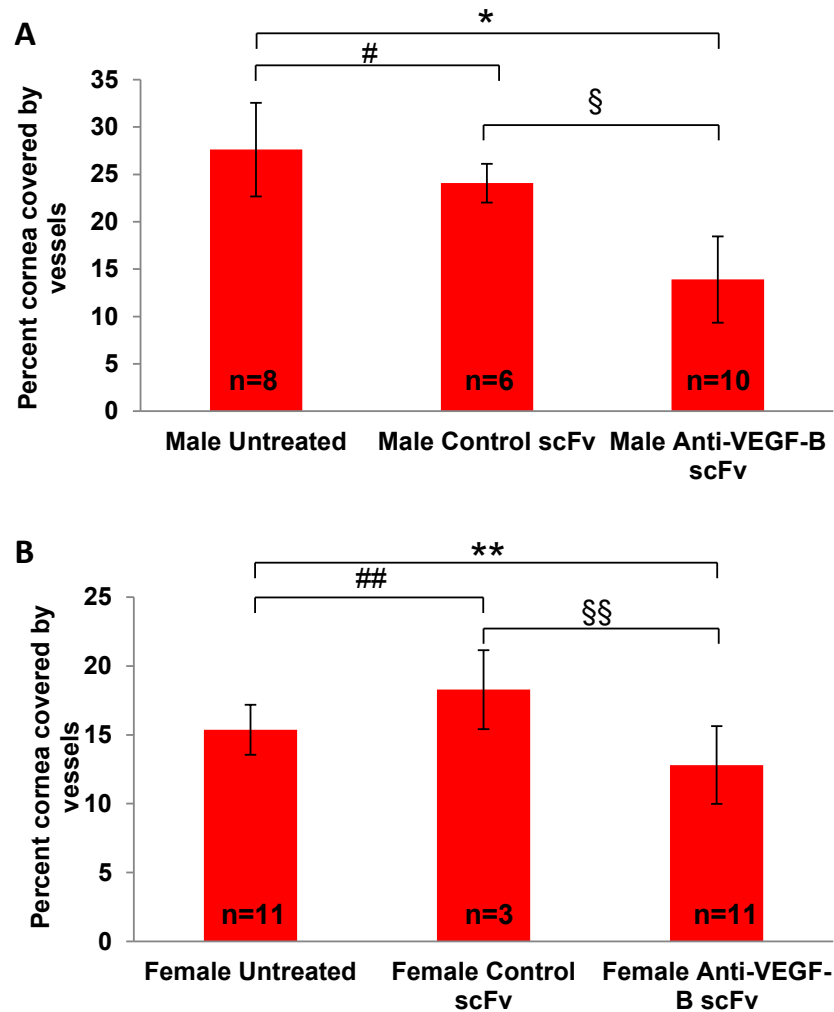


Figure 4-29 Comparison of corneal neovascularization in males and females after combined treatment with topical and subconjunctival anti-VEGF-B scFv

Data from rats treated with topical as well as subconjunctival scFv was separated into (A) males and (B) females. The percent of the cornea covered by vessels was compared between anti-VEGF-B scFv and control treated groups. Rats treated with anti-VEGF-B scFv had a significantly smaller portion of their corneas covered with vessels. *p=0.003, #p=0.525, §p=0.009, **p=0.006, ##p=0.108, § § p=0.048. The bars represent the mean corneal vessel area in biological replicates, and the error bars represent the standard deviation. n = number of rats in each group.

results are summarised in Table 4-2. The scFv did not have an effect on neovascularization when delivered topically as an eye drop. However, topical anti-VEGF-B scFv supplemented with subconjunctival injection resulted in reduced corneal vessel area, compared to a control scFv with irrelevant specificity.

Table 4-2 Summary of results

Group	Percentage of the cornea vascularised			p value
	Untreated	Control scFv	Anti-VEGF-B scFv	
7 days of eye drops, growing vessels		23.9 ±14.5 n=3	21.6 ±14.5 n=3	0.59
7 days of eye drops, established vessels	35 ±9.8 n=3	31 ±14.1 n=3	42.5 ±19 n=3	0.83
14 days of eye drops, growing vessels	33 ±14.1 n=11	33.7 ±14.1 n=6	26.4 ±8.3 n=7	0.46
14 days of eye drops, established vessels	20.5 ±7 n=17	20.9 ±12 n=10	20.1 ±6.7 n=18	0.87
14 days of eye drops + subconjunctival injection, established vessels	20.5 ±7 n=19	22.5 ±7.2 n=9	12.9 ±3.6 n=21	<0.001

4.4 Discussion

The aim of this work was to develop an anti-VEGF-B antibody fragment, in the scFv format, and assess its activity on growing and established vessels in a rat model of corneal neovascularization. An anti-VEGF-B scFv was engineered from a hybridoma that secreted an antibody with activity against human, mouse and rat VEGF-B. The binding of the anti-VEGF-B scFv to human VEGF-B was confirmed by ELISA and surface plasmon resonance, and its functional activity was proven using a cell based assay.

Topical therapy with scFv did not prevent the growth of newly formed vessels nor cause regression of established vessels in a rat model of corneal neovascularization. However, a significant decrease in the corneal neovascular area was observed when treatment with topical scFv was supplemented by subconjunctival injection.

An unexpected finding of this study was a statistically significant difference in the degree of neovascularization between male and female rats. Male rats developed more vessels in response to silver nitrate cautery than female rats. These findings will be discussed and placed in context with the current literature.

4.4.1 VEGF-B as a therapeutic target for corneal neovascularization

Corneal neovascularization is a potentially sight threatening condition, with limited treatment options. The major therapeutic target for the treatment of corneal neovascularization is VEGF-A, which has been shown to stimulate blood vessel growth in the cornea²²⁵. A meta-analysis of prospective human case studies showed that subconjunctival and topical bevacizumab caused a reduction in corneal vessel

area⁴⁸⁸. A recent randomised control trial by Petsoglou *et al*, in 30 patients with recent onset corneal neovascularization, demonstrated that subconjunctival injections of bevacizumab, an anti-VEGF-A antibody, were effective at reducing the area of the cornea covered by vessels by 36% over 12 weeks, as compared to placebo group in whom the area increased by 90%³⁴⁸. However, treatment of established vessels has proved to be more difficult. A study in 12 eyes of 11 patients revealed that subconjunctival bevacizumab did not cause long lasting regression of established corneal vessels³⁴⁶.

An agent that can cause regression of established blood vessels would be useful for the treatment of corneal neovascularization. VEGF-B is closely related to VEGF-A^{236, 237} but does not induce angiogenesis^{248, 249}. However, VEGF-B has been shown to be a survival factor for blood vessels²⁵⁷. This makes VEGF-B an attractive target for the treatment of established blood vessels in the cornea.

4.4.2 Production of an anti-VEGF-B scFv

The 2H10 hybridoma produces an antibody with activity against human, mouse and rat VEGF-B⁴⁸⁵. An agent with cross-species reactivity is particularly attractive, as it allows initial testing in animal models, followed by rapid progression to human trials, without the need for modification. The efficacy of the 2H10 antibody has been trialled in a number of animal models of human diseases. The antibody, when administered prophylactically, resulted in a reduced clinical pathology index in a mouse collagen induced arthritis model⁴⁸⁹. Administration of the antibody to diabetic rats on a high fat diet resulted in normalization of insulin sensitivity and increased glucose uptake in skeletal muscles and heart²⁷⁶. The 2H10 antibody has also shown

an effect on blood vessels in the eye. In a mouse model of oxygen induced retinopathy, intravitreal injection of the antibody increased blood vessel regression, and reduced neovascular tufts²⁵⁷. This effect was brought about by an increase in apoptosis of endothelial cells, as evidenced by co-localization of TUNNEL⁺ cells with IB4 stained endothelial cells²⁵⁷.

Topical application is the preferred option for the delivery of ophthalmic drugs. A locally applied drug for the treatment of established corneal vessels would be a useful addition to the clinician's armamentarium. Antibodies are large molecules and are unable to penetrate the cornea on topical application⁴⁴³. Antibody fragments such as single chain variable fragments (scFv) retain the binding specificity of the parental antibody, but being much smaller, penetrate through the cornea when applied topically⁴⁴³. ScFvs consist of the V_L and V_H of the parent antibody held together with a polypeptide linker. cDNA from the 2H10 hybridoma was used successfully to engineer an anti-VEGF-B scFv.

V(D)J recombination leads to a vast array of specificities for antibody molecules. Plückhtun *et al* have developed specialised sets of primers to capture the large variations in antibody genes⁴³⁹. However recombination can lead to the formation of unproductive immunoglobulin rearrangements in hybridomas that secrete a functional antibody, which complicates the amplification of the functional genes⁴⁹⁰. In order to avoid this, the V regions of the 2H10 antibody were sequenced and specific primers were designed to amplify the V_L and V_H. The amplified V_L and V_H were joined using splice by overlap extension PCR, to yield the anti-VEGF-B scFv gene.

The anti-VEGF-B scFv gene was then cloned into a bacterial vector for expression in *E.coli*. Bacterial expression is an efficient method to produce large quantities of recombinant protein, with yields of up to 40 mg per litre per day achievable using a benchtop fermenter⁴⁹¹. However, protein production in bacteria is associated with endotoxin contamination. Removal of endotoxin from recombinant protein is time-consuming and leads to loss of recombinant protein. Furthermore it is often impossible to reduce the endotoxin levels to an acceptable amount for *in vivo* use. For this reason, recombinant anti-VEGF-B scFv produced in *E.coli* was used for *in vitro* experiments only. All scFv for *in vivo* use was produced at CSL Ltd. using a mammalian expression system, to massively reduce endotoxin levels.

4.4.3 Characterization of the anti-VEGF-B scFv

A scFv produced from an antibody must maintain the binding specificity of the parent antibody to be of use. The binding of the anti-VEGF-B scFv to human VEGF-B was assessed by ELISA and surface plasmon resonance. The VEGF-B scFv demonstrated binding to human VEGF-B at concentrations as low as 7 pg/ml by ELISA. Furthermore, surface plasmon resonance analysis demonstrated that the VEGF-B scFv maintained similar binding characteristics to the parent 2H10 antibody. However, the kinetics of the binding differed slightly. Although an accurate K_d was not calculated, the sensograms revealed that the scFv had a higher association and a higher dissociation rate to and from human VEGF-B than the parental antibody. The faster association rate of the scFv may be due to reduced steric hindrance, owing to the smaller size of the molecule. Furthermore, the scFv being monovalent might also dissociate from the target faster than a divalent antibody molecule. However, the anti-VEGF-B scFv was found to maintain the

binding characteristics of the parental antibody. The next step was to assess the stability of the anti-VEGF-B scFv.

Having a long shelf life is an important quality for a pharmaceutical drug. The stability of the anti-VEGF-B scFv under long-term storage was assessed. The binding of freshly prepared scFv to VEGF-B was assessed by ELISA. The scFv was then stored at 4°C for a period of 20 months, at which point a repeat ELISA was performed. There was no significant difference in the binding of the scFv after 20 months of storage at 4°C. This indicated that the scFv could be stored at 4°C for extended periods, without adversely affecting the binding. This is keeping with previous studies in our laboratory, in which an anti-rat-CD4 scFv was found to be stable at 4°C and room temperature for up to 12 months, and was resistant to protease in rat serum for up to 72 hours⁴⁴³. scFvs have also shown stability in human serum for similar time frames⁴⁹².

The functional effects of the anti-VEGF-B scFv were assessed in a cell based assay at CSL Ltd. BaF3 cells, expressing a recombinant fusion receptor consisting of the extracellular portion of VEGFR1 and the transmembrane and intracellular regions of the erythropoietin receptor, proliferate when exposed to VEGF-B⁴⁹³. The ability of the anti-VEGF-B scFv to inhibit VEGF-B induced proliferation was assessed. The anti-VEGF-B scFv inhibited VEGF-B induced proliferation in BaF3 cells at concentrations in the ng/ml range. This was comparable to the inhibition of proliferation seen with the 2H10 antibody. These data suggested that the anti-VEGF-B scFv maintained the binding specificity of the 2H10 antibody, and was functionally active *in vitro*.

4.4.4 Rat model of corneal neovascularization

The model of corneal neovascularization used in this study was the silver nitrate induced corneal cautery model in the rat. This is a well characterised model which has been used in a number of studies^{311, 327, 494}. Chemical cautery has been used to induce neovascularization in both the rabbit⁴⁹⁵ and the mouse⁴⁹⁶. The advantage of this model is that it is associated with inflammation, which mimics corneal neovascularization in humans, in which neovascularization is usually accompanied by inflammation. It is also simple to induce neovascularization with this model. The disadvantages are uneven neovascularization and the complex pathophysiology of the neovascular response⁴⁹⁷.

Corneal neovascularization has been induced in animals using other models such as the corneal micropocket model and the corneal suture model. The corneal micropocket model was described by Kenyon *et al* in the mouse⁴⁹⁸ and by Loughman *et al* in the rabbit⁴⁹⁹. It involves implanting pellets containing vascular growth factors such as β -fibroblast growth factor into the corneal stroma, to induce neovascularization. It is a fast and inexpensive model, however the neovascularization can be variable and is dependent on the surgeon's technique⁴⁹⁷. Neovascularization can also be induced by placement of sutures in the cornea. This model has been used for induction of corneal neovascularization in the rabbit^{317, 500}. The advantage of this model is that it is a simulated clinical scenario in the context of corneal transplantation. The disadvantages are that it is surgeon-dependent and there is variability in the neovascular response⁴⁹⁷.

The silver nitrate cautery model was chosen because it is a robust model which induces both neovascularization and inflammation. It is relatively easy to perform and although there is some variability in the neovascular response, this can be minimised by careful application of the neovascular stimulus. The effect of anti-VEGF-B scFv therapy on growing and established vessels was assessed using this model.

4.4.5 Topical delivery of scFv for corneal neovascularization

The effect of topical treatment with the anti-VEGF-B scFv on growing vessels was first assessed. Blood vessels sprouted from the limbal plexus 3-4 days following cautery of the central cornea with silver nitrate. The vessels grew in towards the centre of the cornea and generally reached the site of cautery between 7-10 days. To assess the effect of anti-VEGF-B scFv eye drops on growing vessels, therapy was commenced on the day following cautery.

Anti-VEGF-B scFv applied as eye drops did not prevent the growth of vessels in a rat model of corneal neovascularization. This result was not entirely surprising, as VEGF-B has shown little or no angiogenic effect. Transgenic overexpression of VEGF-B does not induce angiogenesis or lymphangiogenesis^{248, 249, 255}. Furthermore, VEGF-B protein does not induce endothelial cell proliferation or migration *in vitro*⁵⁰¹, nor angiogenesis *in vivo* in the brain²⁷¹ or eye²⁷³.

VEGF-B is a potent survival factor for endothelial cells^{245, 257}. VEGF-B deficient endothelial cells underwent apoptosis in response to oxidative stress or serum starvation *in vitro*²⁵⁷. Moreover, VEGF-B caused an increase in blood vessel density

in a cardiac ischaemia model in the mouse^{254, 502}, pig and rabbit⁵⁰³. These studies showed that depletion of VEGF-B was detrimental to blood vessel survival, while addition caused an *increase* in blood vessel survival. These data suggested to us that VEGF-B inhibition might cause regression of existing corneal blood vessels.

The effect of the anti-VEGF-B scFv on established vessels was thus assessed. Blood vessels were allowed to grow and form an anastomosed vascular network for 14 days post-cautery. Anti-VEGF-B scFv eye drops were then applied for 14 days and the percentage of the cornea covered by vessels was assessed. Topical anti-VEGF-B scFv therapy did not reduce the area of the cornea covered by vessels when compared to either untreated or control scFv treated groups.

A possible explanation for the ineffectiveness of the topical therapy was that the anti-VEGF-B scFv did not penetrate through the cornea. However, scFvs have been shown to penetrate the cornea of pigs and cats on topical delivery in the form of an eye drop⁴⁴³. Recently, an anti-TNF α scFv was found to penetrate through the cornea in humans, with a mean aqueous humour concentration of 1.1 ng/ml⁵⁰⁴. It is thus unlikely that the anti-VEGF-B scFv did not penetrate through the rat cornea. Another point to consider was the eye drop regimen. Five eye drops were applied at 2 hour intervals, with ointment applied over the eye after administration of the final eye drop each day. This did leave a significant portion of the day in which no therapy was applied, which might have resulted in the levels of scFv dropping below therapeutically useful levels. We considered that possibly what was required was a depot of drug which was released slowly, and that maintained levels of the scFv. Delivery of the anti-VEGF-B scFv by subconjunctival injection was trialled next.

4.4.6 Supplementation of topical therapy with subconjunctival anti-VEGF-B scFv

Subconjunctival injection is an alternative route for administration of drugs to the anterior segment of the eye, and has been used to deliver anti-inflammatory agents such as triamcinolone^{505, 506}, and antibiotics^{507, 508}. Clinically bevacizumab has been delivered by subconjunctival injection for the treatment of corneal neovascularization^{335, 336, 339, 341, 345, 346, 348, 509, 510}.

The aim of delivering the anti-VEGF-B scFv by subconjunctival injection was to create a depot which would release the scFv slowly, so as to maintain the levels of scFv in the cornea. In preliminary work, subconjunctival injection of scFv in aqueous solution proved to be difficult, as most of the injected solution poured back out of the injection site, despite the use of a 31 G needle. To overcome this issue, the scFv was formulated into a temperature responsive gel using Pluronic F127. Pluronic F127 has been used in the eye for sustained release of pilocarpine hydrochloride, with an increase in the duration of action of the drug reported⁵¹¹⁻⁵¹³. The benefit of using Pluronic F127 was that the scFv-Pluronic solution was liquid at 4°C, allowing injection under the conjunctiva. The normal body temperature of rats is 37°C⁵¹⁴. The body heat of the rat caused the injected scFv-Pluronic solution to gel, thus creating a reservoir of drug-containing gel under the conjunctiva. This method allowed successful delivery of the scFv under the conjunctiva of the rat eye.

The effect of topical anti-VEGF-B scFv therapy supplemented with subconjunctival injection was assessed on established corneal vessels using silver nitrate cautery in the rat model. Anti-VEGF-B scFv therapy significantly reduced the area of the

cornea covered by vessels, when compared to either untreated or control scFv treated groups ($p < 0.001$). This was a noteworthy result, as it demonstrated that the anti-VEGF-B scFv had an effect on established corneal vessels. Complete regression of the vessels was not observed at the concentration of scFv and time point tested. Further work is required to characterise the extent of regression achievable with the use of the anti-VEGF-B scFv, including assessing the effect of subconjunctival injections without topical therapy. There were no observable adverse effects associated with anti-VEGF-B scFv therapy. However, as VEGF-B is a survival factor for multiple cell types, including neurons, assessment of corneal nerves and endothelium needs to be carried out to ensure there are no adverse effects of the therapy.

4.4.7 Difference in neovascular response in male and female rats

An interesting finding of this study was the difference in neovascularization in male and female rats. Male rats developed significantly more vessels at 14 and 28 days post-cautery, than did female rats. A standardised cautery protocol was applied to all animals in order to minimise variation.

Obvious differences between the sexes include size and expression of sex hormones. Male rats are significantly larger than females, and have larger eyes. The differences in the size of the eyes may have played a role in the observed neovascularization. However, the experiments were conducted on animals of varying ages, including young male rats which were the size of an adult female rat. The young males displayed a similar neovascular response when compared to older, larger male rats. It is thus unlikely that the size of the animals had an effect on the neovascular response.

A possible explanation for the sex-based differences in ocular neovascularization observed might be differential responses caused by sex hormones. mRNAs for testosterone, oestrogen and progesterone receptors have been found in the eyes of rabbits and humans⁵¹⁵, and in human corneas⁵¹⁶. Both testosterone and oestrogen have been shown to have an effect on angiogenesis. However, testosterone replacement therapy has been shown to stimulate angiogenesis in a castrated rat myocardial infarct model⁵¹⁷. Exogenous testosterone upregulated HIF1 α and VEGF-A in the prostate glands of castrated rats⁵¹⁸. Testosterone has also been shown to have the opposite effect on angiogenesis. Rats fed with a high fat diet had 70% less testosterone, which led to stromal hyperplasia in their prostate, with increased VEGF-A and angiogenesis⁵¹⁹.

Similarly oestrogen plays a role in the regulation of angiogenesis. Ovariectomy, which results in a reduction of oestrogen and an increase in gonadotropins, resulted in increased tumour angiogenesis in a mouse model⁵²⁰. This might indicate an anti-angiogenic role of oestrogen. Oestrogen has also been shown to inhibit angiogenesis in the uterus of mice⁵²¹. The uteri of mice treated with an oestrogen analogue expressed lower levels of VEGFR2, neuropilin1, and platelet endothelial cell adhesion molecule (PECAM-1), which is a marker of endothelial cells⁵²². In a rat model of colon cancer, oestrogen reduced the levels of HIF1 α and VEGF-A, and was found to be protective against carcinogenesis⁵²³. These data suggest that oestrogen is a potent inhibitor of angiogenesis. However, oestrogen has also demonstrated pro-angiogenic effects. Diosgenin, an oestrogen analogue, and oestrogen both have been shown to upregulate VEGF-A and stabilise HIF1 α *in vitro*^{524, 525}. Oestrogen also induced tumour angiogenesis, with upregulation of VEGF-A in rats⁵²⁶.

The literature on the regulation of angiogenesis by sex hormones is mixed, with testosterone and oestrogen having both pro and anti-angiogenic effects in different contexts. However, the literature demonstrates that sex hormones do have a profound effect on angiogenesis. The differences in the response to silver nitrate cautery in male and female rats might plausibly be a result of inhibition of angiogenesis by oestrogen and exacerbation by testosterone. The mechanisms need to be investigated further. However, anti-VEGF-B scFv eye drops supplemented by subconjunctival injections significantly reduced corneal vessels compared to controls in both males and females.

4.5 Conclusion

An anti-VEGF-B scFv with specificity for human, mouse and rat VEGF-B was engineered from a hybridoma. The scFv demonstrated similar binding characteristics to the parent antibody. The scFv was formulated as an eye drop and for subconjunctival injection and assessed in a rat model of corneal neovascularization. Topically delivered scFv had no effect on growing or established vessels. However, topical therapy supplemented with subconjunctival injection did cause significant regression of established corneal vessels. The safety of anti-VEGF-B therapy needs to be further assessed, in particular effects on corneal nerves and endothelial cells. However, the anti-VEGF-B scFv, delivered by subconjunctival injection, might prove useful for the treatment of human corneal neovascularization.

CHAPTER 5 DISCUSSION

During my PhD candidature, I investigated the use of porous silicon membranes and composite materials as artificial stem cell niches for the transfer of oral mucosal epithelial cells to the rat eye, and anti-VEGF-B scFv therapy in a rat model of corneal neovascularization. In this chapter I will present the major findings of my studies and place them in context with the current literature.

5.1 Overview of study findings

5.1.1 Porous silicon materials as an artificial stem cell niche for the transfer of cells to the rat eye

Porous silicon membranes coated with collagen IV or vitronectin were found to support the growth of rat oral mucosal epithelial cells. The cells expressed the corneal epithelial marker CK3/12 and the transient amplifying cell marker p63. A small proportion of cells also expressed the putative stem cell marker ABCG2. Upon subconjunctival implantation, rat oral mucosal epithelial cells migrated off the pSi membranes, however they were not detected from the central corneal surface.

A novel pressed pSi-PCL composite material was engineered, which supported the growth of human lens epithelial cells and could be loaded with drugs, including biologics, post-fabrication. FDA loaded in the composite materials was released and taken up by lens epithelial cells. Composites loaded with a mixture of biologic growth factors elicited proliferation in BALBc/3T3 cells grown in serum-free medium. However, the restricted biocompatibility of the composite material in the rat eye suggested it was unsuitable for use as an ocular implant.

5.1.2 Anti-VEGF-B therapy for corneal neovascularization

I engineered an anti-VEGF-B scFv from a hybridoma that secreted an antibody with specificity for human, mouse and rat VEGF-B. The binding of the scFv to human VEGF-B was confirmed, and the scFv was formulated for topical delivery as an eye drop. Topical scFv therapy did not have a significant effect on growing or established corneal vessels in a rat model of corneal neovascularization. However, topical anti-VEGF-B scFv supplemented with subconjunctival injection, applied to established corneal vessels, significantly reduced the area of the rat cornea covered by vessels.

5.2 General discussion

5.2.1 The need for a specific limbal epithelial stem cell marker

Ex vivo cultured epithelial cells must contain a population of self-renewing stem cells for long-term maintenance of the corneal epithelium after transplantation. Confirming the presence of stem cells before transplantation might improve outcomes, but currently there is no single, unambiguous marker for LSCs.

Morphologically, LSCs are identified as small⁵²⁷, melanin-containing⁵²⁸ cells with a high nuclear to cytoplasmic ratio⁶⁸. Like other stem cell populations, LSCs are slow cycling¹⁷, retain BrdU labelled DNA⁵²⁹ and have the ability to generate holoclones^{30, 48}. Currently used markers are not specific for LSCs and in addition, mark populations of transient amplifying cells. In a clinical setting the presence of stem cells is not generally confirmed prior to transplantation of epithelial cells to the ocular surface.

Pellegrini *et al* were the first to demonstrate ocular surface reconstruction using *ex vivo* cultured limbal epithelial cells in humans¹⁵⁵. The cultured limbal cells stained positive for CK3¹⁵⁵, indicating they had undergone differentiation into mature corneal epithelium. Schwab *et al* used CK3, which marks differentiated corneal epithelial cells, to confirm re-epithelialization of the ocular surface after transplantation of *ex vivo* cultured limbal epithelial cells, in a rabbit model of OSD¹⁰⁰.

Shortt *et al* treated 10 patients with limbal stem cell dysfunction with *ex vivo* cultured limbal epithelial cells grown on amniotic membrane¹⁵⁰. Cells were collected from the central corneas pre- and post-operatively by impression cytology, and stained for CK3 and CK19. The corneal epithelial marker CK3 was expressed in 12% of cells pre-operatively compared with 69% of cells post-operatively¹⁵⁰. CK19 is expressed by basal epithelial cells in the peripheral cornea, but is also seen in the conjunctiva. Pre-operatively, the conjunctivised ocular surface showed high expression of CK19 (80% of cells); this number reduced to 30% post-operatively. A combination of CK3 and CK19 expression was used to demonstrate the shift from a conjunctival to a more corneal epithelial phenotype.

Rama *et al* demonstrated a correlation between the expression of the transient amplifying cell marker p63 and the stabilization of the ocular surface post-transplant¹⁷⁹. The authors treated 112 patients with autologous limbal epithelial cells cultivated on fibrin sheets. Cultured limbal epithelial cells with greater than 3% of cells expressing p63 (p63alpha bright cells) resulted in a 78% success rate when transplanted into patients¹⁷⁹. Conversely, when less than 3% of the cells expressed p63, ocular surface restoration was achieved in only 11% of patients¹⁷⁹. Although

expression of p63 was predictive of the success of the transplant, it must be noted that it is a marker of transient amplifying cells, not stem cells. However, the Δ Np63 isoform is regarded the most selective for stem cells⁶⁴. A recent study by Zakari *et al* evaluated the expression of putative stem cell markers expressed by *ex vivo* cultured limbal epithelial cells using a standardised non-xenogeneic protocol⁴⁷⁰. Cultured limbal epithelial cells expressed the stem cell markers ABCG2, Δ Np63 and CK14 and were negative for the differentiation markers CK3 and desmoglein 3⁴⁷⁰. The authors used a panel of markers consisting of putative stem cell markers and differentiation to characterise the population of epithelial cells.

Our study also employed a panel of markers for characterization of the rat oral mucosal epithelial cells. The use of CK3 with oral mucosal epithelial cells serves two purposes. Firstly, expression of CK3 demonstrates that the OMECs have a corneal epithelial cell-like phenotype. Secondly, CK3 can be used to confirm the differentiation status of the cells. CK19 marks basal epithelial cells and in conjunction with p63 was used to identify transient amplifying cells. ABCG2 expression was used to identify a population of putative stem cells. Various markers used for the characterization of epithelial cells for ocular surface reconstruction are summarised in Table 5-1.

Table 5-1 Markers used to identify human limbal stem cells

Putative marker	Present (+) absent (-)	Reference
in LESC		
α -enolase	+	530-532
ABCG2	+	57, 59, 68, 533
C/EBP δ	+	534
Carbonic anhydrase	+	535
CD44	+	536
CK19	+	66, 68, 73
CK3/12	-	18, 28, 68, 537
Connexin 43, Connexin 50	-	538-540
Cyclin A, D, E	+	541
Cytochrome oxidase	+	542
Integrin α 9, Integrin β 1	+	543-545
Involucrin	-	68, 538
Na/K-ATPase	+	546
p63 (various isoforms)	+	19, 35, 46, 64, 547, 548
Protein kinase C- γ	+	549
TrKA	+	550-552
Vimentin	+	22, 66, 73

5.2.1.a *Cell surface markers for enrichment of stem cells*

A marker that not only identifies LESC's but can also be used to enrich them from a mixed population would be of great value. Molecules expressed on the surface of cells, such as receptors and adhesion molecules, could potentially be used for enrichment of stem cells by cell sorting methods.

Rabbit limbal side population cells which expressed high levels of ABCG2 were shown to express higher levels of the marker nectin-3 than non-side population cells⁵⁵³. However, the authors noted that a small proportion of the non-side population cells also expressed nectin-3. This indicates that nectin-3 is not a specific marker of LESC's and can only be used to enrich them partially. Horenstein *et al* evaluated the expression of two cell surface molecules, CD38 and CD157, in corneas from 10 human cadaveric donors⁵⁵⁴. CD38 was found to be expressed by suprabasal cells in the limbal epithelium, but was not seen in the central corneal epithelium⁵⁵⁴. CD157 was expressed by a population of p63⁺, CK19⁺ cells in the basal region of the limbus⁵⁵⁴. These markers could potentially be used for the identification and enrichment of LESC's.

In 2014 a novel marker of LESC's, ABCB5, was identified⁵⁵⁵. To date this appears to be the most specific marker identified. ABCB5 expressing cells from the limbus of humans and mouse co-localised with Δ Np63 α ⁺ cells, and retained BrdU-labelled DNA⁵⁵⁵. Furthermore, ABCB5 expression was found to be reduced in patients with limbal stem cell deficiency. ABCB5 positive cells isolated from human and mouse limbus were able to restore the corneal epithelium in limbal stem cell deficient mice

in both a xenogeneic and a syngeneic transplantation model⁵⁵⁵. This is the first report of a molecular marker which correlates with stem cell function.

In summary, a panel of markers is likely to be required for the identification of epithelial stem cells. ABCB5, ABCG2 and Δ Np63 can be used to identify stem cells, while CK3/12 labels differentiated corneal epithelial cells. Furthermore, cell surface markers such as ABCB5 and ABCG2 might possibly be used to enrich for stem cells using cell sorting methods. The former has been shown to correlate with stem cell function and is the most promising for the identification and enrichment of epithelial stem cells.

5.2.2 Is a scaffold necessary for the transfer of cells to the ocular surface?

The majority of studies have transplanted epithelial cells to the ocular surface on a scaffold. The various scaffolds used to transfer cells have been outlined in section 1.4.1.e. However, there is some evidence in the literature of successful transfer of epithelial cells to the ocular surface *without* the use of a scaffold.

In 2004, the Tano group applied a cell sheet composed of autologous oral mucosal epithelial cells to the ocular surface of four patients with limbal stem cell deficiency, without the use of a carrier¹⁰⁷. Oral mucosal biopsies were taken from four patients with bilateral total LCSD and enzymatically dissociated with dispase and trypsin. This was the method used for harvest of tissue in the current study. The authors then cultured the oral mucosal epithelial cells on a temperature responsive polymer, poly(n-isopropylacrylamide). Under normal cell culture conditions at 37°C the cultured cells are adherent to the polymer. However, reducing the temperature below

30°C causes rapid hydration and expansion of the polymer resulting in detachment of the cells in a single contiguous epithelial sheet, with a basement membrane. The oral mucosal epithelial cells formed a stratified epithelium five to six layers thick, expressing CK3/12¹⁰⁷. The cell sheets were transplanted on to the ocular surface of the patients, whose corneas had been denuded to expose the stroma¹⁰⁷. No sutures were required, and a contact lens was used to hold the cell sheet in place. Rapid re-epithelialization was observed, with restoration of corneal transparency. An improvement in visual acuity was observed in all patients, with a mean follow-up time of 14 months¹⁰⁷. The use of temperature-responsive polymers for the generation of epithelial cell sheets is an efficient way of circumventing the need to use a scaffold to carry the cells. However, this was a single, small study and long-term results using this method have not been published. Furthermore, damage to the limbal stem cell niche may need to be repaired for long-term efficacy.

Hyun *et al* have described biomaterial-free epithelial cell sheets prepared from human oral mucosal epithelium⁵⁵⁶. The authors demonstrated that human oral mucosa exhibited a greater colony forming efficiency (44%) when compared to human limbal epithelium (17%). Cultured oral mucosal epithelium expressed the non-keratinised epithelium marker CK4, the corneal epithelium marker CK3/12, the transient amplifying cell marker p63 and the proliferation marker Ki67⁵⁵⁶. Oral mucosal epithelial sheets were detached from the culture plates using dispase. Eighty percent of the cells remained viable after detachment⁵⁵⁶. Transplantation of the cell sheets on to the ocular surface of rabbits with induced limbal stem cell deficiency resulted in re-epithelialization of the ocular surface with marginal epithelial defects⁵⁵⁶. Expression of CK3/12, CK4 and CK13 was observed⁵⁵⁶. The basal

epithelial cells expressed p63, ABCG2 and Ki67⁵⁵⁶. However, this was a xenograft model in which outcomes were reported one week post-transplant. Long-term stabilization of the ocular surface is required in the clinical context, and further evaluation of carrier free oral mucosal epithelial sheets is required.

Zhang *et al* have described a “scaffold free” method for the construction of embryonic stem cell sheets for ocular surface reconstruction⁵⁵⁷. This method employs a centrifugation protocol to deposit a multilayer of mouse embryonic stem cells on to amniotic membrane in a transwell plate. The cells were then transferred to the ocular surface of rabbits with induced limbal stem cell deficiency, with the cells in direct contact with the stroma⁵⁵⁸. The amniotic membrane was removed 10 days post-transplant. In essence this was not a truly scaffold-free method for the transfer of cells to the ocular surface, however, the scaffold was removed shortly after transplantation. The authors reported short-term re-epithelialization of the ocular surface up to 15 days post- transplant, with expression of CK3 and no expression of the conjunctival marker Muc-5AC or the embryonic stem cell marker OCT-4⁵⁵⁸.

The majority of the literature dictates the use of a scaffold to transfer *ex vivo* cultured epithelial cells to the ocular surface. However, the reports described above demonstrate that cell sheets *can* be transplanted on the ocular surface without the use of a scaffold. The use of a scaffold may be more important for the creation of an artificial stem cell niche, rather than simply as a carrier of cells to the ocular surface.

5.2.3 Recreating the limbal epithelial stem cell niche

The majority of studies to treat ocular surface disease have focused on applying cells to the ocular surface, like a bandage. Although this is effective at repairing epithelial defects and restoring transparency, unless the limbal stem cells and their niche are replaced, indefinite renewal of the corneal epithelium is unlikely. Recreating the physical and chemical characteristics of the limbal stem cell niche is one of the biggest challenges in the field of ocular surface reconstruction.

Ortega *et al* have described the engineering of three dimensional scaffolds which resemble the limbus^{468, 469}. They employed a two-step process of microfabrication and electrospinning to generate a 3D scaffold. In the first step, microstereolithography was used to generate a template, followed by electrospinning of poly(lactic-co-glycolic acid) polymer on to the scaffold, to generate a 3D polymer fibre scaffold that incorporated the structural features of the template⁴⁶⁸. The scaffolds were ring or horseshoe shaped and incorporated areas of low fibre density, resembling the structure of limbal crypts. The scaffolds were found to support the growth of rabbit limbal fibroblasts as well as rabbit limbal epithelial cells⁴⁶⁸. Both types of cells were found in the niche, as well as the non-niche areas of the scaffolds. This was an efficient method for the generation of crypt-like regions within the bulk implant. However the authors did not describe the structure of the niche regions in detail. Furthermore, the niche structure was only physically different from the surrounding material and was not chemically modified to resemble the “real” limbal stem cell niche.

The same group has since developed a limbal scaffold using microstereolithography, or 3D printing⁴⁶⁹. The scaffold was made of polyethylene glycol diacrylate and incorporated structures designed to closely resemble the limbal palisades of Vogt. The biggest improvement in the materials was the coating of the niche areas with fibronectin. Coating with fibronectin improved attachment of rabbit limbal epithelial cells and rabbit limbal fibroblasts⁴⁶⁹. Rabbit limbal epithelial cells grown on fibronectin coated scaffolds expressed CK3/12 and were able to migrate on to a denuded rabbit cornea, and to partially re-epithelialise the surface *ex vivo*⁴⁶⁹. Although these results are promising, further work is required to demonstrate the biocompatibility of the scaffolds *in vivo*. Furthermore, coating of the niche structures with multiple factors known to be expressed in the LESC niche, such as collagen IV^{79, 448, 451}, vitronectin^{449, 450, 559}, and tenascin-c^{543, 560} may improve the function of the niche, and allow it to harbour a population of self-renewing epithelial stem cells.

Bray *et al* have described a dual-layer silk fibroin scaffold for the recreation of the limbus¹⁸⁶. The scaffold consisted of mats supporting membranes prepared from silk fibroin. The authors explored co-culture of human limbal epithelial cells and limbal mesenchymal stromal cells on the dual layer scaffolds. Limbal epithelial cells were grown on the silk fibroin membrane while the limbal mesenchymal stromal cells were suspended within the fibres of the silk fibroin mat. The limbal epithelial cells expressed CK3/12 as well as Δ Np63, while the limbal mesenchymal stromal cells expressed CD90 and α -smooth muscle actin¹⁸⁶. This study explored the use of limbal stromal cells as part of the stem cell niche environment, and successful co-culture of limbal epithelial and stromal cells was achieved. However, the biocompatibility of the materials in the eye was not tested. Moreover, the migration of the cells off the

scaffold was not assessed. Silk fibroin scaffolds may prove to be suitable artificial limbal stem cell niches, however further *in vivo* characterization of the materials is required.

The importance of direct association of LESC's and stromal cells has been described by the Daniels group⁵⁶¹. The composition of an artificial stem cell niche may require the presence of accessory cells such as stromal cells and melanocytes to maintain the LESC's. These authors have described the engineering of three dimensional biomimetic limbal crypts, generated from collagen hydrogels using the Real Architecture For 3D Tissue (RAFT) technique⁵⁶². Human limbal epithelial cells formed stratified cell sheets 3-4 layers thick on the collagen constructs, and filled the crypts forming an epithelium that was 6-7 cells thick⁵⁶². Human limbal fibroblasts contained within the RAFT constructs were found in close proximity to the limbal epithelial cells within the artificial crypts. Human limbal epithelial cells at the base of the crypts had a high nuclear to cytoplasmic ratio and expressed the putative stem cell marker p63 α ⁵⁶². The expression of the proliferation marker Ki67 was also observed in the cells within crypts. Furthermore, the superficial epithelial cells expressed CK3 and Pax6, which are markers of corneal epithelial cells⁵⁶². This study attempted to recreate both the physical as well as the chemical characteristics of the limbal stem cell niche, in order to preserve the limbal epithelial cells in a more stem cell like phenotype. The association of the epithelial cells with stromal cell may be essential in maintaining their "stemness".

In the context of using porous silicon-polymer materials as an artificial stem cell niche, the incorporation of three-dimensional architecture to better mimic the physical characteristics stem cell niche may be required. The replication of the

chemical characteristics of the niche is of utmost importance. The maintenance of stem cells is not likely in the absence of factors that support these cells. Our study attempted the recreation of the stem cell niche with the use of collagen IV and vitronectin, with some success. However, the new evidence of the importance of associations between limbal epithelial cells and stromal cells may necessitate the incorporation of stromal cells and/or melanocytes into the construction of future constructs. A long-lived artificial material, which is non-immunogenic, can be fabricated with the physical and chemical properties of the limbal stem cell niche, and can support the growth of epithelial stem cells in close association with stromal cells may prove to be an adequate substitute for the limbus. A porous silicon polycaprolactone composite material with three dimensional architecture mimicking limbal crypts, and loaded with factors and or cells found in the niche environment could prove to be a suitable scaffold to house stem cells able to regenerate the corneal epithelium long-term.

5.2.4 Angiogenesis induced by treatments for ocular surface disease

Ocular surface disease results from the loss of or damage to adult corneal epithelial stem cells or their niche at the limbus, and is characterised by conjunctivization of the corneal epithelium, inflammation and neovascularization. Corneal neovascularization can also result from injury, infection or ocular inflammation^{66, 67}. The common thread in the pathogenesis of the two diseases is inflammation and the growth of blood vessels in otherwise avascular tissue.

Corneal neovascularization has been noted after treatment of OSD with cultivated epithelial cells. Nakamura *et al* transplanted autologous oral mucosal epithelial cells

carried on amniotic membranes in six eyes of four patients. Superficial peripheral neovascularization was observed in all eyes, just below the amniotic membrane¹¹³. Similarly, Inatomi *et al* reported superficial peripheral vascularization in all eyes (n=15), between the amniotic membrane and stroma, after transplantation of epithelial cells on amniotic membrane to the ocular surface¹¹⁶. Peripheral vascularization was apparent within the first post-operative month in most cases. New vessels progressed towards the central cornea between three to six months, but abated thereafter and did not interfere with visual function¹¹⁶. Ma *et al* also observed superficial neovascularization following transplantation of oral mucosal epithelial cells on amniotic membranes in 5 patients with limbal stem cell dysfunction resulting from severe chemical burns⁵⁶³. Stromal vascularization was noted by Nishida *et al* after transplantation of oral mucosal epithelial sheets for the treatment of ocular surface disease. The authors stressed that this vascularization was different from the sub-epithelial vascularization observed with conjunctivization, as it was deep in the stroma¹⁰⁷. In summary, corneal neovascularization may accompany OSD, but may also develop as a result of treatment of OSD.

In vitro studies have shown that decreased expression of the anti-angiogenic molecules thrombospondin-1 (TSP-1)⁵⁶⁴ and soluble fms-like tyrosine kinase-1 (sflt-1)⁵⁶⁵, and increased expression of the pro-angiogenic molecule fibroblast growth factor-2 (FGF-2)⁵⁶⁶ may be responsible for the observed neovascularization associated with cultured oral mucosal epithelial cells. Chen *et al* analysed 6 eyes from patients with limbal stem cell dysfunction and who had received cultivated oral mucosal epithelial cells for the expression of pro- and anti-angiogenic factors. FGF-2 and VEGF-A were expressed in specimens (collected during penetrating

keratoplasty) from all six patients⁵⁶⁷. VEGF-A expression was detected in the stromal cells and blood vessels. The expression of the anti-angiogenic factors TIMP-3, TSP-1 and sflt-1, which are expressed in normal corneal epithelium, was only detected in one of the six patient corneas⁵⁶⁷. These data indicated an imbalance in the levels of pro- and anti-angiogenic factors following epithelial cell transplantation for the treatment of OSD.

Neovascularization post-therapy has been associated with poorer outcomes. A study in eight patients with limbal stem cell deficiency who received cultivated autologous limbal epithelial cells on amniotic membranes, demonstrated a correlation between vascularization and success of therapy⁵⁶⁸. Five of eight patients with a stable ocular surface demonstrated a reduction in the neovascular area, vessel calibre and the invasion area post-therapy⁵⁶⁸. In the three failed cases, there was a worsening of at least one of the vascular parameters⁵⁶⁸. Inhibition of corneal neovascularization post-transplant might thus lead to improved success of the epithelial cell therapy in restoring the ocular surface. A recent case report investigated the use of bevacizumab in conjunction with a limbal stem cell transplant for the treatment of long-standing ocular surface disease⁵⁶⁹. A 59 year old patient with unilateral total LCSD resulting from a 21 year old chemical burn was treated with autologous limbal epithelial cells and two subconjunctival injections of bevacizumab (2.5 mg each injection), administered 2 and 3 months after limbal stem cell transplantation. Four months after transplantation, the ocular surface was stable, transparent, with no signs of limbal neovascularization, and an improvement in visual acuity was noted⁵⁶⁹. Thus, treatment of neovascularization related to ocular surface disease may be associated with improved outcomes for patients.

5.2.5 VEGF-B, angiogenesis and the eye

The majority of studies have shown that VEGF-B does not cause angiogenesis under normal circumstances^{249, 254-256}. In the eye, Reichelt *et al* demonstrated that mice lacking VEGF-B developed normal retinal vasculature²⁵⁰. However, under pathological conditions VEGF-B has been shown to promote capillary growth, survival and perfusion.

Silvestre *et al* assessed the effect of VEGF-B and VEGF-A administration in a surgical model of hind limb ischemia in the mouse²⁵². The angiographic score 28 days post-induction showed a marked improvement in the ischaemic/non-ischaemic leg ratio (1.4 fold in VEGF-B group and 1.5 fold in VEGF-A group)²⁵². Furthermore, perfusion was improved by 1.5 fold in both groups²⁵². Similar results were obtained in a rabbit femoral artery ligation model²⁵³. Treatment with VEGF-B, FGF-2, or VEGF-B+FGF2, increased collateral artery numbers by 53%, 47% and 59% respectively, compared to a 28% increase observed with rabbit serum albumin²⁵³. These data suggest that VEGF-B has a role in angiogenesis related to reperfusion of ischaemic tissue.

VEGF-B is highly expressed in the heart⁵⁷⁰. Li *et al* demonstrated that VEGF-B deficient mice had impaired vessel growth after left coronary artery occlusion²⁵⁴. Overexpression of VEGF-B in wild type mice led to improved revascularization of the infarct and the ischaemic border zone²⁵⁴. Cardiac-specific transgenic overexpression of VEGF-B in mice caused an increase in capillary size, but the number of vessels remained unchanged²⁴⁹. Mice overexpressing VEGF-B in their

hearts had less cardiomyocyte damage in response to ischemia^{249, 259}. These data suggest a protective role of VEGF-B in the heart under ischaemic conditions.

The effect of VEGF-B depletion and overexpression on the vasculature of the eye has also been assessed^{257, 258}. Zhong *et al* overexpressed VEGF-B in the retinae of mice, using transgenic VEGF-B delivered by adeno-associated virus²⁵⁸. Overexpression did not cause retinal neovascularization in normal mice. However, overexpression of VEGF-B in the retina prior to induction of neovascularization, in a laser induced model of choroidal neovascularization, led to an increased neovascular area when compared to controls²⁵⁸. Furthermore, increased retinal neovascularization was observed in mice over-expressing VEGF-B in an oxygen-induced retinopathy model²⁵⁸. These data demonstrate the role of VEGF-B in *pathological* neovascularization in the retina.

The role of VEGF-B in corneal neovascularization and in oxygen induced retinopathy was evaluated by Zhang *et al*²⁵⁷. Corneal vessel growth in response to VEGF-A or bFGF in the mouse corneal pocket assay was comparable in VEGF-B-deficient and wild type mice²⁵⁷. This indicated that in the presence of other angiogenic growth factors VEGF-B was not required for the growth of blood vessels into the normally avascular cornea. However, the authors demonstrated that VEGF-B was essential for the survival of blood vessels. Corneal neovascularization was induced in VEGF-B deficient and wild type mice with exogenous VEGF-A or bFGF. After induction of neovascularization, the exogenous growth factors were removed. Blood vessel survival was decreased in VEGF-B deficient mice²⁵⁷. Furthermore, intravitreal injection of a VEGF-B neutralizing antibody led to greater regression of vessels in an oxygen induced retinopathy model, while intravitreal injection of

VEGF-B inhibited regression²⁵⁷. Taken together, these data suggest that VEGF-B is a potent survival factor for pathological blood vessels in the cornea and the retina. Targeting of VEGF-B in these conditions might thus lead to regression of pathological vessels, an hypothesis that was further tested in the work described in this thesis.

5.2.6 Targeting VEGF-A and VEGF-B in corneal neovascularization

Blockade of VEGF-A signalling with bevacizumab has been shown to be effective at reducing the growth of newly-formed corneal vessels in a randomised clinical trial³⁴⁸. Ranibizumab, a Fab fragment generated from bevacizumab, has been shown to have a similar anti-neovascular effect to bevacizumab in animal⁵⁷¹⁻⁵⁷³ and human studies^{574, 575}. However, treatment of established vessels is still a challenge^{338, 345}.

My study demonstrated that blockade of VEGF-B with an anti-VEGF-B biologic caused regression of established vessels in a rat model of corneal neovascularization. A 37% reduction in corneal vessel area was observed in anti-VEGF-B scFv treated animals when compared to untreated or control scFv treated animals, which is comparable to the anti-neovascular effect observed with bevacizumab treatment of newly formed vessels in humans³⁴⁸. Further work is required to ascertain if anti-VEGF-A treatment with bevacizumab or ranibizumab will be synergistic or additive with anti-VEGF-B therapy.

An agent with activity against both VEGF-A and VEGF-B is currently on the market. Aflibercept is a recombinant fusion protein composed of the second immunoglobulin (Ig) binding domain of VEGF receptor 1 and the third Ig binding

domain of VEGF receptor 2, fused to the Fc region of human IgG1⁵⁷⁶. Aflibercept binds VEGF-A, VEGF-B and PlGF⁵⁷⁷, and is used for the treatment of wet ARMD and macular oedema.

Two randomised, double-masked, active-controlled, phase 3 trials comparing aflibercept to ranibizumab for the treatment of neovascular age related macular degeneration demonstrated that the increase in visual acuity with aflibercept was significantly higher than for ranibizumab at one year post-treatment⁵⁷⁸. However, by two years post-treatment there was no difference between aflibercept or ranibizumab treatment⁵⁷⁸. Due to its increased affinity for VEGF-A⁵⁷⁷, fewer aflibercept injections (11.2 injections) were required over 24 months of therapy compared to ranibizumab (16.5 injections), to achieve a similar anti-neovascular effect⁵⁷⁷.

A recent randomised clinical trial compared the effect of aflibercept, bevacizumab and ranibizumab in 660 patients with diabetic macular oedema. The improvement in the visual acuity letter score, as measured by electronic early treatment of diabetic retinopathy study visual acuity test, was higher in the aflibercept group (13.3) compared with the bevacizumab (9.7) and the ranibizumab (11.2) groups⁵⁷⁹. The authors pointed out that although this difference was statistically significant, it was clinically irrelevant as the difference was due in large part to eyes with worse visual acuity at baseline⁵⁷⁹.

Aflibercept has been assessed for its anti-neovascular activity in a mouse model of corneal neovascularization⁵⁸⁰. Neovascularization was induced by implanting a bFGF pellet into the cornea, and aflibercept was administered by intraperitoneal injection at 12.5 mg/kg. The extent of corneal neovascularization was assessed at 4 and 7 days

post-implant. The area of corneal neovascularization was $1.05 \pm 0.12 \text{ mm}^2$ and $1.53 \pm 0.27 \text{ mm}^2$ at days 4 and 7, respectively. Treatment with aflibercept significantly reduced the area of corneal neovascularization, $0.24 \pm 0.11 \text{ mm}^2$ and $0.35 \pm 0.16 \text{ mm}^2$ at days 4 and 7, respectively⁵⁸⁰. The effect of aflibercept on established vessels was not determined. To my knowledge, there are no reports of aflibercept being used to treat corneal neovascularization in humans.

In summary, aflibercept binds VEGF-A, VEGF-B and PlGF, however studies comparing its anti-neovascular effects to the anti-VEGF-A agents, bevacizumab and ranibizumab, have not found a statistically significant difference in neovascularization. The advantages of using aflibercept are that it can be administered less frequently than the anti-VEGF-A agents. However, it may be beneficial to be able to selectively target VEGF-A and VEGF-B, using different agents. This might be important to prevent off-target effects of the blockade of VEGF-B, which is a survival factor for endothelial cells, neurons and smooth muscle cells²⁸¹, in the context of treatment of well-established pathological vessels.

5.2.7 Is topical therapy for corneal neovascularization appropriate?

The preferred route of administration of ophthalmic drugs is topically, as eye drops. Whole antibodies do not penetrate the cornea on topical application, however, antibody fragments such as scFvs have been shown to penetrate the cornea when applied as eye drops^{443, 504}. A number of studies have looked at the effect of topical therapy with anti-VEGF agents in corneal neovascularization.

Topical bevacizumab has shown some anti-neovascular effect in rodent models of corneal neovascularization. Yoeruek *et al* compared the effect of bevacizumab (25 mg/ml) eye drops on developing as well as established vessels in a rabbit model of corneal neovascularization³²⁹. Bevacizumab eye drops were able to reduce the development of vessels in the early treatment group, while no apoptosis of developed vessels was observed³²⁹. Similar results were observed by Perez-Santonja *et al*⁵⁸¹. Bevacizumab eye drops (5 mg/ml) were administered thrice daily for 14 days, in rabbits with corneal neovascularization induced by placement of silk sutures in the cornea⁵⁸¹. A modest but statistically significant reduction in the corneal vessel area was observed in bevacizumab-treated animals (13%±5.8%) when compared to controls (18%±3.5%)⁵⁸¹. In a silver nitrate induced model in the rat, bevacizumab eye drops (4 mg/ml), administered twice daily for 7 days was able to significantly reduce corneal neovascularization when compared to controls (38%±15% compared to 63%±5% in controls)³²⁷. Habet-Wilner *et al* assessed three doses of bevacizumab eye drops (4 mg/ml, 2 mg/ml and 1 mg/ml) in a rat model of corneal neovascularization³²⁸. Doses above 2 mg/ml were found to have a significant effect on the growth of corneal vessels³²⁸. However, the study did not quantify the percentage of the cornea covered by vessels, but applied the qualitative measure of neovascularization score, as assessed by a masked observer.

Bevacizumab is known to bind to human and non-human primate VEGF-A^{319, 326, 430}. We have compared the binding of bevacizumab to human, mouse and rat VEGF-A by ELISA, and found that it binds to rat and mouse VEGF-A with 5 orders of magnitude less affinity than to human VEGF-A (Figure 5-1). Furthermore, we have shown that whole antibodies do not penetrate the cornea on topical application⁴⁴³. In

light of these data, it is somewhat surprising that topically-delivered bevacizumab has been reported to cause significant reduction in corneal neovascularization in rodent models.

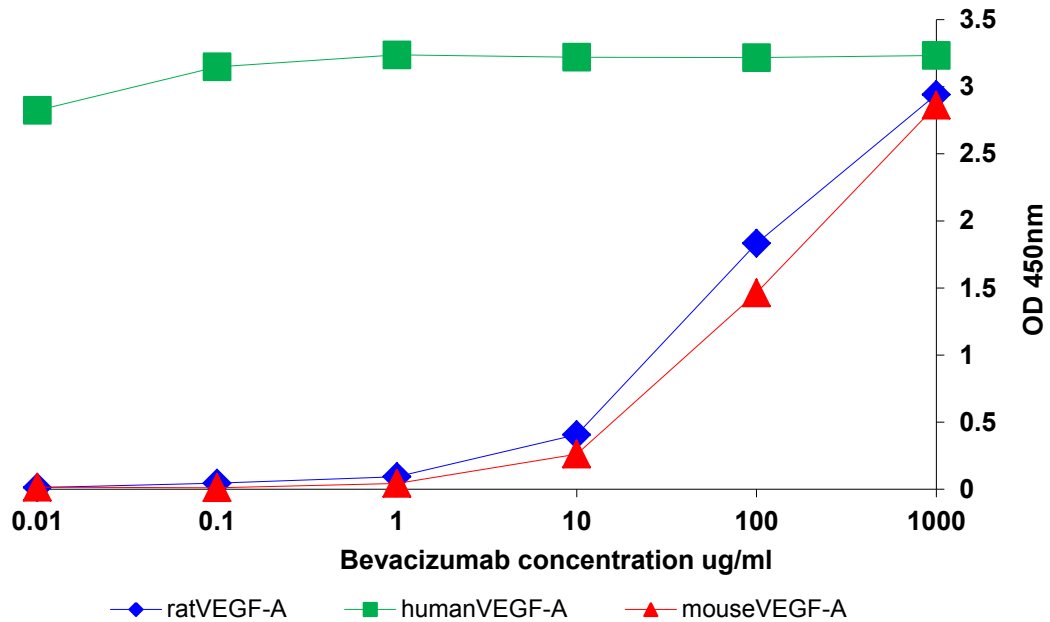


Figure 5-1 Binding of bevacizumab to human, mouse and rat VEGF-A

The binding of bevacizumab to human, mouse and rat VEGF-A was assayed by ELISA. Bevacizumab bound strongly to human VEGF-A above concentrations of 0.01 $\mu\text{g/ml}$. No binding to rat or mouse VEGF-A was observed below 10 $\mu\text{g/ml}$. Binding to rat and mouse VEGF-A at 1000 $\mu\text{g/ml}$ was comparable to binding to human VEGF-A at 0.01 $\mu\text{g/ml}$.

Bevacizumab and ranibizumab have been applied topically in humans and rodents for the treatment of corneal neovascularization. However, penetration through the

cornea on topical application is disputed. Moisseiev *et al* could not detect penetration of bevacizumab in to the anterior chamber or vitreous after topical application at 25 mg/ml in humans⁵⁸². However, Dastjerdi *et al* reported penetration of bevacizumab in the corneas of mice with induced corneal neovascularization³³⁰. The authors did not observe penetration through intact corneas³³⁰, and it is likely that penetration was observed in neovascularised corneas as a result of damage caused during the induction of angiogenesis (implantation of the bFGF pellet).

Bock *et al* described the effect of topical bevacizumab in 5 patients with corneal neovascularization, refractory to steroids³⁴⁰. Eye drops were applied at 5 mg/ml for 0.5-6 months (mean 3.6 months). All patients showed a decrease in corneal vessel area, however this was quite variable ($48\% \pm 28\%$)³⁴⁰. Partial regression of immature vessels was observed, with reduced perfusion of persisting vessels³⁴⁰. The Dana group has reported a prospective, open-label, non-comparative study in 10 patients with corneal neovascularization³⁴⁴. Bevacizumab eye drops (10 mg/ml) were applied two or four times a day for three weeks and follow-up was 24 weeks. A $47\% \pm 36\%$ reduction in neovascular area was observed, with a reduction of $54\% \pm 28\%$ in vessel calibre and a $12\% \pm 42\%$ reduction in invasion area³⁴⁴. The reduction in neovascular area appeared to be driven by the reduction the vessel calibre, as the area of vessel invasion did not reduce significantly.

Waisbourd *et al* tested high-dose (25 mg/ml) bevacizumab eye drops, four times daily for two weeks, in 17 patients with corneal neovascularization⁵⁸³. Partial regression of corneal vascularization was observed in 11 patients, with a modest improvement in visual acuity⁵⁸³. Ferrari *et al* assessed the effect of topical 1% ranibizumab, applied four times daily, on corneal neovascularization⁵⁷⁴. A

statistically significant difference in neovascular area and vessel calibre was observed (55% and 59% respectively), over the 16 weeks of the study, with no significant difference in invasion area⁵⁷⁴. As with previous results using bevacizumab³⁴⁴, the decrease in neovascular area appeared to be mediated by a decrease in the vessel calibre rather than regression of the vessel. Ranibizumab and bevacizumab appear to have similar anti-neovascular effects, however ranibizumab may reduce neovascular area slightly faster than bevacizumab⁵⁸⁴. The difference may be explained by the fact that ranibizumab, being a smaller molecule, displays better tissue penetration than bevacizumab. This modest improvement may not warrant the use of ranibizumab, which comes at a higher cost⁵⁸⁴.

In our study, a topically delivered anti-VEGF-B scFv had no effect on growing or established vessels in a rat model of corneal neovascularization. However, topical therapy supplemented with subconjunctival injection resulted in a statistically significant reduction in the corneal vessel area. These data suggest that the anti-VEGF-B scFv delivered topically as an eye drop did not reach a concentration that was able to cause regression of vessels. Eye drops were applied at two hour intervals five times a day over a fourteen day period. In a clinical setting increasing the frequency of eye drops is clearly impractical. Furthermore, biologic drugs are generally stored at 4°C. The requirement for refrigeration means that a drug cannot practically be applied more than once or twice daily. Hence, for a topically delivered anti-VEGF-B scFv to be an effective and practical anti-neovascular drug, it must be able to be applied once or at the very most twice daily.

A number of strategies might be employed to increase the effective dose of an anti-VEGF-B scFv in the cornea. Firstly, the concentration of the scFv in the eye drop

solution could be increased. The anti-VEGF-B scFv eye drop was formulated at 1 mg/ml in our study. Topically delivered bevacizumab has been applied at doses as high as 25 mg/ml for the treatment of corneal neovascularization⁵⁸³. The eye drop could also be formulated for overnight treatment as an ointment or a temperature responsive gel such as Pluronic F127, to increase the amount of time on the ocular surface, subsequently increasing penetration into the cornea. It is clear that significant improvements are required to be able to use the anti-VEGF-B scFv for topical therapy for corneal neovascularization. Subconjunctival injection might still be a more practical route of delivery, especially if only a few injections are required, compared to long-term use of daily eye drops.

5.2.8 Gender differences in ocular pathology

It is widely recognised that gender-based differences are observed in a number of ocular diseases⁵⁸⁵⁻⁵⁹¹. Our study demonstrated a significant difference in corneal neovascularization in response to chemical cautery in a rat model. Differences in the prevalence of corneal neovascularization in human males and females have not been reported. However, a gender bias has been noted in ocular diseases characterised by aberrant angiogenesis, such as diabetic retinopathy and age-related macular degeneration^{588, 589}.

Evidence from three large population studies, the Beaver Dam Eye Study, the Rotterdam study of the elderly, and the Blue Mountains Eye Study revealed that the prevalence of ARMD was significantly higher in women when compared with men (odds ratio 1.15)⁵⁹², adjusting for 10 year age categories. In the United States the prevalence of ARMD in Caucasian women above the age of 80 is estimated to be

16%, while it is 12% in males above 80 years or age⁵⁹³. A meta-analysis of studies describing the prevalence of ARMD in people with European ancestry suggested that neovascular ARMD is more prevalent in women than men (odds ratio 1.2)⁵⁹⁴. Conversely, a large population study from China and a meta-analysis of ARMD studies in Asian populations put males at increased risk of developing ARMD compared to women^{595, 596}. The mechanisms of the observed differences have not been elucidated. However, exposure to exogenous oestrogen has been associated with a reduced risk of developing ARMD^{597, 598}.

The data surrounding gender differences in diabetic retinopathy are mixed. Increased levels of oestrogen and progesterone during pregnancy have been associated with the progression of diabetic retinopathy^{599, 600}. However in men, high testosterone levels are associated with an increased risk of developing diabetic retinopathy^{601, 602}.

My study demonstrated that male rats developed significantly more vessels in response to corneal cautery than did female rats. It is possible that this difference is caused in part due to differences in expression of steroid hormones and their receptors. The data surrounding the effect of oestrogen, progesterone and testosterone on angiogenesis, are conflicting. However, it is possible that oestrogen has an anti-angiogenic effect and/or testosterone has a pro-angiogenic effect in the rat cornea. Further work is required to determine the mechanism behind these observed differences.

Although a number of studies with conflicting results have been published, it is certain that there are clear gender differences in the prevalence of ocular neovascular diseases. There is a gender bias in preclinical animal models towards the use of

males⁶⁰³. The results from our study demonstrate the need to include both male and female animals, in order to determine any gender differences. Recognising this issue, the National Institutes of Health in the United States of America now recommends the use of both male and female animals and cells in pre-clinical models⁶⁰⁴. The authors point out that the use of a single sex in animal models could be to blame for the results of a number of promising preclinical results not being translated to phase I/II clinical trials. Furthermore, women have been shown to experience higher rates of adverse drug reactions than males⁶⁰⁵.

5.3 Final comments

This study looked to develop novel therapies for two potentially blinding corneal conditions, ocular surface disease and corneal neovascularization. In animal models, the use of porous silicon materials for the transfer of cells and drugs to the eye was assessed, and the anti-neovascular effect of VEGF-B blockade directed at the cornea was investigated.

Oral mucosal epithelial cells were successfully cultured on porous silicon membranes. These cells contained a population of putative stem cells, a large number of transient amplifying cells and some mature epithelial cells. However, transplanted cells could not be detected on the central ocular surface upon implantation under the conjunctiva of rats. The porous silicon membranes were biocompatible, but degraded too rapidly to be used as an artificial stem cell niche. A longer-lived composite material of porous silicon and polycaprolactone was successfully loaded with biologic growth factors that had a functional effect on cells grown on the materials. This provided proof of concept that the materials could be loaded with factors that

might support the growth of stem cells, with the view to creating an artificial stem cell niche. The composite materials supported the growth of mammalian cells, but induced an undesirable inflammatory response on implantation under the rat conjunctiva. These composite materials could potentially be used in the engineering of an artificial stem cell niche, but need to be modified further to display improved biocompatibility.

An anti-VEGF-B scFv was generated from a hybridoma with activity against human, rat and mouse VEGF-B, and its binding to human VEGF-B confirmed. The scFv was formulated for topical delivery as an eye drop. Topically delivered anti-VEGF-B scFv did not prevent the growth of developing vessels nor cause regression of established vessels in a rat model of corneal neovascularization. However, topical scFv supplemented with subconjunctival injection led to regression of established corneal vessels. This anti-VEGF-B scFv might potentially be used for the treatment of human corneal neovascularization, on its own or in conjunction with an anti-VEGF-A agent, because it is human reactive.

Finally, this study reported a difference in the neovascular response to silver nitrate cautery between male and female rats. To my knowledge this is the first study to demonstrate gender differences in neovascularization of the cornea. These findings highlight the importance of including animals of both sexes in preclinical animal models.

A number of advances in the treatment of ocular surface disease have been made over the last 15-20 years. Chiefly, the use of *ex vivo* expanded epithelial cell sheets, rather than limbal tissue grafts has improved outcomes. However, at this stage

indefinite renewal of the corneal epithelium is not possible. Currently, *ex vivo* expanded epithelial cells are applied to the central cornea as a “bandage”. This is an efficient way to restore corneal epithelium, and in turn transparency. However, without a population of self-renewing stem cells these transplants will eventually fail. A number of groups are focusing on recreating an artificial stem cell niche. It is apparent that both the physical and chemical properties of the limbus must be mimicked to be able to house a population of self-renewing stem cells, which are able to regenerate the corneal epithelium. The properties of the ideal artificial limbus are outlined in Table 5-2. On demand “printing” of an artificial stem cell niche using microstereolithography techniques might be possible in the not too distant future.

Table 5-2 Properties of an ideal artificial limbus

1	3D architecture to mimic the limbal stem cell niche
2	Coated with factors found in the limbal stem cell niche
3	Able to support the growth of stem cells
4	Biocompatible in the eye
5	Implantable (at the limbus) – easy to handle
6	Similar Young's modulus (stiffness) to limbal tissue
7	Quick and inexpensive to produce
8	Sterilisable

There are a number of agents on the market for the treatment of corneal neovascularization. However, current treatment regimens have yielded sub-optimal results. The future direction in this field is to establish combinations of agents that

allow treatment of both newly-formed as well as established vessels. An anti-VEGF-B scFv could potentially be used in combination with an anti-VEGF-A agent, delivered by subconjunctival injection, with or without topical steroids, for the management of corneal neovascularization. However, these agents must have minimal side-effects to be a viable therapy, especially given that VEGF-B is a survival factor for a number of cell types. It is nevertheless conceivable that corneal neovascularization might soon be an eminently treatable condition.

APPENDIX A LIST OF GENERAL CHEMICALS

A.1 General chemicals

Table AA.1-1 List of general chemicals

Reagent	Description	Company
2-Propanol	For molecular biology $\geq 99\%$	Sigma, St Louis, MO USA
Absolute alcohol	Ethanol absolute	Merck, Kilsyth, VIC
Acetic acid	Glacial acetic acid	Ajax Finechem, Taren Point, NSW
Albumin, from bovine serum	$\geq 98\%$, catalogue #A7906	Sigma-Aldrich, St Louis, MO USA
Amphotericin B	Antifungal agent 250 $\mu\text{g/ml}$	Sigma-Aldrich, St Louis, MO USA
Bacto™ Agar	Solidifying agent	Becton, Dickson & Co., NJ, USA
Bacto™ Tryptone	Peptone for use in culture media	Becton, Dickson & Co., NJ, USA
Bacto™ Yeast Extract	Extract of autolysed yeast cells	Becton, Dickson & Co., NJ, USA
Betadine® Antiseptic Solution	10% w/v Povidone-Iodine	Betadine, Virginia, QLD
Calcium chloride dihydrate	Transfection reagent, DNA precipitation	VWR International, Leuven, Belgium
CellTiter 96® AQ_{ueous} One Solution	3-(4,5-dimethylthiazol-2-yl)-5-(3-carboxymethoxyphenyl)- 2-(4-sulfophenyl)-2H-tetrazolium	Promega, Madison, WI USA
Chloramphenicol	Antibiotic for microbial selection	Sigma, St Louis, MO USA

Reagent	Description	Company
D-Glucose (anhydrous)	dextrose anhydrous, catalogue #GA018	Ajax Finechem, Taren Point, NSW
Di-sodium hydrogen orthophosphate	Na ₂ HPO ₄ (anhydrous)	Chem-Supply, Gillman, SA
EDTA	Ethylenediaminetetraacetic acid tetrasodium salt hydrate	Sigma, St Louis, MO USA
E-Toxa-Clean[®]	Cleaning glassware for endotoxin-low preparations	Sigma, St Louis, MO USA
Foetal bovine serum (FBS)	Australian characterised Hyclone-Serum heat inactivated	Thermo Scientific, Scoresby, VIC
Formalin	Formaldehyde aqueous solution (10%)	Medvet Science Pty Ltd, SA
Glycerol	analytical reagent, catalogue #A242	Ajax Finechem, Taren Point, NSW
Heparin Sodium	DBL [®] 1000 IU/ml	Hospira Australia, Mulgrave, VIC
Hepes	≥ 99.5%	Sigma, St Louis, MO USA
Hoechst 33342	BisBenzimide, nuclear stain, blue dye	Sigma, St Louis, MO USA
Hydrochloric acid	36%, analytical reagent	Ajax Chemicals, Auburn, NSW
Isoflurane	Attane [™] Isoflurane 1 ml/ml	Bomac, Hornsby, NSW, Australia
L-Glutamine	ReagentPlus [™] ≥99%	Sigma, St Louis, MO USA
Non-essential Amino Acids	10 mM solution	Invitrogen, CA USA

Reagent	Description	Company
Papavarine HCl	30 mg/ml USP	Hameln pharmaceuticals, Gloucester, UK.
Paraffin	Paraplast tissue embedding medium	McCormick Scientific, St Louis, MO USA
Pluronic F127	Catalogue number P2443-250G	Sigma-Aldrich, St. Louis, MO, USA
Penicillin	Penicillin G (benzylpenicillin) potassium salt	Sigma, St Louis, MO USA
Potassium dihydrogen	KH ₂ PO ₄ , catalogue #PA009	Chem-Supply, Gillman, SA
Sodium azide	extra pure	Merck, Kilsyth, VIC
Sodium carbonate	Na ₂ CO ₃	Ajax Chemicals, Auburn, NSW
Sodium chloride	NaCl	Chem-Supply, Gillman, SA
Sodium chloride 0.9% for irrigation	0.9% w/v isotonic, nonpyrogenic, sterile	Baxter, Old Toongabbie, NSW
Sodium di-hydrogen orthophosphate	NaH ₂ PO ₄ .2H ₂ O	Chem-Supply, Gillman, SA
Sodium dodecyl sulphate	SDS, for molecular biology. Approx. 99%	Sigma, St Louis, MO USA
Sodium hydrogen carbonate (sodium	NaHCO ₃	Ajax Finechem, Taren Point, NSW
Sodium hydroxide	NaOH	VWR International, Leuven, Belgium
Streptavidin/HRP	Streptavidin conjugated to horseradish peroxidase. Binds to biotin or biotinylated	DakoCytomation, Glostrup, Denmark

Reagent	Description	Company
Streptomycin	Streptomycin sulphate 765 IU/mg	Sigma-Aldrich, St Louis, MO USA
Sucrose	catalogue #10274.4B	Merck, Kilsyth, VIC
Tris base	Trizma® Base, minimum 99.9% titration	Sigma-Aldrich, St Louis, MO USA
Trypan Blue	Used at 1% w/v in dH2O	Sigma, St Louis, MO USA
Trypsin	from porcine pancreas 1000-2000 BAEE units/mg	Sigma, St Louis, MO USA
Tween-20	Polyoxyethylenesorbitan monolaurate	Sigma, St Louis, MO USA
UltraPure water	Used in PCR	Fisher Biotec Australia, Wembley, WA
Water for injections BP	Sterile, used in endotoxin-low methods (animal work)	Phebra, Lane Cove, NSW
Water for irrigation	Sterile, nonpyrogenic, used in endotoxin-low methods	Baxter, Old Toongabbie, NSW
Xylene	catalogue #1023	BDH Chemicals Australia, Kilsyth, Vic

APPENDIX B BUFFERS AND SOLUTIONS

All chemicals used were of analytical grade unless otherwise mentioned. General chemicals were obtained from the following manufacturers: Ajax Finechem, NSW, Australia, BDH Chemicals, Radnor, PA, USA, Chem-Supply, Gillman, SA, Australia, and Sigma-Aldrich, St Louis, MO, USA.

B.1 2YT medium

16 g tryptone
10 g yeast extract
5 g sodium chloride

Dissolve in 900 ml ddH₂O. Adjust pH to 7.0 ± 0.2 and make up to 1 litre. Autoclave and store at room temperature.

B.2 2YT agar medium

Add 15 g/L bacto agar to 2YT medium before autoclaving.

B.3 6x gel loading dye

72 mg bromophenol Blue (0.25%)
72 mg xylene cyanol FF (0.25%)
4.5 g ficoll (0.25%)

Dissolve in 30 ml ddH₂O for 1-2 h on low heat until the solution turns green. Dispense into 1 ml aliquots and store at room temperature.

B.4 Buffered formalin

50 ml formalin (40% w/v)
2 g sodium di-hydrogen orthophosphate
3.25 g di-sodium hydrogen phosphate
Dissolve in 450 ml ddH₂O and store at room temperature.

B.5 Buffered glycerol

Solution A

0.5 M sodium bicarbonate (5.3 g/100 ml)

Solution B

0.5 M di-sodium hydrogen carbonate (8.4 g/ 200 ml)

Solution C

100% v/v glycerol

0.5 M sodium carbonate buffer pH 8.6

Place 50 ml solution B into a beaker and adjust the pH to 8.6 with solution A (~3 ml)
Add 2 parts glycerol to 1 part 0.5 M buffer solution

B.6 Chrome alum subbing solution for slides

5 g chrome alum
5 g gelatin

Gelatin was dissolved in 500 ml of distilled water, warmed to no more than 60°C. The chrome alum was added and the solution made up to 1 L with distilled water. Filtered through Whatman number 1 filter paper (Whatman, Maidstone, England). Glass microscope slides were washed overnight in Extran[®] soap solution (Merck, Darmstadt, Germany) then rinsed for 30 minutes in running deionised water. Slides were dried before being dipped for 2 – 4 minutes into warmed subbing solution in racks, drained on paper towel then dried overnight with loose covers to prevent dust adhering to surfaces.

B.7 Chloramphenicol for antibiotic selection

0.34 g chloramphenicol was made up to 10 ml with 100% Ethanol (AR grade) and filter sterilised for 34 mg/ml aliquots. Used at 34 µg/ml in selective media.

B.8 Complete medium for OMEC culture

The following components were added to 1 litre MCDB 153 medium (Sigma-Aldrich, St. Louis, MO, USA) to make complete OMEC culture medium:

10%	foetal bovine serum
100 iU/ml	penicillin G
100 ug/ml	streptomycin sulphate
2.5 mg/l	amphotericin B
10 ml	insulin transferrin sodium selenate supplement 100X
5 ng/ml	epidermal growth factor
10 ng/ml	β-nerve growth factor
200 ng/ml	hydrocortisone
50pM	tri-iodothyronine

B.9 ELISA blocking buffer

5% w/v	skim milk powder
5% w/v	sucrose

Add to PBS-azide pH 7.4 (B.21) and mix until dissolved. Make up fresh reagent for every experiment.

B.10 ELISA diluent

0.1% w/v skim milk powder

0.05% v/v Tween-20

Add to TBS pH 7.4 (B.26) and mix well. Make up fresh diluent for every experiment.

B.11 ELISA wash buffer

0.05% v/v Tween-20

Add to PBS pH 7.4 (B.20) and mix thoroughly. Store the solution at room temperature.

B.12 Eosin stock solution

1 g eosin Y

20 ml ddH₂O

80 ml 95% ethanol

Add 25 ml eosin stock to 75 ml ethanol (80%). Add 0.5 ml glacial acetic acid immediately prior to use.

B.13 Eye drop base solution

0.9% sodium chloride

0.5% capric acid (sodium salt)

1.5% hypromellose

10 mM HEPES (free acid)

Heat 15 ml of 0.9% NaCl to 80-90°C. Add 1.5 g of hypromellose, add 35 ml ice cold 0.9% NaCl and mix on ice bath. Add 0.5 g capric acid and mix at room temperature until solution is clear. Filter sterilise using 0.2 µm disposable filter and store at 4°C.

B.14 Haematoxylin stain

1.25 g	haematoxylin powder
75 ml	glycerol
0.25 g	sodium iodate
12.5 g	aluminium potassium sulphate
0.5 ml	glacial acetic acid
A few ml	absolute ethanol
175 ml	distilled water

The haematoxylin powder was dissolved in absolute ethanol. Aluminium potassium sulphate was added to 60 ml of distilled water, heated to dissolve and cooled. The remaining water was added to the aluminium potassium sulphate with the dissolved haematoxylin, sodium iodate, acetic acid and glycerol. The resulting solution was filtered and stored in the dark.

B.15 Haematoxylin perfusion buffer

Mix 1 part haematoxylin solution (B.14) with 3 parts PBS (B.20), add 0.32 ml / 100 ml papaverine HCL, heat to 37°C and filter through #1 Whatman paper.

B.16 IMAC elution buffer

100 mM	sodium di-hydrogen orthophosphate
10 mM	tris-chloride
250 mM	imidazole
pH 8.5	

Make up in 1 litre ddH₂O and store at room temperature.

B.17 IMAC loading buffer

100 mM sodium di-hydrogen orthophosphate

10 mM tris-chloride

10 mM imidazole

pH 8.5

Make up in 1 litre ddH₂O and store at room temperature.

B.18 IMAC wash buffer

100 mM sodium di-hydrogen orthophosphate

10 mM tris-chloride

20 or 30 mM imidazole

pH 8.5

Two separate IMAC wash buffers were prepared, the first with 20 mM imidazole and the second with 30 mM imidazole. The column with bound protein was first washed with wash buffer containing 20 mM imidazole followed by buffer with 30 mM imidazole.

B.19 Luria Bertani (LB) medium

10 g tryptone

5 g yeast extract

10 g sodium chloride

Dissolve in 900 ml ddH₂O. Adjust pH to 7.0 ± 0.2 and make up to 1 litre. Autoclave and store at room temperature. A low salt version of this medium with 5 g/l NaCl is used to prepare electrocompetent cells.

B.20 Phosphate Buffered Saline (PBS) 10X solution

43.5 g sodium chloride
4.25 g di-sodium hydrogen orthophosphate
2.7 g potassium di-hydrogen orthophosphate

Dissolve in 400 ml ddH₂O and adjust pH to 7.4, and make up to 500 ml with ddH₂O.
Autoclave and dilute 1/10 with ddH₂O before use.

B.21 PBS-azide

20 mM sodium azide in PBS

Add 5 ml 4M sodium azide to 995 ml 1x PBS and mix well and stored at room temperature.

B.22 PBS-tween 20

0.05% v/v tween20 in PBS

Add 500 µl tween20 to 1 litre 1x PBS (B.20), mix well and store at room temperature.

B.23 SOC medium

20 g tryptone
5 g yeast extract
0.5 g sodium chloride

Dissolve in 950 ml ddH₂O. Add 10 ml of 250 mM potassium chloride. Adjust pH to 7.0 and adjust volume to 1 litre. Autoclave and store at room temperature. Add 5 ml of sterile solution of 2 M MgCl₂ and 20 ml of sterile 1 M glucose solution.

B.24 Terrific broth (TB)

11.8 g/L tryptone
23.6 g/L yeast extract
9.4 g/L dipotassium hydrogen phosphate
2.2 g/L potassium dihydrogen phosphate
4 ml/L Glycerol (0.4%)

Make up to 1 litre with ddH₂O and autoclave. Store at room temperature.

B.25 TBE (5X stock)

54 g trizma base
27.5 g boric acid
4.65 g ethylene diamine tetra acetic acid

Dissolve in 400 ml ddH₂O and make up to 500 ml with ddH₂O. Dilute 1/10 before use.

B.26 TBS pH 7.4

0.2 M Tris solution was prepared by dissolving 24.23 g of Tris base in 1 L dH₂O. 50 ml of this solution was mixed with 16.5 ml of 0.1 M HCl and made up to 200 ml with dH₂O. This final solution was diluted to 10 mM before use.

B.27 TNT buffer

10 mM tris hydrochloric acid pH 8.0
150 mM sodium chloride
0.05% v/v tween-20

Make up in ddH₂O.

B.28 Trypsin-EDTA

0.5 g trypsin powder 1:250

0.2 g EDTA.4Na (0.05%)

100 ml 10x PBS (endotoxin-low)

Made up to 1 litre with water for irrigation and sterile filtered with a 0.22 µm filter.

APPENDIX C CHARACTERIZATION OF THE ANTI-VEGF-B SCFV AT CSL LTD.

C.1 Binding of the parent 2H10 antibody to human, mouse, and rat VEGF-B

The work described in appendix C.1, C.2 and C.3 was carried out at CSL Ltd. in the laboratories of Dr. Andrew Nash and Dr. Pierre Scotney. The binding of the parent antibody, from which the anti-VEGF-B scFv was generated, to human, mouse and rat VEGF-B was assessed by direct ELISA at CSL Ltd. Binding of the antibody to human, mouse and rat VEGF-B was similar (Figure C-1). These data confirm the feasibility of using the 2H10 antibody to generate a scFv for treatment of induced corneal neovascularization in a rat model. Furthermore, species cross-reactivity allows faster translation from pre-clinical to human trials.

C.2 Analysis of binding of the anti-VEGF-B scFv to human VEGF-B by surface plasmon resonance

The binding of the anti-VEGF-B scFv and the parent anti-VEGF-B antibody to human VEGF-B was assessed by surface plasmon resonance. Human VEGF-B was immobilised on the chip surface, 40 nM anti-VEGF-B mAb or scFv were applied for 10 minutes, and dissociation monitored for 30 minutes. Both anti-VEGF-B mAb and scFv displayed binding to human VEGF-B (Figure C-2). The binding of the two interactions appeared to be similar. However, the kinetics of the binding appeared to differ. Accurate kinetic rates and K_d were not determined. A qualitative observation was made that the anti-VEGF-B scFv retained the ability to bind human VEGF-B. Qualitative evaluation of the sensograms revealed that the scFv displayed a higher binding rate and a higher dissociation rate than the parental antibody. These data

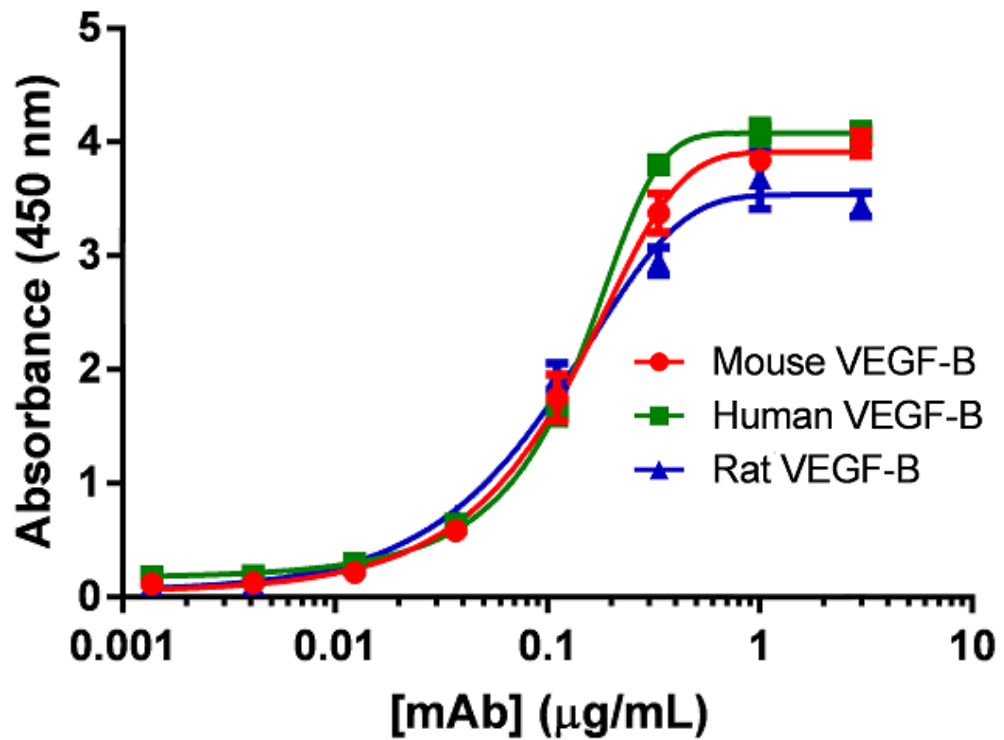


Figure C-1 Binding of the anti-VEGF-B antibody to human, mouse and rat VEGF-B

The binding of the anti-VEGF-B antibody to human, mouse and rat VEGF-B scFv was assayed by direct ELISA. The antibody had a similar binding profile to human, mouse and rat VEGF-B. This work was carried out in the laboratories of Dr. Andrew Nash and Dr. Pierre Scotney at CSL Ltd.

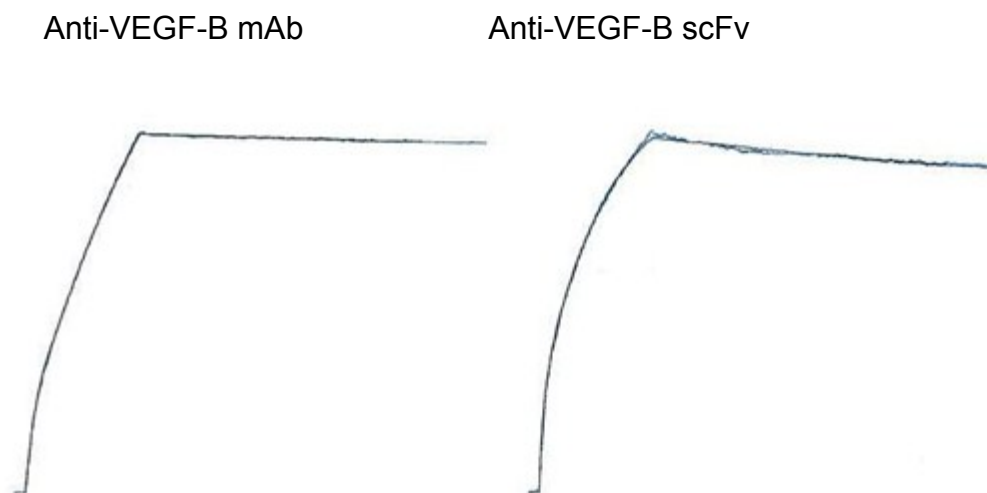


Figure C-2 Characterization of the binding of the anti-VEGF-B scFv to human VEGF-B

The binding of the anti-VEGF-B scFv and mAb to human VEGF-B was assessed by surface plasmon resonance at CSL Ltd. The anti-VEGF-B scFv retained binding to human VEGF-B. The dissociation constant (K_d) could not be determined. However, it was noted that the kinetics of binding and dissociation of the scFv and the whole antibody to VEGF-B differed. This work was carried out by Dr. Pierre Scotney at CSL Ltd. The horizontal axis is time and the vertical axis is relative binding.

confirm that the anti-VEGF-B scFv maintained the binding specificity of the parental antibody.

C.3 Functional characterization of the anti-VEGF-B scFv

The parental 2H10 antibody has been shown to neutralise the effects of VEGF-B⁴⁸⁵. A cell based assay was used to characterise the functional binding of the anti-VEGF-B scFv to human VEGF-B, and its ability to neutralise the effects of VEGF-B. This work was also carried out at CLS Ltd. The anti-VEGF-B scFv or mAb were incubated in cell culture medium containing VEGF-B for 1 hour. BaF3 cells expressing a chimeric receptor, consisting of the extracellular domain of VEGFR1, fused to the transmembrane and intracellular domains of the erythropoietin receptor, were added. The cells were allowed to grow for 72 hours and the proliferation measured by MTS assay. Both the anti-VEGF-B scFv and mAb inhibited VEGF-B induced proliferation of BaF3 cells (Figure C-3). The anti-VEGF-B scFv appeared to inhibit cell proliferation at a lower concentration than the anti-VEGF-B mAb. Complete inhibition of proliferation was observed at 1 µg/ml scFv.

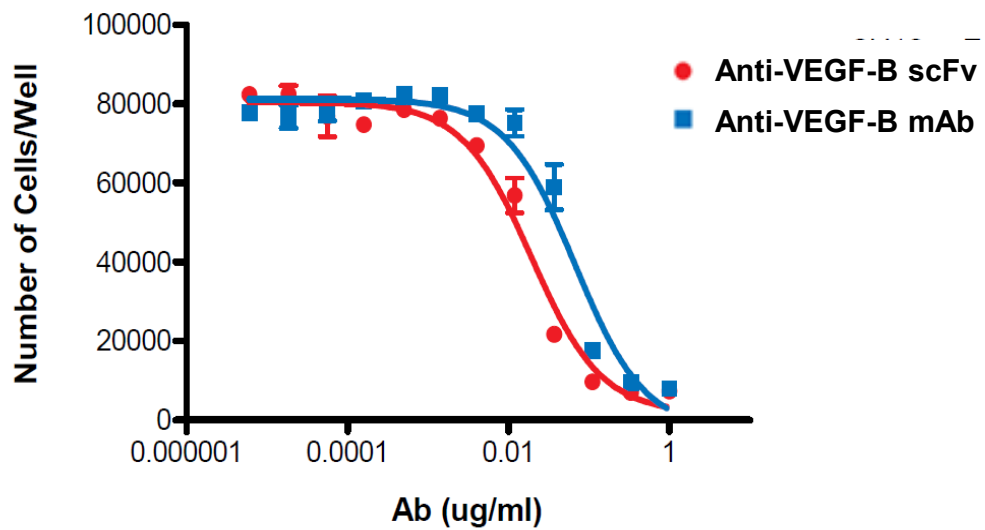


Figure C-3 The anti-VEGF-B scFv neutralises the effect of VEGF-B *in vitro*

The ability of the anti-VEGF-B mAb and scFv to neutralise the biological activity of VEGF-B was assessed in a cell based assay at CSL Ltd. The scFv or mAb were incubated in medium containing VEGF-B before addition of BaF3 cells that expressed a chimeric receptor consisting of the extracellular domain of VEGFR1 and the transmembrane and intracellular domains of the erythropoietin receptor. These cells proliferate in response to VEGF-B. The cells were allowed to grow for 72 hours and the proliferation measured by MTS assay. Both the anti-VEGF-B mAb and scFv inhibited VEGF-B induced proliferation in BaF3 cells. This work was carried out by Dr. Pierre Scotney at CSL Ltd.

APPENDIX D ANIMAL MONITORING SHEETS

D.1 Corneal cautery scoring sheet

Corneal AgNO₃ cautery

Scoring key:

Quadrant: Ns= nasal superior; Ni= nasal inferior; Ts= temporal superior; Ti= temporal inferior

Length%: score % distance between limbus (defined by inner-most limbal vessel arcade) and burn edge that leading vessel has spanned for each quadrant.

Base degrees: score width of the base of new vessels at the limbus. Measured in degrees, where the maximum possible is 90 degrees for each quadrant.

Density %: % of total area of the quadrant occupied by vessels.

Oedema: corneal oedema: 0 = none
1 = some iris detail apparent
2 = little iris detail apparent
3 = no iris detail apparent
4 = complete opacity

Blister: 0 = none
1 = slightly raised above corneal surface; just detectable
2 = moderately raised corneal surface; readily detectable
3 = raised well above corneal surface; concern RE perforation
See diagram on old scoring sheet

Hypopyon: % AC occupied by hypopyon. 0 = none

Hyphaema: % AC occupied by hyphaema. 0 = none

Iris: Degree of injection/ vascular engorgement
0 = none
1 = mild
2 = moderate, intervascular spaces still readily apparent
3 = marked, intervascular spaces difficult to appreciate
NB will be influenced by corneal oedema – impossible to assess where oedema >3

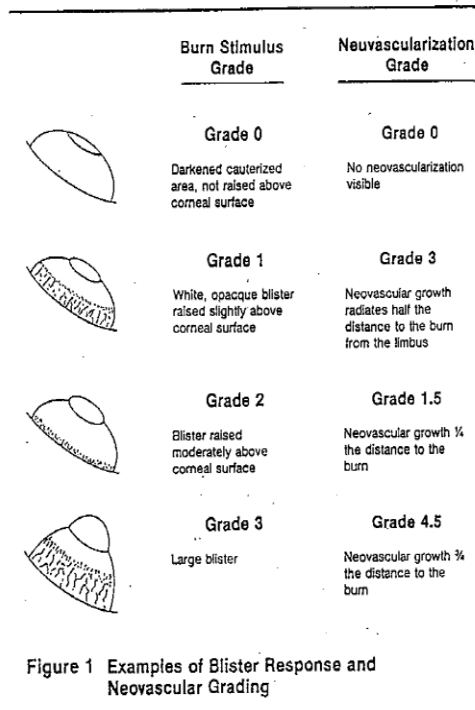
* syn: record in the case of anterior synechia

Blister response scale:

0	No blister: dark cauterised area, not raised above corneal surface
1+	Small blister: raised slightly above corneal surface
2+	Medium blister: raised moderately above corneal surface
3+	Large blister

Neovascularisation grade:

0	No visible corneal vessels
1+	1/4 distance to burn
2+	1/3 distance to burn
3+	1/2 distance to burn
4+	2/3 distance to burn
5+	3/4 distance to burn
6+	vessels reach burn



Corneal AgNO₃ cautery

animal #: _____ TBs: _____ strain: _____ sex: _____ AGE: _____

wt (day 0): _____ eye: _____ burn duration: _____

comment: _____

date	day	quad	length%	base° x/90°	density area %	oedema 0-4	blister 0-3	hypo %	hyph %	iris 0-3 syn
		Ns								
		Ni								
		Ts								
		Ti								
total										
		Ns								
		Ni								
		Ts								
		Ti								
total										
		Ns								
		Ni								
		Ts								
		Ti								
total										
		Ns								
		Ni								
		Ts								
		Ti								
total										
		Ns								
		Ni								
		Ts								
		Ti								
total										
		Ns								
		Ni								
		Ts								
		Ti								
total										
		Ns								
		Ni								
		Ts								
		Ti								
total										
		Ns								
		Ni								
		Ts								
		Ti								
total										
		Ns								
		Ni								
		Ts								
		Ti								
total										

D.3 Rat conjunctival space implant scoring sheet

Experiment:

Animal Number:

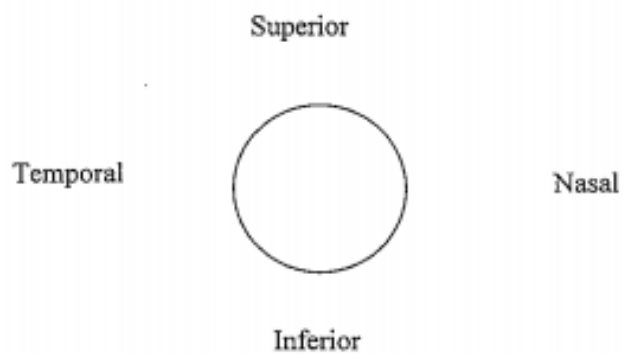
Date of experiment:

Marking:

Recipient Strain:
 Sex:
 Weight:

Operator:

Implant treatment:



Chloromycetin: Yes/No

Suture lid shut: Yes/No

Post-operative treatment:

D.5 n-Heptanol corneal debridement procedure sheet

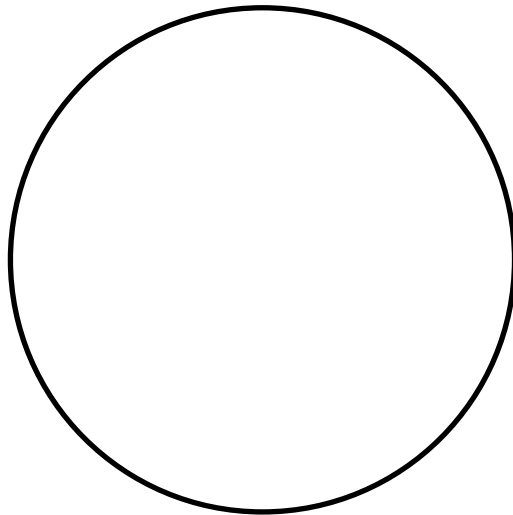
Animal#: Marking: Sex: Strain: Eye:

Date:

Operator:

Topicamide:

Procedure:



Notes:

Disclaimer:
Superficial debridement of the corneal epithelium performed using n-heptanol
A separate sheet will be used for each animal

BIBLIOGRAPHY

1. Tsubota K, Tseng SG, Nordlund M. Anatomy and physiology of the ocular surface. *Ocular Surface Disease Medical and Surgical Management*: Springer New York; 2002:3-15.
2. Bron AJ. *Wolff's anatomy of the eye and orbit*. 8th ed.. ed. London: London : Chapman & Hall Medical; 1997.
3. Remington LA, Remington LA. *Clinical Anatomy and Physiology of the Visual System*. St. Louis, Miss.: St. Louis, Miss. : Elsevier/Butterworth-Heinemann; 2012.
4. Reinstein DZ, Silverman RH, Rondeau MJ, Coleman DJ. Epithelial and corneal thickness measurements by high-frequency ultrasound digital signal processing. *Ophthalmology* 1994;101:140-146.
5. Mathers WD, Lemp MA. Morphology and movement of corneal surface cells in humans. *Curr Eye Res* 1992;11:517-523.
6. Kubawara T. Current concepts in anatomy and histology of the cornea. *Contact Lens Intraoc Lens J* 1978;4:101.
7. Guthoff RF, Zhivov A, Stachs O. In vivo confocal microscopy, an inner vision of the cornea - a major review. *Clin Experiment Ophthalmol* 2009;37:100-117.
8. Wulle KG. Electron microscopy of the fetal development of the corneal endothelium and Descemet's membrane of the human eye. *Invest Ophthalmol* 1972;11:897-904.
9. Joyce NC. Proliferative capacity of the corneal endothelium. *Prog Retin Eye Res* 2003;22:359-389.
10. Kessing SV. Mucous gland system of the conjunctiva. A quantitative normal anatomical study. *Acta Ophthalmol (Copenh)* 1968;Suppl 95:91+.
11. McClellan KA. Mucosal defense of the outer eye. *Surv Ophthalmol* 1997;42:233-246.
12. Gillette TE, Chandler JW, Greiner JV. Langerhans cells of the ocular surface. *Ophthalmology* 1982;89:700-711.
13. Vantrappen L, Geboes K, Missotten L, Maudgal PC, Desmet V. Lymphocytes and Langerhans cells in the normal human cornea. *Invest Ophthalmol Vis Sci* 1985;26:220-225.
14. Gipson IK. The epithelial basement membrane zone of the limbus. *Eye (Lond)* 1989;3 (Pt 2):132-140.
15. Tseng SC. Concept and application of limbal stem cells. *Eye (Lond)* 1989;3 (Pt 2):141-157.
16. Baylis O, Figueiredo F, Henein C, Lako M, Ahmad S. 13 years of cultured limbal epithelial cell therapy: a review of the outcomes. *J Cell Biochem* 2011;112:993-1002.
17. Cotsarelis G, Cheng SZ, Dong G, Sun TT, Lavker RM. Existence of slow-cycling limbal epithelial basal cells that can be preferentially stimulated to proliferate: implications on epithelial stem cells. *Cell* 1989;57:201-209.
18. Schermer A, Galvin S, Sun TT. Differentiation-related expression of a major 64K corneal keratin in vivo and in culture suggests limbal location of corneal epithelial stem cells. *J Cell Biol* 1986;103:49-62.
19. Pellegrini G, Dellambra E, Golisano O, et al. p63 identifies keratinocyte stem cells. *Proc Natl Acad Sci U S A* 2001;98:3156-3161.

20. Goldberg MF, Bron AJ. Limbal palisades of Vogt. *Trans Am Ophthalmol Soc* 1982;80:155-171.
21. Dua HS, Shanmuganathan VA, Powell-Richards AO, Tighe PJ, Joseph A. Limbal epithelial crypts: a novel anatomical structure and a putative limbal stem cell niche. *Br J Ophthalmol* 2005;89:529-532.
22. Schlotzer-Schrehardt U, Kruse FE. Identification and characterization of limbal stem cells. *Exp Eye Res* 2005;81:247-264.
23. Boulton M, Albon J. Stem cells in the eye. *Int J Biochem Cell Biol* 2004;36:643-657.
24. Sharma A, Coles WH. Kinetics of corneal epithelial maintenance and graft loss. A population balance model. *Invest Ophthalmol Vis Sci* 1989;30:1962-1971.
25. Hanna C, Bicknell DS, O'Brien JE. Cell turnover in the adult human eye. *Arch Ophthalmol* 1961;65:695-698.
26. Huang AJ, Tseng SC. Corneal epithelial wound healing in the absence of limbal epithelium. *Invest Ophthalmol Vis Sci* 1991;32:96-105.
27. Majo F, Rochat A, Nicolas M, Jaoude GA, Barrandon Y. Oligopotent stem cells are distributed throughout the mammalian ocular surface. *Nature* 2008;456:250-254.
28. Davanger M, Evensen A. Role of the pericorneal papillary structure in renewal of corneal epithelium. *Nature* 1971;229:560-561.
29. Bron AJ. Vortex patterns of the corneal epithelium. *Trans Ophthalmol Soc U K* 1973;93:455-472.
30. Pellegrini G, Golisano O, Paterna P, et al. Location and clonal analysis of stem cells and their differentiated progeny in the human ocular surface. *J Cell Biol* 1999;145:769-782.
31. Sun TT, Tseng SC, Lavker RM. Location of corneal epithelial stem cells. *Nature* 2010;463:E10-11; discussion E11.
32. Echevarria TJ, Di Girolamo N. Tissue-regenerating, vision-restoring corneal epithelial stem cells. *Stem Cell Rev* 2011;7:256-268.
33. Casaroli-Marano RP, Nieto-Nicolau N, Martinez-Conesa EM. Progenitor Cells for Ocular Surface Regenerative Therapy. *Ophthalmic Res* 2012;49:115-121.
34. Notara M, Shortt AJ, O'Callaghan AR, Daniels JT. The impact of age on the physical and cellular properties of the human limbal stem cell niche. *Age (Dordr)* 2012.
35. Hsueh YJ, Kuo PC, Chen JK. Transcriptional regulators of the DeltaNp63: Their role in limbal epithelial cell proliferation. *J Cell Physiol* 2013;228:536-546.
36. Yoon JJ, Ismail S, Sherwin T. Limbal stem cells: Central concepts of corneal epithelial homeostasis. *World J Stem Cells* 2014;6:391-403.
37. Thoft RA, Friend J. The X, Y, Z hypothesis of corneal epithelial maintenance. *Invest Ophthalmol Vis Sci* 1983;24:1442-1443.
38. Lauweryns B, van den Oord JJ, Missotten L. The transitional zone between limbus and peripheral cornea. An immunohistochemical study. *Invest Ophthalmol Vis Sci* 1993;34:1991-1999.
39. Lauweryns B, van den Oord JJ, Volpes R, Foets B, Missotten L. Distribution of very late activation integrins in the human cornea. An immunohistochemical study using monoclonal antibodies. *Invest Ophthalmol Vis Sci* 1991;32:2079-2085.
40. Buck RC. Measurement of centripetal migration of normal corneal epithelial cells in the mouse. *Invest Ophthalmol Vis Sci* 1985;26:1296-1299.

41. Di Girolamo N, Bobba S, Raviraj V, et al. Tracing the fate of limbal epithelial progenitor cells in the murine cornea. *Stem Cells* 2015;33:157-169.
42. Koester CJ, Auran JD, Rosskothan HD, Florakis GJ, Tackaberry RB. Clinical microscopy of the cornea utilizing optical sectioning and a high-numerical-aperture objective. *J Opt Soc Am A* 1993;10:1670-1679.
43. Hanna C, O'Brien JE. Cell production and migration in the epithelial layer of the cornea. *Arch Ophthalmol* 1960;64:536-539.
44. Wagoner MD. Chemical injuries of the eye: current concepts in pathophysiology and therapy. *Surv Ophthalmol* 1997;41:275-313.
45. German MJ, Pollock HM, Zhao B, et al. Characterization of putative stem cell populations in the cornea using synchrotron infrared microspectroscopy. *Invest Ophthalmol Vis Sci* 2006;47:2417-2421.
46. Arpitha P, Prajna NV, Srinivasan M, Muthukkaruppan V. A subset of human limbal epithelial cells with greater nucleus-to-cytoplasm ratio expressing high levels of p63 possesses slow-cycling property. *Cornea* 2008;27:1164-1170.
47. Figueira EC, Di Girolamo N, Coroneo MT, Wakefield D. The phenotype of limbal epithelial stem cells. *Invest Ophthalmol Vis Sci* 2007;48:144-156.
48. Lindberg K, Brown ME, Chaves HV, Kenyon KR, Rheinwald JG. In vitro propagation of human ocular surface epithelial cells for transplantation. *Invest Ophthalmol Vis Sci* 1993;34:2672-2679.
49. Ebato B, Friend J, Thoft RA. Comparison of limbal and peripheral human corneal epithelium in tissue culture. *Invest Ophthalmol Vis Sci* 1988;29:1533-1537.
50. Wei ZG, Sun TT, Lavker RM. Rabbit conjunctival and corneal epithelial cells belong to two separate lineages. *Invest Ophthalmol Vis Sci* 1996;37:523-533.
51. Kubota M, Shimmura S, Miyashita H, Kawashima M, Kawakita T, Tsubota K. The anti-oxidative role of ABCG2 in corneal epithelial cells. *Invest Ophthalmol Vis Sci* 2010;51:5617-5622.
52. Zhou S, Schuetz JD, Bunting KD, et al. The ABC transporter Bcrp1/ABCG2 is expressed in a wide variety of stem cells and is a molecular determinant of the side-population phenotype. *Nat Med* 2001;7:1028-1034.
53. Kim M, Turnquist H, Jackson J, et al. The multidrug resistance transporter ABCG2 (breast cancer resistance protein 1) effluxes Hoechst 33342 and is overexpressed in hematopoietic stem cells. *Clin Cancer Res* 2002;8:22-28.
54. Goodell MA, Brose K, Paradis G, Conner AS, Mulligan RC. Isolation and functional properties of murine hematopoietic stem cells that are replicating in vivo. *J Exp Med* 1996;183:1797-1806.
55. Murayama A, Matsuzaki Y, Kawaguchi A, Shimazaki T, Okano H. Flow cytometric analysis of neural stem cells in the developing and adult mouse brain. *J Neurosci Res* 2002;69:837-847.
56. Summer R, Kotton DN, Sun X, Ma B, Fitzsimmons K, Fine A. Side population cells and Bcrp1 expression in lung. *Am J Physiol Lung Cell Mol Physiol* 2003;285:L97-104.
57. Watanabe K, Nishida K, Yamato M, et al. Human limbal epithelium contains side population cells expressing the ATP-binding cassette transporter ABCG2. *FEBS Lett* 2004;565:6-10.
58. Wolosin JM, Budak MT, Akinci MA. Ocular surface epithelial and stem cell development. *Int J Dev Biol* 2004;48:981-991.

59. de Paiva CS, Chen Z, Corrales RM, Pflugfelder SC, Li DQ. ABCG2 transporter identifies a population of clonogenic human limbal epithelial cells. *Stem Cells* 2005;23:63-73.
60. Yang A, Schweitzer R, Sun D, et al. p63 is essential for regenerative proliferation in limb, craniofacial and epithelial development. *Nature* 1999;398:714-718.
61. Mills AA, Zheng B, Wang XJ, Vogel H, Roop DR, Bradley A. p63 is a p53 homologue required for limb and epidermal morphogenesis. *Nature* 1999;398:708-713.
62. Celli J, Duijf P, Hamel BC, et al. Heterozygous germline mutations in the p53 homolog p63 are the cause of EEC syndrome. *Cell* 1999;99:143-153.
63. Yang A, Kaghad M, Wang Y, et al. p63, a p53 homolog at 3q27-29, encodes multiple products with transactivating, death-inducing, and dominant-negative activities. *Mol Cell* 1998;2:305-316.
64. Di Iorio E, Barbaro V, Ruzza A, Ponzin D, Pellegrini G, De Luca M. Isoforms of DeltaNp63 and the migration of ocular limbal cells in human corneal regeneration. *Proc Natl Acad Sci U S A* 2005;102:9523-9528.
65. Rodrigues M, Ben-Zvi A, Krachmer J, Schermer A, Sun TT. Suprabasal expression of a 64-kilodalton keratin (no. 3) in developing human corneal epithelium. *Differentiation* 1987;34:60-67.
66. Kasper M, Moll R, Stosiek P, Karsten U. Patterns of cytokeratin and vimentin expression in the human eye. *Histochemistry* 1988;89:369-377.
67. Wiley L, SundarRaj N, Sun TT, Thoft RA. Regional heterogeneity in human corneal and limbal epithelia: an immunohistochemical evaluation. *Invest Ophthalmol Vis Sci* 1991;32:594-602.
68. Chen Z, de Paiva CS, Luo L, Kretzer FL, Pflugfelder SC, Li DQ. Characterization of putative stem cell phenotype in human limbal epithelia. *Stem Cells* 2004;22:355-366.
69. Bickenbach JR, Grinnell KL. Epidermal stem cells: interactions in developmental environments. *Differentiation* 2004;72:371-380.
70. Kurpakus MA, Maniaci MT, Esco M. Expression of keratins K12, K4 and K14 during development of ocular surface epithelium. *Curr Eye Res* 1994;13:805-814.
71. Barnard Z, Apel AJ, Harkin DG. Phenotypic analyses of limbal epithelial cell cultures derived from donor corneoscleral rims. *Clin Experiment Ophthalmol* 2001;29:138-142.
72. Michel M, Torok N, Godbout MJ, et al. Keratin 19 as a biochemical marker of skin stem cells in vivo and in vitro: keratin 19 expressing cells are differentially localized in function of anatomic sites, and their number varies with donor age and culture stage. *J Cell Sci* 1996;109 (Pt 5):1017-1028.
73. Kasper M. Patterns of cytokeratins and vimentin in guinea pig and mouse eye tissue: evidence for regional variations in intermediate filament expression in limbal epithelium. *Acta Histochem* 1992;93:319-332.
74. Schofield R. The relationship between the spleen colony-forming cell and the haemopoietic stem cell. *Blood Cells* 1978;4:7-25.
75. Fuchs E, Tumber T, Guasch G. Socializing with the neighbors: stem cells and their niche. *Cell* 2004;116:769-778.
76. Higa K, Shimmura S, Miyashita H, Shimazaki J, Tsubota K. Melanocytes in the corneal limbus interact with K19-positive basal epithelial cells. *Exp Eye Res* 2005;81:218-223.

77. Schlotzer-Schrehardt U, Dietrich T, Saito K, et al. Characterization of extracellular matrix components in the limbal epithelial stem cell compartment. *Exp Eye Res* 2007;85:845-860.
78. Tuori A, Uusitalo H, Burgeson RE, Terttunen J, Virtanen I. The immunohistochemical composition of the human corneal basement membrane. *Cornea* 1996;15:286-294.
79. Cleutjens JP, Havenith MG, Kasper M, Vallinga M, Bosman FT. Absence of type IV collagen in the centre of the corneal epithelial basement membrane. *Histochem J* 1990;22:688-694.
80. Ljubimov AV, Burgeson RE, Butkowski RJ, Michael AF, Sun TT, Kenney MC. Human corneal basement membrane heterogeneity: topographical differences in the expression of type IV collagen and laminin isoforms. *Lab Invest* 1995;72:461-473.
81. Kolega J, Manabe M, Sun TT. Basement membrane heterogeneity and variation in corneal epithelial differentiation. *Differentiation* 1989;42:54-63.
82. Nishida K, Kinoshita S, Ohashi Y, Kuwayama Y, Yamamoto S. Ocular surface abnormalities in aniridia. *Am J Ophthalmol* 1995;120:368-375.
83. Ahonen P, Myllarniemi S, Sipila I, Perheentupa J. Clinical variation of autoimmune polyendocrinopathy-candidiasis-ectodermal dystrophy (APECED) in a series of 68 patients. *N Engl J Med* 1990;322:1829-1836.
84. Dunaief JL, Ng EW, Goldberg MF. Corneal dystrophies of epithelial genesis: the possible therapeutic use of limbal stem cell transplantation. *Arch Ophthalmol* 2001;119:120-122.
85. Puangsricharern V, Tseng SC. Cytologic evidence of corneal diseases with limbal stem cell deficiency. *Ophthalmology* 1995;102:1476-1485.
86. Jenkins C, Tuft S, Liu C, Buckley R. Limbal transplantation in the management of chronic contact-lens-associated epitheliopathy. *Eye (Lond)* 1993;7 (Pt 5):629-633.
87. Wilson FM, 2nd. Adverse external ocular effects of topical ophthalmic therapy: an epidemiologic, laboratory, and clinical study. *Trans Am Ophthalmol Soc* 1983;81:854-965.
88. Lee GA, Hirst LW. Ocular surface squamous neoplasia. *Surv Ophthalmol* 1995;39:429-450.
89. Foster CS, Calonge M. Atopic keratoconjunctivitis. *Ophthalmology* 1990;97:992-1000.
90. Dushku N, Reid TW. Immunohistochemical evidence that human pterygia originate from an invasion of vimentin-expressing altered limbal epithelial basal cells. *Curr Eye Res* 1994;13:473-481.
91. Chen JJ, Tseng SC. Corneal epithelial wound healing in partial limbal deficiency. *Invest Ophthalmol Vis Sci* 1990;31:1301-1314.
92. Kenyon KR, Tseng SC. Limbal autograft transplantation for ocular surface disorders. *Ophthalmology* 1989;96:709-722; discussion 722-703.
93. Tsai RJ, Tseng SC. Human allograft limbal transplantation for corneal surface reconstruction. *Cornea* 1994;13:389-400.
94. Tsubota K, Satake Y, Kaido M, et al. Treatment of severe ocular-surface disorders with corneal epithelial stem-cell transplantation. *N Engl J Med* 1999;340:1697-1703.
95. Tsubota K, Toda I, Saito H, Shinozaki N, Shimazaki J. Reconstruction of the corneal epithelium by limbal allograft transplantation for severe ocular surface disorders. *Ophthalmology* 1995;102:1486-1496.

96. Tan DT, Ficker LA, Buckley RJ. Limbal transplantation. *Ophthalmology* 1996;103:29-36.
97. Mills RA, Coster DJ, Williams KA. Effect of immunosuppression on outcome measures in a model of rat limbal transplantation. *Invest Ophthalmol Vis Sci* 2002;43:647-655.
98. Ozdemir O, Tekeli O, Ornek K, Arslanpence A, Yalcindag NF. Limbal autograft and allograft transplantations in patients with corneal burns. *Eye (Lond)* 2004;18:241-248.
99. Williams KA, Lowe MT, Keane MC. The Australian Corneal Graft Registry 2012 Report. 2012.
- 100 Schwab IR. Cultured corneal epithelia for ocular surface disease. *Trans Am Ophthalmol Soc* 1999;97:891-986.
- 101 Schwab IR, Reyes M, Isseroff RR. Successful transplantation of bioengineered tissue replacements in patients with ocular surface disease. *Cornea* 2000;19:421-426.
- 102 Koizumi N, Inatomi T, Suzuki T, Sotozono C, Kinoshita S. Cultivated corneal epithelial stem cell transplantation in ocular surface disorders. *Ophthalmology* 2001;108:1569-1574.
103. Koizumi N, Inatomi T, Suzuki T, Sotozono C, Kinoshita S. Cultivated corneal epithelial transplantation for ocular surface reconstruction in acute phase of Stevens-Johnson syndrome. *Arch Ophthalmol* 2001;119:298-300.
104. Nakamura T, Inatomi T, Sotozono C, et al. Transplantation of autologous serum-derived cultivated corneal epithelial equivalents for the treatment of severe ocular surface disease. *Ophthalmology* 2006;113:1765-1772.
105. Satake Y, Dogru M, Yamaguchi T, Tomida D, Hirayama M, Shimazaki J. Immunological rejection following allogeneic cultivated limbal epithelial transplantation. *JAMA Ophthalmology* 2013;131:920-922.
106. Satake Y, Dogru M, Yamane GY, Kinoshita S, Tsubota K, Shimazaki J. Barrier function and cytologic features of the ocular surface epithelium after autologous cultivated oral mucosal epithelial transplantation. *Arch Ophthalmol* 2008;126:23-28.
107. Nishida K, Yamato M, Hayashida Y, et al. Corneal reconstruction with tissue-engineered cell sheets composed of autologous oral mucosal epithelium. *N Engl J Med* 2004;351:1187-1196.
108. Zhang QZ, Nguyen AL, Yu WH, Le AD. Human oral mucosa and gingiva: a unique reservoir for mesenchymal stem cells. *J Dent Res* 2012;91:1011-1018.
109. Obokata H, Yamato M, Yang J, Nishida K, Tsuneda S, Okano T. Subcutaneous transplantation of autologous oral mucosal epithelial cell sheets fabricated on temperature-responsive culture dishes. *J Biomed Mater Res A* 2008;86:1088-1096.
110. Nakamura T, Endo K, Cooper LJ, et al. The successful culture and autologous transplantation of rabbit oral mucosal epithelial cells on amniotic membrane. *Invest Ophthalmol Vis Sci* 2003;44:106-116.
111. Hayashida Y, Nishida K, Yamato M, et al. Ocular surface reconstruction using autologous rabbit oral mucosal epithelial sheets fabricated ex vivo on a temperature-responsive culture surface. *Invest Ophthalmol Vis Sci* 2005;46:1632-1639.
112. Gipson IK, Geggel HS, Spurr-Michaud SJ. Transplant of oral mucosal epithelium to rabbit ocular surface wounds in vivo. *Arch Ophthalmol* 1986;104:1529-1533.

113. Nakamura T, Inatomi T, Sotozono C, Amemiya T, Kanamura N, Kinoshita S. Transplantation of cultivated autologous oral mucosal epithelial cells in patients with severe ocular surface disorders. *Br J Ophthalmol* 2004;88:1280-1284.
114. Nakamura T, Takeda K, Inatomi T, Sotozono C, Kinoshita S. Long-term results of autologous cultivated oral mucosal epithelial transplantation in the scar phase of severe ocular surface disorders. *Br J Ophthalmol* 2011;95:942-946.
115. Satake Y, Higa K, Tsubota K, Shimazaki J. Long-term outcome of cultivated oral mucosal epithelial sheet transplantation in treatment of total limbal stem cell deficiency. *Ophthalmology* 2011;118:1524-1530.
116. Inatomi T, Nakamura T, Koizumi N, Sotozono C, Yokoi N, Kinoshita S. Midterm results on ocular surface reconstruction using cultivated autologous oral mucosal epithelial transplantation. *Am J Ophthalmol* 2006;141:267-275.
117. Sahu SK, Govindswamy P, Sangwan VS, Thomas R. Midterm results on ocular surface reconstruction using cultivated autologous oral mucosal epithelial transplantation. *Am J Ophthalmol* 2007;143:189; author reply 189-190.
118. Chen HC, Chen HL, Lai JY, et al. Persistence of transplanted oral mucosal epithelial cells in human cornea. *Invest Ophthalmol Vis Sci* 2009;50:4660-4668.
119. Krishnan S, Iyer GK, Krishnakumar S. Culture & characterisation of limbal epithelial cells & oral mucosal cells. *Indian J Med Res* 2010;131:422-428.
120. Liu J, Sheha H, Fu Y, Giegengack M, Tseng SC. Oral mucosal graft with amniotic membrane transplantation for total limbal stem cell deficiency. *Am J Ophthalmol* 2011;152:739-747 e731.
121. Burillon C, Huot L, Justin V, et al. Cultured autologous oral mucosal epithelial cell sheet (CAOMECS) transplantation for the treatment of corneal limbal epithelial stem cell deficiency. *Invest Ophthalmol Vis Sci* 2012;53:1325-1331.
122. Oie Y, Hayashi R, Takagi R, et al. A novel method of culturing human oral mucosal epithelial cell sheet using post-mitotic human dermal fibroblast feeder cells and modified keratinocyte culture medium for ocular surface reconstruction. *Br J Ophthalmol* 2010;94:1244-1250.
123. Yokoo S, Yamagami S, Usui T, Amano S, Araie M. Human corneal epithelial equivalents for ocular surface reconstruction in a complete serum-free culture system without unknown factors. *Invest Ophthalmol Vis Sci* 2008;49:2438-2443.
124. Ang LP, Tanioka H, Kawasaki S, et al. Cultivated human conjunctival epithelial transplantation for total limbal stem cell deficiency. *Invest Ophthalmol Vis Sci* 2010;51:758-764.
125. Ono K, Yokoo S, Mimura T, et al. Autologous transplantation of conjunctival epithelial cells cultured on amniotic membrane in a rabbit model. *Mol Vis* 2007;13:1138-1143.
126. Yang X, Moldovan NI, Zhao Q, et al. Reconstruction of damaged cornea by autologous transplantation of epidermal adult stem cells. *Mol Vis* 2008;14:1064-1070.
127. Monteiro BG, Serafim RC, Melo GB, et al. Human immature dental pulp stem cells share key characteristic features with limbal stem cells. *Cell Prolif* 2009;42:587-594.
128. Gomes JA, Geraldes Monteiro B, Melo GB, et al. Corneal reconstruction with tissue-engineered cell sheets composed of human immature dental pulp stem cells. *Invest Ophthalmol Vis Sci* 2010;51:1408-1414.
129. Kim JH, Chun YS, Lee SH, et al. Ocular surface reconstruction with autologous nasal mucosa in cicatricial ocular surface disease. *Am J Ophthalmol* 2010;149:45-53.

130. Blazejewska EA, Schlotzer-Schrehardt U, Zenkel M, et al. Corneal limbal microenvironment can induce transdifferentiation of hair follicle stem cells into corneal epithelial-like cells. *Stem Cells* 2009;27:642-652.
131. Meyer-Blazejewska EA, Call MK, Yamanaka O, et al. From hair to cornea: toward the therapeutic use of hair follicle-derived stem cells in the treatment of limbal stem cell deficiency. *Stem Cells* 2011;29:57-66.
132. Homma R, Yoshikawa H, Takeno M, et al. Induction of epithelial progenitors in vitro from mouse embryonic stem cells and application for reconstruction of damaged cornea in mice. *Invest Ophthalmol Vis Sci* 2004;45:4320-4326.
133. Ma Y, Xu Y, Xiao Z, et al. Reconstruction of chemically burned rat corneal surface by bone marrow-derived human mesenchymal stem cells. *Stem Cells* 2006;24:315-321.
134. Ye J, Yao K, Kim JC. Mesenchymal stem cell transplantation in a rabbit corneal alkali burn model: engraftment and involvement in wound healing. *Eye (Lond)* 2006;20:482-490.
135. Koizumi N, Fullwood NJ, Bairaktaris G, Inatomi T, Kinoshita S, Quantock AJ. Cultivation of corneal epithelial cells on intact and denuded human amniotic membrane. *Invest Ophthalmol Vis Sci* 2000;41:2506-2513.
136. Meller D, Tseng SC. Conjunctival epithelial cell differentiation on amniotic membrane. *Invest Ophthalmol Vis Sci* 1999;40:878-886.
137. Rendal-Vazquez ME, San-Luis-Verdes A, Yebra-Pimentel-Vilar MT, et al. Culture of limbal stem cells on human amniotic membrane. *Cell Tissue Bank* 2012;13:513-519.
138. Balasubramanian S, Jasty S, Sitalakshmi G, Madhavan HN, Krishnakumar S. Influence of feeder layer on the expression of stem cell markers in cultured limbal corneal epithelial cells. *Indian J Med Res* 2008;128:616-622.
139. Baharvand H, Heidari M, Ebrahimi M, Valadbeigi T, Salekdeh GH. Proteomic analysis of epithelium-denuded human amniotic membrane as a limbal stem cell niche. *Mol Vis* 2007;13:1711-1721.
140. Kinoshita S, Koizumi N, Nakamura T. Transplantable cultivated mucosal epithelial sheet for ocular surface reconstruction. *Exp Eye Res* 2004;78:483-491.
141. Song E, Yang W, Cui ZH, et al. Transplantation of human limbal cells cultivated on amniotic membrane for reconstruction of rat corneal epithelium after alkaline burn. *Chin Med J (Engl)* 2005;118:927-935.
142. Koizumi N, Inatomi T, Quantock AJ, Fullwood NJ, Dota A, Kinoshita S. Amniotic membrane as a substrate for cultivating limbal corneal epithelial cells for autologous transplantation in rabbits. *Cornea* 2000;19:65-71.
143. Wan P, Wang X, Ma P, et al. Cell delivery with fixed amniotic membrane reconstructs corneal epithelium in rabbits with limbal stem cell deficiency. *Invest Ophthalmol Vis Sci* 2011;52:724-730.
144. Tsai RJ, Li LM, Chen JK. Reconstruction of damaged corneas by transplantation of autologous limbal epithelial cells. *N Engl J Med* 2000;343:86-93.
145. Nakamura T, Inatomi T, Sotozono C, Koizumi N, Kinoshita S. Successful primary culture and autologous transplantation of corneal limbal epithelial cells from minimal biopsy for unilateral severe ocular surface disease. *Acta Ophthalmol Scand* 2004;82:468-471.
146. Nakamura T, Koizumi N, Tsuzuki M, et al. Successful regrafting of cultivated corneal epithelium using amniotic membrane as a carrier in severe ocular surface disease. *Cornea* 2003;22:70-71.

147. Tseng SC, Prabhasawat P, Barton K, Gray T, Meller D. Amniotic membrane transplantation with or without limbal allografts for corneal surface reconstruction in patients with limbal stem cell deficiency. *Arch Ophthalmol* 1998;116:431-441.
148. Tsai RJ, Li L, Chen J. Reconstruction of damaged corneas by transplantation of autologous limbal epithelial cells(1). *Am J Ophthalmol* 2000;130:543.
149. Gomes JA, Romano A, Santos MS, Dua HS. Amniotic membrane use in ophthalmology. *Curr Opin Ophthalmol* 2005;16:233-240.
150. Shortt AJ, Secker GA, Rajan MS, et al. Ex vivo expansion and transplantation of limbal epithelial stem cells. *Ophthalmology* 2008;115:1989-1997.
151. Basu S, Ali H, Sangwan VS. Clinical outcomes of repeat autologous cultivated limbal epithelial transplantation for ocular surface burns. *Am J Ophthalmol* 2012;153:643-650.
152. Di Girolamo N, Chui J, Wakefield D, Coroneo MT. Cultured human ocular surface epithelium on therapeutic contact lenses. *Br J Ophthalmol* 2007;91:459-464.
153. Zhang H, Brown KD, Lowe SP, et al. Acrylic acid surface-modified contact lens for the culture of limbal stem cells. *Tissue Eng Part A* 2014;20:1593-1602.
154. Brown KD, Low S, Mariappan I, et al. Plasma polymer-coated contact lenses for the culture and transfer of corneal epithelial cells in the treatment of limbal stem cell deficiency. *Tissue Eng Part A* 2014;20:646-655.
155. Pellegrini G, Traverso CE, Franzi AT, Zingirian M, Cancedda R, De Luca M. Long-term restoration of damaged corneal surfaces with autologous cultivated corneal epithelium. *Lancet* 1997;349:990-993.
156. Di Girolamo N, Bosch M, Zamora K, Coroneo MT, Wakefield D, Watson SL. A contact lens-based technique for expansion and transplantation of autologous epithelial progenitors for ocular surface reconstruction. *Transplantation* 2009;87:1571-1578.
157. Feng Y, Borrelli M, Reichl S, Schrader S, Geerling G. Review of alternative carrier materials for ocular surface reconstruction. *Curr Eye Res* 2014;39:541-552.
158. Kozak I, Trbolova A, Kolodzieyski L, Juhas T, Ledecy V. Experimental anterior lens capsule transplantation for chronic corneal ulcers-Bowman's layer replacement? *Cornea* 2003;22:359-362.
159. Galal A, Perez-Santonja JJ, Rodriguez-Prats JL, Abad M, Alio J. Human anterior lens capsule as a biologic substrate for the ex vivo expansion of limbal stem cells in ocular surface reconstruction. *Cornea* 2007;26:473-478.
160. Elsdale T, Bard J. Collagen substrata for studies on cell behavior. *J Cell Biol* 1972;54:626-637.
161. Fagerholm P, Lagali NS, Carlsson DJ, Merrett K, Griffith M. Corneal regeneration following implantation of a biomimetic tissue-engineered substitute. *Clin Transl Sci* 2009;2:162-164.
162. Geggel HS, Friend J, Thoft RA. Collagen gel for ocular surface. *Invest Ophthalmol Vis Sci* 1985;26:901-905.
163. He YG, McCulley JP. Growing human corneal epithelium on collagen shield and subsequent transfer to denuded cornea in vitro. *Curr Eye Res* 1991;10:851-863.
164. McIntosh Ambrose W, Salahuddin A, So S, et al. Collagen Vitrigel membranes for the in vitro reconstruction of separate corneal epithelial, stromal, and endothelial cell layers. *J Biomed Mater Res B Appl Biomater* 2009;90:818-831.

165. Dravida S, Gaddipati S, Griffith M, et al. A biomimetic scaffold for culturing limbal stem cells: a promising alternative for clinical transplantation. *J Tissue Eng Regen Med* 2008;2:263-271.
166. Mi S, Chen B, Wright B, Connon CJ. Plastic compression of a collagen gel forms a much improved scaffold for ocular surface tissue engineering over conventional collagen gels. *J Biomed Mater Res A* 2010;95:447-453.
167. Levis HJ, Brown RA, Daniels JT. Plastic compressed collagen as a biomimetic substrate for human limbal epithelial cell culture. *Biomaterials* 2010;31:7726-7737.
168. Shimmura S, Doillon CJ, Griffith M, et al. Collagen-poly(N-isopropylacrylamide)-based membranes for corneal stroma scaffolds. *Cornea* 2003;22:S81-88.
169. Liu W, Merrett K, Griffith M, et al. Recombinant human collagen for tissue engineered corneal substitutes. *Biomaterials* 2008;29:1147-1158.
170. Merrett K, Fagerholm P, McLaughlin CR, et al. Tissue-engineered recombinant human collagen-based corneal substitutes for implantation: performance of type I versus type III collagen. *Invest Ophthalmol Vis Sci* 2008;49:3887-3894.
171. Lagali N, Griffith M, Fagerholm P, Merrett K, Huynh M, Munger R. Innervation of tissue-engineered recombinant human collagen-based corneal substitutes: a comparative in vivo confocal microscopy study. *Invest Ophthalmol Vis Sci* 2008;49:3895-3902.
172. Fagerholm P, Lagali NS, Merrett K, et al. A biosynthetic alternative to human donor tissue for inducing corneal regeneration: 24-month follow-up of a phase 1 clinical study. *Sci Transl Med* 2010;2:46ra61.
173. Llamas SG, Del Rio M, Larcher F, et al. Human plasma as a dermal scaffold for the generation of a completely autologous bioengineered skin. *Transplantation* 2004;77:350-355.
174. Meana A, Iglesias J, Del Rio M, et al. Large surface of cultured human epithelium obtained on a dermal matrix based on live fibroblast-containing fibrin gels. *Burns* 1998;24:621-630.
175. Han B, Schwab IR, Madsen TK, Isseroff RR. A fibrin-based bioengineered ocular surface with human corneal epithelial stem cells. *Cornea* 2002;21:505-510.
176. Sheth R, Neale MH, Shortt AJ, Massie I, Vernon AJ, Daniels JT. Culture and characterization of oral mucosal epithelial cells on a fibrin gel for ocular surface reconstruction. *Curr Eye Res* 2014;1-11.
177. Talbot M, Carrier P, Giasson CJ, et al. Autologous transplantation of rabbit limbal epithelia cultured on fibrin gels for ocular surface reconstruction. *Mol Vis* 2006;12:65-75.
178. Rama P, Bonini S, Lambiase A, et al. Autologous fibrin-cultured limbal stem cells permanently restore the corneal surface of patients with total limbal stem cell deficiency. *Transplantation* 2001;72:1478-1485.
179. Rama P, Matuska S, Paganoni G, Spinelli A, De Luca M, Pellegrini G. Limbal stem-cell therapy and long-term corneal regeneration. *N Engl J Med* 2010;363:147-155.
180. Harkin DG, George KA, Madden PW, Schwab IR, Hutmacher DW, Chirila TV. Silk fibroin in ocular tissue reconstruction. *Biomaterials* 2011;32:2445-2458.
181. Lawrence BD, Cronin-Golomb M, Georgakoudi I, Kaplan DL, Omenetto FG. Bioactive silk protein biomaterial systems for optical devices. *Biomacromolecules* 2008;9:1214-1220.

182. Lawrence BD, Marchant JK, Pindrus MA, Omenetto FG, Kaplan DL. Silk film biomaterials for cornea tissue engineering. *Biomaterials* 2009;30:1299-1308.
183. Higa K, Takeshima N, Moro F, et al. Porous silk fibroin film as a transparent carrier for cultivated corneal epithelial sheets. *J Biomater Sci Polym Ed* 2010.
184. Chirila T, Barnard Z, Zainuddin, Harkin DG, Schwab IR, Hirst L. Bombyx mori silk fibroin membranes as potential substrata for epithelial constructs used in the management of ocular surface disorders. *Tissue Eng Part A* 2008;14:1203-1211.
185. Bray LJ, George KA, Ainscough SL, Hutmacher DW, Chirila TV, Harkin DG. Human corneal epithelial equivalents constructed on Bombyx mori silk fibroin membranes. *Biomaterials* 2011;32:5086-5091.
186. Bray LJ, George KA, Hutmacher DW, Chirila TV, Harkin DG. A dual-layer silk fibroin scaffold for reconstructing the human corneal limbus. *Biomaterials* 2012;33:3529-3538.
187. Ang LP, Cheng ZY, Beuerman RW, Teoh SH, Zhu X, Tan DT. The development of a serum-free derived bioengineered conjunctival epithelial equivalent using an ultrathin poly(epsilon-caprolactone) membrane substrate. *Invest Ophthalmol Vis Sci* 2006;47:105-112.
188. Sharma S, Mohanty S, Gupta D, Jassal M, Agrawal AK, Tandon R. Cellular response of limbal epithelial cells on electrospun poly-epsilon-caprolactone nanofibrous scaffolds for ocular surface bioengineering: a preliminary in vitro study. *Mol Vis* 2011;17:2898-2910.
189. Deshpande P, McKean R, Blackwood KA, et al. Using poly(lactide-co-glycolide) electrospun scaffolds to deliver cultured epithelial cells to the cornea. *Regen Med* 2010;5:395-401.
190. Rimmer S, Johnson C, Zhao B, et al. Epithelialization of hydrogels achieved by amine functionalization and co-culture with stromal cells. *Biomaterials* 2007;28:5319-5331.
191. Ma A, Zhao B, Bentley AJ, et al. Corneal epithelialisation on surface-modified hydrogel implants: artificial cornea. *J Mater Sci Mater Med* 2011;22:663-670.
192. Oelker AM, Grinstaff MW. Synthesis, characterization, and in vitro evaluation of a hydrogel-based corneal onlay. *IEEE Trans Nanobioscience* 2012;11:37-45.
193. Philipp W, Speicher L, Humpel C. Expression of vascular endothelial growth factor and its receptors in inflamed and vascularized human corneas. *Invest Ophthalmol Vis Sci* 2000;41:2514-2522.
194. Chang JH, Gabison EE, Kato T, Azar DT. Corneal neovascularization. *Curr Opin Ophthalmol* 2001;12:242-249.
195. Ambati BK, Nozaki M, Singh N, et al. Corneal avascularity is due to soluble VEGF receptor-1. *Nature* 2006;443:993-997.
196. Stuart PM, Pan F, Plambeck S, Ferguson TA. FasL-Fas interactions regulate neovascularization in the cornea. *Invest Ophthalmol Vis Sci* 2003;44:93-98.
197. Mwaikambo BR, Sennlaub F, Ong H, Chemtob S, Hardy P. Activation of CD36 inhibits and induces regression of inflammatory corneal neovascularization. *Invest Ophthalmol Vis Sci* 2006;47:4356-4364.
198. Risau W. Mechanisms of angiogenesis. *Nature* 1997;386:671-674.
199. Carmeliet P, Jain RK. Angiogenesis in cancer and other diseases. *Nature* 2000;407:249-257.
200. Carmeliet P. Angiogenesis in health and disease. *Nat Med* 2003;9:653-660.
201. Semenza GL, Wang GL. A nuclear factor induced by hypoxia via de novo protein synthesis binds to the human erythropoietin gene enhancer at a site required for transcriptional activation. *Mol Cell Biol* 1992;12:5447-5454.

202. Wang GL, Jiang BH, Rue EA, Semenza GL. Hypoxia-inducible factor 1 is a basic-helix-loop-helix-PAS heterodimer regulated by cellular O₂ tension. *Proc Natl Acad Sci U S A* 1995;92:5510-5514.
203. Risau W, Flamme I. Vasculogenesis. *Annu Rev Cell Dev Biol* 1995;11:73-91.
204. Yancopoulos GD, Davis S, Gale NW, Rudge JS, Wiegand SJ, Holash J. Vascular-specific growth factors and blood vessel formation. *Nature* 2000;407:242-248.
205. D'Amore PA, Thompson RW. Mechanisms of angiogenesis. *Annu Rev Physiol* 1987;49:453-464.
206. Reynolds LP, Killilea SD, Redmer DA. Angiogenesis in the female reproductive system. *FASEB J* 1992;6:886-892.
207. Smith SK. Angiogenesis, vascular endothelial growth factor and the endometrium. *Hum Reprod Update* 1998;4:509-519.
208. Rees M, Hague S, Oehler MK, Bicknell R. Regulation of endometrial angiogenesis. *Climacteric* 1999;2:52-58.
209. Folkman J, Shing Y. Angiogenesis. *J Biol Chem* 1992;267:10931-10934.
210. Otrock ZK, Mahfouz RA, Makarem JA, Shamseddine AI. Understanding the biology of angiogenesis: review of the most important molecular mechanisms. *Blood Cells Mol Dis* 2007;39:212-220.
211. Ferrara N, Henzel WJ. Pituitary follicular cells secrete a novel heparin-binding growth factor specific for vascular endothelial cells. *Biochem Biophys Res Commun* 1989;161:851-858.
212. Leung DW, Cachianes G, Kuang WJ, Goeddel DV, Ferrara N. Vascular endothelial growth factor is a secreted angiogenic mitogen. *Science* 1989;246:1306-1309.
213. Plate KH, Breier G, Weich HA, Risau W. Vascular endothelial growth factor is a potential tumour angiogenesis factor in human gliomas in vivo. *Nature* 1992;359:845-848.
214. Shweiki D, Itin A, Soffer D, Keshet E. Vascular endothelial growth factor induced by hypoxia may mediate hypoxia-initiated angiogenesis. *Nature* 1992;359:843-845.
215. Stein I, Neeman M, Shweiki D, Itin A, Keshet E. Stabilization of vascular endothelial growth factor mRNA by hypoxia and hypoglycemia and coregulation with other ischemia-induced genes. *Mol Cell Biol* 1995;15:5363-5368.
216. Flamme I, Breier G, Risau W. Vascular endothelial growth factor (VEGF) and VEGF receptor 2 (flk-1) are expressed during vasculogenesis and vascular differentiation in the quail embryo. *Dev Biol* 1995;169:699-712.
217. Breier G, Risau W. The role of vascular endothelial growth factor in blood vessel formation. *Trends Cell Biol* 1996;6:454-456.
218. Jakeman LB, Winer J, Bennett GL, Altar CA, Ferrara N. Binding sites for vascular endothelial growth factor are localized on endothelial cells in adult rat tissues. *J Clin Invest* 1992;89:244-253.
219. Otrock ZK, Makarem JA, Shamseddine AI. Vascular endothelial growth factor family of ligands and receptors: review. *Blood Cells Mol Dis* 2007;38:258-268.
220. Senger DR, Galli SJ, Dvorak AM, Perruzzi CA, Harvey VS, Dvorak HF. Tumor cells secrete a vascular permeability factor that promotes accumulation of ascites fluid. *Science* 1983;219:983-985.
221. Muller YA, Li B, Christinger HW, Wells JA, Cunningham BC, de Vos AM. Vascular endothelial growth factor: crystal structure and functional mapping of

- the kinase domain receptor binding site. *Proc Natl Acad Sci U S A* 1997;94:7192-7197.
222. Tischer E, Mitchell R, Hartman T, et al. The human gene for vascular endothelial growth factor. Multiple protein forms are encoded through alternative exon splicing. *J Biol Chem* 1991;266:11947-11954.
 223. Neufeld G, Cohen T, Gengrinovitch S, Poltorak Z. Vascular endothelial growth factor (VEGF) and its receptors. *FASEB J* 1999;13:9-22.
 224. Nicosia RF, Nicosia SV, Smith M. Vascular endothelial growth factor, platelet-derived growth factor, and insulin-like growth factor-1 promote rat aortic angiogenesis in vitro. *Am J Pathol* 1994;145:1023-1029.
 225. Phillips GD, Stone AM, Jones BD, Schultz JC, Whitehead RA, Knighton DR. Vascular endothelial growth factor (rhVEGF165) stimulates direct angiogenesis in the rabbit cornea. *In Vivo* 1994;8:961-965.
 226. Mesri EA, Federoff HJ, Brownlee M. Expression of vascular endothelial growth factor from a defective herpes simplex virus type 1 amplicon vector induces angiogenesis in mice. *Circ Res* 1995;76:161-167.
 227. Alon T, Hemo I, Itin A, Pe'er J, Stone J, Keshet E. Vascular endothelial growth factor acts as a survival factor for newly formed retinal vessels and has implications for retinopathy of prematurity. *Nat Med* 1995;1:1024-1028.
 228. Carmeliet P, Ferreira V, Breier G, et al. Abnormal blood vessel development and lethality in embryos lacking a single VEGF allele. *Nature* 1996;380:435-439.
 229. Ferrara N, Gerber HP, LeCouter J. The biology of VEGF and its receptors. *Nat Med* 2003;9:669-676.
 230. Adamis AP, Miller JW, Bernal MT, et al. Increased vascular endothelial growth factor levels in the vitreous of eyes with proliferative diabetic retinopathy. *Am J Ophthalmol* 1994;118:445-450.
 231. Aiello LP, Avery RL, Arrigg PG, et al. Vascular endothelial growth factor in ocular fluid of patients with diabetic retinopathy and other retinal disorders. *N Engl J Med* 1994;331:1480-1487.
 232. Pe'er J, Folberg R, Itin A, Gnessin H, Hemo I, Keshet E. Upregulated expression of vascular endothelial growth factor in proliferative diabetic retinopathy. *Br J Ophthalmol* 1996;80:241-245.
 233. Boulton M, Foreman D, Williams G, McLeod D. VEGF localisation in diabetic retinopathy. *Br J Ophthalmol* 1998;82:561-568.
 234. Kvanta A, Sarman S, Fagerholm P, Seregard S, Steen B. Expression of matrix metalloproteinase-2 (MMP-2) and vascular endothelial growth factor (VEGF) in inflammation-associated corneal neovascularization. *Exp Eye Res* 2000;70:419-428.
 235. Cursiefen C, Rummelt C, Kuchle M. Immunohistochemical localization of vascular endothelial growth factor, transforming growth factor alpha, and transforming growth factor beta1 in human corneas with neovascularization. *Cornea* 2000;19:526-533.
 236. Grimmond S, Lagercrantz J, Drinkwater C, et al. Cloning and characterization of a novel human gene related to vascular endothelial growth factor. *Genome Res* 1996;6:124-131.
 237. Olofsson B, Pajusola K, Kaipainen A, et al. Vascular endothelial growth factor B, a novel growth factor for endothelial cells. *Proc Natl Acad Sci U S A* 1996;93:2576-2581.
 238. Olofsson B, Pajusola K, von Euler G, Chilov D, Alitalo K, Eriksson U. Genomic organization of the mouse and human genes for vascular endothelial growth

- factor B (VEGF-B) and characterization of a second splice isoform. *J Biol Chem* 1996;271:19310-19317.
- 239.Li X, Kumar A, Zhang F, Lee C, Tang Z. Complicated life, complicated VEGF-B. *Trends Mol Med* 2011.
 - 240.Aase K, Lymboussaki A, Kaipainen A, Olofsson B, Alitalo K, Eriksson U. Localization of VEGF-B in the mouse embryo suggests a paracrine role of the growth factor in the developing vasculature. *Dev Dyn* 1999;215:12-25.
 - 241.Li X, Aase K, Li H, von Euler G, Eriksson U. Isoform-specific expression of VEGF-B in normal tissues and tumors. *Growth Factors* 2001;19:49-59.
 - 242.Olofsson B, Korpelainen E, Pepper MS, et al. Vascular endothelial growth factor B (VEGF-B) binds to VEGF receptor-1 and regulates plasminogen activator activity in endothelial cells. *Proc Natl Acad Sci U S A* 1998;95:11709-11714.
 - 243.Makinen T, Olofsson B, Karpanen T, et al. Differential binding of vascular endothelial growth factor B splice and proteolytic isoforms to neuropilin-1. *J Biol Chem* 1999;274:21217-21222.
 - 244.Cao Y. Positive and negative modulation of angiogenesis by VEGFR1 ligands. *Sci Signal* 2009;2:re1.
 - 245.Li X, Lee C, Tang Z, et al. VEGF-B: a survival, or an angiogenic factor? *Cell Adh Migr* 2009;3:322-327.
 - 246.Bellomo D, Headrick JP, Silins GU, et al. Mice lacking the vascular endothelial growth factor-B gene (*Vegfb*) have smaller hearts, dysfunctional coronary vasculature, and impaired recovery from cardiac ischemia. *Circ Res* 2000;86:E29-35.
 - 247.Aase K, von Euler G, Li X, et al. Vascular endothelial growth factor-B-deficient mice display an atrial conduction defect. *Circulation* 2001;104:358-364.
 - 248.Mould AW, Greco SA, Cahill MM, et al. Transgenic overexpression of vascular endothelial growth factor-B isoforms by endothelial cells potentiates postnatal vessel growth in vivo and in vitro. *Circ Res* 2005;97:e60-70.
 - 249.Karpanen T, Bry M, Ollila HM, et al. Overexpression of vascular endothelial growth factor-B in mouse heart alters cardiac lipid metabolism and induces myocardial hypertrophy. *Circ Res* 2008;103:1018-1026.
 - 250.Reichelt M, Shi S, Hayes M, et al. Vascular endothelial growth factor-B and retinal vascular development in the mouse. *Clin Experiment Ophthalmol* 2003;31:61-65.
 - 251.Abraham D, Taghavi S, Riml P, et al. VEGF-A and -C but not -B mediate increased vascular permeability in preserved lung grafts. *Transplantation* 2002;73:1703-1706.
 - 252.Silvestre JS, Tamarat R, Ebrahimian TG, et al. Vascular endothelial growth factor-B promotes in vivo angiogenesis. *Circ Res* 2003;93:114-123.
 - 253.Wafai R, Tudor EM, Angus JA, Wright CE. Vascular effects of FGF-2 and VEGF-B in rabbits with bilateral hind limb ischemia. *J Vasc Res* 2009;46:45-54.
 - 254.Li X, Tjwa M, Van Hove I, et al. Reevaluation of the role of VEGF-B suggests a restricted role in the revascularization of the ischemic myocardium. *Arterioscler Thromb Vasc Biol* 2008;28:1614-1620.
 - 255.Rissanen TT, Markkanen JE, Gruchala M, et al. VEGF-D is the strongest angiogenic and lymphangiogenic effector among VEGFs delivered into skeletal muscle via adenoviruses. *Circ Res* 2003;92:1098-1106.
 - 256.Bhardwaj S, Roy H, Gruchala M, et al. Angiogenic responses of vascular endothelial growth factors in periadventitial tissue. *Hum Gene Ther* 2003;14:1451-1462.

257. Zhang F, Tang Z, Hou X, et al. VEGF-B is dispensable for blood vessel growth but critical for their survival, and VEGF-B targeting inhibits pathological angiogenesis. *Proc Natl Acad Sci U S A* 2009;106:6152-6157.
258. Zhong X, Huang H, Shen J, et al. Vascular endothelial growth factor-B gene transfer exacerbates retinal and choroidal neovascularization and vasopermeability without promoting inflammation. *Mol Vis* 2011;17:492-507.
259. Kivela R, Bry M, Robciuc MR, et al. VEGF-B-induced vascular growth leads to metabolic reprogramming and ischemia resistance in the heart. *EMBO Mol Med* 2014;6:307-321.
260. Wanstall JC, Gambino A, Jeffery TK, et al. Vascular endothelial growth factor-B-deficient mice show impaired development of hypoxic pulmonary hypertension. *Cardiovasc Res* 2002;55:361-368.
261. Huusko J, Lottonen L, Merentie M, et al. AAV9-mediated VEGF-B gene transfer improves systolic function in progressive left ventricular hypertrophy. *Mol Ther* 2012;20:2212-2221.
262. Zhao T, Zhao W, Chen Y, Liu L, Ahokas RA, Sun Y. Differential expression of vascular endothelial growth factor isoforms and receptor subtypes in the infarcted heart. *Int J Cardiol* 2013;167:2638-2645.
263. Bry M, Kivela R, Holopainen T, et al. Vascular endothelial growth factor-B acts as a coronary growth factor in transgenic rats without inducing angiogenesis, vascular leak, or inflammation. *Circulation* 2010;122:1725-1733.
264. Huusko J, Merentie M, Dijkstra MH, et al. The effects of VEGF-R1 and VEGF-R2 ligands on angiogenic responses and left ventricular function in mice. *Cardiovasc Res* 2010;86:122-130.
265. Serpi R, Tolonen AM, Huusko J, et al. Vascular endothelial growth factor-B gene transfer prevents angiotensin II-induced diastolic dysfunction via proliferation and capillary dilatation in rats. *Cardiovasc Res* 2011;89:204-213.
266. Dhondt J, Peeraer E, Verheyen A, et al. Neuronal FLT1 receptor and its selective ligand VEGF-B protect against retrograde degeneration of sensory neurons. *FASEB J* 2011;25:1461-1473.
267. Yue X, Hariri DJ, Caballero B, et al. Comparative study of the neurotrophic effects elicited by VEGF-B and GDNF in preclinical in vivo models of Parkinson's disease. *Neuroscience* 2014;258:385-400.
268. Falk T, Zhang S, Sherman SJ. Vascular endothelial growth factor B (VEGF-B) is up-regulated and exogenous VEGF-B is neuroprotective in a culture model of Parkinson's disease. *Mol Neurodegener* 2009;4:49.
269. Falk T, Yue X, Zhang S, et al. Vascular endothelial growth factor-B is neuroprotective in an in vivo rat model of Parkinson's disease. *Neurosci Lett* 2011;496:43-47.
270. Sun Y, Jin K, Childs JT, Xie L, Mao XO, Greenberg DA. Vascular endothelial growth factor-B (VEGFB) stimulates neurogenesis: evidence from knockout mice and growth factor administration. *Dev Biol* 2006;289:329-335.
271. Poesen K, Lambrechts D, Van Damme P, et al. Novel role for vascular endothelial growth factor (VEGF) receptor-1 and its ligand VEGF-B in motor neuron degeneration. *J Neurosci* 2008;28:10451-10459.
272. Sun Y, Jin K, Childs JT, Xie L, Mao XO, Greenberg DA. Increased severity of cerebral ischemic injury in vascular endothelial growth factor-B-deficient mice. *J Cereb Blood Flow Metab* 2004;24:1146-1152.

- 273.Li Y, Zhang F, Nagai N, et al. VEGF-B inhibits apoptosis via VEGFR-1-mediated suppression of the expression of BH3-only protein genes in mice and rats. *J Clin Invest* 2008;118:913-923.
- 274.Guaiquil VH, Pan Z, Karagianni N, Fukuoka S, Alegre G, Rosenblatt MI. VEGF-B selectively regenerates injured peripheral neurons and restores sensory and trophic functions. *Proc Natl Acad Sci U S A* 2014;111:17272-17277.
- 275.Hagberg CE, Falkevall A, Wang X, et al. Vascular endothelial growth factor B controls endothelial fatty acid uptake. *Nature* 2010;464:917-921.
- 276.Hagberg CE, Mehlem A, Falkevall A, et al. Targeting VEGF-B as a novel treatment for insulin resistance and type 2 diabetes. *Nature* 2012;490:426-430.
- 277.Bartelt A, Bruns OT, Reimer R, et al. Brown adipose tissue activity controls triglyceride clearance. *Nat Med* 2011;17:200-205.
- 278.Lu X, Ji Y, Zhang L, et al. Resistance to obesity by repression of VEGF gene expression through induction of brown-like adipocyte differentiation. *Endocrinology* 2012;153:3123-3132.
- 279.Elias I, Franckhauser S, Ferre T, et al. Adipose tissue overexpression of vascular endothelial growth factor protects against diet-induced obesity and insulin resistance. *Diabetes* 2012;61:1801-1813.
- 280.Sun K, Wernstedt Asterholm I, Kusminski CM, et al. Dichotomous effects of VEGF-A on adipose tissue dysfunction. *Proc Natl Acad Sci U S A* 2012;109:5874-5879.
- 281.Bry M, Kivela R, Leppanen VM, Alitalo K. Vascular endothelial growth factor-B in physiology and disease. *Physiol Rev* 2014;94:779-794.
- 282.Lee P, Wang CC, Adamis AP. Ocular neovascularization: an epidemiologic review. *Surv Ophthalmol* 1998;43:245-269.
- 283.Qazi Y, Maddula S, Ambati BK. Mediators of ocular angiogenesis. *J Genet* 2009;88:495-515.
- 284.Burger PC, Chandler DB, Klintworth GK. Experimental corneal neovascularization: biomicroscopic, angiographic, and morphologic correlation. *Cornea* 1985;4:35-41.
- 285.Yaylali V, Ohta T, Kaufman SC, Maitchouk DY, Beuerman RW. In vivo confocal imaging of corneal neovascularization. *Cornea* 1998;17:646-653.
- 286.Ahmad N, Mukhtar H. Mechanism of photodynamic therapy-induced cell death. *Methods Enzymol* 2000;319:342-358.
- 287.Zheng M, Deshpande S, Lee S, Ferrara N, Rouse BT. Contribution of vascular endothelial growth factor in the neovascularization process during the pathogenesis of herpetic stromal keratitis. *J Virol* 2001;75:9828-9835.
- 288.Sheppard JD, Jr., Epstein RJ, Lattanzio FA, Jr., Marcantonio D, Williams PB. Argon laser photodynamic therapy of human corneal neovascularization after intravenous administration of dihematoporphyrin ether. *Am J Ophthalmol* 2006;141:524-529.
- 289.Marsh RJ, Marshall J. Treatment of lipid keratopathy with the argon laser. *Br J Ophthalmol* 1982;66:127-135.
- 290.Gerten G. Bevacizumab (avastin) and argon laser to treat neovascularization in corneal transplant surgery. *Cornea* 2008;27:1195-1199.
- 291.Nirankari VS, Baer JC. Corneal argon laser photocoagulation for neovascularization in penetrating keratoplasty. *Ophthalmology* 1986;93:1304-1309.
- 292.Pai VH, Handary SV. Necrotizing scleritis following laser therapy for corneal vascularization. *Ann Ophthalmol (Skokie)* 2009;41:50-51.

293. Fossarello M, Peiretti E, Zucca I, Serra A. Photodynamic therapy of corneal neovascularization with verteporfin. *Cornea* 2003;22:485-488.
294. Brooks BJ, Ambati BK, Marcus DM, Ratanasit A. Photodynamic therapy for corneal neovascularisation and lipid degeneration. *Br J Ophthalmol* 2004;88:840.
295. Yoon KC, You IC, Kang IS, et al. Photodynamic therapy with verteporfin for corneal neovascularization. *Am J Ophthalmol* 2007;144:390-395.
296. Gordon YJ, Mann RK, Mah TS, Gorin MB. Fluorescein-potentiated argon laser therapy improves symptoms and appearance of corneal neovascularization. *Cornea* 2002;21:770-773.
297. Gupta D, Illingworth C. Treatments for corneal neovascularization: a review. *Cornea* 2011;30:927-938.
298. Pillai CT, Dua HS, Hossain P. Fine needle diathermy occlusion of corneal vessels. *Invest Ophthalmol Vis Sci* 2000;41:2148-2153.
299. Wertheim MS, Cook SD, Knox-Cartwright NE, Van DL, Tole DM. Electrolysis-needle cauterization of corneal vessels in patients with lipid keratopathy. *Cornea* 2007;26:230-231.
300. Trikha S, Parikh S, Osmond C, Anderson DF, Hossain PN. Long-term outcomes of Fine Needle Diathermy for established corneal neovascularisation. *Br J Ophthalmol* 2014;98:454-458.
301. Boneham GC, Collin HB. Steroid inhibition of limbal blood and lymphatic vascular cell growth. *Curr Eye Res* 1995;14:1-10.
302. Jones IS, Meyer K. Inhibition of vascularization of the rabbit cornea by local application of cortisone. *Proc Soc Exp Biol Med* 1950;74:102-104.
303. Ahuja OP, Nema HV. Experimental corneal vascularization and its management. *Am J Ophthalmol* 1966;62:707-710.
304. McDonald PR, Leopold IH, Vogel AW, Mulberger RD. Hydrocortisone (compound F) in ophthalmology; clinical and experimental studies. *AMA Arch Ophthalmol* 1953;49:400-412.
305. Phillips K, Arffa R, Cintron C, et al. Effects of prednisolone and medroxyprogesterone on corneal wound healing, ulceration, and neovascularization. *Arch Ophthalmol* 1983;101:640-643.
306. Lavergne G, Colmant IA. Comparative study of the action of thiotepa and triamcinolone on corneal vascularization in rabbits. *Br J Ophthalmol* 1964;48:416-422.
307. Nakao S, Hata Y, Miura M, et al. Dexamethasone inhibits interleukin-1beta-induced corneal neovascularization: role of nuclear factor-kappaB-activated stromal cells in inflammatory angiogenesis. *Am J Pathol* 2007;171:1058-1065.
308. Robin JB, Regis-Pacheco LF, Kash RL, Schanzlin DJ. The histopathology of corneal neovascularization. Inhibitor effects. *Arch Ophthalmol* 1985;103:284-287.
309. Beutler B, Krochin N, Milsark IW, Luedke C, Cerami A. Control of cachectin (tumor necrosis factor) synthesis: mechanisms of endotoxin resistance. *Science* 1986;232:977-980.
310. Ebrahim Q, Minamoto A, Hoppe G, Anand-Apte B, Sears JE. Triamcinolone acetonide inhibits IL-6- and VEGF-induced angiogenesis downstream of the IL-6 and VEGF receptors. *Invest Ophthalmol Vis Sci* 2006;47:4935-4941.
311. Mahoney JM, Waterbury LD. Drug effects on the neovascularization response to silver nitrate cauterization of the rat cornea. *Curr Eye Res* 1985;4:531-535.

312. Dana MR, Streilein JW. Loss and restoration of immune privilege in eyes with corneal neovascularization. *Invest Ophthalmol Vis Sci* 1996;37:2485-2494.
313. Takahashi K, Saishin Y, Mori K, et al. Topical nepafenac inhibits ocular neovascularization. *Invest Ophthalmol Vis Sci* 2003;44:409-415.
314. Kahan BD. Cyclosporin A: a selective anti-T cell agent. *Clin Haematol* 1982;11:743-761.
315. Nirankari VS. Laser photocoagulation for corneal stromal vascularization. *Trans Am Ophthalmol Soc* 1992;90:595-669.
316. Kachi S, Hirano K, Takesue Y, Miura M. Unusual corneal deposit after the topical use of cyclosporine as eyedrops. *Am J Ophthalmol* 2000;130:667-669.
317. Williams KA, Grutzmacher RD, Roussel TJ, Coster DJ. A comparison of the effects of topical cyclosporine and topical steroid on rabbit corneal allograft rejection. *Transplantation* 1985;39:242-244.
318. Andreoli CM, Miller JW. Anti-vascular endothelial growth factor therapy for ocular neovascular disease. *Curr Opin Ophthalmol* 2007;18:502-508.
319. Presta LG, Chen H, O'Connor SJ, et al. Humanization of an anti-vascular endothelial growth factor monoclonal antibody for the therapy of solid tumors and other disorders. *Cancer Res* 1997;57:4593-4599.
320. Pytowski B, Goldman J, Persaud K, et al. Complete and specific inhibition of adult lymphatic regeneration by a novel VEGFR-3 neutralizing antibody. *J Natl Cancer Inst* 2005;97:14-21.
321. Witte L, Hicklin DJ, Zhu Z, et al. Monoclonal antibodies targeting the VEGF receptor-2 (Flk1/KDR) as an anti-angiogenic therapeutic strategy. *Cancer Metastasis Rev* 1998;17:155-161.
322. Aiello LP, Pierce EA, Foley ED, et al. Suppression of retinal neovascularization in vivo by inhibition of vascular endothelial growth factor (VEGF) using soluble VEGF-receptor chimeric proteins. *Proc Natl Acad Sci U S A* 1995;92:10457-10461.
323. Singh N, Higgins E, Amin S, et al. Unique homologous siRNA blocks hypoxia-induced VEGF upregulation in human corneal cells and inhibits and regresses murine corneal neovascularization. *Cornea* 2007;26:65-72.
324. Strawn LM, McMahan G, App H, et al. Flk-1 as a target for tumor growth inhibition. *Cancer Res* 1996;56:3540-3545.
325. Fong TA, Shawver LK, Sun L, et al. SU5416 is a potent and selective inhibitor of the vascular endothelial growth factor receptor (Flk-1/KDR) that inhibits tyrosine kinase catalysis, tumor vascularization, and growth of multiple tumor types. *Cancer Res* 1999;59:99-106.
326. Ferrara N, Hillan KJ, Novotny W. Bevacizumab (Avastin), a humanized anti-VEGF monoclonal antibody for cancer therapy. *Biochem Biophys Res Commun* 2005;333:328-335.
327. Manzano RP, Peyman GA, Khan P, et al. Inhibition of experimental corneal neovascularisation by bevacizumab (Avastin). *Br J Ophthalmol* 2007;91:804-807.
328. Habet-Wilner Z, Barequet IS, Ivanir Y, Moisseiev J, Rosner M. The inhibitory effect of different concentrations of topical bevacizumab on corneal neovascularization. *Acta Ophthalmol* 2010;88:862-867.
329. Yoeruek E, Ziemssen F, Henke-Fahle S, et al. Safety, penetration and efficacy of topically applied bevacizumab: evaluation of eyedrops in corneal neovascularization after chemical burn. *Acta Ophthalmol* 2008;86:322-328.

330. Dastjerdi MH, Sadrai Z, Saban DR, Zhang Q, Dana R. Corneal penetration of topical and subconjunctival bevacizumab. *Invest Ophthalmol Vis Sci* 2011;52:8718-8723.
331. Barros LF, Belfort R, Jr. The effects of the subconjunctival injection of bevacizumab (Avastin) on angiogenesis in the rat cornea. *An Acad Bras Cienc* 2007;79:389-394.
332. Hashemian MN, Moghimi S, Kiumehr S, Riazi M, Amoli FA. Prevention and treatment of corneal neovascularization: comparison of different doses of subconjunctival bevacizumab with corticosteroid in experimental rats. *Ophthalmic Res* 2009;42:90-95.
333. Hurmeric V, Mumcuoglu T, Erdurman C, Kurt B, Dagli O, Durukan AH. Effect of subconjunctival bevacizumab (Avastin) on experimental corneal neovascularization in guinea pigs. *Cornea* 2008;27:357-362.
334. Chen WL, Lin CT, Lin NT, et al. Subconjunctival injection of bevacizumab (avastin) on corneal neovascularization in different rabbit models of corneal angiogenesis. *Invest Ophthalmol Vis Sci* 2009;50:1659-1665.
335. Kim TI, Kim SW, Kim S, Kim T, Kim EK. Inhibition of experimental corneal neovascularization by using subconjunctival injection of bevacizumab (Avastin). *Cornea* 2008;27:349-352.
336. Papathanassiou M, Theodossiadis PG, Liarakos VS, Rouvas A, Giamarellos-Bourboulis EJ, Vergados IA. Inhibition of corneal neovascularization by subconjunctival bevacizumab in an animal model. *Am J Ophthalmol* 2008;145:424-431.
337. Su W, Li Z, Li Y, et al. Doxycycline enhances the inhibitory effects of bevacizumab on corneal neovascularization and prevents its side effects. *Invest Ophthalmol Vis Sci* 2011;52:9108-9115.
338. Erdurmus M, Totan Y. Subconjunctival bevacizumab for corneal neovascularization. *Graefes Arch Clin Exp Ophthalmol* 2007;245:1577-1579.
339. Bahar I, Kaiserman I, McAllum P, Rootman D, Slomovic A. Subconjunctival bevacizumab injection for corneal neovascularization. *Cornea* 2008;27:142-147.
340. Bock F, Konig Y, Kruse F, Baier M, Cursiefen C. Bevacizumab (Avastin) eye drops inhibit corneal neovascularization. *Graefes Arch Clin Exp Ophthalmol* 2008;246:281-284.
341. Doctor PP, Bhat PV, Foster CS. Subconjunctival bevacizumab for corneal neovascularization. *Cornea* 2008;27:992-995.
342. Kim SW, Ha BJ, Kim EK, Tchah H, Kim TI. The effect of topical bevacizumab on corneal neovascularization. *Ophthalmology* 2008;115:e33-38.
343. Uy HS, Chan PS, Ang RE. Topical bevacizumab and ocular surface neovascularization in patients with Stevens-johnson syndrome. *Cornea* 2008;27:70-73.
344. Dastjerdi MH, Al-Arfaj KM, Nallasamy N, et al. Topical bevacizumab in the treatment of corneal neovascularization: results of a prospective, open-label, noncomparative study. *Arch Ophthalmol* 2009;127:381-389.
345. You IC, Kang IS, Lee SH, Yoon KC. Therapeutic effect of subconjunctival injection of bevacizumab in the treatment of corneal neovascularization. *Acta Ophthalmol* 2009;87:653-658.
346. Benayoun Y, Adenis JP, Casse G, Forte R, Robert PY. Effects of subconjunctival bevacizumab on corneal neovascularization: results of a prospective study. *Cornea* 2012.

347. Qian CX, Bahar I, Levinger E, Rootman D. Combined use of superficial keratectomy and subconjunctival bevacizumab injection for corneal neovascularization. *Cornea* 2008;27:1090-1092.
348. Petsoglou C, Balaggan KS, Dart JK, et al. Subconjunctival bevacizumab induces regression of corneal neovascularisation: a pilot randomised placebo-controlled double-masked trial. *Br J Ophthalmol* 2013;97:28-32.
349. Uhlir A. Electrolytic shaping of germanium and silicon. *Bell System Technical Journal* 1956;35:333-347.
350. Foraker A, Walczak R, Cohen M, Boiarski T, Grove C, Swaan P. Microfabricated porous silicon particles enhance paracellular delivery of insulin across intestinal Caco-2 cell monolayers. *Pharmaceutical Research* 2003;20:110-116.
351. Andersson J, Rosenholm J, Areva S, Lindén M. Influences of material characteristics on ibuprofen drug loading and release profiles from ordered micro- and mesoporous silica matrices. *Chemistry of Materials* 2004;16:4160-4167.
352. Coffey JL, Whitehead MA, Nagesha DK, et al. Porous silicon-based scaffolds for tissue engineering and other biomedical applications. *Physica Status Solidi (a)* 2005;202:1451-1455.
353. Schwartz MP, Derfus AM, Alvarez SD, Bhatia SN, Sailor MJ. The smart petri dish: a nanostructured photonic crystal for real-time monitoring of living cells. *Langmuir* 2006;22:7084-7090.
354. McInnes SJP, Voelcker NH. Silicon-polymer hybrid materials for drug delivery. *Future Medicinal Chemistry* 2009;1:1051-1074.
355. Gentile F, La Rocca R, Marinaro G, et al. Differential cell adhesion on mesoporous silicon substrates. *ACS Appl Mater Interfaces* 2012.
356. Haidary SM, #xf3, rcoles EP, Ali NK. Nanoporous silicon as drug delivery systems for cancer therapies. *Journal of Nanomaterials* 2012;2012:15.
357. McInnes SJ, Irani Y, Williams KA, Voelcker NH. Controlled drug delivery from composites of nanostructured porous silicon and poly(L-lactide). *Nanomedicine (Lond)* 2012.
358. McInnes SJ, Szili EJ, Al-Bataineh SA, et al. Combination of iCVD and porous silicon for the development of a controlled drug delivery system. *ACS Appl Mater Interfaces* 2012;4:3566-3574.
359. Canham L. Properties of Porous Silicon. London: Institution of Engineering and Technology; 1997.
360. Anglin EJ, Cheng L, Freeman WR, Sailor MJ. Porous silicon in drug delivery devices and materials. *Adv Drug Deliv Rev* 2008;60:1266-1277.
361. Canham LT. Bioactive silicon structure fabrication through nanoetching techniques. *Advanced Materials* 1995;7:1033-1037.
362. Canham LT, Newey JP, Reeves CL, et al. The effects of DC electric currents on the in-vitro calcification of bioactive silicon wafers. *Advanced Materials* 1996;8:847-849.
363. Rosengren A, Wallman L, Bengtsson M, Laurell T, Danielsen N, Bjursten LM. Tissue reactions to porous silicon: A comparative biomaterial study. *Physica Status Solidi (A)* 2000;182:527-531.
364. Coffey JL, Montchamp J-L, Aimone JB, Weis RP. Routes to calcified porous silicon: implications for drug delivery and biosensing. *Physica Status Solidi (A)* 2003;197:336-339.

365. Seregin VV, Coffey JL. Bias-assisted in vitro calcification of calcium disilicide growth layers on spark-processed silicon. *Biomaterials* 2006;27:3726-3737.
366. Bowditch AP, Waters K, Gale H, et al. In-Vivo assessment of tissue compatibility and calcification of bulk and porous silicon. *MRS Online Proceedings Library* 1998;536.
367. Low SP, Williams KA, Canham LT, Voelcker NH. Evaluation of mammalian cell adhesion on surface-modified porous silicon. *Biomaterials* 2006;27:4538-4546.
368. Bayliss SC, Buckberry LD, Harris PJ, Tobin M. Nature of the silicon-animal cell interface. *Journal of Porous Materials* 2000;7:191-195.
369. Bayliss SC, Heald R, Fletcher DI, Buckberry LD. The culture of mammalian cells on nanostructured silicon. *Advanced Materials* 1999;11:318-321.
370. Chin V, Collins BE, Sailor MJ, Bhatia SN. Compatibility of primary hepatocytes with oxidized nanoporous silicon. *Advanced Materials* 2001;13:1877-1880.
371. Sapelkin AV, Bayliss SC, Unal B, Charalambou A. Interaction of B50 rat hippocampal cells with stain-etched porous silicon. *Biomaterials* 2006;27:842-846.
372. Alvarez SD, Derfus AM, Schwartz MP, Bhatia SN, Sailor MJ. The compatibility of hepatocytes with chemically modified porous silicon with reference to in vitro biosensors. *Biomaterials* 2009;30:26-34.
373. Bellia JP, Birchall JD, Roberts NB. Beer: a dietary source of silicon. *Lancet* 1994;343:235.
374. Reffitt DM, Jugdaohsingh R, Thompson RP, Powell JJ. Silicic acid: its gastrointestinal uptake and urinary excretion in man and effects on aluminium excretion. *J Inorg Biochem* 1999;76:141-147.
375. Petrova-Koch V, Muschik T, Kux A, Meyer BK, Koch F, Lehmann V. Rapid-thermal-oxidized porous Si - The superior photoluminescent Si. *Applied Physics Letters* 1992;61:943-945.
376. Pacholski C, Sartor M, Sailor MJ, Cunin F, Miskelly GM. Biosensing using porous silicon double-layer interferometers: reflective interferometric fourier transform spectroscopy. *J Am Chem Soc* 2005;127:11636-11645.
377. Tessmar JK, Gopferich AM. Matrices and scaffolds for protein delivery in tissue engineering. *Adv Drug Deliv Rev* 2007;59:274-291.
378. Horcajada P, Rámila A, Pérez-Pariente J, et al. Influence of pore size of MCM-41 matrices on drug delivery rate. *Microporous and Mesoporous Materials* 2004;68:105-109.
379. Vallet-Regi M, Rámila A, del Real RP, Pérez-Pariente J. A new property of MCM-41: drug delivery system. *Chemistry of Materials* 2000;13:308-311.
380. Song SW, Hidajat K, Kawi S. Functionalized SBA-15 Materials as carriers for controlled drug delivery: influence of surface properties on matrix-drug interactions. *Langmuir* 2005;21:9568-9575.
381. Charnay C, Bégu S, Tourné-Péteilh C, Nicole L, Lerner DA, Devoisselle JM. Inclusion of ibuprofen in mesoporous templated silica: drug loading and release property. *Eur J Pharm Biopharm* 2004;57:533-540.
382. Salonen J, Kaukonen AM, Hirvonen J, Lehto VP. Mesoporous silicon in drug delivery applications. *J Pharm Sci* 2008;97:632-653.
383. Batra I, Coffey J, Canham L. Electronically-responsive delivery from a calcified mesoporous silicon structure. *Biomedical Microdevices* 2006;8:93-97.

384. Canham LT, Stewart MP, Buriak JM, et al. Derivatized porous silicon mirrors: implantable optical components with slow resorbability. *Physica Status Solidi (A)* 2000;182:521-525.
385. Anderson SHC, Elliott H, Wallis DJ, Canham LT, Powell JJ. Dissolution of different forms of partially porous silicon wafers under simulated physiological conditions. *Physica Status Solidi (A)* 2003;197:331-335.
386. Anglin EJ, Schwartz MP, Ng VP, Perelman LA, Sailor MJ. Engineering the chemistry and nanostructure of porous silicon Fabry-Perot films for loading and release of a steroid. *Langmuir* 2004;20:11264-11269.
387. Dancil K-PS, Greiner DP, Sailor MJ. A porous silicon optical biosensor: detection of reversible binding of IgG to a protein A-modified surface. *J Am Chem Soc* 1999;121:7925-7930.
388. Cheng L, Anglin E, Cunin F, et al. Intravitreal properties of porous silicon photonic crystals: a potential self-reporting intraocular drug-delivery vehicle. *Br J Ophthalmol* 2008;92:705-711.
389. Chhablani J, Nieto A, Hou H, et al. Oxidized porous silicon particles covalently grafted with daunorubicin as a sustained intraocular drug delivery system. *Invest Ophthalmol Vis Sci* 2013;54:1268-1279.
390. Hartmann KI, Nieto A, Wu EC, et al. Hydrosilylated porous silicon particles function as an intravitreal drug delivery system for daunorubicin. *J Ocul Pharmacol Ther* 2013;29:493-500.
391. Low SP, Voelcker NH, Canham LT, Williams KA. The biocompatibility of porous silicon in tissues of the eye. *Biomaterials* 2009;30:2873-2880.
392. Jay T, Canham LT, Heald K, Reeves CL, Downing R. Autoclaving of porous silicon within a hospital environment: potential benefits and problems. *Physica Status Solidi (A)* 2000;182:555-560.
393. Khung Y-L, Graney SD, Voelcker NH. Micropatterning of porous silicon films by direct laser writing. *Biotechnology Progress* 2006;22:1388-1393.
394. Janshoff A, Dancil K-PS, Steinem C, et al. Macroporous p-type silicon Fabry-Perot layers. fabrication, characterization, and applications in biosensing. *J Am Chem Soc* 1998;120:12108-12116.
395. Stewart MP, Buriak JM. Chemical and biological applications of porous silicon technology. *Advanced Materials* 2000;12:859-869.
396. Bimbo LM, Sarparanta M, Makila E, et al. Cellular interactions of surface modified nanoporous silicon particles. *Nanoscale* 2012.
397. Whitehead MA, Fan D, Mukherjee P, Akkaraju GR, Canham LT, Coffey JL. High-porosity poly(epsilon-caprolactone)/mesoporous silicon scaffolds: calcium phosphate deposition and biological response to bone precursor cells. *Tissue Eng Part A* 2008;14:195-206.
398. Natta FJv, Hill JW, Carothers WH. Studies of polymerization and ring formation. XXIII.1 epsilon-caprolactone and its polymers. *J Am Chem Soc* 1934;56:455-457.
399. Woodruff MA, Hutmacher DW. The return of a forgotten polymer—polycaprolactone in the 21st century. *Prog Polym Sci* 2010;35:1217-1256.
400. Luciani A, Coccoli V, Orsi S, Ambrosio L, Netti PA. PCL microspheres based functional scaffolds by bottom-up approach with predefined microstructural properties and release profiles. *Biomaterials* 2008;29:4800-4807.
401. Lee KH, Kim HY, Khil MS, Ra YM, Lee DR. Characterization of nanostructured poly(epsilon-caprolactone) nonwoven mats via electrospinning. *Polymer* 2003;44:1287-1294.

402. Marrazzo C, Di Maio E, Iannace S. Conventional and nanometric nucleating agents in poly(ϵ -caprolactone) foaming: Crystals vs. bubbles nucleation. *Polym Eng Sci* 2008;48:336-344.
403. Huang H, Oizumi S, Kojima N, Niino T, Sakai Y. Avidin–biotin binding-based cell seeding and perfusion culture of liver-derived cells in a porous scaffold with a three-dimensional interconnected flow-channel network. *Biomaterials* 2007;28:3815-3823.
404. Zein I, Hutmacher DW, Tan KC, Teoh SH. Fused deposition modeling of novel scaffold architectures for tissue engineering applications. *Biomaterials* 2002;23:1169-1185.
405. Vert M. Degradable and bioresorbable polymers in surgery and in pharmacology: beliefs and facts. *J Mater Sci Mater Med* 2009;20:437-446.
406. Middleton JC, Tipton AJ. Synthetic biodegradable polymers as orthopedic devices. *Biomaterials* 2000;21:2335-2346.
407. Gunatillake PA, Adhikari R. Biodegradable synthetic polymers for tissue engineering. *Eur Cell Mater* 2003;5:1-16; discussion 16.
408. Pitt CG, Chasalow FI, Hibionada YM, Klimas DM, Schindler A. Aliphatic polyesters. I. The degradation of poly(ϵ -caprolactone) in vivo. *J Appl Polym Sci* 1981;26:3779-3787.
409. Sun H, Mei L, Song C, Cui X, Wang P. The in vivo degradation, absorption and excretion of PCL-based implant. *Biomaterials* 2006;27:1735-1740.
410. Woodward SC, Brewer PS, Moatamed F, Schindler A, Pitt CG. The intracellular degradation of poly(epsilon-caprolactone). *J Biomed Mater Res* 1985;19:437-444.
411. Menei P, Croué A, Daniel V, Pouplard-Barthelaix A, Benoit JP. Fate and biocompatibility of three types of microspheres implanted into the brain. *J Biomed Mater Res* 1994;28:1079-1085.
412. Sawyer AA, Song SJ, Susanto E, et al. The stimulation of healing within a rat calvarial defect by mPCL-TCP/collagen scaffolds loaded with rhBMP-2. *Biomaterials* 2009;30:2479-2488.
413. Schantz JT, Hutmacher DW, Lam CX, et al. Repair of calvarial defects with customised tissue-engineered bone grafts II. Evaluation of cellular efficiency and efficacy in vivo. *Tissue Eng* 2003;9 Suppl 1:S127-139.
414. Yoon MS, Ahn KH, Cheung RW, et al. Covalent crosslinking of 1-D photonic crystals of microporous Si by hydrosilylation and ring-opening metathesis polymerization. *Chemical Communications* 2003;680-681.
415. Jane A, Dronov R, Hodges A, Voelcker NH. Porous silicon biosensors on the advance. *Trends Biotechnol* 2009;27:230-239.
416. Kilian KA, Bocking T, Gooding JJ. The importance of surface chemistry in mesoporous materials: lessons from porous silicon biosensors. *Chemical Communications* 2009;630-640.
417. Bonanno LM, Segal E. Nanostructured porous silicon-polymer-based hybrids: from biosensing to drug delivery. *Nanomedicine (Lond)* 2011;6:1755-1770.
418. Wu J, Sailor MJ. Chitosan Hydrogel-Capped Porous SiO₂ as a pH Responsive Nano-Valve for Triggered Release of Insulin. *Advanced Functional Materials* 2009;19:733-741.
419. Heinrich JL, Lee A, Sailor MJ. Porous silicon used as an initiator in polymerization reactions. *MRS Online Proceedings Library* 1994;358.
420. DeLouise LA, Fauchet PM, Miller BL, Pentland AA. Hydrogel-supported optical-microcavity sensors. *Advanced Materials* 2005;17:2199-2203.

421. Park JH, Gu L, von Maltzahn G, Ruoslahti E, Bhatia SN, Sailor MJ. Biodegradable luminescent porous silicon nanoparticles for in vivo applications. *Nat Mater* 2009;8:331-336.
422. Kashanian S, Harding F, Irani Y, et al. Evaluation of mesoporous silicon/polycaprolactone composites as ophthalmic implants. *Acta Biomater* 2010;6:3566-3572.
423. Underdown BJ, Schiff JM. Immunoglobulin A: strategic defense initiative at the mucosal surface. *Annu Rev Immunol* 1986;4:389-417.
424. *Immunology, infection, and immunity*. Washington, D.C.: Washington, D.C. : ASM Press; 2004.
425. Kohler G, Milstein C. Continuous cultures of fused cells secreting antibody of predefined specificity. *Nature* 1975;256:495-497.
426. Miller RA, Maloney DG, McKillop J, Levy R. In vivo effects of murine hybridoma monoclonal antibody in a patient with T-cell leukemia. *Blood* 1981;58:78-86.
427. Schroff RW, Foon KA, Beatty SM, Oldham RK, Morgan AC, Jr. Human anti-murine immunoglobulin responses in patients receiving monoclonal antibody therapy. *Cancer Res* 1985;45:879-885.
428. Boulianne GL, Hozumi N, Shulman MJ. Production of functional chimaeric mouse/human antibody. *Nature* 1984;312:643-646.
429. Gussow D, Seemann G. Humanization of monoclonal antibodies. *Methods Enzymol* 1991;203:99-121.
430. Ferrara N, Hillan KJ, Gerber HP, Novotny W. Discovery and development of bevacizumab, an anti-VEGF antibody for treating cancer. *Nat Rev Drug Discov* 2004;3:391-400.
431. Avery RL, Pearlman J, Pieramici DJ, et al. Intravitreal bevacizumab (Avastin) in the treatment of proliferative diabetic retinopathy. *Ophthalmology* 2006;113:1695 e1691-1615.
432. Arevalo JF, Wu L, Sanchez JG, et al. Intravitreal bevacizumab (Avastin) for proliferative diabetic retinopathy: 6-months follow-up. *Eye (Lond)* 2009;23:117-123.
433. Avery RL, Pieramici DJ, Rabena MD, Castellarin AA, Nasir MA, Giust MJ. Intravitreal bevacizumab (Avastin) for neovascular age-related macular degeneration. *Ophthalmology* 2006;113:363-372 e365.
434. Iliev ME, Domig D, Wolf-Schnurrbursch U, Wolf S, Sarra GM. Intravitreal bevacizumab (Avastin) in the treatment of neovascular glaucoma. *Am J Ophthalmol* 2006;142:1054-1056.
435. Iturralde D, Spaide RF, Meyerle CB, et al. Intravitreal bevacizumab (Avastin) treatment of macular edema in central retinal vein occlusion: a short-term study. *Retina* 2006;26:279-284.
436. Arevalo JF, Maia M, Garcia-Amaris RA, et al. Intravitreal bevacizumab for refractory pseudophakic cystoid macular edema: the Pan-American Collaborative Retina Study Group results. *Ophthalmology* 2009;116:1481-1487, 1487 e1481.
437. Arevalo JF, Sanchez JG, Fromow-Guerra J, et al. Comparison of two doses of primary intravitreal bevacizumab (Avastin) for diffuse diabetic macular edema: results from the Pan-American Collaborative Retina Study Group (PACORES) at 12-month follow-up. *Graefes Arch Clin Exp Ophthalmol* 2009;247:735-743.
438. Hudson PJ, Souriau C. Engineered antibodies. *Nat Med* 2003;9:129-134.

- 439.Pluckthun A, Krebber A, Krebber C, et al. Producing antibodies in *Escherichia coli*: from PCR to fermentation. In: Mccafferty J, Hoogenboom HR, Chiswell DJ (eds), *Antibody Engineering: A practical approach*: Oxford University Press; 1996.
- 440.Filpula D. Antibody engineering and modification technologies. *Biomol Eng* 2007;24:201-215.
- 441.Tang L, Persky AM, Hochhaus G, Meibohm B. Pharmacokinetic aspects of biotechnology products. *J Pharm Sci* 2004;93:2184-2204.
- 442.Mahmood I, Green MD. Pharmacokinetic and pharmacodynamic considerations in the development of therapeutic proteins. *Clin Pharmacokinet* 2005;44:331-347.
- 443.Thiel MA, Coster DJ, Standfield SD, et al. Penetration of engineered antibody fragments into the eye. *Clin Exp Immunol* 2002;128:67-74.
- 444.Bottenstein J, Hayashi I, Hutchings S, et al. The growth of cells in serum-free hormone-supplemented media. *Methods Enzymol* 1979;58:94-109.
- 445.Rubin JS, Chan AM, Bottaro DP, et al. A broad-spectrum human lung fibroblast-derived mitogen is a variant of hepatocyte growth factor. *Proc Natl Acad Sci U S A* 1991;88:415-419.
- 446.Karlsson LM, Tengvall P, Lundström I, Arwin H. Adsorption of human serum albumin in porous silicon gradients. *Physica Status Solidi (A)* 2003;197:326-330.
- 447.Li DQ, Chen Z, Song XJ, de Paiva CS, Kim HS, Pflugfelder SC. Partial enrichment of a population of human limbal epithelial cells with putative stem cell properties based on collagen type IV adhesiveness. *Exp Eye Res* 2005;80:581-590.
- 448.Igarashi T, Shimmura S, Yoshida S, Tonogi M, Shinozaki N, Yamane GY. Isolation of oral epithelial progenitors using collagen IV. *Oral Dis* 2008;14:413-418.
- 449.Ainscough SL, Barnard Z, Upton Z, Harkin DG. Vitronectin supports migratory responses of corneal epithelial cells to substrate bound IGF-I and HGF, and facilitates serum-free cultivation. *Exp Eye Res* 2006;83:1505-1514.
- 450.Echevarria TJ, Chow S, Watson S, Wakefield D, Di Girolamo N. Vitronectin: a matrix support factor for human limbal epithelial progenitor cells. *Invest Ophthalmol Vis Sci* 2011;52:8138-8147.
- 451.Newsome DA, Foidart JM, Hassell JR, Krachmer JH, Rodrigues MM, Katz SI. Detection of specific collagen types in normal and keratoconus corneas. *Invest Ophthalmol Vis Sci* 1981;20:738-750.
- 452.Cameron JD, Hagen ST, Waterfield RR, Furcht LT. Effects of matrix proteins on rabbit corneal epithelial cell adhesion and migration. *Curr Eye Res* 1988;7:293-301.
- 453.Masaki Y, Hirasawa A, Okuyama S, et al. Microchimerism and heart allograft acceptance. *Transplant Proc* 1995;27:148-150.
- 454.Rotman B, Papermaster BW. Membrane properties of living mammalian cells as studied by enzymatic hydrolysis of fluorogenic esters. *Proc Natl Acad Sci U S A* 1966;55:134-141.
- 455.Persidsky MD, Baillie GS. Fluorometric test of cell membrane integrity. *Cryobiology* 1977;14:322-331.
- 456.Vaccari L, Canton D, Zaffaroni N, Villa R, Tormen M, di Fabrizio E. Porous silicon as drug carrier for controlled delivery of doxorubicin anticancer agent. *Microelectronic Engineering* 2006;83:1598-1601.

457. Anglin EJ, Schwartz MP, Ng VP, Perelman LA, Sailor MJ. Engineering the chemistry and nanostructure of porous silicon Fabry-Pérot films for loading and release of a steroid. *Langmuir* 2004;20:11264-11269.
458. DeLouise LA, Miller BL. Enzyme Immobilization in porous silicon: quantitative analysis of the kinetic parameters for glutathione-S-transferases. *Anal Chem* 2005;77:1950-1956.
459. Maia MdMD, Vasconcelos EAd, Maia PFCdMD, et al. Immobilization of urease on vapour phase stain etched porous silicon. *Process Biochem* 2007;42:429-433.
460. Collins A, Mikeladze E, Bengtsson M, Kokaia M, Laurell T, Csöregi E. Interference elimination in glutamate monitoring with chip integrated enzyme microreactors. *Electroanalysis* 2001;13:425-431.
461. Solomon A, Rosenblatt M, Monroy D, Ji Z, Pflugfelder SC, Tseng SC. Suppression of interleukin 1alpha and interleukin 1beta in human limbal epithelial cells cultured on the amniotic membrane stromal matrix. *Br J Ophthalmol* 2001;85:444-449.
462. Hao Y, Ma DH, Hwang DG, Kim WS, Zhang F. Identification of antiangiogenic and antiinflammatory proteins in human amniotic membrane. *Cornea* 2000;19:348-352.
463. Basu S, Fernandez MM, Das S, Gaddipati S, Vemuganti GK, Sangwan VS. Clinical outcomes of xeno-free allogeneic cultivated limbal epithelial transplantation for bilateral limbal stem cell deficiency. *Br J Ophthalmol* 2012;96:1504-1509.
464. Marangon FB, Alfonso EC, Miller D, Remonda NM, Muallem MS, Tseng SC. Incidence of microbial infection after amniotic membrane transplantation. *Cornea* 2004;23:264-269.
465. Liu J, Lawrence BD, Liu A, Schwab IR, Oliveira LA, Rosenblatt MI. Silk fibroin as a biomaterial substrate for corneal epithelial cell sheet generation. *Invest Ophthalmol Vis Sci* 2012;53:4130-4138.
466. Reichl S, Borrelli M, Geerling G. Keratin films for ocular surface reconstruction. *Biomaterials* 2011;32:3375-3386.
467. Borrelli M, Reichl S, Feng Y, Schargus M, Schrader S, Geerling G. In vitro characterization and ex vivo surgical evaluation of human hair keratin films in ocular surface reconstruction after sterilization processing. *J Mater Sci Mater Med* 2013;24:221-230.
468. Ortega I, Ryan AJ, Deshpande P, Macneil S, Claeysens F. Combined microfabrication and electrospinning to produce 3-D architectures for corneal repair. *Acta Biomater* 2012.
469. Ortega I, Deshpande P, Gill AA, MacNeil S, Claeysens F. Development of a microfabricated artificial limbus with micropockets for cell delivery to the cornea. *Biofabrication* 2013;5:025008.
470. Zakaria N, Possemiers T, Dhuhghaill SN, et al. Results of a phase I/II clinical trial: standardized, non-xenogenic, cultivated limbal stem cell transplantation. *J Transl Med* 2014;12:58.
471. Chien Y, Liao YW, Liu DM, et al. Corneal repair by human corneal keratocyte-reprogrammed iPSCs and amphiphatic carboxymethyl-hexanoyl chitosan hydrogel. *Biomaterials* 2012;33:8003-8016.
472. Sotozono C, Inatomi T, Nakamura T, et al. Visual improvement after cultivated oral mucosal epithelial transplantation. *Ophthalmology* 2013;120:193-200.

473. Meyer-Blazejewska EA, Kruse FE, Bitterer K, et al. Preservation of the limbal stem cell phenotype by appropriate culture techniques. *Invest Ophthalmol Vis Sci* 2010;51:765-774.
474. Liu CY, Zhu G, Westerhausen-Larson A, et al. Cornea-specific expression of K12 keratin during mouse development. *Curr Eye Res* 1993;12:963-974.
475. Doyle LA, Yang W, Abruzzo LV, et al. A multidrug resistance transporter from human MCF-7 breast cancer cells. *Proc Natl Acad Sci U S A* 1998;95:15665-15670.
476. Dua HS, Gomes JA, Singh A. Corneal epithelial wound healing. *Br J Ophthalmol* 1994;78:401-408.
477. Yang Q, Peng J, Guo Q, et al. A cartilage ECM-derived 3-D porous acellular matrix scaffold for in vivo cartilage tissue engineering with PKH26-labeled chondrogenic bone marrow-derived mesenchymal stem cells. *Biomaterials* 2008;29:2378-2387.
478. Bernards DA, Bhisitkul RB, Wynn P, et al. Ocular biocompatibility and structural integrity of micro- and nanostructured poly(caprolactone) films. *J Ocul Pharmacol Ther* 2013;29:249-257.
479. Natu MV, Gaspar MN, Ribeiro CA, et al. A poly(epsilon-caprolactone) device for sustained release of an anti-glaucoma drug. *Biomed Mater* 2011;6:025003.
480. Iyer S, Scotney PD, Nash AD, Ravi Acharya K. Crystal structure of human vascular endothelial growth factor-B: identification of amino acids important for receptor binding. *J Mol Biol* 2006;359:76-85.
481. Allansmith M, de Ramus A, Maurice D. The dynamics of IgG in the cornea. *Invest Ophthalmol Vis Sci* 1979;18:947-955.
482. Stebbings R, Poole S, Thorpe R. Safety of biologics, lessons learnt from TGN1412. *Curr Opin Biotechnol* 2009;20:673-677.
483. Bennett MJ, Karki S, Moore GL, et al. Engineering fully human monoclonal antibodies from murine variable regions. *J Mol Biol* 2010;396:1474-1490.
484. Lichtlen P, Lam TT, Nork TM, Streit T, Urech DM. Relative contribution of VEGF and TNF-alpha in the cynomolgus laser-induced CNV model: comparing the efficacy of bevacizumab, adalimumab, and ESBA105. *Invest Ophthalmol Vis Sci* 2010;51:4738-4745.
485. Scotney PD, MacKenzie A, Maccarone P, et al. Human vascular endothelial growth factor B: characterization of recombinant isoforms and generation of neutralizing monoclonal antibodies. *Clin Exp Pharmacol Physiol* 2002;29:1024-1029.
486. Irani Y, Brereton HM, Tilton RG, Coster DJ, Williams KA. Production of scFv antibody fragments from a hybridoma with functional activity against human vascular endothelial growth factor. *Hybridoma (Larchmt)* 2009;28:205-209.
487. Turner ML, Cockerell EJ, Brereton HM, et al. Antigens of selected *Acanthamoeba* species detected with monoclonal antibodies. *Int J Parasitol* 2005;35:981-990.
488. Papathanassiou M, Theodoropoulou S, Analitis A, Tzonou A, Theodossiadis PG. Vascular endothelial growth factor inhibitors for treatment of corneal neovascularization: a meta-analysis. *Cornea* 2012.
489. Mould AW, Scotney P, Greco SA, Hayward NK, Nash A, Kay GF. Prophylactic but not therapeutic activity of a monoclonal antibody that neutralizes the binding of VEGF-B to VEGFR-1 in a murine collagen-induced arthritis model. *Rheumatology* 2008;47:263-266.

490. Irani Y, Tea M, Tilton RG, Coster DJ, Williams KA, Brereton HM. PCR amplification of the functional immunoglobulin heavy chain variable gene from a hybridoma in the presence of two aberrant transcripts. *J Immunol Methods* 2008;336:246-250.
491. Thiel MA, Coster DJ, Mavrangelos C, Zola H, Williams KA. An economical 20 litre bench-top fermenter. *Protein Expr Purif* 2002;26:14-18.
492. Li F, Meng F, Jin Q, et al. Fusion protein of single-chain variable domain fragments for treatment of myasthenia gravis. *Neural Regen Res* 2014;9:851-856.
493. Achen MG, Roufail S, Domagala T, et al. Monoclonal antibodies to vascular endothelial growth factor-D block its interactions with both VEGF receptor-2 and VEGF receptor-3. *Eur J Biochem* 2000;267:2505-2515.
494. Maurice DM, Zauberman H, Michaelson IC. The stimulus to neovascularization in the cornea. *Exp Eye Res* 1966;5:168-184.
495. Cogan DG. Vascularization of the cornea; its experimental induction by small lesions and a new theory of its pathogenesis. *Arch Ophthalmol* 1949;41:406-416.
496. Moromizato Y, Stechschulte S, Miyamoto K, et al. CD18 and ICAM-1-dependent corneal neovascularization and inflammation after limbal injury. *Am J Pathol* 2000;157:1277-1281.
497. Montezuma SR, Vavvas D, Miller JW. Review of the ocular angiogenesis animal models. *Semin Ophthalmol* 2009;24:52-61.
498. Kenyon BM, Voest EE, Chen CC, Flynn E, Folkman J, D'Amato RJ. A model of angiogenesis in the mouse cornea. *Invest Ophthalmol Vis Sci* 1996;37:1625-1632.
499. Loughman MS, Chatzistefanou K, Gonzalez EM, et al. Experimental corneal neovascularisation using sucralfate and basic fibroblast growth factor. *Aust N Z J Ophthalmol* 1996;24:289-295.
500. Corrent G, Roussel TJ, Tseng SC, Watson BD. Promotion of graft survival by photothrombotic occlusion of corneal neovascularization. *Arch Ophthalmol* 1989;107:1501-1506.
501. Sands M, Howell K, Costello CM, McLoughlin P. Placenta growth factor and vascular endothelial growth factor B expression in the hypoxic lung. *Respir Res* 2011;12:17.
502. Claesson-Welsh L. VEGF-B taken to our hearts: specific effect of VEGF-B in myocardial ischemia. *Arterioscler Thromb Vasc Biol* 2008;28:1575-1576.
503. Lahtenvuo JE, Lahtenvuo MT, Kivela A, et al. Vascular endothelial growth factor-B induces myocardium-specific angiogenesis and arteriogenesis via vascular endothelial growth factor receptor-1- and neuropilin receptor-1-dependent mechanisms. *Circulation* 2009;119:845-856.
504. Thiel MA, Wild A, Schmid MK, et al. Penetration of a topically administered anti-tumor necrosis factor alpha antibody fragment into the anterior chamber of the human eye. *Ophthalmology* 2013;120:1403-1408.
505. Athanasiadis Y, Tsatsos M, Sharma A, Hossain P. Subconjunctival triamcinolone acetonide in the management of ocular inflammatory disease. *J Ocul Pharmacol Ther* 2013;29:516-522.
506. Roufas A, Jalaludin B, Gaskin C, McCluskey P. Subconjunctival triamcinolone treatment for non-necrotising anterior scleritis. *Br J Ophthalmol* 2010;94:743-747.
507. Vazirani J, Basu S. Role of topical, subconjunctival, intracameral, and irrigative antibiotics in cataract surgery. *Curr Opin Ophthalmol* 2013;24:60-65.

508. Baum J. Treatment of bacterial ulcers of the cornea in the rabbit: a comparison of administration by eye drops and subconjunctival injections. *Trans Am Ophthalmol Soc* 1982;80:369-390.
509. Yeung SN, Lichtinger A, Kim P, Amiran MD, Slomovic AR. Combined use of subconjunctival and intracorneal bevacizumab injection for corneal neovascularization. *Cornea* 2011;30:1110-1114.
510. You IC, Im SK, Lee SH, Yoon KC. Photodynamic therapy with verteporfin combined with subconjunctival injection of bevacizumab for corneal neovascularization. *Cornea* 2011;30:30-33.
511. Desai SD, Blanchard J. Evaluation of pluronic F127-based sustained-release ocular delivery systems for pilocarpine using the albino rabbit eye model. *J Pharm Sci* 1998;87:1190-1195.
512. Desai SD, Blanchard J. Pluronic F127-based ocular delivery system containing biodegradable polyisobutylcyanoacrylate nanocapsules of pilocarpine. *Drug Deliv* 2000;7:201-207.
513. Lin HR, Sung KC. Carbopol/pluronic phase change solutions for ophthalmic drug delivery. *J Control Release* 2000;69:379-388.
514. Poole S, Stephenson JD. Body temperature regulation and thermoneutrality in rats. *Q J Exp Physiol Cogn Med Sci* 1977;62:143-149.
515. Wickham LA, Gao J, Toda I, Rocha EM, Ono M, Sullivan DA. Identification of androgen, estrogen and progesterone receptor mRNAs in the eye. *Acta Ophthalmologica Scandinavica* 2000;78:146-153.
516. Suzuki T, Kinoshita Y, Tachibana M, et al. Expression of sex steroid hormone receptors in human cornea. *Curr Eye Res* 2001;22:28-33.
517. Chen Y, Fu L, Han Y, et al. Testosterone replacement therapy promotes angiogenesis after acute myocardial infarction by enhancing expression of cytokines HIF-1 α , SDF-1 α and VEGF. *Eur J Pharmacol* 2012;684:116-124.
518. Rudolfsson SH, Bergh A. Testosterone-stimulated growth of the rat prostate may be driven by tissue hypoxia and hypoxia-inducible factor-1 α . *J Endocrinol* 2008;196:11-19.
519. Silva SA, Gobbo MG, Pinto-Fochi ME, et al. Prostate hyperplasia caused by long-term obesity is characterized by high deposition of extracellular matrix and increased content of MMP-9 and VEGF. *Int J Exp Pathol* 2015;96:21-30.
520. Schiffenbauer YS, Abramovitch R, Meir G, et al. Loss of ovarian function promotes angiogenesis in human ovarian carcinoma. *Proc Natl Acad Sci U S A* 1997;94:13203-13208.
521. Ma W, Tan J, Matsumoto H, et al. Adult tissue angiogenesis: evidence for negative regulation by estrogen in the uterus. *Mol Endocrinol* 2001;15:1983-1992.
522. Yamashita S, Kudo A, Kawakami H, Okada Y. Mechanisms of angiogenic suppression in uteri exposed to diethylstilbestrol neonatally in the mouse. *Biol Reprod* 2013;88:116.
523. Yang J, Xiong LJ, Xu F, et al. Estrogen inhibits colon polyp formation by reducing angiogenesis in a carcinogen-induced rat model. *Int J Endocrinol* 2013;2013:453898.
524. Yen ML, Su JL, Chien CL, et al. Diosgenin induces hypoxia-inducible factor-1 activation and angiogenesis through estrogen receptor-related phosphatidylinositol 3-kinase/Akt and p38 mitogen-activated protein kinase pathways in osteoblasts. *Mol Pharmacol* 2005;68:1061-1073.

525. Yun SP, Lee MY, Ryu JM, Song CH, Han HJ. Role of HIF-1alpha and VEGF in human mesenchymal stem cell proliferation by 17beta-estradiol: involvement of PKC, PI3K/Akt, and MAPKs. *Am J Physiol Cell Physiol* 2009;296:C317-326.
526. Banerjee SK, Sarkar DK, Weston AP, De A, Campbell DR. Over expression of vascular endothelial growth factor and its receptor during the development of estrogen-induced rat pituitary tumors may mediate estrogen-initiated tumor angiogenesis. *Carcinogenesis* 1997;18:1155-1161.
527. Romano AC, Espana EM, Yoo SH, Budak MT, Wolosin JM, Tseng SC. Different cell sizes in human limbal and central corneal basal epithelia measured by confocal microscopy and flow cytometry. *Invest Ophthalmol Vis Sci* 2003;44:5125-5129.
528. Wolosin JM, Xiong X, Schutte M, Stegman Z, Tieng A. Stem cells and differentiation stages in the limbo-corneal epithelium. *Prog Retin Eye Res* 2000;19:223-255.
529. Lehrer MS, Sun TT, Lavker RM. Strategies of epithelial repair: modulation of stem cell and transit amplifying cell proliferation. *J Cell Sci* 1998;111 (Pt 19):2867-2875.
530. Zieske JD, Bukusoglu G, Yankauckas MA. Characterization of a potential marker of corneal epithelial stem cells. *Invest Ophthalmol Vis Sci* 1992;33:143-152.
531. Zieske JD, Bukusoglu G, Yankauckas MA, Wasson ME, Keutmann HT. Alpha-enolase is restricted to basal cells of stratified squamous epithelium. *Dev Biol* 1992;151:18-26.
532. Chung EH, DeGregorio PG, Wasson M, Zieske JD. Epithelial regeneration after limbus-to-limbus debridement. Expression of alpha-enolase in stem and transient amplifying cells. *Invest Ophthalmol Vis Sci* 1995;36:1336-1343.
533. Budak MT, Alpdogan OS, Zhou M, Lavker RM, Akinci MA, Wolosin JM. Ocular surface epithelia contain ABCG2-dependent side population cells exhibiting features associated with stem cells. *J Cell Sci* 2005;118:1715-1724.
534. Barbaro V, Testa A, Di Iorio E, Mavilio F, Pellegrini G, De Luca M. C/EBPdelta regulates cell cycle and self-renewal of human limbal stem cells. *J Cell Biol* 2007;177:1037-1049.
535. Steuhl KP, Thiel HJ. Histochemical and morphological study of the regenerating corneal epithelium after limbus-to-limbus denudation. *Graefes Arch Clin Exp Ophthalmol* 1987;225:53-58.
536. Kumagai Y, Kurokawa MS, Ueno H, et al. Induction of corneal epithelium-like cells from cynomolgus monkey embryonic stem cells and their experimental transplantation to damaged cornea. *Cornea* 2010;29:432-438.
537. Espana EM, Di Pascuale M, Grueterich M, Solomon A, Tseng SC. Keratolimbic allograft in corneal reconstruction. *Eye (Lond)* 2004;18:406-417.
538. Chen Z, Evans WH, Pflugfelder SC, Li DQ. Gap junction protein connexin 43 serves as a negative marker for a stem cell-containing population of human limbal epithelial cells. *Stem Cells* 2006;24:1265-1273.
539. Matic M, Petrov IN, Chen S, Wang C, Dimitrijevic SD, Wolosin JM. Stem cells of the corneal epithelium lack connexins and metabolite transfer capacity. *Differentiation* 1997;61:251-260.
540. Dong Y, Roos M, Gruijters T, et al. Differential expression of two gap junction proteins in corneal epithelium. *Eur J Cell Biol* 1994;64:95-100.

541. Joyce NC, Mekler B, Joyce SJ, Zieske JD. Cell cycle protein expression and proliferative status in human corneal cells. *Invest Ophthalmol Vis Sci* 1996;37:645-655.
542. Hayashi K, Kenyon KR. Increased cytochrome oxidase activity in alkali-burned corneas. *Curr Eye Res* 1988;7:131-138.
543. Stepp MA, Zhu L. Upregulation of alpha 9 integrin and tenascin during epithelial regeneration after debridement in the cornea. *J Histochem Cytochem* 1997;45:189-201.
544. Stepp MA, Zhu L, Sheppard D, Cranfill RL. Localized distribution of alpha 9 integrin in the cornea and changes in expression during corneal epithelial cell differentiation. *J Histochem Cytochem* 1995;43:353-362.
545. Pajooesh-Ganji A, Ghosh SP, Stepp MA. Regional distribution of alpha9beta1 integrin within the limbus of the mouse ocular surface. *Dev Dyn* 2004;230:518-528.
546. Zieske JD. Perpetuation of stem cells in the eye. *Eye (Lond)* 1994;8 (Pt 2):163-169.
547. Di Iorio E, Barbaro V, Ferrari S, Ortolani C, De Luca M, Pellegrini G. Q-FIHC: quantification of fluorescence immunohistochemistry to analyse p63 isoforms and cell cycle phases in human limbal stem cells. *Microsc Res Tech* 2006;69:983-991.
548. Arpitha P, Prajna NV, Srinivasan M, Muthukkaruppan V. High expression of p63 combined with a large N/C ratio defines a subset of human limbal epithelial cells: implications on epithelial stem cells. *Invest Ophthalmol Vis Sci* 2005;46:3631-3636.
549. Tseng SC, Li DQ. Comparison of protein kinase C subtype expression between normal and aniridic human ocular surfaces: implications for limbal stem cell dysfunction in aniridia. *Cornea* 1996;15:168-178.
550. Lambiase A, Bonini S, Micera A, Rama P, Bonini S, Aloe L. Expression of nerve growth factor receptors on the ocular surface in healthy subjects and during manifestation of inflammatory diseases. *Invest Ophthalmol Vis Sci* 1998;39:1272-1275.
551. Touhami A, Grueterich M, Tseng SC. The role of NGF signaling in human limbal epithelium expanded by amniotic membrane culture. *Invest Ophthalmol Vis Sci* 2002;43:987-994.
552. Grueterich M, Espana EM, Tseng SC. Ex vivo expansion of limbal epithelial stem cells: amniotic membrane serving as a stem cell niche. *Surv Ophthalmol* 2003;48:631-646.
553. Kusanagi R, Umemoto T, Yamato M, et al. Nectin-3 expression is elevated in limbal epithelial side population cells with strongly expressed stem cell markers. *Biochem Biophys Res Commun* 2009;389:274-278.
554. Horenstein AL, Sizzano F, Lusso R, et al. CD38 and CD157 ectoenzymes mark cell subsets in the human corneal limbus. *Mol Med* 2009;15:76-84.
555. Ksander BR, Kolovou PE, Wilson BJ, et al. ABCB5 is a limbal stem cell gene required for corneal development and repair. *Nature* 2014;511:353-357.
556. Hyun DW, Kim YH, Koh AY, et al. Characterization of biomaterial-free cell sheets cultured from human oral mucosal epithelial cells. *J Tissue Eng Regen Med* 2014.
557. Zhang W, Xiao J, Li C, et al. Rapidly constructed scaffold-free cornea epithelial sheets for ocular surface reconstruction. *Tissue Eng Part C Methods* 2011;17:569-577.

558. Zhang W, Yang W, Liu X, Zhang L, Huang W, Zhang Y. Rapidly constructed scaffold-free embryonic stem cell sheets for ocular surface reconstruction. *Scanning* 2014;36:286-292.
559. Chow S, Di Girolamo N. Vitronectin: a migration and wound healing factor for human corneal epithelial cells. *Invest Ophthalmol Vis Sci* 2014;55:6590-6600.
560. Sumioka T, Fujita N, Kitano A, Okada Y, Saika S. Impaired angiogenic response in the cornea of mice lacking tenascin C. *Invest Ophthalmol Vis Sci* 2011;52:2462-2467.
561. Dziasko MA, Armer HE, Levis HJ, Shortt AJ, Tuft S, Daniels JT. Localisation of epithelial cells capable of holoclone formation in vitro and direct interaction with stromal cells in the native human limbal crypt. *PLoS One* 2014;9:e94283.
562. Levis HJ, Massie I, Dziasko MA, Kaasi A, Daniels JT. Rapid tissue engineering of biomimetic human corneal limbal crypts with 3D niche architecture. *Biomaterials* 2013;34:8860-8868.
563. Ma DH, Kuo MT, Tsai YJ, et al. Transplantation of cultivated oral mucosal epithelial cells for severe corneal burn. *Eye (Lond)* 2009;23:1442-1450.
564. Sekiyama E, Nakamura T, Kawasaki S, Sogabe H, Kinoshita S. Different expression of angiogenesis-related factors between human cultivated corneal and oral epithelial sheets. *Exp Eye Res* 2006;83:741-746.
565. Kanayama S, Nishida K, Yamato M, et al. Analysis of soluble vascular endothelial growth factor receptor-1 secreted from cultured corneal and oral mucosal epithelial cell sheets in vitro. *Br J Ophthalmol* 2009;93:263-267.
566. Kanayama S, Nishida K, Yamato M, et al. Analysis of angiogenesis induced by cultured corneal and oral mucosal epithelial cell sheets in vitro. *Exp Eye Res* 2007;85:772-781.
567. Chen HC, Yeh LK, Tsai YJ, et al. Expression of angiogenesis-related factors in human corneas after cultivated oral mucosal epithelial transplantation. *Invest Ophthalmol Vis Sci* 2012;53:5615-5623.
568. Guarnieri A, Moreno-Montanes J, Alfonso-Bartolozzi B, et al. Quantification of corneal neovascularization after ex vivo limbal epithelial stem cell therapy. *Int J Ophthalmol* 2014;7:988-995.
569. Cavallini GM, Pellegrini G, Volante V, et al. Chemical injury treated with autologous limbal epithelial stem cell transplantation and subconjunctival bevacizumab. *Clin Ophthalmol* 2014;8:1671-1673.
570. Nash AD, Baca M, Wright C, Scotney PD. The biology of vascular endothelial growth factor-B (VEGF-B). *Pulm Pharmacol Ther* 2006;19:61-69.
571. Dursun A, Arici MK, Dursun F, et al. Comparison of the effects of bevacizumab and ranibizumab injection on corneal angiogenesis in an alkali burn induced model. *Int J Ophthalmol* 2012;5:448-451.
572. Spitzer MS, Yoeruek E, Sierra A, et al. Comparative antiproliferative and cytotoxic profile of bevacizumab (Avastin), pegaptanib (Macugen) and ranibizumab (Lucentis) on different ocular cells. *Graefes Arch Clin Exp Ophthalmol* 2007;245:1837-1842.
573. Akar EE, Oner V, Kucukerdonmez C, Aydin Akova Y. Comparison of subconjunctivally injected bevacizumab, ranibizumab, and pegaptanib for inhibition of corneal neovascularization in a rat model. *Int J Ophthalmol* 2013;6:136-140.
574. Ferrari G, Dastjerdi MH, Okanobo A, et al. Topical ranibizumab as a treatment of corneal neovascularization. *Cornea* 2013;32:992-997.

575. Kim JH, Seo HW, Han HC, Lee JH, Choi SK, Lee D. The effect of bevacizumab versus ranibizumab in the treatment of corneal neovascularization: a preliminary study. *Korean J Ophthalmol* 2013;27:235-242.
576. Ohr M, Kaiser PK. Aflibercept in wet age-related macular degeneration: a perspective review. *Ther Adv Chronic Dis* 2012;3:153-161.
577. Papadopoulos N, Martin J, Ruan Q, et al. Binding and neutralization of vascular endothelial growth factor (VEGF) and related ligands by VEGF Trap, ranibizumab and bevacizumab. *Angiogenesis* 2012;15:171-185.
578. Schmidt-Erfurth U, Kaiser PK, Korobelnik JF, et al. Intravitreal aflibercept injection for neovascular age-related macular degeneration: ninety-six-week results of the VIEW studies. *Ophthalmology* 2014;121:193-201.
579. Diabetic Retinopathy Clinical Research N, Wells JA, Glassman AR, et al. Aflibercept, bevacizumab, or ranibizumab for diabetic macular edema. *N Engl J Med* 2015;372:1193-1203.
580. Oliveira HB, Sakimoto T, Javier JA, et al. VEGF Trap(R1R2) suppresses experimental corneal angiogenesis. *Eur J Ophthalmol* 2010;20:48-54.
581. Perez-Santonja JJ, Campos-Mollo E, Lledo-Riquelme M, Javaloy J, Alio JL. Inhibition of corneal neovascularization by topical bevacizumab (Anti-VEGF) and Sunitinib (Anti-VEGF and Anti-PDGF) in an animal model. *Am J Ophthalmol* 2010;150:519-528 e511.
582. Moisseiev E, Waisbourd M, Ben-Artzi E, et al. Pharmacokinetics of bevacizumab after topical and intravitreal administration in human eyes. *Graefes Arch Clin Exp Ophthalmol* 2014;252:331-337.
583. Waisbourd M, Levinger E, Varssano D, et al. High-dose topical bevacizumab for corneal neovascularization. *Pharmacology* 2013;92:310-314.
584. Stevenson W, Cheng SF, Dastjerdi MH, Ferrari G, Dana R. Corneal neovascularization and the utility of topical VEGF inhibition: ranibizumab (Lucentis) vs bevacizumab (Avastin). *Ocul Surf* 2012;10:67-83.
585. Clayton JA, Davis AF. Sex/gender disparities and women's eye health. *Curr Eye Res* 2015;40:102-109.
586. Eisner A. Sex, eyes, and vision: male/female distinctions in ophthalmic disorders. *Curr Eye Res* 2015;40:96-101.
587. Handa RJ, McGivern RF. Steroid hormones, receptors, and perceptual and cognitive sex differences in the visual system. *Curr Eye Res* 2015;40:110-127.
588. Kaarniranta K, Machalinska A, Vereb Z, Salminen A, Petrovski G, Kauppinen A. Estrogen signalling in the pathogenesis of age-related macular degeneration. *Curr Eye Res* 2015;40:226-233.
589. Ozawa GY, Bearse MA, Jr., Adams AJ. Male-female differences in diabetic retinopathy? *Curr Eye Res* 2015;40:234-246.
590. Schmidl D, Schmetterer L, Garhofer G, Popa-Cherecheanu A. Gender differences in ocular blood flow. *Curr Eye Res* 2015;40:201-212.
591. Sen HN, Davis J, Ucar D, Fox A, Chan CC, Goldstein DA. Gender disparities in ocular inflammatory disorders. *Curr Eye Res* 2015;40:146-161.
592. Smith W, Mitchell P, Wang JJ. Gender, oestrogen, hormone replacement and age-related macular degeneration: results from the Blue Mountains Eye Study. *Aust N Z J Ophthalmol* 1997;25 Suppl 1:S13-15.
593. Friedman DS, O'Colmain BJ, Munoz B, et al. Prevalence of age-related macular degeneration in the United States. *Arch Ophthalmol* 2004;122:564-572.

594. Rudnicka AR, Jarrar Z, Wormald R, Cook DG, Fletcher A, Owen CG. Age and gender variations in age-related macular degeneration prevalence in populations of European ancestry: a meta-analysis. *Ophthalmology* 2012;119:571-580.
595. Kawasaki R, Yasuda M, Song SJ, et al. The prevalence of age-related macular degeneration in Asians: a systematic review and meta-analysis. *Ophthalmology* 2010;117:921-927.
596. You QS, Xu L, Yang H, et al. Five-year incidence of age-related macular degeneration: the Beijing Eye Study. *Ophthalmology* 2012;119:2519-2525.
597. Feskanich D, Cho E, Schaumberg DA, Colditz GA, Hankinson SE. Menopausal and reproductive factors and risk of age-related macular degeneration. *Arch Ophthalmol* 2008;126:519-524.
598. Fraser-Bell S, Donofrio J, Wu J, Klein R, Azen SP, Varma R. Sociodemographic factors and age-related macular degeneration in Latinos: the Los Angeles Latino Eye Study. *Am J Ophthalmol* 2005;139:30-38.
599. Errera MH, Kohly RP, da Cruz L. Pregnancy-associated retinal diseases and their management. *Surv Ophthalmol* 2013;58:127-142.
600. Negrato CA, Mattar R, Gomes MB. Adverse pregnancy outcomes in women with diabetes. *Diabetol Metab Syndr* 2012;4:41.
601. Chaurasia RK, Singh R, Agrawal JK, Maurya OP. Sex hormones and diabetic retinopathy. *Ann Ophthalmol* 1993;25:227-230.
602. Haffner SM, Klein R, Dunn JF, Moss SE, Klein BE. Increased testosterone in type I diabetic subjects with severe retinopathy. *Ophthalmology* 1990;97:1270-1274.
603. Beery AK, Zucker I. Sex bias in neuroscience and biomedical research. *Neurosci Biobehav Rev* 2011;35:565-572.
604. Clayton JA, Collins FS. Policy: NIH to balance sex in cell and animal studies. *Nature* 2014;509:282-283.
605. Franconi F, Brunelleschi S, Steardo L, Cuomo V. Gender differences in drug responses. *Pharmacol Res* 2007;55:81-95.